Constructive Motives and Scattering

M. D. Sheppeard

Preface

This elementary textbook is for anyone interested in combinatorial methods in modern particle physics. Whenever advanced concepts are mentioned, an attempt is made to give some explanation. It assumes some physics knowledge, but not too much mathematics. There is a development of ideas through the book, but hopefully each chapter is also of some use on its own. All diagrams and tables are embedded in the text, just like equations.

At the heart of particle physics is the problem of *localisation*. As of 2012, nobody really understands what this is, just as mathematicians lack a proof of the famous Riemann hypothesis. There is however general agreement that the answers to these big questions involve the concept of *motive*. Throughout the book, our aim is to understand a little about motives, not from the standard mathematical point of view, but using a physicist's intuition. This can be done at an elementary level, because the underlying philosophy is a constructive one, meaning that theorems about motives should depend on their concrete construction. Motives are about both geometry and number theory, which means they must have something to do with knots. Of course, there are also many relevant topics that cannot be covered.

The essential physical ideas do not appear before chapter 6, but are an integral part of the methods discussed. The last chapter mentions several interesting observations related to these methods. If the reader *really* wants to skip the abstract nonsense on a first reading, they may do so.

The whole book is typeset in LaTeX, using mostly XY-pic for diagrams. It was written with essentially no resources and no library access, and no doubt contains errors. The author is a theoretical physicist who has contributed to professional research since 1987. In the years 1994-1997 she studied mathematical physics in Australia, focusing on knots, category theory and cohomological field theories. In the years 2004-2009 she gave many technical seminars on these topics and on their applications to twistor physics and the new cosmology, when the subject was still extremely unpopular.

Thanks to wikipedia for an endless supply of free information. It cannot all be acknowledged. This work was made possible by the kindness of Kerie and Allan.

Contents

1 Introduction

Twentieth century physics was created in a world that envisions a clock-work universe, where concrete objects inhabit a vast emptiness, ordained to exist forever from the beginning. When general relativity was formulated, the only suitable mathematics available was the Riemannian geometry of classical continua. But this theory was inspired by the non local dynamical principles of Mach and his circle. Many physicists scoff at Mach for his determined anti-atomism, because atoms do exist after all, but the key issue was always the clumsy separability of the atoms from the spaces they inhabit. In local quantum field theories, the atomic nature of matter is described by gauge fields on a spacetime continuum. These fields do not create their own dynamical spacetime.

We now know for certain that an alternative exists. Modern twistor methods for particle scattering amplitudes do not explicitly impose locality on the basic combinatorial input that specifies particle data. Amplitudes for n particles are computed on a space whose dimension increases with n, suggesting the increasing complexity of abstract information rather than an external reality of a fixed number of dimensions. Their structure is completely reducible to combinatorial data.

The physical framework is that of M theory, although its reduction to string theories is of no interest to us. Abstractly, the modern methods revolve around the concept of *motive*. A motive is a gadget much beloved by mathematicians, although nobody really understands what it is. Technically, motives define some category of spaces, from which one hopes the key to a universal cohomology theory will be revealed. What is cohomology to a physicist? It is an algorithm for cutting spaces down to their essential physical content. Today, physicists seek a mathematics to describe the emergence of classical spaces from algebras of quantum measurement, so motives cannot be based on purely commutative geometry, or a priori continua.

Motives already play a role in traditional quantum field theory [1][2], where renormalisation is studied using the underlying noncommutative geometry. They were originally described by Grothendieck [3], who pioneered the study of higher dimensional categories with arithmetic structure. In this text, we assume that the universal cohomology is intimately related to higher dimensional categories themselves. As pointed out by Street [4], the basic axioms of cohomology may be interpreted in almost any category.

First let us recall the basic idea of singular homology, with coefficients in $\mathbb{Z}$ [5][6]. A well behaved topological space M is triangulated to provide the combinatorial data for the computation of invariants. Usually M has a fixed classical dimension, so that all its pieces are triangular n-simplices, or subsimplices of lower dimension. An *m-chain* is a linear combination, with coefficients in $\mathbb{Z}$, of the m dimensional simplices of M. The sign of an integer coefficient may be used to orient cells. In this way, an edge between

two faces contributes positively to one face and negatively to the other, canceling out in a boundary sum. This cancelation allows the rule $\partial^2 = 0$ for the boundary operator. The collection of all chains for M fit into a chain complex

$$\cdots \to C^m \to C^{m-1} \to \cdots \to C^0 \tag{1}$$

where the arrows are given by the boundary map, which sends a simplex to a sum of its boundary elements. Similarly, a *cochain* complex is based on a coboundary map, which increases the dimension of a cochain. For a classical manifold M, the cochains may be the differential n-forms of de Rham cohomology.

If M is geometrically a category, rather than a set, a simplex is naturally oriented [4]. For example, the 2-simplex triangle

$$\tag{2}$$

may denote a cohomological cocycle condition. Oriented simplices are little categories in their own right. When the vertices are labeled $\{0, 1, \cdots, n\}$ they denote an ordinal n in $\mathbb{N}$, with inclusion maps. Every edge is modeled by a fundamental $0 \to 1$ arrow. To a category theorist, this arrow is the very foundation of topology, because the simplest topological space consists of one point and the empty set [7]. In the category of topological spaces, there is a unique arrow from this space to any other space.

Speaking of classical spaces, recall that the source free Maxwell's equations may be expressed simply as cohomological conditions, $d\omega = 0$ and $d * \omega = 0$, for a star operation defined with respect to the Lorentzian metric. The 2-form ω has the components (E_X, E_Y, E_Z) and (B_X, B_Y, B_Z) of the electromagnetic field. The star operation swaps these vectors around as coefficients in ω and $*\omega$. From the constructive point of view, it is electric magnetic duality that creates the metric, and not the other way around.

In M theory, this duality becomes the S duality between strong and weak couplings [8][9]. In the perturbative field theory we expect to see electric charges, as observed in nature. Magnetic charges are the counterpart to these fundamental states. The exchange of couplings is initially described by the modular group $SL_2(\mathbb{Z})$ acting on a complex parameter. Under S duality the gauge group G is sent to a dual group, known as the Langlands dual. This process belongs in the domain of number theory rather than representation theory, which is fortunate, because an emergent spacetime requires emergent symmetries.

The modular group is itself extended to the diagrammatic braid group on three strands. In the particle spectrum of chapter 7, we see that all electric and magnetic charges are naturally accounted for by braided ribbon

diagrams. The ribbons carry a $U(1)$ charge, not unlike Maxwell's original intuition for vortices in the aether, remembering that this aether is an abstraction.

The ribbons thicken line diagrams into surface diagrams, so a zero dimensional point becomes a one dimensional edge. Categories that look like collections of points are *sets*, but now that means that sets are lying below the very idea of topology. Actually, there are many reasons to give up on set theory. In particular, the axiom of choice creates horrendously unphysical paradoxes. The Banach-Tarski [10] paradox says that an orange can be cut up in a certain way, and put back together as two oranges. Whether or not quantum oranges have this property, a physicist requires real numbers that behave themselves. Secondly, the category **Set** of sets is a *topos*, a structure within which the real numbers do not even have a unique definition.

Giving up sets requires working with strictly categorical concepts. A constructive view of number theory is essential. This is a relatively underdeveloped subject, since constructivism has historically focused on real analysis and number theorists on set theoretic mathematics. We will talk about sets, but usually they will be finite and objects of a category.

In the late 19th century, Peano and Frege axiomatised basic arithmetic [11][12]. Peano also defined the first space filling curve. A modern example is Thurston's fractal curves [13]. Spaces of higher dimension are also filled with a one dimensional space, giving any continuum equal cardinality. But in category theory, the power of space filling first appears in dimension 3, with the Crans-Gray tensor product [14]. Conveniently, we focus on one dimensional curves in dimension 3, the subject of knots. The ambient dimension is always taken to be a categorical one, so that we must work with a collection of axioms that may be impossible to write down by hand.

There is a topology for which the integers $\mathbb{Z}$ appear to be three dimensional. Many mathematicians hope that knots will explain this mysterious fact. To physicists, knots are Wilson loops in a three dimensional quantum field theory known as Chern-Simons theory [15]. It does not bother us that spacetime appears to be four dimensional, because in twistor physics it is really a three dimensional complex space. The complexification of knots is the key to the emergence of causality.

In twistor theory, a non zero rest mass was studied in the 1980s [16] using higher dimensional sheaf cohomology. In nature, rest mass takes on quantised values. As a three valued quantum number, we investigate rest mass using quantum information theory. In chapter 7 we look at the Koide relations for the rest masses of the fundamental particles in the Standard Model.

The kinematic rules governing mass operators are well accounted for by $N = 8$ supergravity [17][18], which is described using twistor methods. In [19][20] a full formula for the S matrix of supergravity at tree level is given, using a tree matrix correspondence. This is a deeply motivic result, because

the trees provide geometry alongside their own matrix algebra. Such a natural combination of geometric and algebraic data is the modern extension of Descartes' original creation of Cartesian coordinates. Although the matrices initially contain unrestricted complex entries, the eventual aim is constrain every possible number within its proper geometric context.

Both Descartes and Newton accepted an absolute physical space, heralding the age of materialism, but they only did so reluctantly. In his *Opticks*, Newton introduces an aether and considers the particle nature of light. His objection to the wave hypothesis of the time was its premise of an inert stage in which waves could propagate. In contrast, the aether was itself a collection of the finest particles, with a tendency to disperse, not unlike a dark energy fluid in the standard cosmology. Light was refracted through its interactions with both matter and the aether, and empty space did not exist.

In a truly quantum universe, where measurement events obtain an ontological status that wave functions cannot, one would like to reconsider Newton's action at a distance as a statement about separated bodies that does not depend on a fixed background. Consider the first law: objects tend to remain in a state of uniform motion. The two distinct objects being dropped from a leaning tower, by Galileo, begin at rest with respect to each other. According to the literal law, there is no reason for these two objects to develop a separation, whether or not the Earth is present.

In general relativity, the equivalence principle ensures that the falling mass and inertial mass are equal. But how do we *measure* differences in inertia? In a modern laboratory, imagine that a mass spectrometer uses a magnetic field to separate a fixed velocity beam of charged electrons, muons and tau particles. The inertia of the heavier particles gives their trajectories a larger radius. The masses are thus measured by the local rods and clocks of the laboratory, via a circular motion.

If this inertia stands for a gravitational mass, what is the object about which the mass orbits? The circular motion brings to mind Newton's spinning bucket. Imagine first an ideal liquid in a perfect bucket, so that when the bucket is at rest relative to the human observer, the medium of fluid particles creates a flat surface inside the bucket. When the bucket spins, the surface appears to be curved. Our observer does not see the individual particles of the fluid, or the motion of the perfect bucket, but rather one of two static states: a flat surface or a curved surface. Only *under the hypothesis of particles* do these static observations correspond to rest and circular motion respectively.

According to Mach's classical principle, the spinning occurs relative to distant objects in the universe [21]. This implies that the gravitational mass is being measured using rods and clocks that reach far beyond the human laboratory. The equivalence principle becomes a statement of equality for two very distinct laboratories, one local and one cosmic. Precision locality is

a high energy concept, while cosmic distances are a low energy one, linking the equivalence principle to the physical dualities of M theory.

Multiple time twistor physics has a long history, notably in the work of Carr, Sparling [22] and Bars [23]. Most importantly, it allows us to discuss the cosmological arrow of time without assuming the same perfect time reversal symmetry afforded to laboratory clocks. The classical argument that thermodynamics derives this arrow of time from statistical behaviour does not hold water at a fundamental level, because the universe is *not* classical, nor specified as a single quantum state.

In quantum gravity, the universe is *observer dependent*. Every observer has access to multiple types of clock, be it laboratory ticks based on the motion of the sun, or the temperature of the cosmic microwave background radiation. Thermodynamics appears in the observer's environment, and as a matter of principle is interpreted using black hole geometry. Today, black hole thermodynamics in M theory is investigated using quantum information theory [24][25] and twistor physics [26]. Once again the subject is combinatorial.

Black hole entropy is given quantitatively in terms of generalised matrix invariants via the black hole qubit correspondence. These invariants are used to classify entanglement classes for n qudit systems, under the assumption of local operations and classical communication. The entanglement of particle pairs is crucial to the twistor methods for $N = 4$ Yang-Mills theory. Recent developments [19][20][27] have also illuminated the structure of $N = 8$ supergravity using matrix techniques.

Understanding gravity in twistor physics means a careful study of the breaking of conformal invariance. We can also consider this from the point of view of statistical mechanics. Near the critical points of phase transitions, the divergence of a correlation length can correspond to the scale invariance of a massless field theory. In particular, local conformal field theories in two dimensions start with the conformal transformations of a two dimensional world sheet. These form an infinite dimensional Lie group, composed of both the holomorphic and antiholomorphic coordinate transformations. At the quantum level the appropriate Lie algebra generators form the Virasoro algebra V, with relations [28]

$$[L_m, L_n] = \frac{c}{12}m(m^2 - 1)\delta_{m+n,0} + (m - n)L_{m+n} \tag{3}$$

so that the full Lie algebra is $V \oplus \overline{V}$. The constant c is the *central charge* associated to a central generator C. The generators L_0 and $L_{\pm 1}$ form an $sl_2(\mathbb{C})$ subalgebra.

When conformal field theory and two dimensional gravity were considered together, consistency demanded that $c = 26$. The continuum picture is not of direct interest here, but these are the 26 dimensions of bosonic string theory. The *conformal bootstrap* says that the fields $\phi(z, \overline{z})$ form an opera-

7

tor algebra, which is closely connected to the categorical concept of *operad*. The primary fields of interest have a vacuum creation property given by $L_n\phi = 0$ for $n > 0$ and $L_0\phi = h\phi$, where h and c characterise modules for V. Similarly for the antiholomorphic part. Now let a world sheet torus be given by its modular parameter t on the upper half plane. Then there is a partition function of the form [28]

$$Z(t) = \mathrm{Tr} e^{2\pi i t L_0} e^{-2\pi i \overline{t} \overline{L}_0} \tag{4}$$

for a simple Hamiltonian $H = L_0 + \overline{L}_0$. The trace splits into a sum over the primary fields, which have L_0 eigenvalues h, and other fields. The terms now include the phases $\exp(2\pi i t (L_0 - c/24))$, from which we can pull out the factor $\exp(-\pi i t c/12)$. Roughly speaking, these are zero point energies. Under the modular transformations there is then a phase factor of $\exp(2\pi i (h_j - c/24))$ for each primary ϕ_j. Modular invariance demands $h_j - \overline{h}_k \in \mathbb{Z}$.

At the critical value $c = 1$, there is a persistent phase $\exp \pi i/12$. This central charge is the limiting case of a special discrete set $c \in [0, 1]$ for which the algebra modules are nicely behaved. This basic phase appears throughout the book, in various guises.

To a category theorist, a conformal field theory is a study of ribbon graphs [29][30]. The behaviour of the operator algebra is governed by the axioms of braided ribbon categories. Intriguingly, all knotted strings in three dimensions can be embedded into branched surface diagrams, using the templates of dynamical systems theory [31][32]. The Lorenz attractor is an example of such a template, when drawn as glued ribbon pieces. Thus an extension of conformal field theory to branched surfaces should be associated to the $2 + 1$ dimensional field theories for knots [15].

In [33], Witten considers the $c = 24k$ conformal field theories, for $k \in \mathbb{N}$. This results in a partition function that is basically the j-invariant. This very special function is a complex map on the moduli space for four points, namely $\mathbb{CP}^1$ without $\{0, 1, \infty\}$,

$$j(z) = \frac{4}{27} \frac{(z^2 - z + 1)^3}{z^2(z-1)^2}. \tag{5}$$

It is really a function of an elliptic curve, because z can be expressed in terms of the three roots of a cubic polynomial in six different ways, which results in an action of the permutation group S_3. In the world of moonshine, the j-invariant has a Fourier expansion at the modular parameter $t \mapsto i\infty$, as a series in $q \equiv \exp(2\pi i t)$. The coefficients of this series are dimensions of modules that show up in the bosonic string theory.

Today M theorists are interested in six dimensional field theories, since this is the dimension of twistor space. Naively, one begins with three copies of a massless $1 + 1$ dimensional conformal theory, one for each generation.

8

The generations are governed by *triality*, since rest mass is notably a three valued quantum number. While many forms of duality are studied, triality remains relatively mysterious.

In real dimension six there are three distinct complex moduli spaces for Riemann surfaces, namely the genus zero case with six punctures $\mathcal{M}_{0,6}$, along with $\mathcal{M}_{1,3}$ and $\mathcal{M}_{2,0}$. We imagine that this set exhibits a triality, generalising the important relation between the two dimensional $\mathcal{M}_{1,1}$ for elliptic curves and the punctured Riemann sphere $\mathcal{M}_{0,4}$ [34].

It turns out that moduli spaces are very amenable to categorical description. Moreover, a physicist can imagine a path integral over all geometries to be a cohomological invariant for such index spaces. When moduli spaces are combinatorial, this becomes more tractable than dealing with the usual pathological spaces.

So the land of motives is a place where the numerical symbols that we write down have many interpretations: as geometry and algebra, and as the logic of observation itself. It is a place where arithmetic and combinatorics obey new rules, and where continua only exist when all their sub geometries have been constructively described. And it may be a place where the measurement of gravity finally makes some sense.

2   Numbers and Sets

Number constructivism starts with the idea that a real number should be much more than an element of a set. In mathematics, number fields and arithmetic are often given a priori, without much regard for the underlying axioms. Manifolds are modeled on number fields as if the notion of continuum is naturally specified. Physically, this is an unsatisfactory state of affairs. Numbers are, after all, the actual outcomes of measurement, and the relations between them are contingent upon our theoretical frameworks.

Category theory offers a natural way to add structure to numbers. A counting number $n \in \mathbb{N}$ is both the cardinality of an n element set and the dimension of a category. When n stands for a set with n elements, the permutations of the set become part of the structure of the number n. Important structures in number theory should arise in the canonical structures that appear whenever one raises the categorical dimension.

We use cycle notation for permutations σ in the permutation group S_d on d objects. For example, $\sigma = (312)$ in S_3 is the cycle

$$\begin{pmatrix} 0 & 0 & 1 \\ 1 & 0 & 0 \\ 0 & 1 & 0 \end{pmatrix}. \tag{6}$$

For operations that act on *sets*, the matrix entries act to select one element of the set with each row. This has an interpretation in terms of binary logic, since one can either select the element X or not select it, and hence the choice of 1 or 0.

Boolean logic has two valuations, namely *true* and *false*. These are often represented by the numbers 1 and 0 respectively. The system of logic evaluates propositional statements, which are built from an alphabet of objects and operations on these objects. In Boolean logic, one permits the binary operations AND (denoted by the symbol $\wedge$) and OR (denoted $\vee$). Since these operations are binary, there are only four basic statements involving them. For $\vee$ these are $1 \vee 1 = 1$, $1 \vee 0 = 1$, $0 \vee 1 = 1$ and $0 \vee 0 = 0$, which is summarised in the matrix table

$$\vee : \begin{pmatrix} 0 & 1 \\ 1 & 1 \end{pmatrix}, \tag{7}$$

where the matrix index always starts with 0. The operation $\vee$ is commutative, since $X \vee Y = Y \vee X$, so an extension of the matrix tables to a larger index set of objects always results in a symmetric matrix. However, even in Boolean logic there are operations that are not commutative. The unary operation NOT sends X to $\neg X$, and in Boolean logic only one of X and $\neg X$ can be true. Combining $\wedge$ and $\neg$ we have the table for statements like $0 \wedge \neg 0 = 0$,

$$\begin{pmatrix} 0 & 0 \\ 1 & 0 \end{pmatrix}. \tag{8}$$

Observe that 0 and 1 are letters in the alphabet that indexes a matrix. Every such 2×2 matrix, and there are 16, is permitted as a truth table. Operations in logic may then be used to define matrix multiplication.

Example 2.1 The finite field $\mathbb{F}_2$ has addition and multiplication tables

$$+ : \begin{pmatrix} 0 & 1 \\ 1 & 0 \end{pmatrix} \quad \times : \begin{pmatrix} 0 & 0 \\ 0 & 1 \end{pmatrix} \tag{9}$$

generating ordinary matrix multiplication over $\mathbb{F}_2$.

Example 2.2 The Boolean logic tables

$$\vee : \begin{pmatrix} 0 & 1 \\ 1 & 1 \end{pmatrix} \quad \wedge : \begin{pmatrix} 0 & 0 \\ 0 & 1 \end{pmatrix} \tag{10}$$

specify a matrix product, for matrices with 0 and 1 entries, such that there are 11 projectors satisfying $P^2 = P$. These are

$$\begin{pmatrix} 0 & 0 \\ 0 & 0 \end{pmatrix}, \quad \begin{pmatrix} 0 & 0 \\ 0 & 1 \end{pmatrix}, \quad \begin{pmatrix} 1 & 0 \\ 0 & 0 \end{pmatrix}, \quad \begin{pmatrix} 1 & 1 \\ 1 & 1 \end{pmatrix}, \tag{11}$$

$$\begin{pmatrix} 1 & 0 \\ 1 & 1 \end{pmatrix}, \quad \begin{pmatrix} 1 & 1 \\ 0 & 1 \end{pmatrix}, \quad \begin{pmatrix} 1 & 0 \\ 1 & 0 \end{pmatrix}, \quad \begin{pmatrix} 0 & 1 \\ 0 & 1 \end{pmatrix},$$

$$\begin{pmatrix} 1 & 1 \\ 0 & 0 \end{pmatrix}, \quad \begin{pmatrix} 0 & 0 \\ 1 & 1 \end{pmatrix}, \quad \begin{pmatrix} 1 & 0 \\ 0 & 1 \end{pmatrix}.$$

Projectors $P^2 = P$ reflect the real world process of quantum measurement. When a product is represented by a string vertex, the dual diagram for $P^2 = P$ is the commutative triangle

$$\tag{12}$$

When string networks are unlabeled, the assumption is that each string represents the same object, and $P^2 = P$ is only weakened through the addition of higher dimensional cells, starting with the interior of the triangle.

Finite sets are sometimes labeled by ordinals $\{0, 1, 2, \cdots, n\}$, and more generally by variable elements $\{X, Y, Z, \cdots\}$. The two element set $\Omega \equiv \{0, 1\}$ characterises the logic of the category **Set** [7]. In general, a binary operation for an n element set gives an $n \times n$ matrix table of truth values, as in

$$\begin{pmatrix} XX & XY & XZ \\ YX & YY & YZ \\ ZX & ZY & ZZ \end{pmatrix}. \tag{13}$$

Similarly, a ternary operation would specify an $n \times n \times n$ array. Partial domains for operations allow a generalisation to $n_1 \times n_2 \times \cdots \times n_k$ rectangular arrays. Note that the dimension l of the array is the word length of the components. The next few chapters focus on square matrices, which all correspond to truth tables of word length 2.

2.1 The Word Monoid

Polynomials are a lot like numbers. They can be added and multiplied, and usually inherit the distributivity of the coefficient field. The existence of noncommutative geometry in M theory suggests looking also at noncommutative polynomials. These are closely connected to quantum path spaces, since a monomial like XZX is interpreted as a sequence of noncommutative operations. A noncommutative monomial contains words in the letters of a given variable alphabet. The number of letters d determines the dimension d of a discrete cubic path space, defined by marking one letter steps along each axis. In this book, d is the dimension of a quantum state space. When $d = 2$, we think of states of a *qubit* [35].

The *word monoid* is the collection of all finite noncommutative monomials, with concatenation of words as a noncommutative product. The qubit words are graded by the diagonals of the path square.

$$(14)$$
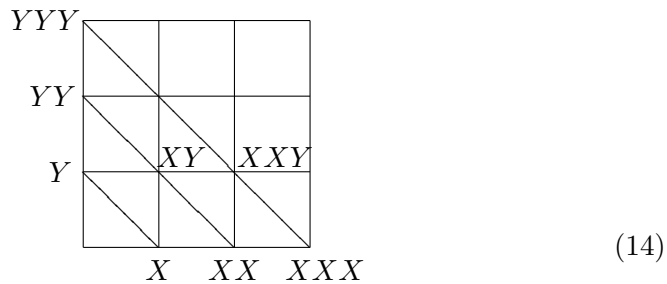
where both XY and YX end at the same point. Similarly, the qutrit words sit on the triangular diagonal simplices of a path cube.

$$(15)$$
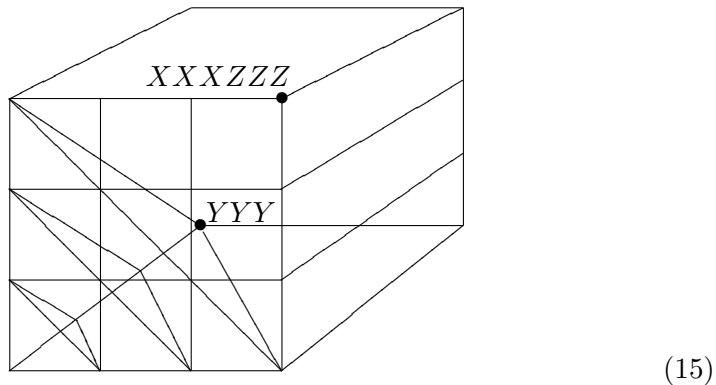
Note that the edges of the triangle at word length l are divided into l pieces. The first few simplices are labeled

$$(16)$$
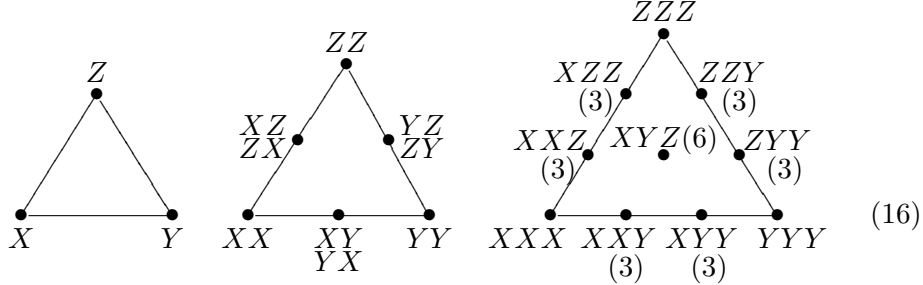
so that the ten sets of unordered monomials on the tetractys contain a total of 27 paths. The length 1 words in a d letter alphabet form a standard triangular simplex in dimension $d-1$. The measured simplices of longer word length will be used in the construction of interesting polytopes, starting in chapter 5.

The entire word monoid is graded in a table indexed by both l and d. The first column, for $l = 1$ letters, gives the standard simplex of dimension $d - 1$. The $l = 2$ column gives the halved simplices with d^2 paths. For the tetractys and beyond, we have the further option of bracketing words, distinguishing $(XY)Z$ and $X(YZ)$. We talk about $(d-1, l)$ simplices, where $d - 1$ is the simplex dimension and l numbers the divisions along an edge.

A divided simplex is canonically coordinatised in the integer lattice $\mathbb{Z}^d$. Since the monomials are of homogeneous degree, the sum of degrees is always a constant. For the length two words in three letters, we can then choose six vectors in $\mathbb{Z}^3$ that correspond to the degrees of X, Y and Z in each monomial. These are $(2, 0, 0)$, $(0, 2, 0)$, $(0, 0, 2)$, $(1, 1, 0)$, $(1, 0, 1)$ and $(0, 1, 1)$. Canonical coordinates will be used to study entropic volumes.

A $(d-1, l)$ path simplex in path space is naturally expanded into a cubic array. For example, the $(2, 3)$ *tensor cube* looks like

$$(17)$$
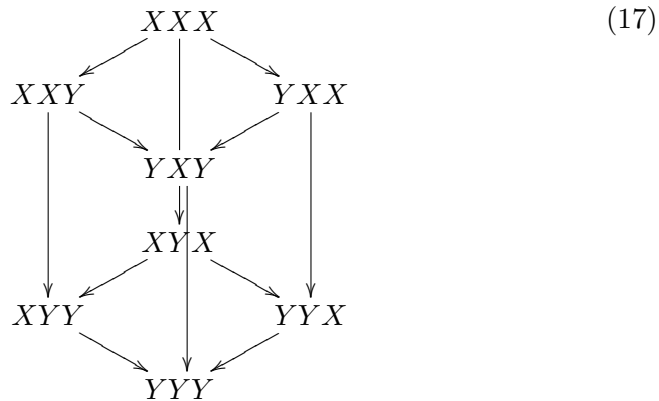
where we have shown how the cube can be oriented by $X \rightarrow Y$. See what has happened here. Path space gives both $(d - 1, l)$ divided *simplices* and

13

$(l, d-1)$ divided *cubes*. The two integers of the grading are swapped between simplices and cubes. A tensor cube is a model for a matrix or an array, like in (13). Any diagram that decomposes into paths can be assigned a tensor array. Arrays may be decomposed into symmetric and antisymmetric parts, as in

$$\begin{pmatrix} XX & XY \\ XY & YY \end{pmatrix} + \begin{pmatrix} 0 & 0 \\ YX - XY & 0 \end{pmatrix}. \tag{18}$$

The square arrays pick out two numbers, in this case 3 and 1, that partition d^2 into two triangular simplices. One of these simplices accounts for the commutative path set. The second may be drawn inside the first using the midpoints of the divided simplex. For $d = 4$ this gives an octahedron with vertices XY, YZ, ZW, XZ, XW and YW.

Any braid may be represented as a word in four letters, on the universal ribbon graph of Ghrist [31]. Knots are embedded in this special branched surface as loops around four attractor holes, with crossing points at the branches. Although we look mostly at algebraic representations for braids, the attractor word is always in the back of our minds.

2.2 Constructive Numbers

Since we don't want any unnecessary set theoretic axioms, particularly the axiom of choice, sets are merely zero dimensional categories. If the geometry and algebra of interest *looks* more than zero dimensional, it almost certainly should be. Continuum fields like $\mathbb{R}$ and $\mathbb{C}$ require dissection into infinite dimensional structures. This is a very concrete idea. For instance, as everyone knows, the sixth complex root of unity $\omega_6 = \exp(2\pi i/3)$ is actually the infinite sequence

$$\omega_6 = 1 + 1 + 2 + 5 + 14 + 42 + \cdots \tag{19}$$

of integer Catalan numbers [36][37]. As we will see, the Catalan numbers count planar binary trees, so ω_6 is the *cardinality* of an infinite set of trees. This suggests that complex numbers operate with multiple kinds of infinity. We focus on infinite sets of trees and braids.

Moving beyond set theory, we can do arithmetic using the first infinite cardinal, usually called ω. In the surreal number [38] construction of $\mathbb{R}$, ω appears after an infinite number of binary branchings on the surreal number tree. At each branching node, one can take a $+$ or $-$ step. The tree root marks the number 0, which branches to ± 1. Then ω is the infinite sequence $(+ + + + + \cdots)$. Similarly, ω^{-1} is the sequence $(- - - - - \cdots)$. After 1 we obtain $3/2$ or $1/2$, and the rule thereafter uses the difference $\pm 2^{-n}$ at step $n + 1$. Only the dyadic numbers are obtained in a finite number of steps, and then all the reals appear at step ω. The number ω^{-1} behaves much like an infinitesimal real. In the surreals, this process continues beyond ω, to polynomials in ω and to ω^ω and beyond.

To begin with, we think of $z \in \mathbb{C}$ as the sum of real and imaginary parts. The complex i has various roles to play in what follows, and it will be handy to keep track of it. For example, it is represented by the quantum Fourier transform F_d in dimension d, which obeys $F_d{}^4 = I$ whenever $d > 2$. Thus $z \in \mathbb{C}$ is like a Fourier pair of objects. Ordinary complex vector spaces are of no use to us, because a category of such spaces would take $\mathbb{C}$ as a given set.

Quantum mechanically we work with measurement operators, rather than vectors themselves, and finite dimensional vector spaces are characterised simply by the ordinal d that is their dimension. The category of ordinals and $m \times n$ matrices between them reminds us of **FinSet**, the category of finite sets. Actually, a matrix is like a binary relation $m \times n \to t$ to the set t of allowed truth values. We start with the binary entries 0 and 1, gradually adding further numbers as information structures are considered. Observe that the basic permutation

$$(21) = \begin{pmatrix} 0 & 1 \\ 1 & 0 \end{pmatrix}$$

can represent the number -1, since $(21)^2 = I_2$. Thus $k \times k$ matrices with entries in $\{0, \pm 1\}$ can be written as $2k \times 2k$ matrices with entries in $\{0, 1\}$. For instance, the Pauli matrix σ_Z becomes the controlled NOT gate [35]. The permutation (2341) also represents the complex i, so 2×2 matrices with entries in $\{0, \pm 1, \pm i\}$ could be expressed as 8×8 matrices with entries in $\{0, 1\}$. The Pauli matrices then become permutations in S_8. With this scheme, the entire set of complex numbers would require an uncountable matrix index! Fortunately, in practice we never work with all complex numbers at once. Rather than write out larger and larger binary matrices, we sensibly consider small sets of complex $d \times d$ matrices with special properties. We will often restrict to those of circulant form for $d = 2$ and $d = 3$, since these are combinations of the permutation matrices.

For many purposes, when $\mathbb{R}$ is mentioned, the rationals $\mathbb{Q}$ suffice. In reduced a/b form, rationals fit neatly into a Farey sequence F_n containing rationals with denominator $\leq n$ [39]. For example,

$$F_3 = \{0, \frac{1}{3}, \frac{1}{2}, \frac{2}{3}, 1\}. \tag{20}$$

Elements are listed in order. Let $a_k = n_k/d_k$ be a term in F_n for $k = 0, 1, \cdots, m_n$. Neighbouring pairs in the sequence F_n have the remarkable property that $d_k n_{k+1} - n_k d_{k+1} = 1$, which is a determinant 1 condition for the integer matrix

$$\begin{pmatrix} d_k & d_{k+1} \\ n_k & n_{k+1} \end{pmatrix}. \tag{21}$$

Now let $d_k = a_k - k/m_n$. For example, the F_3 set takes values in $\{0, \pm 1/12\}$. It has been shown [40] that the famous Riemann hypothesis is equivalent to

the statement that

$$\sum_{k=1}^{m_n} |d_k| \tag{22}$$

is of order n^x for some $x > 1/2$. These days one suspects that this is itself an axiomatic question. What is the value of m_n? It follows from the recursion $m_n = m_{n-1} + \phi(n-1)$, where $\phi(n)$ is Euler's totient function [41]

$$\phi(n) = n \prod_{p|n} (1 - \frac{1}{p}), \tag{23}$$

a product over the primes dividing n. This function counts the number of ordinals less than or equal to n that are relatively prime to n. It is also a multiplicative function, meaning that $\phi(a)\phi(b) = \phi(ab)$. Such a rule is always interpreted as the functor law for a 1-category, meaning here that $\mathbb{N}$ with multiplication is a monoid.

Another multiplicative function on $\mathbb{N}$ is Ramanujan's τ function, which satisfies $\tau(ab) = \tau(a)\tau(b)$ whenever a and b have no common primes. It appears as coefficients in the modular discriminant

$$\Delta(q) \equiv \sum_{n=1}^{\infty} \tau(n)q^n = q(\prod_{n=1}^{\infty}(1 - q^n))^{24} \tag{24}$$

where $q = \exp(2\pi i z)$, and z is in the upper half complex plane. The discriminant $\Delta(z)$ equals $\eta(z)^{24}$. This Dedekind η function deforms the modular group transformations by

$$\eta(z+1) = e^{\pi i/12} \eta(z) \qquad \eta(-1/z) = \sqrt{-iz}\eta(z). \tag{25}$$

A complex parameter q is used to define a noncommutative ordinal, a *q-number* [28],

$$\llcorner n \lrcorner_q = \frac{q^{n/2} - q^{-n/2}}{q^{1/2} - q^{-1/2}} \tag{26}$$

and such q parameters are used to deform commutative algebras. This is a function of $n \in \mathbb{N}$, but any real number similarly has a quantum deformation. The parameter q is used to deform permutation algebras into braided ones. When $\mathbb{C}$ is itself constructed, we care about each individual choice for q. Typically it is a root of unity, and the ordinals $\mathbb{N}$ are mapped to phases which project onto an axis in the complex plane. That is, quantum ordinals are non integral because of the higher dimensionality of phases. If we don't insist that a dimension has to be real, the complex phase itself is so interpreted.

We can also use real numbers to define ring like structures with unusual binary operations. The *tropical max semiring* $(\mathbb{R} \cup (-\infty), \oplus, \odot)$ uses the operations [42][43]

$$a \oplus b = \max(a, b) \qquad a \odot b = a + b \tag{27}$$

so that $-\infty$ behaves like zero for $\odot$ and one for $\oplus$. There is a similar min semiring, and we can restrict to $\mathbb{R}^+$ if we don't care about additive inverses. This structure is distributive. Using $\oplus$ and $\odot$, we can create tropical polynomials.

Example 2.3 The degree two conic in three variables with coefficients in X, Y and Z is

$$(X^2 \odot z_1 \odot z_1) \oplus (XY \odot z_1 \odot z_2) \oplus (XZ \odot z_1 \odot z_3)$$

$$\oplus (Y^2 \odot z_2 \odot z_2) \oplus (YZ \odot z_2 \odot z_3) \oplus (Z^2 \odot z_3 \odot z_3).$$

The reason for the strange coefficients is that this polynomial defines a trivalent graph
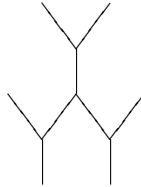
which is dual to the coordinatised two qutrit simplex. Tropical polynomials naturally define polytopes [43]. A trivalent vertex here is a tropical line.

The tropical semiring is closely related to the logarithm, as noted in [44]. That is, when a physical parameter $\hbar \to 0$, we observe that

$$\hbar \log(e^{x_1/\hbar} + e^{x_2/\hbar}) \sim \max(x_1, x_2). \tag{28}$$

This classical limit reduces two dimensional pictures to the one dimensional tropical curves. In chapter 6, a modern diagram calculus for logarithmic functions is described. This is important in the analysis of scattering amplitudes.

2.3 Union, Disjoint Union and Cohomology

To a mathematician, motives provide a universal theory for cohomological invariants. To a physicist however, the invariants themselves are responsible for the emergence of classical structure. Motives need to construct not only invariants but the spaces themselves! It is surely a chicken and egg problem, trying to say that a torus has a hole without looking at the torus. A few introductory comments on cohomology are in order.

As usual, $A_1 \cup A_2$ denotes the union of two sets, A_1 and A_2, and $A_1 \cap A_2$ their intersection. We write $A_1 \coprod A_2$ for the disjoint union. For a three element set $\{0, 1, 2\}$, the union of subsets is illustrated on the cubic lattice

of set inclusions

$$\tag{29}$$

$$\{\} $$

Diagram showing set inclusions from {} branching to {2}, {0}, to {0,2}, to {1}, to {2,1}, {1,0}, to {0,1,2}.
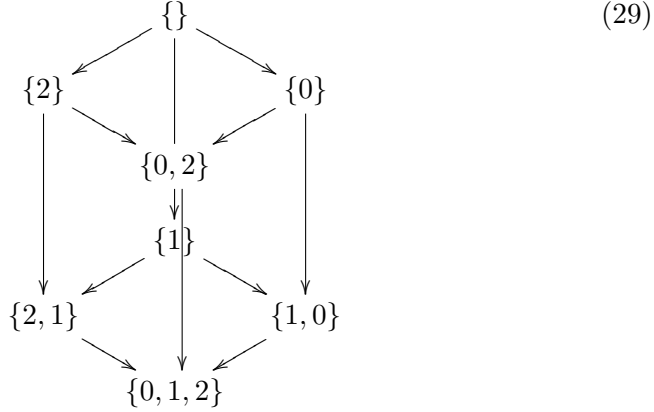
ending in $\{0, 1, 2\}$. The six elements at path length 2 actually give *two* copies of $\{0, 1, 2\}$, so somehow one copy is taken away to recover $\{0, 1, 2\}$. Since, in category theory, the cardinalities of sets are derived from sets, we would like the algebra of cardinalities to agree with operations on sets. Consider the principle of *inclusion exclusion*. Although usually expressed in terms of cardinalities, we can write

$$A \cup B \cup C = A \coprod B \coprod C - A \cap B - B \cap C - C \cap A + A \cap B \cap C \tag{30}$$

for three sets, where it is understood that the cardinality of $A \coprod B$ equals $|A| + |B|$. In general

$$\bigcup_i A_i = \coprod A_i - \sum_{i,j} A_i \cap A_j + \sum_{i,j,k} A_i \cap A_j \cap A_k - \cdots \tag{31}$$

Classically, this is not correct. It is an amazing paradoxical fact that, when A and B are open, $A \coprod B$ is *contained in* $A \cup B$. Usually for finite sets, where the open sets are the singletons in the discrete topology, complementary sets such as $\{0, 2\}$ above are not open, and there is no problem. If A and B have empty intersection, then $A \coprod B$ is the same as $A \cup B$, and there is no problem. But the above formula suggests that $A \coprod B$ should in general be larger! This is of great interest to us, because these alternating sums of intersections are responsible for the alternating sums that appear in Čech cohomology [45][46], which uses open covers of a classical manifold.

A classical cover of open sets U_i for a space M is a *good cover* if all intersections $U_i \cap U_j$ are either empty or contractible. For example, the Riemann sphere $\mathbb{CP}^1$ takes three open sets. Two is not sufficient, because an equatorial intersection is not contractible to a point. In this example, all

possible intersections up to $U_1 \cap U_2 \cap U_3$ give the cube

$$\begin{array}{c}
U_1 \cap U_2 \cap U_3 \qquad\qquad (32)
\end{array}$$

which is indexed by the original cube above. All arrows are inclusions. For all good covers, the nested intersections define a cube. Tracing a path backwards from M, one may encounter an empty intersection $U_i \cap \cdots \cap U_k$. In that case, all objects above $U_i \cap \cdots \cap U_k$ must be empty. Thus the cube is partitioned into two pieces: a top part marked with empty sets and the base with non empty ones. The shape of this partition defines the data of M. For example, the space of two disjoint sets U_1 and U_2 has empty intersection $U_1 \cap U_2$. The incidence data for the intersection lattice is the matrix

$$\begin{pmatrix} 0 & 1 \\ 1 & 1 \end{pmatrix}.$$

The topological data of any classical manifold defines such a binary matrix. The lattice of open sets for M is itself a category, which we call $O(M)$. A reversal of the inclusion arrows, to restrictions, defines the opposite category $O(M)^*$. A *presheaf* on M is a functor F from $O(M)^*$ into an algebraic category, such as the category of abelian groups.

For any such presheaf F, the 0-cochains of Čech cohomology [45] are the maps that send U_i to an element in $F(U_i)$. Then the 1-cochains come from $U_i \cap U_j$, and so on. The inclusion maps on the lattice induce a sequence of homomorphisms in the algebraic data, and the coboundary operator δ from d-cochains to $(d+1)$-cochains is defined as usual by an alternating sum. For $d = 0$, $\delta \equiv F(i_1) - F(i_2)$ on the two inclusion arrows i_1 and i_2 for $U_i \cap U_j \to U_i$. That is, for two open sets U and V there are inclusion maps

$$U \cap V \rightrightarrows U \coprod V \rightrightarrows U \cup V \qquad\qquad (33)$$

where a map on the left chooses one of the two sets, ignoring the other. Classically, there is only one inclusion on the right, but we need to be quite clear that U and V in $U \coprod V$ may use distinct inclusions.

The Mayer-Vietoris principle for the de Rham cohomology of manifolds uses the differential form functor, applied to the sequence (33). We do not

19

begin with manifolds at all, but what is the useful intuition behind Mayer-Vietoris? When the differential form functor F is applied, it gives a reversed sequence of restriction maps

$$F(U \cup V) \rightarrowtail F(U) \oplus F(V) \rightarrowtail F(U \cap V) \tag{34}$$

where the double map is absorbed into the algebraic splitting $F(U) \oplus F(V)$. Clearly there should be more differential forms in $F(U \cup V)$ than in the disjoint $F(U) \oplus F(V)$, which has no joining information. The strictness of the 1-functor F forces us to accept the bizarre behaviour of the underlying sets. However, in our study of a more general kind of cohomology we do not restrict attention to one dimensional functors. Notice also that the sequence of inclusions

$$\coprod_{ijk} U_i \cap U_j \cap U_k \rightrightarrows \coprod_{ij} U_i \cap U_j \rightrightarrows \coprod_i U_i \rightarrow M \tag{35}$$

on a cube forms a simplex, in this case a tetrahedron. Instead, with a fixed number n of arrows at each step, there are a total of n^2 edges. In the previous section, n^2 enumerated the noncommutative paths fitting on a simplex with halved edges. For example, two sets U and V give the four paths UU, VV, UV and VU. The noncommutative paths of length 2 are thus decomposed into an ordinary simplex and a second complementary simplex, providing extra arrows in the basic map sequence. So we consider general categorical incidence data, where the cubes and simplices can become more general polytopes.

2.4   A Category of Relations

See Appendix A for the basic definitions of categories. In the category **Set**, the inclusion of disjoint union in union is given in a coproduct diagram

(36)

where ! is the unique inclusion of the empty set in any set. The coproduct property of $\coprod$ states that for any maps a and b, there exists an inclusion i. When one does not adopt **Set** as a base category, this assumption may be weakened. Actually, we should start with an even better category of sets.

Let a finite index set be denoted J. It has cardinality $n = |J|$. An $n \times n$ matrix of zeroes and ones is a map $J \times J \rightarrow \Omega$. For example, when $n = 3$

20

the permutation (231) picks out the elements (X, Y), (Y, Z) and (Z, X) in $J \times J$. That is, (231) sends the vector (X, Y, Z) to the vector (Y, Z, X). This is a one to one function $J \to J$, but the use of a *relation* $J \times J \to \Omega$ is closer to the idea of a truth table.

Every square matrix may be viewed as a map $J \times J \to T$ for some set T of allowed truth values. The reason for choosing 0 and 1 as truth values is that these actually correspond to the cardinalities of the empty set and a one element set, respectively. More generally, for arbitrary relations between sets, T can have any cardinality. The evaluation of larger propositions depends on the basic ones, which for sets give the maps $\Omega \times \Omega \to \Omega$.

If the alphabet contained all of $\mathbb{R}^+$, we would begin by allowing T to be $\mathbb{R}^+$. However, the aim is to *construct* the real and complex number fields more carefully. The axioms of a field are of secondary concern and the selected subsets are specified by different criteria. It is then assumed that *any* numerical matrix entry should have an interpretation in logic and geometry.

The choice of 0 or 1 as a means of selecting a subset J of K may be expressed using a diagram of functions between sets, where χ is the *characteristic function* that sends elements of J to 1 and the other elements to 0.

$$
\begin{array}{ccc}
J & \longrightarrow & K \\
{\scriptstyle !}\downarrow & & \downarrow{\scriptstyle \chi} \\
1 & \underset{t}{\longrightarrow} & \Omega
\end{array}
\qquad (37)
$$

In the diagram, the set 1 is any one element set, and the function t picks out *true*, namely the element 1 in Ω. The vertical arrow ! is unique, because there is only one function into a one element set. This diagram lives in the category **Set**, which is then a *topos* [47][7]. Similarly, the category **Rel** of sets and relations contains the square

$$
\begin{array}{ccc}
(J \times J) \times (J \times J) & \overset{r_1 \times r_2}{\Longrightarrow} & K \times K \\
{\scriptstyle !}\downarrow & & \downarrow{\scriptstyle \chi} \\
1 \simeq 1 \times 1 & \underset{t}{\longrightarrow} & \Omega
\end{array}
\qquad (38)
$$

where any one point set is isomorphic to the Cartesian product of two one point sets. When $J \times J$ is a subset of K, via both r_1 and r_2, the square commutes, in the sense that both paths lead to the same relation $(J \times J)^2 \to \Omega$. In general, however, the square will not commute.

When $K = \Omega$, the relations r_i stand for matrices of zeroes and ones, and χ is a basic 2×2 table. We would like $r_1 \times r_2$ to be a tensor product of matrices, with respect to χ, because $|J \times J| = |J|^2$. In fact, Cartesian product is the tensor product for the category **Set**.

3 Duality and the Fourier Transform

Engineers and physicists learn that complex numbers are perfect for describing the interaction of waves, but in information theory waves do not necessarily give the ideal picture of what happens when quantum objects interact. Instead, consider the following. In a real plane, $(1, 1)$ and $(1, -1)$ are eigenvectors for the real Pauli matrix σ_X, which represents a spin measurement in the direction X. Together they give an orthogonal basis for the plane. However, real versions of σ_Y and σ_Z can only give one further basis for the plane, when two more are required in order to separate the Y and Z directions. All three directions are implicit in the physical meaning of spin, since spin states are separated in a Stern-Gerlach experiment using magnetic fields. In this chapter we will see that $\mathbb{C}^2$ is the natural home for the three required bases.

The real eigenvectors $(1, 1)$ and $(1, -1)$ form the columns of the 2×2 Hadamard gate [35] of quantum computation,

$$\frac{1}{\sqrt{2}} \begin{pmatrix} 1 & 1 \\ 1 & -1 \end{pmatrix}. \tag{39}$$

When it acts via conjugation $F_d M F_d^\dagger$ on a matrix M, this is the quantum Fourier transform F_2 in dimension 2. Unlike in higher dimensions, where $F_d{}^4$ is the identity, $F_2{}^2$ is already I_2. This is another way of saying that we need a complex i in dimension 2, so that iF_2 shares this property of higher dimensional transforms.

The quantum Fourier transform is the analogue, for a discrete set of noncommuting points, of the classical Fourier transform. The small finite sets of quantum numbers that we deal with are thus not simply sets, under an assumed background of axioms like Zermelo-Frenkel. They come with a good deal more structure than an ordinary set, using axioms from category theory.

The classical duality for the Fourier transform is given via richer notions of duality, using the language of two dimensional categories. These are first introduced in appendix A. The next section introduces the Fourier transform, and the following the important arithmetic concept of *mutually unbiased basis*.

3.1 The Quantum Fourier Transform

As usual, the indices of a finite matrix take values $i, j \in 0, 1, 2, \cdots, d-1$. The primitive dth root of unity $\exp(2\pi i/d)$ will be denoted ω_d. The d dimensional Fourier transform F_d is then a matrix transform $FMF^\dagger$ on a $d \times d$ matrix M, defined by [35]

$$(F_d)_{ij} = \frac{1}{\sqrt{d}} (\omega_d)^{ij}. \tag{40}$$

The choice of ω_d rather than $\overline{\omega_d}$ is arbitrary, as is the choice of row and column order. That is, there are a total of $2d^2$ matrices that we might have written down for F_d. All are elements of the unitary group $U(d)$, since $F_d F_d^\dagger$ equals the identity matrix I_d.

Let D_d be the democratic probability matrix with entries all equal to $1/\sqrt{d}$. For example,

$$D_3 = \frac{1}{\sqrt{3}} \begin{pmatrix} 1 & 1 & 1 \\ 1 & 1 & 1 \\ 1 & 1 & 1 \end{pmatrix}.$$

The elementary matrix E_{ij}, with only one non zero entry equal to 1 in the position ij, is given by $E_{ij} = F_d(D_d)$ for one of the d^2 choices for F_d. This is a decomposition of the basis matrices for all square matrices. The democratic matrix D_d is a unit for the Schur product of matrices, defined entrywise by $(AB)_{ij} = A_{ij} B_{ij}$.

A quantum *Fourier series* is a $d \times d$ 1-circulant matrix, which is specified by its first row, with each successive row a right cyclic shift, by one step, of the first row. For $d = 3$ it is given by $a_1 I + a_2(231) + a_3(312)$. The Fourier transform of such a circulant is a diagonal matrix, as in

$$\frac{1}{2} \begin{pmatrix} 1 & 1 \\ 1 & -1 \end{pmatrix} \begin{pmatrix} a & b \\ b & a \end{pmatrix} \begin{pmatrix} 1 & 1 \\ 1 & -1 \end{pmatrix} = \begin{pmatrix} a+b & 0 \\ 0 & a-b \end{pmatrix} \tag{41}$$

for the simplest 2×2 case. Thus a Fourier series is a linear combination of cyclic permutation matrices from S_d. In reverse, the Fourier transform of a diagonal matrix is a 1-circulant matrix.

Observe that the entries of F_d only take values in the complex dth roots of unity. When $d+1$ is a prime power, these d roots represent the d non zero elements of the field $\mathbb{F}_{d+1}$ with $d+1$ elements, along with their multiplication table. When $d = 3$, we choose

$$F_3 = \frac{1}{\sqrt{3}} \begin{pmatrix} 1 & 1 & 1 \\ 1 & \omega_3 & \overline{\omega}_3 \\ 1 & \overline{\omega}_3 & \omega_3 \end{pmatrix} \tag{42}$$

and its complex conjugate $F_3^\dagger$. For $d = 3$ there are both 1-circulants, for the odd elements of S_3, and 2-circulants, for even permutations. Including the determinant zero 0-circulants, there are always d classes of circulant. There is one basic 1-circulant and one basic diagonal. For $d = 3$, let

$$x = \begin{pmatrix} 0 & 1 & 0 \\ 0 & 0 & 1 \\ 1 & 0 & 0 \end{pmatrix} \qquad p = \begin{pmatrix} 1 & 0 & 0 \\ 0 & \omega_3 & 0 \\ 0 & 0 & \overline{\omega}_3 \end{pmatrix}. \tag{43}$$

Observe that $xp = \omega_3 px$. This is a Weyl commutation relation [48], usually written with an $\hbar$. Cycles of x define three points for the space, and there are similarly 3 forms for p, giving a six point phase space.

A $d \times d$ circulant is an element of the group algebra $\mathbb{C}S_d$ for the permutation group S_d. These Hopf algebras appear in appendix C. In much of what follows, we would like to restrict attention to circulant matrices, because their Hopf algebra gives a natural string network.

3.2   Unitary Bases and Decompositions

The normalised Pauli spin matrices

$$\sigma_X = \frac{1}{\sqrt{2}} \begin{pmatrix} 0 & 1 \\ 1 & 0 \end{pmatrix} \quad \sigma_Y = \frac{1}{\sqrt{2}} \begin{pmatrix} 0 & i \\ -i & 0 \end{pmatrix} \quad \sigma_Z = \frac{1}{\sqrt{2}} \begin{pmatrix} 1 & 0 \\ 0 & -1 \end{pmatrix} \quad (44)$$

define three directions in laboratory space. These matrices, along with the identity I_2, form a basis for the quaternions $\mathbb{H}$, in the form

$$Q = x^0 I_2 + x^1 \sigma_X + x^2 \sigma_Y + x^3 \sigma_Z = \frac{1}{\sqrt{2}} \begin{pmatrix} x^3 + x^0 & x^1 + ix^2 \\ x^1 - ix^2 & x^3 - x^0 \end{pmatrix}. \quad (45)$$

When the x^i are complex, (x^0, x^1, x^2, x^3) is a point in complexified Minkowski space $\mathbb{C}^4$, with x^0 playing the role of time. This 2×2 form leads naturally to twistor geometry [49][50]. We will always take Minkowski space to be in matrix form, since it introduces the concept of spinor. The Pauli matrices are used to create projectors that are normalised forms of $I_2 + \sigma_i$,

$$X = \frac{1}{2} \begin{pmatrix} 1 & 1 \\ 1 & 1 \end{pmatrix} \quad Y = \frac{1}{2} \begin{pmatrix} 1 & i \\ -i & 1 \end{pmatrix} \quad Z = \begin{pmatrix} 1 & 0 \\ 0 & 0 \end{pmatrix}. \quad (46)$$

A noncommutative path with the same end points, such as $XYZX$, is an analogue to a loop in a commutative space. The loop is directed because $YZ \neq ZY$. A point X is a kind of trivial loop. Observe that the product $XYZX$ equals $\exp(-\pi i/4)X$. In order to cancel the anomalous phase, and maintain a law $XYZX \simeq X$, each of X, Y and Z is multiplied by the basic phase $\omega_{24} = \exp(\pi i/12)$. Then X^2 no longer equals X exactly, but does so up to this phase factor.

The classical fundamental group $\pi_1(M, x)$ of a space M is the group of all loops based at a point x, with loop reversal as an inverse. The rule $XYZX \simeq X$ on noncommutative points is a statement of *contractibility*, saying that loops can be shrunk without hitting any obstacles. The rule is not strict, because there is a scale factor of $1/2\sqrt{2}$ on traversing the loop. In chapter 7, this data is used to create a cyclic 3×3 rest mass operator

$$\begin{pmatrix} 2\sqrt{2}^{-1} & \omega_{24} & 0 \\ \overline{\omega_{24}} & 2\sqrt{2}^{-1} & 0 \\ 0 & 0 & 0 \end{pmatrix} + \begin{pmatrix} 2\sqrt{2}^{-1} & 0 & \overline{\omega_{24}} \\ 0 & 0 & 0 \\ \omega_{24} & 0 & 2\sqrt{2}^{-1} \end{pmatrix} + \begin{pmatrix} 0 & 0 & 0 \\ 0 & 2\sqrt{2}^{-1} & \omega_{24} \\ 0 & \overline{\omega_{24}} & 2\sqrt{2}^{-1} \end{pmatrix},$$
$$(47)$$

which is used to parameterise Standard Model data. Note that the entries of X, Y and Z select three planes in Minkowski space, namely (x^1, x^3), (x^2, x^3) and (x^0, x^3) respectively. Note also that the Pauli matrices are a noncommutative analogue of the cubed roots of unity, since

$$1 + \overline{\omega_3} = -\omega_3 \qquad \omega_3 + 1 = -\overline{\omega_3} \qquad \overline{\omega_3} + \omega_3 = -1. \tag{48}$$

The *Pauli group* [35] for one qubit is the group generated by $\{I_2, \sigma_X, \sigma_Y, \sigma_Z\}$ with coefficients in $\{\pm 1, \pm i\}$.

Each Pauli matrix has a pair of eigenvectors, one for each eigenvalue $\pm 1/2$. The eigenvector pair forms the columns of another 2×2 matrix. Since an eigenvector is unchanged under multiplication by a complex scalar, there are many equivalent forms for such operators. But the probabilistic interpretation of quantum mechanical amplitudes means that the sum of norm squares in each row and column should sum to 1.

These three matrices form what is known as a set of *mutually unbiased bases* for dimension $d = 2$ [51][52][53]. That is, any two members M_1 and M_2 of the set have the property that the inner product $\langle v_1 | v_2 \rangle$, for an eigenvector v_1 in M_1 and eigenvector v_2 in M_2, is always of norm square $1/d$. For example, take the eigenvectors $(1, -1)$ and $(1, 0)$, and remember the normalisation factor of $1/\sqrt{2}$ for $(1, -1)$. The Pauli matrices provide a maximal set of $d + 1 = 3$ such bases for dimension 2.

The $d + 1$ mutually unbiased bases [52][53] in prime power dimension $d = p^k$ are given by a $d \times d$ matrix set $\{F_d, R_d, R_d{}^2, \cdots, R_d{}^d\}$, where R_d is a unitary circulant matrix. First,

$$R_2 = \frac{1}{\sqrt{2}} \begin{pmatrix} 1 & i \\ i & 1 \end{pmatrix}. \tag{49}$$

We can use $R_2{}^8 = I$ to specify the three mutually unbiased bases $\{F_2, R_2, I\}$ in dimension 2, since

$$R_2{}^2 = e^{i\pi/4} \sigma_X$$

has a zero diagonal, and so provides essentially the same eigenvectors as the identity I_2. In dimension 3 a convenient choice is

$$R_3 = \frac{1}{\sqrt{3}} \begin{pmatrix} 1 & \omega_3 & 1 \\ 1 & 1 & \omega_3 \\ \omega_3 & 1 & 1 \end{pmatrix} \tag{50}$$

for ω_3 the cubed root of unity, so that $R_3{}^3 = I_3$ up to a phase i. The set of four mutually unbiased bases is $\{F_3, R_3, R_3{}^2, I\}$. Since $4 = 2^2$ is a prime power, these bases represent multiplication in the finite field $\mathbb{F}_4$. The elements $\{R_3, R_3{}^{-1}, I\}$ give the cyclic group C_3 of non zero elements, just like the cubed roots of unity. The Fourier matrix F_3 represents zero in the

sense that $F_3 R_3$ is another form of F_3. The general circulant R_d in odd dimension d is

$$(R_d)_{ij} = \frac{1}{\sqrt{d}} (\omega_d)^{(k-j)(j-k+1)/2} \tag{51}$$

for $i, j \in \{0, 1, \cdots, d-1\}$ [54][55].

When $d = 1$ any phase defines a basis that is mutually unbiased with respect to another phase, since phases always multiply to a number of norm 1. In this way $\mathbb{C}$ is of uncountable dimension. However, we imagine that two bases are sufficient to characterise the one dimensional space. These should be F_1 and $I_1 = 1$, where F_1 must be i in order to have the Fourier property.

Let us look closer at the Pauli bases in dimension 2. Later on, the diagonal element 1 of R_2 will be generalised to a braid phase parameter, which is $\pi/2$ for R_2. The phase $t = \pm\pi/2$ is special as a fixed point under the map $t \mapsto -1/t$. But any real diagonal in R_2 has a corresponding braid parameter for a unitary matrix representation. With the normalisation factors taken as given, a circulant generalisation of R_2 in $\mathbb{C}S_2$ is

$$R_2(r) \equiv R(r) = \begin{pmatrix} r & i \\ i & r \end{pmatrix} \tag{52}$$

for $r \in \mathbb{R}^+$. Observe that this is the general Fourier transform of a diagonal

$$\begin{pmatrix} z & 0 \\ 0 & \bar{z} \end{pmatrix} \tag{53}$$

for z a complex number, under the scaling invariance $z \mapsto \lambda z$ with λ real. With the normalisation convention we are free to put the ratio of real to imaginary parts into the parameter r. Such an $R_2(r)$ is no longer unbiased with respect to F_2 and I_2, but instead stands for a general 2×2 probability matrix.

When $r > 1$, $(R(r))^2$ has non zero diagonal elements $r_2 \equiv r^2 - 1$, as does the nth power $(R(r))^n$. However, as $n \to \infty$ the parameter r_n approaches zero, because it goes as r/n. The recursion is given by

$$r_{j+1} = \frac{rr_j - 1}{r_j + r} \tag{54}$$

where $r = r_1$. Thus $(R(r))^\infty$ looks like $R_2{}^2$. Observe that the sequence is monotonic if and only if $r \geq \phi$, where $\phi \sim 1.618$ is the Golden ratio. Since an infinite number of time steps was never a problem for tortoises or hares, we can repeat the process and observe that

$$(R(r)^\infty)^4 R(r) = R(r). \tag{55}$$

Thus for any $r \geq 1$, $R(r)$ has cyclicity. Moreover,

$$(R(r))^{\infty+1} = \begin{pmatrix} r & i \\ i & r \end{pmatrix} \begin{pmatrix} 0 & i \\ i & 0 \end{pmatrix} = \begin{pmatrix} \frac{-1}{r} & i \\ i & \frac{-1}{r} \end{pmatrix} \tag{56}$$

so the parameters $r < 1$ appear naturally after the first infinite number of steps. When $r < 1$, there is no convergence in the $R(r_j)$, as is easily seen by looking at the first few terms of the sequence. However, the pseudoidentity

$$R(0) = \begin{pmatrix} 0 & i \\ i & 0 \end{pmatrix} = \begin{pmatrix} r & i \\ i & r \end{pmatrix} \begin{pmatrix} \frac{-1}{r} & i \\ i & \frac{-1}{r} \end{pmatrix} \tag{57}$$

relates the two parameter types. Observe that $r \in \{0, \pm 1\}$ sets up a binary alternating sequence in 0 and -1. A small r takes a few iterations to come close to 0.

The Pauli matrices provide a basis for the Lie algebra $su(2)$ of traceless Hermitian matrices. The group $SU(2)$ is obtained by exponentiating elements of the Lie algebra. Since 1-circulants always commute with each other, the 1-circulants

$$\begin{pmatrix} 0 & x \\ x & 0 \end{pmatrix} \tag{58}$$

in $su(2)$, where $x \in \mathbb{R}$, are exponentiated using the basic series

$$\exp A = I + A + \frac{A^2}{2!} + \frac{A^3}{3!} + \cdots \tag{59}$$

resulting in unitary circulants of the form

$$\begin{pmatrix} \cos(x^2) & i\sin(x^2) \\ i\sin(x^2) & \cos(x^2) \end{pmatrix}. \tag{60}$$

This corresponds to the parameter $r = \cot(x^2)$. In the case of the R_2 basis, we get $x = \sqrt{\pi}/2$. The inverse parameter $-1/r$ arises from the tangent of $-x^2$, which comes from pure imaginary elements of the form

$$\begin{pmatrix} 0 & ix \\ ix & 0 \end{pmatrix}. \tag{61}$$

Thus 1-circulants in the Minkowski algebra map to circulants in the group. Unlike in the Lie algebra $su(2)$, the Pauli matrices are each playing different roles in information theory. Note that σ_X is the only 1-circulant, providing the matrices of most interest to us. What is special about σ_X? For any $d \geq 2$, this basic 1-circulant $V_d = (234 \cdots d1)$ always has an eigenvector set giving the columns of F_d. The eigenvalues happen to be $\{\omega_d, \omega_d^2, \cdots, 1\}$.

So $V_2 = \sigma_X$ is dual to F_2, the only *non circulant* in the canonical set of mutually unbiased bases. The circulant set $\{\sigma_X, R_2, I_2\}$ gives all Pauli matrices and their unbiased bases, in the sense that R_2 is dual to σ_Y and I_2 dual to σ_Z. There is a similar set of $d + 1$ circulants in any prime power dimension, where V_d substitutes for the basis F_d.

As noncommutative operations, the mutually unbiased bases may define arbitrary monomials from the word monoid. Consider a noncommutative

polynomial in two variables X and Y. In the plane $\mathbb{C}$, words in X and Y define square paths on the lattice of Gaussian integers $\mathbb{Z} + \mathbb{Z}i$. Following Kapranov [56], we can consider a general polynomial

$$\sum c_{ijkl\ldots} X^i Y^j X^k Y^l \cdots \tag{62}$$

as a sum of abstract paths. This generalises a complex number z, which we get for the natural values $X = 1$ and $Y = i$. The arbitrary strings $(ijkl\cdots)$ of ordinals are instances of 2-ordinals, defined in the next chapter.

The duality of the Fourier transform is a specific instance of the phenomenon of Stone duality [57], which underlies attempts at unifying spaces and algebras in a motivic context. The next chapter discusses the basic elements of such dualities.

4   Duality, Triality and Ordinals

Dualities are ubiquitous in mathematics and physics. Geometrically, in dimension 2 duality swaps vertices for faces and edges for edges. It sends a triangle to a trivalent vertex. In a category, this turns 2-arrows f and g into little box points
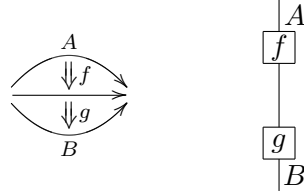
where it is understood that edges are directed downwards, and these edges are 1-arrows. The two unmarked areas are source and target objects. Since a monoidal category is really a bicategory, such strings may be used to represent its objects [58], with the concatenation

$$A \otimes A$$
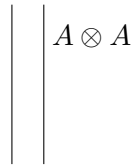
of strings standing for tensor product. Now an algebra object has a basic trivalent vertex, namely the multiplication $A \otimes A \to A$. In a braided monoidal category the strings may pass over and under one another, but in the symmetric case an ambiguous crossing

is sufficient. In a higher dimensional category, arrows may be reversed at any level, defining many distinct notions of duality. An adjoint dual $f^\dagger$ to a map f can be represented by a flipped box [59][60]
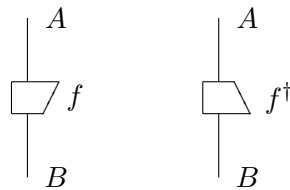
The $\dagger$ structure for a symmetric monoidal category satisfies $f^{\dagger\dagger} = f$, coming from an identity natural transformation in the adjunction. When we want both dual objects and dual arrows, we need the extra structure of *basis object*. Object duals A^* and B^* induce another dual arrow $f^* : B^* \to A^*$

given by *both* a left right and an up down box flip.
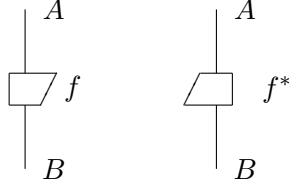
Starting with an adjoint f_*, we similarly define f_*, so that $\dagger$ is the composition of upper and lower star maps. This kind of double diagram flipping appears everywhere in this book.

A $\dagger$ *Frobenius structure* [61][60] is a cocommutative comonoid object A, with $\Delta_A : A \to A \otimes A$ and $\epsilon : A \to I$, such that $\Delta_A{}^\dagger \Delta_A = 1_A$ and

$$\Delta_A \Delta_A{}^\dagger = (\Delta_A{}^\dagger \otimes 1_A) \circ (1_A \otimes \Delta_A).$$

The arrows $\Delta_A : A \to A \otimes A$ and $\Delta_A{}^\dagger : A \otimes A \to A$ define dual trivalent vertices

(63)
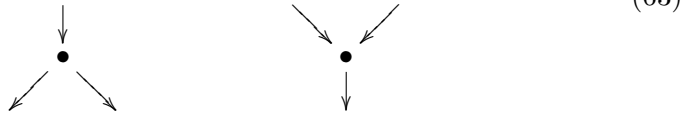
in the category, subject to the Frobenius axioms. Using the category of finite dimensional Hilbert spaces as a guide, the $\dagger$ Frobenius structures are in one to one correspondence with orthonormal bases for the spaces A. Since our special bases are associated to measurement operators, string networks are used to construct quantum circuit diagrams. Mixing $\dagger$ Frobenius structures with duals $\theta_A : A \to A^*$ allows a proper axiomatisation of bases, with $\theta_{A^*} = \theta_A{}^\dagger$. The θ_A are permutations. They allow a symbol
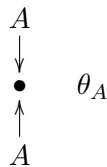
with a reversed pair of object arrows, which are both reversed for the adjoint. The ability to reverse object arrows with the θ maps is a time reversal operation for quantum computation. It permits the acausal logical processes of standard protocols [62] to be replaced with objects for which the observed time flows in one direction.

In all such categorical structures the inputs and outputs fit on a one dimensional line, creating a rigid concept of *before* and *after* for unitary processes. In contrast, the twistor diagrams of chapter 6 aim to capture the cyclicity of color structure in the Yang-Mills theory. The usual diagrammatic

representation for permutations, from n points to n points, is replaced by a cyclic structure within a twistor space picture. Then trivalent vertices such as $A \to A \otimes A$ no longer belong in the quantum mechanical scheme. However, there should be a breaking of the cyclic symmetry that recovers the standard planar diagram rules.

In other words, the simplest manifestation of *triality* is one in which there are reduced binary directions, given by a root choice on a tree or polygon. The next chapter focuses on these binary structures, which also play a key role in twistor physics. We start with the arithmetic importance of rooted trees.

The globule 2-arrows also correspond to trees. The ordinary ordinals $n \in \mathbb{N}$ are represented by single level planar, rooted trees

$$\mid \quad \bigvee \quad \bigvee\!\!\!\bigvee \quad \bigvee\!\!\!\bigvee\!\!\!\bigvee \quad \cdots \tag{64}$$
$$0 \quad 1 \quad\; 2 \quad\;\; 3$$

with $n+1$ leaves. These are the 1-ordinals. A dual way to draw the 1-ordinals is

$$\to \qquad \to\to \qquad \to\to\to \quad \cdots \tag{65}$$
$$0 \qquad\;\; 1 \qquad\qquad 2$$

so that the tree root stands for the n compositions along a string of arrows, just as a closed polygon is geometrically dual to a tree without orientation. Why does the number 1 have two leaves? As a polytope, the two leaves will represent a geometric point, because there is only one way to draw a binary tree with two leaves. This point set of one tree has cardinality 1. The single leaf is like an empty binary tree, and has cardinality 0.

Alternative conventions are possible. We could take the two leaved tree to be 0, since 0 is the *dimension* of a point. Then the single leaf represents the geometric empty set, and is the number -1. Often we count the root as another edge, so that the tree 2 has 4 edges and the tree 3 has 5. This has the advantage that $2 + 3$ is correctly represented by a total of 7 edges, under a tree composition that deletes one leaf from each component.

4.1 The d-Ordinals

A d-*ordinal* is specified by a planar tree with $d+1$ node levels, including the root [63]. For example, the trees

$$\tag{66}$$

represent a 2-ordinal and 3-ordinal respectively. As the number of levels increases so does the categorical dimension, as indicated by the equivalent

31

globule diagram. The 2-ordinal on the left becomes the pasting diagram

$$(67)$$

with five edges on the tree giving the five 1-arrows, the tree root specifying the horizontal composition, and the vertical composition occurring at the higher node. Similarly, the right hand tree is a diagram with five 3-arrows and three directions of composition.

The 2-ordinals are specified by strings of 1-ordinals $(n_1, n_2, \cdots, n_k)$, since a two level tree has k base edges at the root and each higher node has n_i leaves attached. The horizontal and vertical arrow compositions correspond to the trees

$$(68)$$

with a root node or a higher node respectively. All 1-ordinals can be extended to 2-ordinals with the addition of a root edge. Addition $m + n$ of 1-ordinals is then essentially recovered with vertical composition. Similarly, all 1-ordinals can be extended by adding another leaf to every leaf. Then horizontal composition recovers addition. The globule form of the two leaved trees

$$(69)$$

makes the composition rules clear. Note that horizontal composition

$$(70)$$

preserves the number of lowest level edges, while vertical composition does not. The globule representation turns the basic associator edge

$$(71)$$

into an arrow between two dimensional pictures $((ab)c)$ and $(a(bc))$. Higher dimensional representations of word association appear naturally, because words are often shorthand for tensor products, such as $a \otimes b \otimes c$, which may not be associative. Recall that the axioms for a monoidal category use the fact that $\otimes$ is itself an arrow composition. There is then a unique underlying

object, so that the word objects $a, b, a \otimes b, \cdots$ are treated as 1-arrows, and the arrows between words are now 2-arrows.

A globule picture for association raises the dimension yet again, but it becomes too unwieldy to work with higher dimensions, unless the categorical structure requires it. It often does! The most common form of monoidal category is a symmetric monoidal one, where $a \otimes b$ is the same as $b \otimes a$, but this is secretly a four dimensional category, because the symmetry rule is an equation for 3-arrows in a *braided* monoidal category. It turns out that a braiding structure $\gamma_{ab} : a \otimes b \rightarrow b \otimes a$ is another kind of categorical product, which raises the dimension much as $\otimes$ did [64].

Observe that the 3-ordinals have three possible binary compositions. A binary tree with four leaves, which has three levels, should then represent a three dimensional object. Taking this globule correspondence seriously, all the polytopes of the next chapter are thought of as reductions of higher dimensional ones, since they are defined by level trees.

The interplay of the two binary composition types for the 2-ordinals leads to a powerful representation of duality. This is illustrated with the special example of the Tamarkin tree [65][66], which is the 2-ordinal
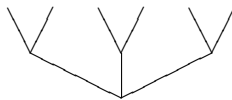
$$\tag{72}$$

representing the composition of six 2-arrows. If these 2-arrows represent dual structure, the Tamarkin tree is an initial instance of a triple of duals. This 2-ordinal indexes a six dimensional polytope, and was instrumental in extending compactifications for classical configuration spaces beyond a surprising six point anomaly [67]. Six dimensions are physically special, because that is the dimension of twistor space.

4.2 The Fourier Transform and Topology

The classical Fourier transform is associated to Pontrjagin duality [68] between a category of locally compact abelian groups and a category of Hausdorff spaces [57]. Given such a group G, the dual $G^\wedge$ is the set of *characters* $G \rightarrow S^1$ into the unit circle. The circle S^1 is very special, in being both an abelian group and a space. It extends the special role of the two point set $\{0, 1\}$ in the category **Set**. Recall that $\{0, 1\}$ stands for the elementary one point topological space, including an empty set [7]. Then S^1 is a large extension to the foundation of topology, if it can be constructed from scratch.

The functor $\wedge$ is an endofunctor $\mathbf{C} \rightarrow \mathbf{C}$ for some category $\mathbf{C}$ that has objects that are both spatial and algebraic. This is a feature of emergence, where *all* objects in $\mathbf{C}$ should have a property analogous to $\{0, 1\}$ and S^1.

33

Our matrices are full of characters in the form of complex phases, but every phase is supposed to have representations in terms of sequences of trees or strings. We must therefore understand how trees and strings are always *self dual* objects in this topological sense. We have seen that trees and arrow diagrams are dual, and that arrow diagrams and strings are dual, and later we will look at how braids and trees are related.

The Pontrjagin duality is a natural transformation $\eta : (G^\wedge)^\wedge \simeq G$ between the double dual of G and G. That is, for every arrow $f : G_1 \to G_2$ in the group category, there is a commutative square

$$
\begin{array}{ccc}
G_1{}^{\wedge\wedge} & \xrightarrow{\ f^{\wedge\wedge}\ } & G_1{}^{\wedge\wedge} \\
\eta_{G_1} \downarrow & & \downarrow \eta_{G_2} \\
G_1 & \xrightarrow{\ f\ } & G_2
\end{array}
\tag{73}
$$

in the category of abelian groups. When the categorical dimension is not restricted, all such dualities may be weakened by higher dimensional arrows. The important example is the Fourier duality between $\mathbb{Z}$ and S^1. For us, $\mathbb{Z}$ is the braid group B_2 on two strands, and it defines the fundamental group $\pi_1(S^1)$ for the circle. A positive braid crossing comes from anticlockwise windings.

With the quantum Fourier transform, the increasing dimension d of a finite dimensional state space is associated to increasing categorical dimension. For each d the underlying *space* only has d points, and the mutually unbiased bases in dimensions p^n are associated to the ring $\mathbb{Z}/\mathbb{Z}_{p^n}$. This suggests that $\mathbb{Z} \simeq B_2$ secretly lives at ω, and we have already assumed that continua such as S^1 are emergent. The Fourier duality of $\mathbb{Z}$ and S^1 is approached first with the inverse limits $\mathbb{Z}_p$

$$
\mathbb{Z}/\mathbb{Z}_p \to \mathbb{Z}/\mathbb{Z}_{p^2} \to \cdots \to \mathbb{Z}/\mathbb{Z}_{p^3} \cdots \to \mathbb{Z}_p
\tag{74}
$$

of the p-dit rings. The set $\mathbb{Z}_p$ is the p-adic integers, and it defines the division field $\mathbb{Q}_p$ of p-adic numbers [69]. A p-adic integer is a sequence of elements $x_n \in \mathbb{Z}/\mathbb{Z}_{p^n}$ such that for $n \leq m$, $x_n = x_m \mathrm{mod} p^n$. These numbers are also written as series sums $\sum a_n p^n$ with $a_n < p$, given p-adic arithmetic. Amazingly, $\mathbb{Z}_p$ is an uncountable set with the cardinality of the continuum.

As it happens, the Fourier dual of $\mathbb{Z}_p$ is the group of all p^n-th roots of unity on S^1 [70]. The only other phases we recognise are the rational ones, differing from the roots by a factor of $1/\pi$.

For a nice classical space X, p-adic cohomology $H^i(X, \mathbb{Z}_p)$ is also defined as an inverse limit of the groups $H^i(X, R_n)$ as $n \to \infty$. Finally, note that there are interesting ways to embed the p-adic numbers into the complex plane [71]. So quantum Fourier duality is carrying arithmetic into $\mathbb{C}$, building S^1 by the rules of the underlying categorical Stone duality [57].

34

5 Trees, Polytopes and Braids

A rooted tree is an example of a one dimensional contractible space. In this chapter we look at rooted, planar trees, mostly with binary branchings. The choice of a root turns cyclic trees into d-ordinals. Reading a tree downwards from the leaves, a binary node represents a product operation $a \cdot b$. Many types of product occur. A bracketing (ab) is a kind of binary product on a and b, and this is the default interpretation of binary tree nodes.

Permutations can be trees, where the permutation acts on the spaces between leaves. For example, a permutation in S_3 acts on the $\otimes$ operations in the word $a \otimes b \otimes c \otimes d$. A categorical braiding is also a kind of product.

Categorical polytopes are specified by certain sets of trees. For example, the binary planar trees with five leaves give the vertices of a polytope in three dimensions. The edges correspond to a tree with one internal edge collapsed, the faces to a tree with two internal edges collapsed, and the whole polytope to the unique one node tree with five leaves, namely the 1-ordinal 4. The basic arithmetic of ordinals is initially given by a matrix representation for trees, starting with the permutations.

5.1 Permutations and Planar Trees

First, consider the binary, rooted, planar trees such that every node is distinguished by its unique vertical height. The empty permutation on the empty set is represented by a single leaf. A two leaf tree

represents the trivial permutation (1) on one object, because there is only one node beneath the leaves. In general, a binary tree with $n + 1$ leaves gives a permutation in S_n, as in the example

$$(75)$$

where each entry in (132) is given by the appearance of a new area between leaves, moving down the page. The permutation really acts on the nodes of the tree. Each permutation group S_d corresponds to a set of $d!$ trees. The

35

hexagon of S_3 is the diagram

$$(76)$$
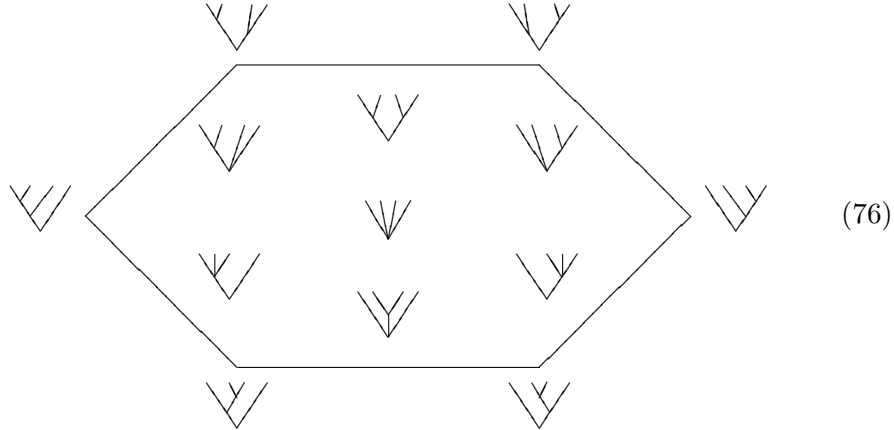
indexed by a one level tree with 4 leaves. Observe that the other geometric elements of the hexagon, namely vertices and edges, correspond to expansions of nodes into edges. Only two expansions are required to turn a 4 leaf node into a binary tree, giving the dimension of the hexagon.

An S_d diagram in dimension $d-1$ is known as a *permutohedron* [72]. The *associahedra* polytopes, also indexed by $d \in \mathbb{N}$, are given by trees which do not distinguish node levels. In this case (132) and (312) in S_3 denote equivalent trees, and the six vertices of the hexagon are reduced to the five vertices of a pentagon associahedron, by shrinking the one edge that is not labeled with a trivalent node. This pentagon is the Mac Lane axiom for monoidal categories, as given in appendix A. The set of associahedra were originally introduced by Tamari [73] and then by Stasheff [74], to discuss homotopy for classical spaces.

The left right reflection symmetry of permutation trees will be associated to S, T and U dualities, when permutations are reduced to their signature classes. The signature signs label the vertices of a parity cube. In dimension 3 these eight vertices are the components of a three qubit state, and hence label the electric and magnetic charges of black hole states [24]. In order to see the categorical importance of parity cubes, consider the following *categorification* of the bracketing process.

An associahedron binary tree with $d+1$ leaves represents a full bracketing of $d+1$ objects, such as in $((a(bc)d)e)$. Using edges oriented by the basic (21) flip, four objects are bracketed in the steps shown in the cube on the

36

right.

$$
\begin{array}{cc}
\text{(diagram of parity cube } P_4 \text{ with signs)} & \text{(hexagon with bracket labels)} \qquad (77)
\end{array}
$$
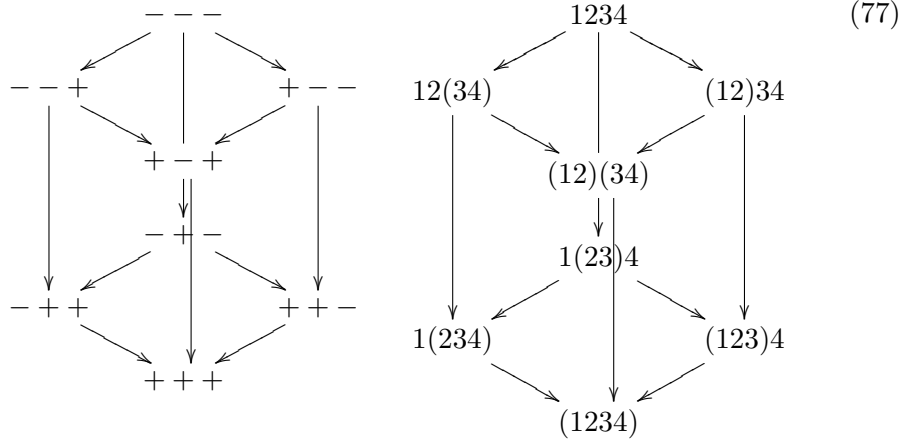
The signs are an alternative representation of the bracket choices, giving a parity cube P_4. Observe that each face of the cube stands for one edge on the hexagon (76). The cube is a categorification of the hexagon, in the sense that each geometric element is raised by one dimension. Categorically speaking, a face is now a pseudonatural transformation in a 2-category. This cube is naturally associated with three dimensional categories [75][76]. Every face except the top face represents an associator edge $(xy)z \Rightarrow x(yz)$. The double arrow labels the face itself, indicating its dimensionality and the homotopy between the two paths around the square. Now the top square

$$
\qquad (78)
$$
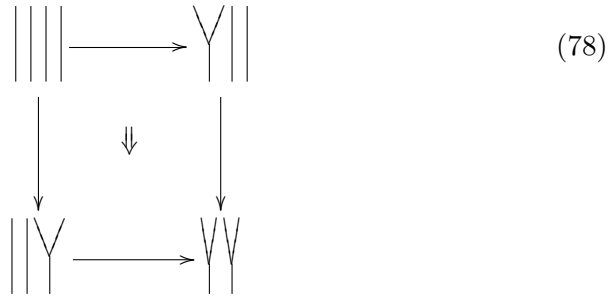
breaks the Mac Lane axiom for monoidal categories [77]. This square will make more sense in chapter 8, where the partial bracket diagrams are related to braids.

Since permutations are fundamental to us, and the categorical dimension is not arbitrarily restricted, this square allows for the deviation in tree node levels. When the vertical direction denotes a time coordinate, as it often does in physical applications, the S_d level splitting breaks the forward backward symmetry of time.

In the next section, the three dimensional associahedron A_4 is indexed by rooted hexagons, which are geometrically dual to the trees with 5 leaves.

Two vertices on this polytope are geometrically distinguished, and these are the ones given by the ambiguous level 4-leaved tree above. Thus the 24 vertices of the S_4 permutohedron are reduced to only 14 vertices for the associahedron. There also exist more complicated polytopes combining these types, such the *permutoassociahedra* [78]. In fact, every d-ordinal defines a special polytope.

Now every permutation matrix is associated to a rooted, binary tree. The S_2 edge associahedron

$$(79)$$

corresponds to the sum

$$\begin{pmatrix} 1 & 0 \\ 0 & 1 \end{pmatrix} + \begin{pmatrix} 0 & 1 \\ 1 & 0 \end{pmatrix} = \begin{pmatrix} 1 & 1 \\ 1 & 1 \end{pmatrix} = 2. \qquad (80)$$

In [79] Loday explains how the arithmetic of $1 + 1 = 2$ works with trees. The point is that we could start with the left hand 1 and then add the right hand 1, or vice versa. Trees or matrices respect this handedness.

For the contracted trees, where at least one node is not binary, the dimension of a permutation matrix may be reduced, as several leaves are joined into one object. This is a substitution process, which eventually reduces any tree to the index tree $d \in \mathbb{N}$ and the trivial permutation (1). Letting the matrix entry 1 be generalised to $k \in \mathbb{N}$, the hexagon edges of (76) should become matrices with the sum of entries totalling d. There is however a problem. Some trees group together objects from opposite ends of a string, so that no single permutation matrix can represent the contracted tree. We therefore generalise the matrices to include sums of permutations, weighted so that the total of d is maintained. The hexagon edges are then specified unambiguously by the matrices

$$\begin{pmatrix} 2 & 0 \\ 0 & 1 \end{pmatrix} \quad \begin{pmatrix} 1 & 0 & 1 \\ 1 & 0 & 1 \\ 0 & 2 & 0 \end{pmatrix} \quad \begin{pmatrix} 0 & 2 \\ 1 & 0 \end{pmatrix}$$

$$\begin{pmatrix} 1 & 0 \\ 0 & 2 \end{pmatrix} \quad \begin{pmatrix} 0 & 2 & 0 \\ 1 & 0 & 1 \\ 1 & 0 & 1 \end{pmatrix} \quad \begin{pmatrix} 0 & 1 \\ 2 & 0 \end{pmatrix} \qquad (81)$$

where the normalisation factors are understood. The 2×2 matrices are reductions of the obvious 3×3 ones, reflecting the ordinal substitution from S_3 into S_2. Observe that all six 3×3 matrices are norms of an F_2 Fourier matrix embedding into three dimensions. The other three possibilities for

F_2 are obtained via composition of edges. Two trees do not reduce to 2×2 operators, and these are the ones corresponding to full left right reflections. Now there is a reduction from the hexagon to the pentagon, and then to a square of 2×2 trees, which is the parity square $S_2 \times S_2$. The sum of matrix hexagon edges gives the democratic matrix

$$3 = \frac{1}{3} \begin{pmatrix} 1 & 1 & 1 \\ 1 & 1 & 1 \\ 1 & 1 & 1 \end{pmatrix} \tag{82}$$

representing the hexagon face. For all d, the integral matrices of the permutation vertices of S_d clearly sum to a scaled democratic matrix. Each vertex contributes equally to its incident edges, and has a fixed valency.

Since the two trees of type (75) are combined in the pentagon vertex $(132) + (312)$, the pentagon face sums to the asymmetric probability matrix

$$\frac{1}{10} \begin{pmatrix} 3 & 4 & 3 \\ 3 & 4 & 3 \\ 4 & 2 & 4 \end{pmatrix}. \tag{83}$$

This embeds in a 4×4 matrix as a pentagon face of A_4. A square face on S_4 is given by

$$(1234) + (2134) + (1243) + (2143) = \frac{1}{2} \begin{pmatrix} 1 & 1 & 0 & 0 \\ 1 & 1 & 0 & 0 \\ 0 & 0 & 1 & 1 \\ 0 & 0 & 1 & 1 \end{pmatrix} \tag{84}$$

but on A_4 we include (4123) and (4213) to obtain the magic square

$$\frac{1}{16} \begin{pmatrix} 7 & 7 & 0 & 2 \\ 8 & 8 & 0 & 0 \\ 1 & 1 & 8 & 6 \\ 0 & 0 & 8 & 8 \end{pmatrix}. \tag{85}$$

Finally, one can easily verify the parity square and cube matrices

$$\frac{1}{8} \begin{pmatrix} 3 & 2 & 3 \\ 2 & 4 & 2 \\ 3 & 2 & 3 \end{pmatrix} \qquad \frac{1}{10} \begin{pmatrix} 3 & 2 & 2 & 3 \\ 2 & 3 & 3 & 2 \\ 2 & 3 & 3 & 2 \\ 3 & 2 & 2 & 3 \end{pmatrix}. \tag{86}$$

Observe that the up down reflection of a parity cube matrix corresponds to a left right reversal of the sign string, with all signs flipped. Flipping all signs corresponds to the left right matrix symmetry.

In the search for motives, we want algebraic objects that explicitly manifest the properties of their diagrams. These S_d objects do not achieve this, and this is the main motivation for braid algebras.

5.2 Solomon's Descent Algebra

The *signature* class for a permutation group S_d is a string of $d-1$ signs, and a collection of signature classes determines a parity cube in dimension $d-1$. For example, the signature of (32145) is $(--++)$, with the signs determined by the direction of change in the digits as one reads out the permutation from left to right. Thus S_3 has four signature classes, giving a parity square, and the 8 corners of the parity cube come from the 24 elements of S_4.

Example 5.1 The eight signature classes of S_4, and their orders, are

$(---)$	(4321)	1
$(--+)$	$(4312), (4213), (3214)$	3
$(-+-)$	$(4231), (4132), (2143), (3142), (3241)$	5
$(+--)$	$(3421), (2431), (1432)$	3
$(++-)$	$(1243), (1342), (2341)$	3
$(+-+)$	$(3412), (1423), (1324), (2413), (2314)$	5
$(-++)$	$(4123), (3124), (2134)$	3
$(+++)$	(1234)	1

For the permutation polytopes, there is an obvious source and target with which to orient the cube edges and faces. Let ρ denote a signature class for S_d. H_ρ is defined to be the sum of all permutations in the class, which is an element in the group Hopf algebra KS_d, for any suitable K that contains zero and one. Solomon's theorem [80] is the statement that $H_{\rho_1} H_{\rho_2}$ is a linear combination of the H_ρ for S_d. When it is obvious, the notation H_ρ may be neglected.

Example 5.2 For the S_4 group algebra over $\mathbb{N}$,

$$(-++)(--+) = [(4123) + (3124) + (2134)][(4312) + (4213) + (3214)]$$

$$= (+--) \quad + \quad (+-+) \quad + \quad (---)$$

Signature classes may also be labeled by *ordered partitions* as follows. The identity element of $(++\cdots+)$ is the single component partition d, as in the ordinal index. The descending $(--\cdots-)$ element is the partition $1+1+\cdots+1$ of all ones. For S_3 there are two remaining classes, $(-+)$ and $(+-)$, each containing two permutations. These are the partitions $1+2$ and $2+1$ respectively. That is, the minus signs are used to indicate a tendency for ones. The more plus signs, the further one moves away from partitions built from ones.

Atkinson [81] defines a matrix $M_{\rho_1 \rho_2}$ using any pair of ordered partitions ρ_1 and ρ_2. The row sums are given by the ordinals in ρ_1 and the column sums by the ordinals in ρ_2. For example, let $\rho_1 = 1+2$ and $\rho_2 = 1+1+1$. Then there are three possibilities for the matrix $M_{\rho_1 \rho_2}$, namely

$$\begin{pmatrix} 0 & 1 & 0 \\ 1 & 0 & 1 \end{pmatrix} \begin{pmatrix} 1 & 0 & 0 \\ 0 & 1 & 1 \end{pmatrix} \begin{pmatrix} 0 & 0 & 1 \\ 1 & 1 & 0 \end{pmatrix} \tag{87}$$

The matrices give the coefficients in the products $H_{\rho_1} H_{\rho_2}$. For example, $H_{1+2}H_{1+1+1} = 3H_{1+1+1}$, since the three matrices each give a copy of H_{1+1+1}. The general rule, for an $n \times m$ matrix, is

$$H_{\rho_1} H_{\rho_2} = \sum_M H_{M_{11}, M_{22}, \cdots, M_{1m}, M_{21}, \cdots, M_{2m}, \cdots, M_{n1}, \cdots, M_{nm}} \qquad (88)$$

where it is understood that zeroes are omitted. These matrices make for easy computations in KS_d. Let KD_∞ be the disjoint union of all descent Hopf algebras KD_d, for $d \geq 0$, and similarly, let KS_∞ be $\oplus KS_d$. For most purposes, the ground field K may be taken to be the rationals $\mathbb{Q}$.

It is shown in [82] that Solomon's descent algebra KD_∞ is a sub Hopf algebra of KS_∞, for any ground field K. Moreover, KD_∞, as a Hopf algebra, is the image under a map $(\phi\psi)^*$, where

- using signed leaves on binary trees, ϕ_d maps the associahedron A_d to the parity cube for S_d by noting the signs of interior leaves. The dual ϕ^* is the linear dual in the Hopf algebra.

- ψ_d is the reduction of S_d to A_d obtained by leveling tree nodes.

In other words, there is an intimate link between S_d, its parity cube and the intermediary associahedron. For a tree T in A_d, the inclusion $\psi^*(T)$ in the Hopf algebra KS_∞ is the sum $\sum \sigma$ of permutations corresponding to T. This is an unweighted version of the matrix sums that appeared in the last section. In particular, the pentagon A_3 maps to the parity square in such a way that both permutations $\sigma \in (+-)$ are correctly sent to $(+-)$.

The descent algebra is a statement about magic probability matrices, since these are sums of permutations. They are not elements of the linear matrix group GL_n, because many of these matrices have determinant zero.

5.3 Associahedra, Permutohedra and Polygons

A genus zero polytope in Euclidean dimension $d-1$ will define a categorical axiom if it arises as an expansion set for an index d-ordinal tree [63]. Instead of trees, we may use the rooted polygons that are dual to rooted trees. For

example, the A_3 polytope is the pentagon of chorded pentagons

$$(89)$$
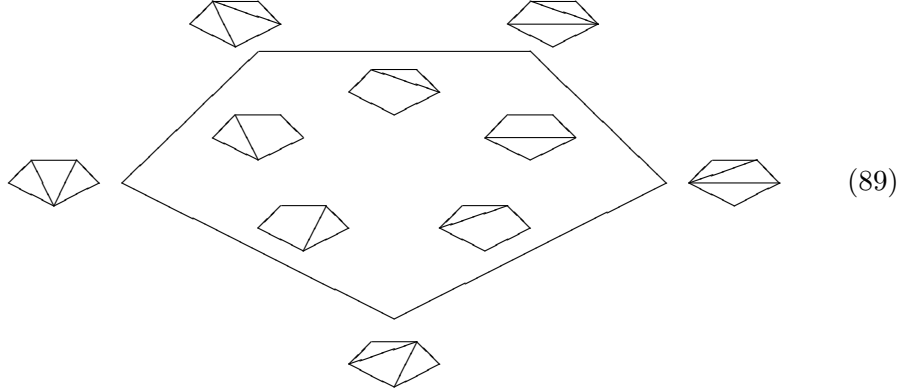
The number of chords on an index polygon clearly indicates the codimension of the face. The nine face A_4 polytope, without labels, looks like

$$(90)$$
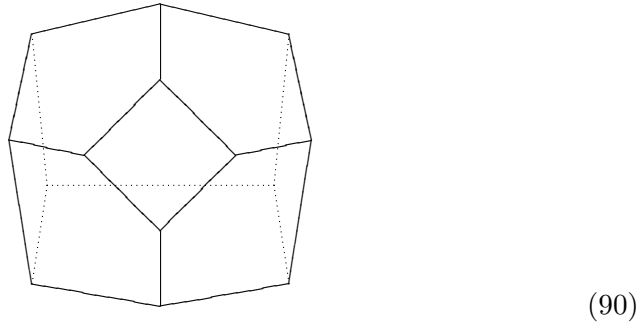
The square faces come from a chorded hexagon, such that the chord cuts the hexagon in two. The 6 pentagonal faces are labeled by the other single chorded hexagons, the 21 edges by hexagons with two chords, and the 14 vertices by hexagons with three chords.

The *source* of A_4 is the tree (1234) and the *target* the tree (4321). This orients all edges on A_4, and fills all faces with a 2-arrow that breaks the Mac Lane pentagon axiom. The set of all associahedra for $d \in \mathbb{N}$ give an example of an *operad*, as in appendix A. The object $d \in \mathbb{N}$ is just the 1-ordinal tree d, but it is often thought of as the topological space of the polytope in $\mathbb{R}^{d-1}$. Morally, however, the topological spaces go to infinite dimension, and should be thought of as an ω-*operad*. Every time one adds an edge through the expansion of a tree node, one increases the number of levels in the tree, creating an ordinal globule diagram of higher dimension.

Let us enumerate the codimension k faces of A_d. The number of vertices on A_d is given by the Catalan number

$$C_d = \frac{1}{d+1} \begin{pmatrix} 2d \\ d \end{pmatrix}. \qquad (91)$$

42

This is seen by dualising rooted trees with d leaves and one root edge to obtain rooted polygons with $d + 1$ sides. The Catalan number counts the triangulated polygons. It is further divided into Narayana numbers

$$N_{d,k} = \frac{1}{d} \left(\begin{array}{c} d \\ k \end{array} \right) \left(\begin{array}{c} d \\ k-1 \end{array} \right) \qquad \sum_{k=1}^{d} N_{d,k} = C_d \qquad (92)$$

This partition groups trees with d leaves according to the number of internal right directed leaves. For example, on A_4 we have $N_{4,k} \in (1, 6, 6, 1)$. The decomposition of A_3 into Narayana sets is

$$(93)$$

giving $N_{3,k} \in (1, 3, 1)$. This takes care of the maximal codimension. For codimension k, the cardinality of the A_d face set is

$$F_{d,k} = \frac{1}{d+1} \left(\begin{array}{c} d+k+1 \\ k+1 \end{array} \right) \left(\begin{array}{c} d-1 \\ k \end{array} \right), \qquad (94)$$

which is similar to the sequence $A033282$ in the online sequence database [83]. This result was first proved by Cayley in 1891 [84]. Related polytopes include the *cyclohedra* [85], which bracket objects on a loop rather than on a line. This is the natural polytope for theories that use cyclic tree diagrams, such as $N = 4$ Yang-Mills theory.

There is much more to the A_4 associahedron. The 21 edges are symmetrically divided into seven sets of the objects $\{a, b, c\}$, with each pentagon carrying a label set of the form *ababc*. Each vertex carries an $\{a, b, c\}$ triplet. A full triangulation of the 9 faces results in 24 triangles, defining 24 tetrahedra when a central vertex is added. Since this triangulation creates 36 edges, the Poincare dual polytope is the permutohedron S_4.

For the permutohedron S_d there are $d!$ vertices and $d!(d-1)/2$ edges. The permutohedron always tiles $\mathbb{R}^{d-1}$, as do cubes and their decompositions. The polytope S_4

$$(95)$$

is coordinatised neatly as follows. First, think of the 24 permutations as integral coordinates in $\mathbb{R}^4$, so that (2341) sits at $(2, 3, 4, 1)$. These points

43

clearly lie on the $\mathbb{R}^3$ plane $x_1 + x_2 + x_3 + x_4 = 10$. This can be turned into the plane $y_1 + y_2 + y_3 + y_4 = 0$ by sending each digit n to $(2n - 5)/2$, giving the vertex $(-1/2, 1/2, 3/2, -3/2)$.

The *permutoassociahedron* in dimension three has $120 = 5!$ vertices, and blends categorical associator and braiding arrows, by turning each vertex of S_4 into a pentagon.

In [72], Postnikov defines the *mixed Eulerian* numbers, which come from volumes for simplices in polytopes. For the permutohedron at the integral vertices $\sigma \in S_{d+1}$ in $\mathbb{Z}^{d+1}$, the volume V_d equals $(d + 1)^{d-1}$. This is a cardinality of *parking functions*, defined below. Postnikov studies volume formulas for general coordinates $(x_1, \cdots, x_{d+1})$. A generalised permutohedron is defined to be a sum

$$\sum_I \alpha_I \Delta_I \qquad (96)$$

in terms of subsets I of the standard d-simplex in $\mathbb{R}^{d+1}$, where Δ_I is the subset of faces of the simplex, given by $i \in I$. These polytopes include the associahedra and cyclohedra. The associahedra come from the interval subsets of I of form $\{i, i + 1, \cdots, j\}$, for $1 \leq i \leq j \leq d$. A *hypersimplex* $\Delta_{k,d}$ is defined to be the generalised permutohedron at coordinates $(1, 1, \cdots, 0, 0, \cdots, 0)$ with k ones at the start, and $d - k + 1$ zeroes. Now define a polytope as a sum

$$P_d \equiv z_1 \Delta_{1d} + z_2 \Delta_{2d} + \cdots + z_d \Delta_{dd} \qquad (97)$$

where $z_1 = x_1 - x_2$ and so on. Consider the vectors $c = (c_1, \cdots, c_d)$ for $c_i \geq 0$ such that $\sum c_i = d$. Let V_c be an integral volume for the collection $(\Delta_{1d}{}^{c_1}, \cdots, \Delta_{dd}{}^{c_d})$ of hypersimplices. These V_c are the mixed Eulerian numbers of interest. Their properties include a decomposition

$$\sum_c \frac{V_c}{c_1! \cdots c_d!} = (d + 1)^{d-1} \qquad (98)$$

of the parking functions. The polytope volume may now be expressed as

$$V(P_d) = \sum_c V_c \frac{z_1{}^{c_1} \cdots z_n{}^{c_n}}{c_1! \cdots c_d!} \qquad (99)$$

The mixed Eulerian numbers include the classical Eulerian numbers E_{kd}, defined for $c = (0, 0, \cdots, 0, d, 0, \cdots 0)$, with the d in the kth position. In other words, the volume of Δ_{kd} is $E_{kd}/d!$. When $c_1 + \cdots + c_i \geq i$ for all i, then

$$V_c = 1^{c_1} 2^{c_2} \cdots d^{c_d} \qquad (100)$$

and there are C_d such vectors c. Moreover, the volumes also decompose the Catalan numbers via $d! \sum V_c = C_d$. The Eulerian numbers appear in recent matrix structures in $N = 8$ supergravity [19].

Example 5.3 When $d = 4$, the 14 c vectors that satisfy $c_1 + \cdots + c_i \geq i$ give volumes V_c that are graded by the Narayana numbers.

|	
1	$V_{4000} = 1$
6	$V_{1300} = 8$, $V_{3100} = 2$, $V_{3010} = 3$, $V_{3001} = 4$, $V_{2020} = 9$, $V_{2200} = 4$
6	$V_{1120} = 18$, $V_{1210} = 12$, $V_{1201} = 16$, $V_{2110} = 6$, $V_{2101} = 8$, $V_{2011} = 12$
1	$V_{1111} = 24$

The special c vectors show up in the factorisation of ordinary ordinals. Consider homogeneous coordinates in $\mathbb{Z}^4$ for the parity cube. It is necessary to add a coordinate, because the strings of zeroes and ones have distinct totals. We choose to put the extra variable at the start of the vector, where it will only pick up a Postnikov volume of 1. The cube, including all integral volumes,

$$(101)$$
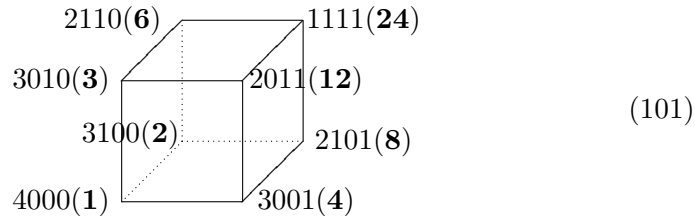
clearly shows all factors of $24 = 4!$. Opposite corner pairs give multiplication to the target 24. This process works on all parity cubes up to dimension 4, with a target volume $120 = 5!$, since all numbers up to 5 are prime powers.

In this way, any natural coordinate set is turned into a set of integral volumes. The parity cube in any dimension gives strings satisfying the special c vector condition, when homogeneous coordinates are used.

Any rooted planar tree defines a set of *linear orders*. Each node of the linear order is a node on the tree, and the nodes are connected by internal edges from the tree. That is, the leaves are all deleted. The n nodes are then labeled by the numbers $1, 2, \cdots, n$, with each number used only once. Note that this is how tree nodes get labeled in the S_n picture. The restriction on labels is that they must *decrease* as one travels on a downward path. The linear orders at $n = 2$ and $n = 3$ are then

$$(102)$$
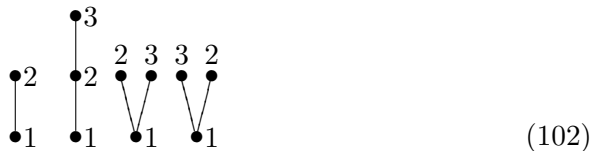
Consider the five vertex trees of the pentagon A_3. Linear orders allow us to distinguish the special tree $(312) + (132)$ from the other four trees, and recover the hexagon S_3. There is a unique order 321 associated to each of the four trees, but $(312) + (132)$ has two distinct orders, each with two leaves. Clearly, each order corresponds to a component permutation.

Given a *forest*, namely a finite union of rooted trees, one associates unions of linear orders, one order for each tree in the forest. Forests are graded according to the total number of nodes. To begin with, the tree set is itself unordered. For $n = 4$, the forest orders and their cardinalities are then

$$\begin{array}{c}\text{(forest diagram with cardinalities } 24,\ 1,\ 4,\ 12,\ 12,\ 2,\ 8,\ 3,\ 3,\ 1)\end{array} \qquad (103)$$
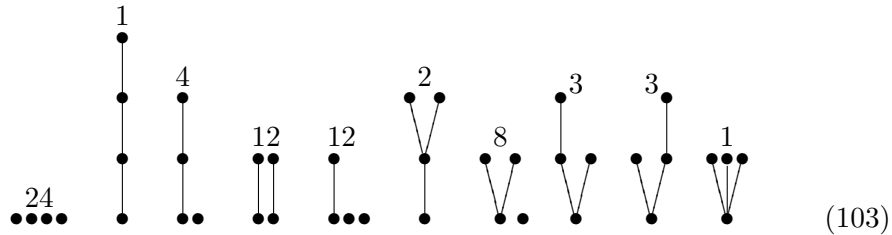
containing 70 distinct objects. Without labels, forests form the Connes-Kreimer renormalisation algebra of rooted trees, as given in appendix C. The *forest coefficient* [86] on unlabeled forests is the integer defined by the product of cardinalities

$$f = \prod_v |\{w : w \geq v\}| \qquad (104)$$

where v is the node set and $w \geq v$ if it lies above it on a path. For example, the vertical tree at $n = 3$ has $f = 6$, because the bottom node contributes three nodes, the middle contributes two, and the top node only itself. At $n = 3$, the sum of f values equals 12. The labeled orders also give a count of 12 for $n = 3$ forests. Verify that these two counts are *dual* in the sense that they swap pairs of forests. For instance, the vertical order is exchanged for the horizontal point set.

A noncommutative analogue orders the tree set within the forest [87]. There are then five distinct forests at $n = 3$, rather than four, and 14 at $n = 4$. These are again the Catalan numbers. Now choose an order from *left to right* on nodes at a level within a forest. Verify that there are then 3 forests at $n = 2$, and 16 at $n = 3$. Ignore left right tree flips for asymmetric trees. The horizontal point set now has only one labeling, since it must be ordered 123. These diagrams are known as *parking functions* [88][89]. The count for general n is

$$p_n = (n + 1)^{n-1}$$

The correspondence between the order types and the standard parking func-

tions [90] at $n = 3$ is

$$123, 231, 312, 213, 321, 132$$

$$111$$

$$221, 212, 122$$

$$112, 121, 211$$

$$311, 131, 113$$
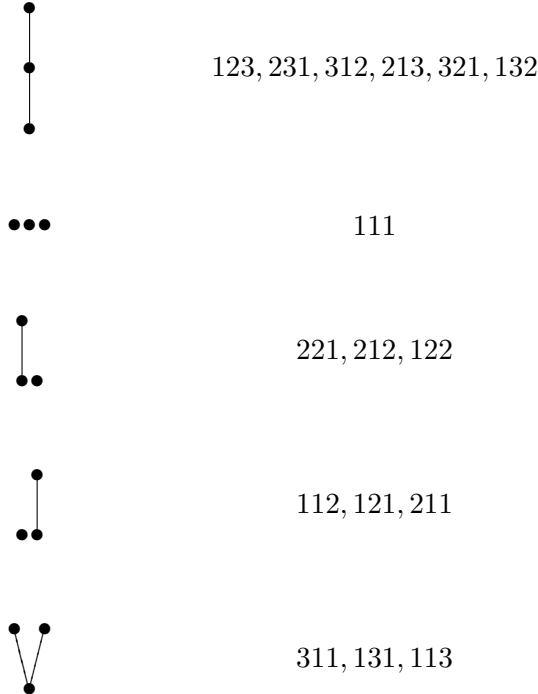
where parking functions are permutations of sequences $i_1 i_2 \cdots i_n$ such that $i_k \leq k$. On the vertical tree, the parking function entries just label the nodes freely. The 111 forest starts at 1 again for each root. The 212 forest chooses 13 for the root labels, as does 121. Label the $p_4 = 125$ forests to check that the partition on unlabeled forests is

$$125 = 1 + 4 + 4 + 4 + 4 + 6 + 6 + 12 + 12 + 12 + 12 + 24 + 24. \quad (105)$$

The number $p_3 = 16$ is associated to the A_4 associahedron in a nice way: it counts the 3-simplices in a natural triangulation of A_4. If the c vector process is extended to any integral vector, then p_3 is also the sum of the ten permutohedra volumes for the three qutrit tetractys diagram, using canonical coordinates. In this case, the mixed Eulerian coefficients are in the set $\{1, 2, 3, 4, 6\}$, which are also the volumes on the pentagon sitting at the $(3, 0, 0)$ corner of the tetractys. This pentagon picks out the points satisfying the special c vector condition.

One could divide A_4 into 24 simplices, by triangulating each face and placing a new node in the centre of the polytope, but the more efficient 16 simplex picture uses parking functions. Consider first A_3. The 3 non-commutative forests at $n = 2$ label three triangles on an oriented chorded

pentagon [90]. One selects chords that aim for the target vertex.

(106)
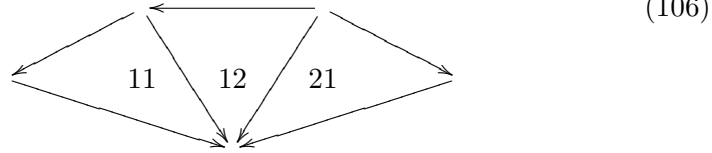
This also demonstrates the chording for a square. On the oriented A_4, all faces are chorded in this manner. The 16 base triangles sit on four pentagons and two squares, with pentagons fixed by their leftmost entry. The diagram is built from the central pentagon, where the A_4 source sits.

(107)
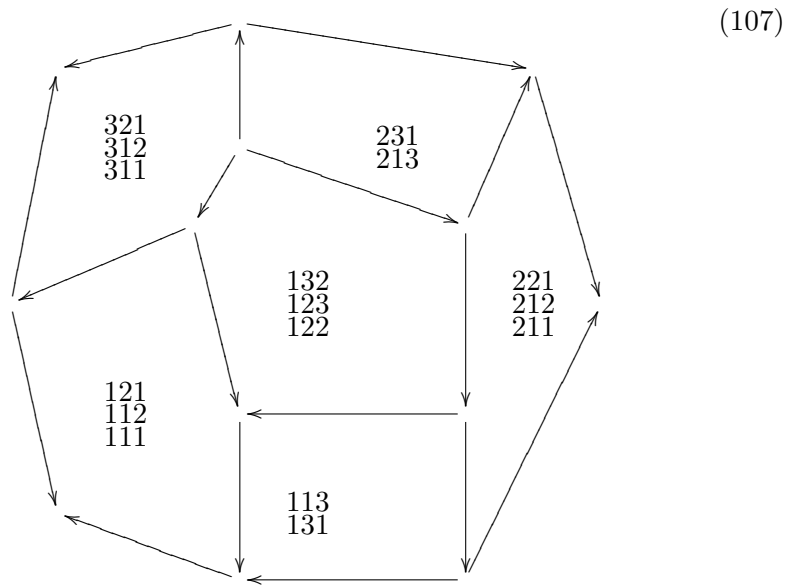
Observe that the source vertex defines an S_3 hexagon, because only the S_3 triangles meet at the source. The other 8 triangles in a triangulation, lying on two pentagons and one square at the back of the diagram, might be labeled with

$$223, 232, 222 \qquad 331, 313, 333 \qquad 233, 323 \qquad (108)$$

bringing us to 24 out of 27 three qutrit words. The missing three labels in this example would be 133, 322 and 332. Note that the associated Postnikov volumes for the whole homogeneous tetractys are $\{1, 2, 3, 4, 6, 8, 9, 12, 18, 27\}$. These will be interpreted as probabilities. In particular, the central $6/27$ point plays an important role.

A *decorated* rooted planar tree has labels on all external leaves, including the root. Decorations take values in a set S. Decorated forests are disjoint collections of decorated trees. We define a tree *splitting contraction* [91], which sends a decorated tree with n edges to one with $n-1$ edges. On an internal edge, it simply contracts the edge. On an outside edge it (i)

48

contracts the edge (ii) moves the label to the second vertex, and (iii) splits the tree at this vertex, giving all subtrees the same label at that vertex. The contraction of a tree T at an edge e is denoted T/e.

Example 5.4 The (21) tree splits into two at T/b,
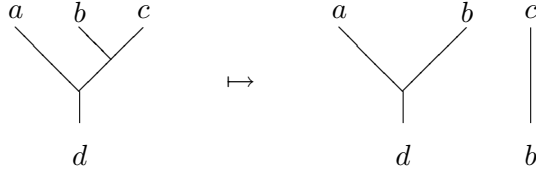
Example 5.5 The tree

splits into four unary edges, with one edge carrying the root label.

All tree contractions within an A_d polytope are internal edge contractions, which do not create disjoint forests. Let $\mathbf{T}_e$ denote the set of all decorated forests, graded by the total number of edges e. A differential $d : \mathbf{T}_e \to \mathbf{T}_{e-1}$ is defined using the splitting contracti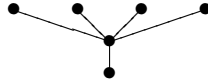on [91]. It also requires an *orientation* for a tree T, defined on the set of edges E. One orientation is written $w = e_1 \wedge e_2 \wedge \cdots \wedge e_m$, where m is the cardinality of E. This defines the orientation class $+$. Then given any permutation $\sigma \in S_m$, the orientation $e_{\sigma(1)} \wedge \cdots \wedge e_{\sigma(m)}$ differs from $+$ by the sign of σ. Let iw be the contraction $e_2 \wedge \cdots \wedge e_m$. The differential is given by

$$d(T, w) \equiv \sum_{e \in E} (T/e, iw). \tag{109}$$

It satisfies $d^2 = 0$. Under the disjoint union product and $\otimes$ on orientation, it satisfies the Leibniz rule [91]

$$d((T_1, w_1)(T_2, w_2)) = d(T_1, w_1) \cdot (T_2, w_2) + (-1)^{e(T_1)} (T_1, w_1) \cdot d(T_2, w_2). \tag{110}$$

5.4 Three Dimensional Traces

Tracing really belongs to the realm of ribbon categories, where there are dual objects to create arcs in a diagram. However, trees will be considered instances of flat ribbon networks, allowing a trace operation.

When two trees are glued together as a composition $1 \to m \to 1$, there is only one input and one output to be traced. These are joined by a loop segment, drawn in the plane. Because planar binary trees have trivalent

nodes, they always glue to form surfaces in three dimensions. The gluing of an upside down (12) and a (21) from S_2 gives the tetrahedron

$$(111)$$
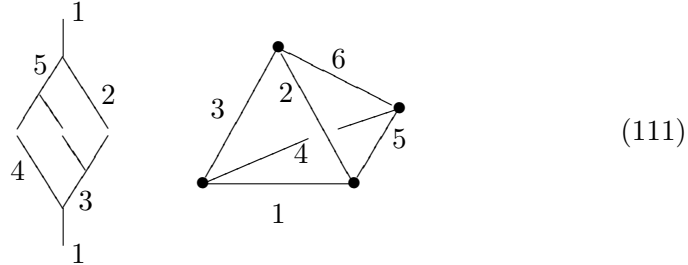
in line form. Let us denote an upside down tree in S_d by σ^*, where σ is the underlying permutation. The *trace* of two objects in S_d takes the tree σ^* and glues it to τ. For example, the trace of (23415) with (15432) gives a pentagonal prism

$$(112)$$

as does $\operatorname{tr}((23415),(51432))$. A similar trace diagram for S_d always gives a d-gon prism. Even for S_2 there is the squashed can, or globule prism.

$$(113)$$
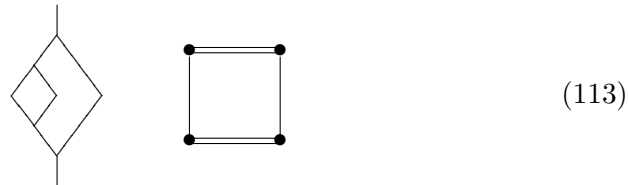
For S_3 the trace $\operatorname{tr}((312),(231))$ of 1-circulants is the triangular prism. Other shapes also occur. The triangular prism is geometrically dual to a pair of tetrahedra

$$(114)$$
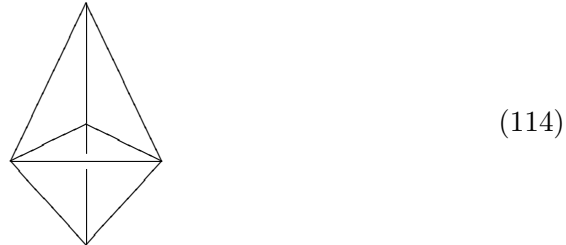
glued along one face. This is the polytope obtained by shrinking the square faces of the A_4 associahedron, so that the pentagons become triangles. Similarly, shrinking the six square faces of S_4 gives an octahedron, which is dual to a cube.

50

Binary tree tracing is a method for turning open ended diagrams into closed ones. In joining the root edges at the top and bottom of a diagram, we still have a planar diagram, but this is interpreted as a three dimensional diagram by allowing a point at infinity on the plane, turning $\mathbb{C}$ into the Riemann sphere $\mathbb{CP}^1$.

A typical braid or multitree diagram has n inputs and n outputs. The standard trace matches the upper and lower points *in order*, a process that requires n joining strings. For trees, one can also construct a reverse gluing, like for a density matrix in quantum mechanics. This also requires more than one joining string. For example, an associator $(21) \rightarrow (12)$ is glued using three strings
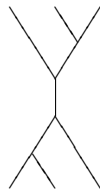
$$(115)$$

to give another form of the tetrahedron with six edges.

When arcs are freely available in the category, other types of trace are possible [92]. A *plat* trace can be defined when there are $2n$ strands, which is the case for ribbon diagrams. Instead of tracing from the top of the diagram to the bottom, strings are used to join top points and also to join bottom points. Most simply, one connects according to $(12)(34)(56) \cdots ((n-1)n)$, using the same connections at the top and the bottom of the diagram. We will also use the *cyclic plat* trace, which joins the points according to $(23)(45)(67) \cdots (n1)$.

Example 5.6
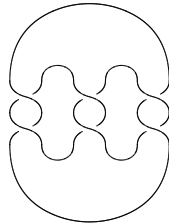
$$(116)$$

Three twists $\tau_1{}^2\tau_3{}^2\tau_5{}^2$ are glued to form a closed ribbon diagram, which is a three component link.

5.5 Associated Braids and Knot Invariants

Permutations in S_d are usually represented by crossing strings, running from d points to d points in the plane. A braid diagram

$$(117)$$

permits crossing information in the third dimension. The braid group B_n on n strings composes two diagrams by joining one vertically to the other to create a new braid. Thus the diagram above is the composition of two single crossing diagrams. Clearly the group is non abelian.

As in appendix B, let τ_i represent the diagram with a crossing between the i-th and $(i+1)$-th strings, so that the left string passes over the right string, as in the top half of the diagram above. Then τ_i^{-1} is the diagram with the opposite crossing. Each group B_n has d generators $\{\tau_1, \tau_2, \cdots, \tau_{n-1}\}$. Along with $\tau_i\tau_j = \tau_j\tau_i$ for $|i-j| > 1$, the group laws state that

$$\tau_i\tau_{i+1}\tau_i = \tau_{i+1}\tau_i\tau_{i+1} \tag{118}$$

for all i. The braid group B_n will now be represented by $(n-1) \times (n-1)$ matrices. This choice agrees with the role of B_3 as the cover of the 2×2 modular group $PSL_2(\mathbb{Z})$ of integer matrices up to ± 1 [93]. The modular group includes the generators

$$t_1 = \begin{pmatrix} 1 & 1 \\ 0 & 1 \end{pmatrix} \qquad t_2 = \begin{pmatrix} 1 & 0 \\ -1 & 1 \end{pmatrix}. \tag{119}$$

These satisfy $t_1 t_2 t_1 = t_2 t_1 t_2$, but this braid rule collapses under the additional relation $(t_1 t_2)^3 = I_2$.

There are two natural representations of B_n, one n and one $(n-1)$ dimensional, known as the *Burau representation* [94][95]. Both are important. The Burau representation of dimension n has a generator τ_i, sent to a 2×2 block in the $n \times n$ matrix,

$$I_{i-1} \oplus \begin{pmatrix} 1-t & t \\ 1 & 0 \end{pmatrix} \oplus I_{n-i-1} \tag{120}$$

with entries in the polynomial ring $\mathbb{Z}[t, t^{-1}]$, assuming $t \neq 0$. At $t = 1$ the permutations in S_n are recovered. The $(n-1)$ dimensional representation is obtained [95] by observing that the matrices above act on n-vectors to leave invariant vectors whose entries sum to zero. The two B_3 generators are then given by

$$\tau_1 = \begin{pmatrix} -t & 0 \\ -1 & 1 \end{pmatrix} \qquad \tau_2 = \begin{pmatrix} 1 & -t \\ 0 & -t \end{pmatrix}. \tag{121}$$

The pattern for higher n is indicated by the central B_5 generator

$$\tau_2 = \begin{pmatrix} 1 & -t & 0 & 0 \\ 0 & -t & 0 & 0 \\ 0 & -1 & 1 & 0 \\ 0 & 0 & 0 & 1 \end{pmatrix}. \tag{122}$$

In this representation, $(\tau_1\tau_2)^3 = t^3 I_2$, so it does not collapse to the modular group if $t \neq 1$ or $t \neq \omega_3$. It is faithful for B_2 and B_3 but not for higher

dimensional n [94]. However, in analogy to the construction of all permutations from S_2, we aim to understand braids by looking at B_2 and B_3. The B_3 generators are

$$\tau_1 = \begin{pmatrix} -t & 0 \\ -1 & 1 \end{pmatrix} \qquad \tau_1^{-1} = \begin{pmatrix} -1/t & 0 \\ -1/t & 1 \end{pmatrix} \tag{123}$$

$$\tau_2 = \begin{pmatrix} 1 & -t \\ 0 & -t \end{pmatrix} \qquad \tau_2^{-1} = \begin{pmatrix} 1 & -1 \\ 0 & -1/t \end{pmatrix}.$$

Braid diagrams are traced like trees, with one connecting loop for each braid strand. This creates a closed knot or link diagram. Modern link invariants [96][97] specialise to the older Alexander polynomial $\Delta_L(t)$, and this may be recovered from the $(n-1)$ dimensional Burau representation as follows. Let the unnormalised Alexander polynomial be defined by

$$\Delta_L(t) = (1 + t + \cdots + t^{n-1})^{-1} \ \det(1 - L) \tag{124}$$

where L is the matrix for the link L, formed from the τ_i generators. We will see that the polynomial coefficient comes from the determinants for unknot braids. Using B_3, verify that the unknot invariant $\Delta_L = 1$ is obtained from $\tau_1 \tau_2$. The unknot invariant should also be obtained from a diagram of the form (117), such as $\tau_1^{-1} \tau_2$, but this gives

$$\Delta_L = (1 + t + t^2)^{-1} \cdot ((1 + \frac{1}{t})t + \frac{1}{t}) = \frac{1}{t}, \tag{125}$$

using I_2 for the identity braid in B_3. In order to find the correct normalisation factor, consider first the newer knot invariant, the Jones polynomial.

The Jones link invariant $V_L(t)$ is defined by a *skein relation*. If three link diagrams differ by only one crossing, there is a relation between their invariants. Let V_τ stand for the invariant when τ sits at the distinctive crossing. Then $V_L(t)$ is given by [96][95]

$$t^{-1} V_{\tau_1} - t V_{\tau_1^{-1}} = (t^{1/2} + t^{-1/2}) V_{I_2} \tag{126}$$

This is recursive, because we can always switch crossings in a messy knot to obtain a simpler knot, and evaluate invariants using the simpler diagrams. Note that the substitution $-t$ introduces the complex i.

Example 5.7 The three B_3 unknot diagrams, $\tau_1^{-1} \tau_2$, $\tau_1 \tau_2$ and τ_2, differ in only one crossing. The generator τ_2 is a two loop link, but the other diagrams must satisfy $V_L = 1$. Thus V_L for two loops is $(t^{1/2} - t^{-1/2})$.

Example 5.8 The trefoil knot $\tau_1{}^3$ in B_2

is computed using a few steps. Focus on changing the top right crossing. The two skein alternatives turn the trefoil into either a Hopf link or an unknot. We have computed the Hopf link $V_H = t^{1/2} + t^{5/2}$. The skein relation then states that V_T for the trefoil satisfies

$$(t^{1/2} + t^{-1/2})V_T = t^{-1}(t^{1/2} + t^{5/2}) - t$$

implying that $V_T = 1 + 1/t + t - t^{1/2} - t^{3/2} + t^2$. One often chooses a variable $q = t^{1/2}$, and a form of the skein relation that pulls out the determinant $1 + 1/t + t$. In that case, the trefoil polynomial takes the standard form $V_T = q^4 - q^3 - q$.

Fixing a value of V_L for the unknot is in fact sufficient to prove that V_L is a link invariant. But what has happened to the matrix invariant? We would really like an invariant that makes direct use of the matrix representations. Recall that the unknot $\tau_1^{-1}\tau_2$ gave $\Delta_L = 1/t$. Let us list all such two crossing braids in B_3.

$$\tau_1\tau_2 = \begin{pmatrix} -t & t^2 \\ -1 & 0 \end{pmatrix} \qquad \tau_1^{-1}\tau_2^{-1} = \begin{pmatrix} -1/t & 1/t \\ -1/t & 0 \end{pmatrix} \qquad (127)$$

$$\tau_2\tau_1 = \begin{pmatrix} 0 & -t \\ t & -t \end{pmatrix} \qquad \tau_2^{-1}\tau_1^{-1} = \begin{pmatrix} 0 & -1 \\ 1/t^2 & -1/t \end{pmatrix}$$

$$\tau_1\tau_2^{-1} = \begin{pmatrix} -t & t \\ -1 & 1 - 1/t \end{pmatrix} \qquad \tau_1^{-1}\tau_2 = \begin{pmatrix} -1/t & 1 \\ -1/t & 1 - t \end{pmatrix}$$

$$\tau_2\tau_1^{-1} = \begin{pmatrix} 1 - 1/t & -t \\ 1 & -t \end{pmatrix} \qquad \tau_2^{-1}\tau_1 = \begin{pmatrix} 1 - t & -1 \\ 1/t & -1/t \end{pmatrix}$$

Observe that in order to obtain $\Delta_L = 1$ for these unknots, it seems we require a correction factor of t^k, where k is the number of *under* crossings in the braid diagram. Recall that the writhe w of a link is the difference $j - k$ between the number j of over crossings and the number k of under crossings. Note that an inverse braid b^{-1} has j and k swapped, so that $w(b^{-1}) = -w(b)$. This suggests considering a modified Alexander polynomial $\widetilde{\Delta}_L(t) = t^x \Delta_L(t)$ for some x depending on w and n, so that all one loop unknot diagrams have $\widetilde{\Delta}_L(t) = 1$. Since I_2 and powers of the B_3 generators all have $\widetilde{\Delta}_L(t) = 0$, a factor such as t^{j+k} would not appear in $b \cdot b^{-1}$. But what about longer braids in B_3? The unknot $\tau_1\tau_2^{-1}\tau_1^{-1}\tau_2$ needs a factor of t, but it has $k = 2$. This suggests instead the definition

$$\widetilde{\Delta}_L(t) = t^{-w/2+1}\Delta_L(t) \qquad (128)$$

which yields $\widetilde{\Delta}_L(t) = 1$ for all the above braids. This is the correct normalisation for B_3. For general n [95] we have the matrix invariant

$$\widetilde{\Delta}_L(t) = (-1)^{w-n+1}t^{-w/2+(n-1)/2}\Delta_L(t). \qquad (129)$$

Consider B_3 braids using the 2×2 representation. Let τ denote any one of the four basic generators. Given a braid word b, we would like to know that the invariant for $b\tau$ is given simply in terms of the invariant for b. For any 2×2 matrices, the characteristic polynomials give directly

$$\det(I - AB) = 1 + \det(A)\det(B) - \mathrm{tr}(AB), \tag{130}$$

so that it is easy to evaluate $\Delta_L(t)$ for any braid product AB. For example, check that $\tau_1^{-1}\tau_2$ gives the determinant $1 + 1/t + t$.

The Jones polynomial agrees with $\widetilde{\Delta}_L$ for B_3 braids. For $L \in B_3$ a knot, it is given by

$$V_L(t) = t^{w/2-1}(1 + t + t^2 + t^{w+1} - t \cdot \det(I - L)). \tag{131}$$

At $w = 0$ this reduces to

$$V_L{}^0(t) = 1 + \frac{1}{t} + t - \det(I - L) + 1. \tag{132}$$

That is, the special determinant for unknots is canceled out and the normalisation set at 1. Writhe zero knots have a simple skein relation for evaluating $V_L{}^0(t)$ known as the *Kauffman bracket* [98] K_L. This does not give a true knot invariant in general, because it does not account for the non planar writhe. Instead of two crossings, it uses both the I_2 diagram and its rotation by $\pi/2$. This mixture of arc pictures is fundamental to all the combinatorics in this book. The initial normalisation is 1, and additional loops carry a factor of $-(t^{1/2} + t^{-1/2})$. Using diagram pieces to denote the invariant itself, the bracket says

$$\Big\slash\!\!\!\!\backslash \;\; = \;\; t^{1/4}\,\Big|\Big| \;\; + \;\; t^{-1/4}\,{\overline{\underline{}}} \tag{133}$$

When suitably normalised, the Kauffman bracket becomes the standard Jones invariant V_L on multiplication by a writhe factor $(-1)^w(t)^{3w/4}$. One can see the three dimensional invariance problem by considering a braid $b\tau_d^{\pm 1}$ in B_{d+1}, for any braid b. The addition of the extra crossing $\tau_d^{\pm 1}$ clearly does not change the actual knot, although it shifts w by ± 1. Yet such a move would alter the Kauffman bracket. Chapter 8 looks more closely at the relation between the Kauffman bracket and the Jones invariant.

A change of variables of the form $t \mapsto 1/t$ gives a distinct set of Burau matrices representing B_n, and exchanges a knot for its mirror image. Note that this is a crossing swap in B_2. The parameter t acts to deform S_{n-1} by extending planar diagrams into the third dimension.

Braids appear in the renormalisation Hopf algebras of the Standard Model [99][100][101]. As discussed in chapter 8, the one particle irreducible

Feynman diagrams are turned into braids. The braids contain extra information coming from loops in the diagram, and this is encoded in chords joining two strands in a braid diagram.

Since we hope eventually to build matrix invariants for physical computations, from now on we imagine that trees, or even diagrams with loops, secretly come from braid and ribbon diagrams. The Standard Model particle spectrum [102] is given as ribbon diagrams in chapter 7, using the writhe 0 unknots in B_3.

6 Twistor Quantum Field Theory

Instead of working with Feynman diagrams, twistor scattering theory uses diagrams in twistor space. Although it is still a continuum theory, it works towards throwing away the underlying spaces by describing amplitudes in a purely combinatorial way. In this chapter we look at techniques in $N = 4$ planar Yang-Mills theory and $N = 8$ supergravity. While this is not the Standard Model, there can be no doubt of its relevance to the true non local formulation for the Standard Model. However, whereas the supersymmetry N usually provides additional variables to the background geometry, in an emergent theory this background is itself derived from the fermionic degrees of freedom. For this reason, we omit a full description of the geometry and focus on the crucial combinatorial elements.

Twistor space is the transform of complexified Minkowski space $\mathbb{M}$ to the complex projective space $\mathbb{CP}^3$ [49][50]. We start with a matrix form for a vector in Minkowski space, namely a path matrix

$$P = \begin{pmatrix} X\overline{X} & X\overline{Y} \\ Y\overline{X} & Y\overline{Y} \end{pmatrix} = \begin{pmatrix} x_3 + x_0 & x_1 + ix_2 \\ x_1 - ix_2 & x_3 - x_0 \end{pmatrix}, \tag{134}$$

where (x_0, x_1, x_2, x_3) are the usual coordinates of Minkowski space $\mathbb{M}$. For commutative variables $X, Y \cdots$, the determinant of P is clearly zero, giving the lightlike Lorentzian metric. Physically, a *null twistor* replaces a light ray in $\mathbb{M}$. The points of $\mathbb{M}$ need to be complexified, and $\mathbb{M}$ then compactified, for the twistor correspondence to work.

First note that, as a Hermitian matrix, P is an element of the quaternions $\mathbb{H}$. In general, such a P is a projection in a 2×2 Jordan algebra. The group $SL_2(\mathbb{C})$ of unit determinant matrices G acts on P by conjugation

$$G^\dagger \begin{pmatrix} X\overline{X} & X\overline{Y} \\ Y\overline{X} & Y\overline{Y} \end{pmatrix} G. \tag{135}$$

Here $SL_2(\mathbb{C})$ is locally the Lorentz group, because it clearly preserves the determinant

$$X\overline{X}Y\overline{Y} - X\overline{Y}Y\overline{X} = -x_0{}^2 + x_1{}^2 + x_2{}^2 + x_3{}^2 \tag{136}$$

which is the Lorentzian metric. As the double cover of the Lorentz group, it includes spin. Here the qudit determinant is non zero only for noncommutative monomials in a word alphabet which has four letters.

Twistor space $\mathbb{T}$ is defined by pairs of spinors λ and μ, so that a standard twistor $Z = (\lambda, \mu)$ is a vector in $\mathbb{C}^4$. The transformation between projective twistor space $\mathbb{PT}$ and Minkowski space is a span 1-arrow

$$\mathbf{F}_{12}(\mathbb{T}) \tag{137}$$

$$\mathbb{M} = \mathbf{F}_2(\mathbb{T}) \qquad\qquad \mathbb{PT} = \mathbf{F}_1(\mathbb{T})$$

in a category of *flag manifolds* [50], which are sequences $V_1 \subset \cdots \subset V_n$ of subspaces of a vector space. Here $\mathbb{PT}$ is $\mathbb{CP}^3$, the one dimensional subspaces of $\mathbb{C}^4 = \mathbb{T}$. Complexified Minkowski space $\mathbb{M}$ is a flag manifold when viewed as a Grassmannian, namely the set of all 2-planes in $\mathbb{C}^4$. This is what $\mathbf{F}_2$ means here. The local coordinates P may be expressed in Grassmannian form as a 4×2 matrix, $[P, I_2]$. The projective space $\mathbb{CP}^3$ similarly has homogeneous 4-vector coordinates $[iPv, v]$, where $v = [v_0, v_1]$ are homogeneous coordinates for $\mathbb{CP}^1$, the Riemann sphere. A point in $\mathbb{M}$ is mapped under the span to such a sphere in $\mathbb{PT}$, which we think of as a celestial sphere. The coordinates for $\mathbf{F}_{12}$ are $[P, v]$, making it a five dimensional space.

The standard coordinates for $\mathbb{T}$ start with the spinor μ, which is usually written with an index as $\mu_{A'} = (\mu_{0'}, \mu_{1'})$. A twistor is a spinor pair $Z = (\lambda^A, \mu_{A'})$ wherein we use local coordinates. One works with a dual pair of twistor spaces, with the dual twistor $W \equiv (\overline{\mu}, \overline{\lambda})$. When $\mathbb{T}$ is equipped with a 4×4 Hermitian form so that $SL_2(\mathbb{C})$ acts separately on each spinor, the spinors may be considered independent. When the spinors are real, the conformal group acts simply as $SL_4(\mathbb{R})$ on $\mathbb{R}^4$, covering the Lorentz group.

As 4-vectors, an independent Z and W define a two dimensional plane in $\mathbb{T}$. These planes form a fibre bundle over the Grassmannian manifold $Gr(2,4)$. Recall that a fibre bundle over a manifold M is an arrow $\pi : E \to M$ with fibre F such that M is covered with sets U_i and there are homeomorphisms $\phi_i : E \simeq U_i \times F$ on E restricted to U_i [45]. In particular, a vector bundle has F a vector space. The transition functions $g_{ij} = \phi_i \phi_j^{-1}$ on F take values in a structure group G. Although fibre bundles do not particularly concern us, we need the following example.

Example 6.1 The space $\mathbb{CP}^3 \times \mathbb{C}^4$ is a trivial vector bundle over $\mathbb{CP}^3$. Inside this bundle is a *universal bundle* $U_{1,4}$, which is defined so that the projection $\pi : U_{1,4} \to \mathbb{CP}^3$ sends the line that represents x in $\mathbb{CP}^3$ to the point x. This works using the standard vector coordinates for $\mathbb{CP}^3$, which contain the projection information. This generalises to any Grassmannian with its local matrix coordinates [50].

A useful characterisation of the Grassmannian $G(2,4)$ is into $\mathbb{P}(\bigwedge^2 \mathbb{C}^4)$, for the exterior algebra $\bigwedge^2 \mathbb{C}^4$. The exterior algebra has basis 2-forms $\{v_1 \wedge v_2, v_1 \wedge v_3, v_1 \wedge v_4, v_2 \wedge v_3, v_2 \wedge v_4, v_3 \wedge v_4\}$ in terms of the basis v_i for $\mathbb{C}^4$. The Minkowski Grassmannian is given by $[U, V] \mapsto [U \wedge V]$, which defines the *Klein quadric* in $\mathbb{CP}^5$ [50]. This is the set of complex v_{ij} satisfying the Plücker relation

$$v_{12}v_{34} - v_{13}v_{24} + v_{23}v_{14} = 0, \tag{138}$$

where v_{ij} is shorthand for homogeneous coordinates in $\mathbb{P}(\bigwedge^2 \mathbb{C}^4)$. Later on we will see that Plücker coordinates are closely connected to the entanglement classification for three qubits, where the $\mathbb{C}^6$ is viewed naturally as a three qubit state space.

Note that we could have written the noncommutative P as a submatrix of the length 2, $d = 4$ monoid matrix

$$\begin{pmatrix} XX & XY & X\overline{X} & X\overline{Y} \\ YX & YY & Y\overline{X} & Y\overline{Y} \\ \overline{X}X & \overline{X}Y & \overline{X}X & \overline{X}Y \\ \overline{Y}X & \overline{Y}Y & \overline{Y}X & \overline{Y}Y \end{pmatrix}, \qquad (139)$$

so that P determines a square, formed between the edges of the divided tetrahedron on the monoid alphabet $\{\overline{X}, X, Y, \overline{Y}\}$. Then the first two terms of the Plücker relation are the determinant of P, and the whole relation comes from the tetrahedron.

The twistor transform not only transforms Minkowski space to twistor space. It also transforms the solutions of field equations to cohomology classes on twistor space [103][50]. The long term difficulty in extending this functor cohomology to massive fields is a major motivation for studying universal noncommutative cohomology. Notably, classical massive solutions to the Klein-Gordon equation are possible [16] using a pair of massless spin $1/2$ fields, and H^2 cohomology.

We would like to construct twistor scattering amplitudes using categorical polytopes and their combinatorics, and notions of quantum entanglement. Such a procedure shows that the Standard Model is reformulated using discrete structures, from which classical spacetime and locality emerges.

6.1 Scattering Amplitudes in Twistor Space

In category land, supersymmetry is about the choice of underlying number field [104]. In particular, saying that a theory has $N = 4$ supersymmetry just means that it is expressed in quaternionic geometry. Twistor theory currently focuses on the planar $N = 4$ supersymmetric Yang-Mills theory, wherein we consider the S matrix for massless particle scattering, with each particle characterised by a momentum p and helicity $\pm$. The color stripped scattering amplitude components are $M(\lambda_i, \overline{\lambda}_i, h_i)$, where h_i is the $\pm$ helicity [106][107][108][109]. For gluons, these fit into the full tree amplitude

$$A_n = g^{n-2} \sum \text{Tr}[T^{i_1} T^{i_2} \cdots T^{i_n}] M(\lambda_i, \overline{\lambda}_i, h_i) \qquad (140)$$

which includes the T^i matrices of the fundamental representation of $SU(3)$ color.

The helicity sign is often given by a left or right leaning tree leaf, since helicity will be given by the handedness of a particle braid and the tree orientation picks out a direction of propagation. However, this breaks the natural cyclicity of the theory, which is also considered here.

Recall the Mandelstam variables for the s, t and u channels [105]

$$(141)$$

with $s + t + u = \sum_i m_i{}^2$. That is, $s = (p_1 + p_4)^2$, $t = (p_1 - p_2)^2$ and $u = (p_1 - p_3)^2$. Momentum conservation holds when reading the interaction from left to right. In the zero mass limit, $s \simeq 2p_1 \cdot p_4$ and so on.

The particle momentum is now expressed in twistor variables as $p_i = \lambda_i \overline{\lambda}_i$, where in general the variables are independent. The full twistor variables are $Z^A = (\lambda, \mu)$ and the dual $W_A = (\overline{\mu}, \overline{\lambda})$. Each leg i in a scattering diagram carries both a helicity and a momentum. Momentum conservation $\sum_i p_i = 0$ is used to define closed polygons of momenta in a dual twistor space, given by n coordinates such that $x_{i+1} - x_i \equiv p_i$. These polygons are dual to the tree diagrams that usually label the A_d polytopes, or their cyclic variant, the cyclohedra. In what follows we restrict to real spinors [106].

Under a $SL_2(\mathbb{C})$ Lorentzian transformation

$$\lambda_i \mapsto \phi_i \lambda_i \qquad \overline{\lambda}_i \mapsto \phi_i^{-1} \overline{\lambda}_i \qquad (142)$$

the amplitudes for a spin s particle should transform as

$$M(\phi Z, -) = \phi^{2(s-1)} M(Z, -) \qquad M(\phi Z, +) = \phi^{-2(s+1)} M(Z, +). \quad (143)$$

The degrees here come from the *anti self dual* and *self dual* character of the components, via cohomology. In the basic $\mathbb{CP}^1$ sheaf cohomology there is Serre duality between H^0 and H^1 [50]. For the more complicated $\mathbb{CP}^3$ case, the dimensions of H^0 and H^1 still complement each other, as they vary with spin and helicity, as in the table [110].

s	-3/2	-1	-1/2	0	1/2	1
dim H^0	0	0	0	1	2	3
dim H^1	3	2	1	0	0	0
degree	-3	-2	-1	0	1	2

In the last row the homogeneity degree is $2s$. For positive helicity the degree $-2s - 2$ comes from the structure sheaf $O(E^{\otimes(-2s-2)})$, where $E^{\otimes m}$ is the m-th power of the hyperplane section bundle E. A hyperplane in $\mathbb{CP}^3$ is given by an equation $\sum_{i=1}^4 c_i z_i = 0$. The section bundle is a line bundle with transition functions $g_{ab} \equiv f_a/f_b$ on the intersections $U_a \cap U_b$, where [50]

$$f_a \equiv c_1 \frac{z_1}{z_a} + c_2 \frac{z_2}{z_a} + c_3 \frac{z_3}{z_a} + c_4 \frac{z_4}{z_a}.$$

For example, the real permutohedron hyperplane $z_1 + z_2 + z_3 + z_4 = 0$, which gives S_4 coordinates via permutations of $(-1/2, 1/2, 3/2, -3/2)$, has

$$g_{23} = \frac{z_3{}^2 + z_3(1 + z_1 + z_4)}{z_2{}^2 + z_2(1 + z_1 + z_4)}$$

and similarly for the other g_{ab}. The transition functions for E^m are given by $g_{ab}{}^m$. The bundle E^{-1} is the universal bundle (6) for the Grassmannian

manifold $\mathbb{CP}^3$. It turns out that E^{-1} generates its cohomology group H^1 over $\mathbb{CP}^3$, as the integers $\mathbb{Z}$. Note the analogy with the braid group B_2 representation by powers $(-t)^m$ for $m \in \mathbb{Z}$. Then the homogeneity offset coming from $E^{\otimes(-2)} = E^{-1} \otimes E^{-1}$ is associated to one full twist, so to speak. Only with this extra factor does the sheaf cohomology recover the physical solutions on Minkowski space, via the Penrose transform.

Amplitudes are expressed in terms of basic invariants for the Lorentz group. They are

$$[\bar{\lambda}_1 \bar{\lambda}_2] \equiv \epsilon^{ij}(\bar{\lambda}_1)_i(\bar{\lambda}_2)_j \quad \langle \lambda_1 \lambda_2 \rangle \equiv \epsilon^{ij}(\lambda_1)_i(\lambda_2)_j \tag{144}$$

for the antisymmetric tensor ϵ. That is, one is in terms of W coordinates and the other in terms of Z. In the amplitudes, they are often abbreviated to $[12]$ and $\langle 12 \rangle$ for particles 1 and 2. Although one should use dots to differentiate the indices for different spinors, this is unnecessary given a consistent variable convention. A Mandelstam variable takes the form $s = \langle 14 \rangle [14]$, and so on.

An n particle Yang-Mills amplitude is abbreviated to $M(123 \cdots n)$. The first non trivial $M(123 \cdots n)$ have two negative (resp. two positive) helicities, and these are known as MHV (resp. $\overline{\text{MHV}}$) amplitudes [111]. We write $M(- - + \cdots +)$ for the helicity configuration. For the minimal three point $\overline{\text{MHV}}$ configuration $(+ + -)$, the amplitude is given by

$$M(+ + -) = \frac{[12]^3}{[13][23]} \delta(\lambda_1 \bar{\lambda}_1 + \lambda_2 \bar{\lambda}_2 + \lambda_2 \bar{\lambda}_2) \tag{145}$$

including the momentum conservation delta function. Ignoring the delta function, the four point MHV amplitude

$$M(- - + +) = \frac{\langle 12 \rangle^4}{\langle 23 \rangle \langle 34 \rangle \langle 41 \rangle} \tag{146}$$

indicates the general MHV pattern. The conditions of momentum conservation and zero rest mass reduce the number of independent kinematic variables in the four point function from four to two, but the three variable (s, t, u) symmetry is useful, not least because it is related to the basic axioms for the gauge algebra.

For k *extra* negative helicities, we have the N^{k}MHV amplitudes. The first interesting six gluon MHV amplitude $(- - + + + +)$ equals simply

$$\frac{\langle 12 \rangle^4}{\langle 23 \rangle \langle 34 \rangle \langle 45 \rangle \langle 56 \rangle \langle 61 \rangle}$$

There is also a delta function for momentum conservation $\sum p = 0$, but this is understood. Observe how the negative helicity homogeneity $|2s - 2| = 4$ appears in the numerator for the particles 1 and 2, giving the required phase

61

scaling. For a general MHV amplitude, the numerator is the same and there are $n-1$ invariants on the denominator. Note how the MHV amplitudes are easily written in the Z variables, while the $\overline{\text{MHV}}$ ones use the W.

These expressions originally arose from scrutinising concrete calculations using the Feynman method. In the 1980s, Parke and Taylor [112] noticed the simple form of the MHV amplitudes. Since then, it has become clear that the twistor form of the amplitudes is vastly simpler than the original Feynman form [113]. The modern advantage is our willingness to disallow spacetime locality its separate existence.

In [114], scattering was considered in terms of on shell processes, which do not permit arbitrary momenta in internal loops. The *BCFW shift* selects two legs, $n-1$ and n, and transforms the twistor variables

$$\lambda_n \mapsto \lambda_n + z\lambda_{n-1} \qquad \overline{\lambda}_{n-1} \mapsto \overline{\lambda}_{n-1} - z\lambda_n \tag{147}$$

using a continuum parameter z, which may be considered a physical scale parameter. The BCFW ansatz leads to an elegant formula for tree amplitudes. For n particles, this rule [114][115] takes the form

$$M(123\cdots n) = \sum_{+,-}\sum_{i=1}^{n-3} M(\overline{n}123\cdots i(-P_{n,i}^{\pm}))\frac{1}{P(n,i)^2}M((P_{n,i}^{\mp})(i+1)\cdots(n-2)(\overline{n-1})) \tag{148}$$

where $P(n,i)$ is the sum of momenta $p_n + p_1 + p_2 + \cdots + p_i$. In other words, there is a recursion rule that factorises an n point amplitude into a sum over products of smaller ones. The two particles $n-1$ and n have been singled out in this expression, breaking the cyclic invariance. Given such a BCFW cut, the n particle cyclic tree is turned into a familiar rooted tree with $n-2$ leaves. As a *twistor diagram* [116], the two legs obtain a BCFW bridge.

$$\tag{149}$$

The black dots will stand for the Z variables and the white dots for the W [106]. In the newer twistor diagrams, these define ribbon vertices [117]

$$\tag{150}$$

where the anticlockwise and clockwise vertex orientation is given respectively by the permutations (312) and (231). The boundary of the diagram is now cyclic. The permutations (12) and (21) are now ribbon strips, with an orientation. Such a twistor diagram always defines a decorated permutation

[27][117]. For four legs, the associahedron edge becomes a flip of Z and W nodes on the index squares.

$$\tag{151}$$
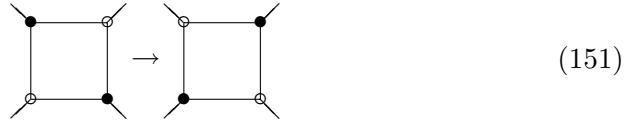
A permutation in S_4 defines four paths through the diagram disc, giving 8 edges on a ribbon graph. The identity (1234) can be drawn with no crossing points

$$\tag{152}$$

using ribbon edges that loop back to the same vertex. Thus the S_2 permutations are given by the pictures

$$\tag{153}$$

This is a crucial reinterpretation of the identity ribbon strip, because as we will see in the next two chapters, the usual planar pictures for S_2 are precisely the other way around. This dual representation of S_2 will result in mixing, with values in a group algebra $\mathbb{F}S_2$. The permutation (3412) requires a twistor square to cover the six path crossings.

$$\tag{154}$$
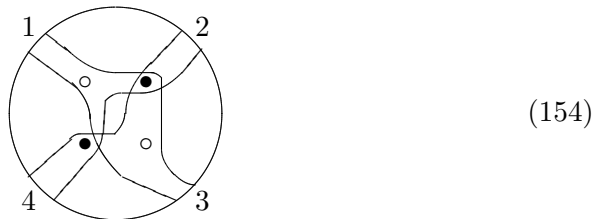
The line edges are omitted in this diagram, but are defined by the four legs and path contours around the square. The permutation σ determines the ribbon edge orientations, sending a path inwards from its source. This chooses the position of all $2n$ ribbon edges on the boundary disc.

To each permutation $\sigma \in S_n$ of the form $(\sigma_1 \cdots \sigma_n)$ one assigns a sequence $p(\sigma) = (p(\sigma_1) \cdots p(\sigma_n))$ of consecutive ordinals such that there exists an $x \in \mathbb{N}$ with $x+1 \le p(\sigma_i) \le x+n$. For example, (3412) is mapped to (3456), with $x = 2$. The offset is given by [117]

$$x = \frac{1}{n} \sum_i (p(\sigma_i) - \sigma_i) \tag{155}$$

For an S_6 example:

$$(156)$$
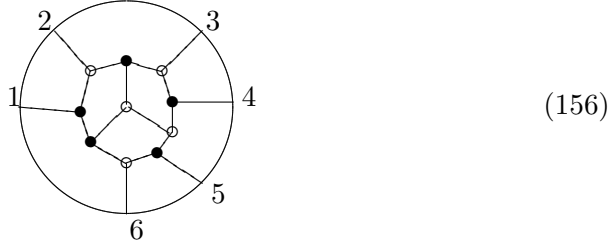
In another example, (465123) is mapped to (465789) with $x = 3$. This can be done by placing two ribbon edges around every edge on the twistor disc. On such twistor diagrams, ribbon edges specify a $U(1)$ gauge field, and as in the next chapter ribbon twists are used to specify electromagnetic charges. Note that the nine faces of the six point diagram resemble the A_4 faces, although the disc boundary gives a distinct surface, and the cyclohedra polytopes are more appropriate for cyclic structure. These polytopes are all generalised permutohedra. Including boundary vertices, there are $4(n-2)$ vertices in the twistor diagram.

These decorated permutations give a natural choice of Grassmannian variables for a $(k+2) \times n$ matrix [117]. These are the $G(k+2, n)$ Grassmannian homogeneous coordinates, where a $(k+2) \times (k+2)$ submatrix is fixed at I_{k+2}. This generalises the Minkowski space $G(2, 4)$ coordinates, which now correspond to 4 particles in a $(--++)$ configuration. With a BCFW cut, this basic configuration is represented by a two leaved tree

$$(157)$$

with a double edged root. Recall that this tree stands for the unique associahedron point A_1. In other words, the MHV rule, which says one must have at least two negative helicities, comes down to the emptiness of associahedra below the fundamental point. A three particle tree can only have one leaf, either left or right leaning, so it is no longer a proper binary tree.

The columns of the Grassmannian matrix span a planar subspace of n dimensional space. The homogeneity sets $k + 2$ columns to the identity matrix, as in

$$M_{13} \equiv \begin{pmatrix} c_{12} & 1 & c_{32} & 0 \\ c_{14} & 0 & c_{34} & 1 \end{pmatrix} \qquad (158)$$

for the alternative Minkowski space configuration $(+-+-)$. As always, M_{ij} is indexed by the column choices, so that the remaining indices are used for

the rows. In total, there are

$$m = \begin{pmatrix} n \\ k+2 \end{pmatrix}$$

such matrix minors, the full set giving coordinates M_{ij} for the projective space $\mathbb{P}^{m-1}$ via the Plücker map. The Plücker relation (138) holds between the determinants of the minors in the four point case. The interesting part of the Grassmannian is positive [118][119], meaning that all the minors are positive. This is interpreted using tropical geometry.

For these $N = 4$ diagrams, there is a globule reduction rule. This is just the categorical rule (292)

 (159)

which assumes that the points belong to the same entanglement class. The full loop recursion rule for the n particle l loop amplitude is then given by the sum over BCFW bridge tree factorisations and on shell loop terms

 (160)

where the little loop has an ingoing $\lambda_j \bar{\lambda}_j$ momentum and outgoing $-\lambda_j \bar{\lambda}_j$ one.

In the twistor formalism, there is a close link between the $N = 4$ theory and $N = 8$ supergravity. The amount of supersymmetry, $N = 8$, means that $\mathbb{CH}$, or the split octonions, now underlies the matrix algebra. The spin 2 tensors required for perturbative gravity are, in a suitable sense, squares of the Yang-Mills ones [120][121]. This is known as *color kinematic duality*. First, let the numerator of a term in a Yang-Mills tree amplitude be expressed as $c_j n_j$, where c_j are color factors related to the structure constants of the Lie algebra. Duality imposes a relation between the c_j and n_j. That is, given three terms that are related by the Jacobi rule

 (161)

a relation $c_1 \pm c_2 \pm c_3 = 0$ implies that $n_1 \pm n_2 \pm n_3 = 0$ [121]. The supergravity amplitudes have numerators like $n_j{}^2$, namely two kinematic factors. The three particle spin 2 amplitude is just M^2, for M the spin 1

65

Yang-Mills amplitude. Instead of color trace factors in (140), one considers kinematic factors $\tau(12\cdots n)$.

These terms come from the two distinct cyclic ribbon vertices. At four points, using the pieces of (153), there is a four leg ribbon vertex. In general, the $\tau(12\cdots n)$ obey Kleiss-Kuijf identities. For digit strings A and B,

$$\tau(1AnB) = (-1)^{|B|} \sum_{\sigma \in \text{sh}} \tau(1\sigma n) \tag{162}$$

expresses the relation between shuffles of the indices (AB^T), that is with the string B reversed.

Example 6.2 The four point graviton amplitude in $N = 8$ supergravity is

$$M(++--) = G_N \frac{\langle 34 \rangle^4 [12]^4}{\langle 14 \rangle [14] \langle 12 \rangle [12] \langle 13 \rangle [13]}$$

where G_N is Newton's constant. The denominator is an stu factor, using the convention above. This clearly resembles the product of Yang-Mills $M(--++)$ and $M(++--)$ amplitudes. The three point case

$$M(--+) = \frac{\langle 12 \rangle^6}{\langle 13 \rangle^2 \langle 23 \rangle^2}$$

does not mix Z and W invariants, and only makes sense for complex momenta.

Physical localisation in scattering comes from the observation that factors in internal propagators, such as $(p_1 + p_2 + p_3 + p_4)^{-1}$, give singularities precisely when the internal particle is real, since then the sum of momenta is zero. This is now an *extra* condition on the amplitudes, and a strong constraint on the spin s. For spin 2 there was an stu factor in the four point case. The only other solution for a fixed s theory is a factor $s^{-1} + t^{-1} + u^{-1}$, for a spin zero ϕ^3 scalar field theory [122]. Of course a physical theory must mix particle spins.

There is also a straightforward recursion rule for the gravity amplitudes. Recent results include an exact tree level formula for the $N = 8$ theory. In [19][27], the N^kMHV kinematic invariants are defined by an $n \times n$ matrix $K(k+2)$. This is paired with a matrix $\overline{K}$ for dual variables. We mention the MHV case only. Define the phases [27]

$$\phi_{ij} = \frac{[ij]}{\langle ij \rangle} \qquad i \neq j \tag{163}$$

$$\phi_{ii} = -\sum_{j \neq i} \frac{[ij]\langle jx \rangle \langle jy \rangle}{\langle ij \rangle \langle ix \rangle \langle iy \rangle}$$

which are independent of the choices x and y, for momentum conservation on the n points. Now let

$$c_{ijk} = (\langle ij \rangle \langle jk \rangle \langle ki \rangle)^{-1}. \tag{164}$$

Then the n point amplitude is expressed in terms of the c_{ijk} and ϕ_{ij} as a new kind of determinant for the symmetric matrix K_{ij}, which has entries ϕ_{ij}. One needs to delete 3 rows and 3 columns from K_{ij}, namely ijk and the complementary rst respectively. These give a $(n-3) \times (n-3)$ minor, called $\Phi_{rst,ijk}$. Let $\sigma_{rst,ijk}$ be the permutation in S_n sending $(ijk12\cdots n)$ to $(rst12\cdots n)$. Then the important part of the gravity amplitude is just

$$M'(12\cdots n) = (-1)^{n+1}\text{sgn}(\sigma_{rst,ijk})c_{ijk}c_{rst}\Phi_{rst,ijk}. \tag{165}$$

It does not depend on permutations. The full amplitude $M(12\cdots n)$ requires a product $\det(\overline{K})\det(K)$ of reduced determinants [19]. The reduced determinant at N^kMHV requires $n-k-3$ contractions, and we note that this is the dimension of the A_{n-2} codimension k faces, labeled by trees with contracted edges.

In summary, with a BCFW cut the four point diagram becomes the two leaved A_1 tree, which is a basic causal point. Localisation splits A_1 into a left $(-)$ and right $(+)$ leaf, defining the left right tree symmetry for all A_d.

6.2 Grassmannians and Associahedra

With two rows for a $k=0$ $\overline{\text{MHV}}$ Grassmannian matrix, there are $(d-1)(d+2)/2+1$ minors M_{ij}, for $d = n-1$. Note that this is not the usual correspondence $d = n-2$, given by the sides on the polygon. Recall that $(d-1)(d+2)/2$ counts the number $f_{1,d}$ of codimension 1 faces of A_d.

d	2	3	4	5	6	7
$f_{1,d}$	2	5	9	14	20	27

To account for the one missing minor, we choose to ignore the sign configuration $(+-\cdots-+)$ that puts the two $+$ helicities at the start and end. This leaves $f_{1,d}$ signature classes for the permutation group S_n. For example, the pentagon A_3 has edges labeled by the five minors

$$\tag{166}$$

In general, this gives a projection $S_{n+1} \to A_{n-1}$ that selects the signature classes of $\overline{\text{MHV}}$ type. Similarly for the MHV case. These signatures are

vertices on the parity cube in the central dimension n. For codimension x on A_d, the number of faces is

$$f_{x,d} = \frac{1}{n} \begin{pmatrix} n-2 \\ x \end{pmatrix} \begin{pmatrix} n+x \\ x+1 \end{pmatrix} \tag{167}$$

in terms of $n = d + 1$. This selects minors for both $n - 2$ particles and $n + x$ particles, where x specifies k. The number of minors for $k + 2$ negative helicities and n particles is counted by lattice paths of length n. The paths are drawn on a $(k + 2) \times (n - k - 2)$ rectangle. Alternatively, we can use marked boxes in a rectangular Young diagram of the same shape.

Example 6.3 For the four particles that label the pentagon edges, omit the empty Young diagram. The five remaining lattice paths are anchored at the top right corner of the diagrams.
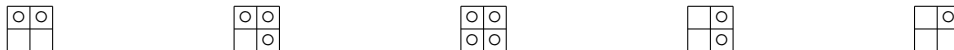
These diagrams label the Minkowski space minors of $Gr(2, 4)$.

Recall from appendix C that lattice paths count the $(k + 2, n - k - 2)$ shuffles in S_n. Shuffles will be important in the next section, where we look at the symbol calculus for scattering amplitudes.

We have seen that the BCFW rules pair two legs to create a tree with $n - 2$ leaves. Now the n particle scattering amplitudes match the associahedra A_{n-1}, A_{n-2} and A_{n-3}. The A_{n-2} is indexed by polygons with n sides, and A_{n-3} works when a cut reduces the number of legs by one. Although the directionality of tree roots breaks the cyclic symmetry of the theory, it offers insight into the underlying categorical structure.

Consider labeling the interior nodes of the binary tree so that each edge has ends forming a $\pm$ pair [123]. On the dual polygons, this corresponds to labeling both outer edges and chords, so that all triangles in the chorded diagram have mixed sign sets. That is, no triangles of form $(- - -)$ or $(+ + +)$ are allowed. This is just an MHV rule. Let us see how signed polygons or trees force an extension of the A_d structure. The pentagon of

pentagons

$$(168)$$
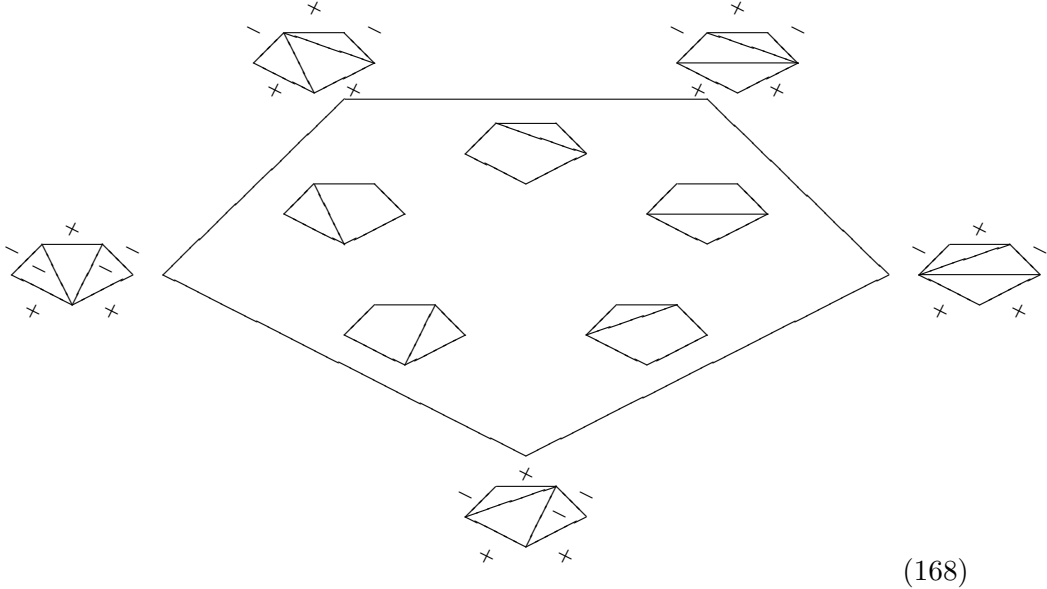
is marked with signs. The horizontal chord in the top right pentagon must be a $-$ by the triangle rule. This forces the one other chord to be marked with a $+$ sign. Moving around four sides of the large pentagon, all chord signs are fixed by associator edges. But then the ends of the fifth side will have opposite signs on the same internal chord. An additional sign flip edge would turn the pentagon into a hexagon, just as for the categorified pentagon on the faces of a parity cube.

Observe that only three vertices of the pentagon have some freedom in assigning signs to chords. These are all equivalent under cyclic shifts. In the end, there is only one vertex for the $(- - + - +)$ sequence and one for $(- - - + +)$, counting C_2. As n increases, however, there are more possibilities for the chordings.

Now look at how the physical set of signed polygons may be mapped to the vertices of the ordinary associahedron, with the shift $\Delta d = -1$. Once again let $k + 2$ be the total number of minus signs, and let r be the number of $+$ signs. For a given k, the number of terms in a scattering amplitude is given by the Narayana numbers. Recall from chapter 5 that the collection of Narayana numbers, for all possible k, gives the Catalan number associated to n. For n points, the correct count is given by

$$C_n \equiv \frac{1}{n-2} \binom{2(n-3)}{n-3} \qquad (169)$$

for $n \geq 3$. For example, at $n = 5$ we take the polygon with $n - 1 = 4$ sides, and this has two possible chordings, giving C_5. The Catalan numbers are decomposed into Narayana numbers $N(k, j)$ such that $C_k = \sum_{j=1}^{k} N(k, j)$.

In terms of n and r,

$$N(n,r) = \frac{1}{n-3} \begin{pmatrix} n-3 \\ r-1 \end{pmatrix} \begin{pmatrix} n-3 \\ r-2 \end{pmatrix} \tag{170}$$

so that $N(6,3) = 3$ recovers the three internal vertices of the pentagon A_3. The A_3 signs are given in (93). After choosing a root, the other helicity signs correspond to the direction of the leaves, with $-$ for a left branching and $+$ for right. The double $\pm$ root with two leaves gives the $n = 4$ point A_1.

Since the signs are canonical, all the higher dimensional cells of this A_d are defined as usual. We view such Δd shifts as homological operations, since they shift the dimension of a homological cell. But particle scattering is picking up a new ternary structure for homology, with three distinct dimensions contributing directly to n point amplitudes.

6.3 Symbology and Polylogarithms

Multiple polylogarithms are ubiquitous in the components of scattering amplitudes. This large class of functions satisfies numerous functional relations. Symbology [124][125][126] is the process of mapping a given polylogarithm to a unique object in a categorical algebra so that the combinatorics of functional relations are respected by this algebra. Polylogarithms are defined [127] recursively in terms of complex parameters by

$$G(a_1, a_2, \cdots, a_{n-1}; x) = \int_0^x \frac{\mathrm{d}t}{t - a_1} G(a_2, a_2, \cdots, a_{n-1}; t) \tag{171}$$

starting with $G(0) = 0$ and $G(x) = 1$ for $x \neq 0$, and then $G(0; x) = \log x$. This class includes the classical polylogarithms $\mathrm{Li}_{n-1}(x) = -G(0, \cdots, 0, 1; x)$ and nested sums such as

$$G(0, 0, \frac{1}{x_3}, 0, \frac{1}{x_2 x_3}, \frac{1}{x_1 x_2 x_3}; 1) = (-1)^3 \sum_{i_1 < i_2 < i_3} \frac{x_1^{i_1} x_2^{i_2} x_3^{i_3}}{i_1^{1} i_2^{2} i_3^{3}}.$$

Sometimes the shorthand 0_m is used for a string of m zeroes. In particular, the multiple zeta values $\zeta(s_1, \cdots, s_k)$ [128][129] for $s_i \in \mathbb{N}$, called MZVs, are given by $G(0_{s_k-1}, 1, 0_{s_{k-1}-1}, \cdots, 0_{s_1-1}, 1; 1)$. These MZVs occur in the basic n point Veneziano amplitudes, which may be obtained through motivic integration on spaces described by categorical polytopes [130][131]. A multiple zeta value of *depth* j and *weight* n is a function of the form

$$\zeta(k_1, k_2, \cdots, k_j) = \sum_{n_1 > n_2 > \cdots > n_k \geq 1} \frac{1}{n_1^{k_1} n_2^{k_2} n_3^{k_3} \cdots n_j^{k_j}} \tag{172}$$

for positive integers $k_1, k_2, \cdots$ such that $n = \sum k_i$. Higher order classical polylogarithms [132] are defined iteratively as

$$\mathrm{Li}_n(z) = \int_0^z \mathrm{Li}_{n-1}(z) \frac{\mathrm{d}z}{z}$$

and in particular $\mathrm{Li}_n(1) = \zeta(n)$. The symbol $\mathcal{S}(G)$ associated to an MZV will always be zero, due to the parameters occurring in G. For instance, when some $s_i \geq 2$ the MZV symbol contains at least one term equal to 1, coming from a $(0, 1)$ subsequence in the arguments.

Thus by construction the symbol algebra is *torsion free*, meaning that any occurrence of a root of unity, such as 1 itself, kills the symbol. This reflects the simple fact that $\mathcal{S}(\log x) = x$ with $\log 1 = 0$. In particular, the pole of the Riemann zeta function at $s = 1$, which equals $-G(1; 1)$, has symbol 0. This is a special case of $-\log(1 - x)$ at $x = 1$.

Since $\mathcal{S}(\log x) = x$, we may think of the symbol $\mathcal{S}(G)$ as a kind of exponentiation map, which turns arithmetic sums into products. Moreover, since $\mathcal{S}$ acts on functions, it might be viewed as a functor on a subcategory of functions on $\{\mathbb{C}^n\}$, with terminal object $\mathbb{C}$. The pointwise product $G_1 G_2$ of two functions should then be sent by $\mathcal{S}$ to a product for the symbol algebra. At the level of universal algebra, the shuffle rule

$$x \sqcup\!\sqcup y \equiv x \otimes y + y \otimes x$$

interprets $x \sqcup\!\sqcup y$ as $\mathcal{S}(\log x \log y)$ in the target category. This becomes the functorality law for the symbol algebra.

Given a vector $(a_1, a_2, \cdots, a_{n-1})$ of complex singularities, a general polylogarithm function $G(a_1, a_2, \cdots, a_{n-1}; x)$ of weight $n - 1$ will be referred to simply as a *polylog*. The symbol $\mathcal{S}(G)$ [124][125] of a polylog G is an object in a tensor algebra of functions in the parameters $(a; x) \equiv (a_1, a_2, \cdots, a_{n-1}; x)$ of G. Words W of the form $w_1 \otimes \cdots \otimes w_k$ in the tensor algebra form an algebra with respect to the shuffle product $W_1 \sqcup\!\sqcup W_2$. This product is defined in appendix C. Finally, the full symbol algebra satisfies the following axiomatic properties.

- **Functorality:** $\mathcal{S}(G(a_1, a_2, \cdots, a_j; x) G(a_1, a_2, \cdots, a_k; y))$

$$= \mathcal{S}(G(a_1, a_2, \cdots, a_j; x)) \sqcup\!\sqcup \mathcal{S}(G(a_1, a_2, \cdots, a_k; y)).$$

- **Distributivity:** function products split, as in $U \otimes (xy) \otimes V = U \otimes x \otimes V + U \otimes y \otimes V$.

- **Scale Invariance:** since, for all $\lambda \in \mathbb{C}^*$, $G(\lambda a; \lambda x) = G(a; x)$ provided $a \neq 0$, the symbol must satisfy $\mathcal{S}(G(\lambda a; \lambda x)) = \mathcal{S}(G(a; x))$.

- **No Torsion:** for ω_n the nth root, $U \otimes \omega_n \otimes V = 0$, for all $n \in \mathbb{Z}$.

71

To begin with,

$$\mathcal{S}(\log x) = \mathcal{S}(G(0; x)) = x \qquad (173)$$

and functorality then implies

$$\mathcal{S}(\log x \log y) = \mathcal{S}(\log x) \sqcup\!\sqcup \mathcal{S}(\log y) = x \otimes y + y \otimes x. \qquad (174)$$

The symmetric tensor $x \otimes y + y \otimes x$ is associated to the concatenation xy, since the exponential of $\log x \log y$ is xy.

An example of a classical polylog is $\text{Li}_2(x) = -G(0, 1; x)$, which has symbol $-(1-x) \otimes x$. A similar example will be determined in the next section by a set of three chorded, labeled polygons P, along with the basic function assignment f, which sends the simplest two variable diagram $P(y; x)$ to

$$f(P(y; x)) = 1 - x/y \qquad (175)$$

when $y \neq 0$, and to x otherwise [124][125][126]. Why this particular function assignment? Firstly, the ratio x/y enforces scale invariance on all $\mathcal{S}(G)$. When $y = 0$, $P(0; x)$ must recover $\mathcal{S}(\log x) = x$. The basic polylog $-\text{Li}_1(x) = G(1; x)$ has symbol $(1 - x)$, since this is just $\log(1 - x)$. The expression $1 - x/y$ is also projective, for $\mathbb{PF}^1$ [91].

The next section describes the diagrams used to construct symbols.

6.4 Decorated Polygons for Symbols

Decorated trees appeared in section (5.3). Their dual polygons are used to construct the symbol for a polylog. This is another point of view on the new twistor ribbon graphs.

To each polylog G we first assign a decorated, rooted polygon $P(G)$ following [91][133]. For an n argument polylog $G(a_1, a_2, \cdots, a_{n-1}; x)$ there is an n-gon with halved sides, forming a $2n$-gon with alternating black and white vertices, such that the white vertices mark the midpoints on the sides of the original n-gon. The sides of the n-gon are labeled with the arguments of $G(a_1, a_2, \cdots, a_{n-1}; x)$, so that x marks a root edge. The *orientation* of $P(G)$, left or right, is specified by choosing a vertex at either the left or right hand side of the root edge.

A *maximal chord diagram* is a set of $n - 2$ non intersecting chords on the $2n$-gon, with each chord joining one black and one white vertex, but not an adjacent vertex, as in the figure

$$(176)$$
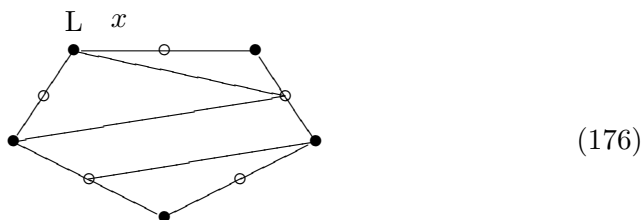
where the top edge is a left oriented root edge, taking the x variable. The symbol $\mathcal{S}(G)$ is constructed from the set of all maximal chord diagrams. This set is enumerated below. In what follows we assume a left orientation for the polygons, so that labels are read in an anticlockwise direction. The chording turns the $2n$-gon into a polygon chopped into squares. To start with, at $n = 3$ there are three chorded triangles for $G(a, b; x)$.

$$(177)$$
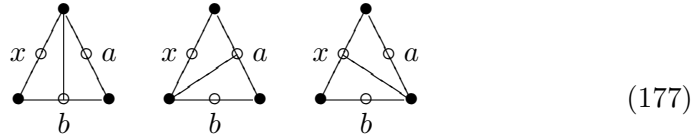
These chorded polygons are always cut into squares, suggesting the existence of dual trees with $2n$ legs and *ternary* branchings. First, the dual decorated tree to the n-gon may be considered a flat ribbon graph, by thickening the edges as they meet the vertices [91]. This has n legs including the root, but $2n$ external ribbon edges. The polygon is decomposed using the splitting contraction of (5.3) on the edge at the head of the chord. Thus the first chorded triangle becomes

$$(178)$$
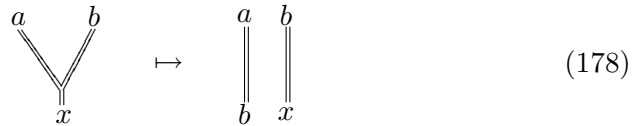
The ribbon strips of the decomposed graph are dual to globule diagrams with two sides. The top label is taken to be the root side of the globule. Ribbon graphs have no automatic internal edges, but here each chord defines an internal edge, which can be represented

$$(179)$$
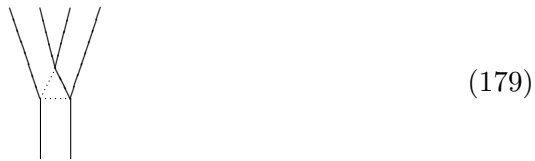
on an overlapping ribbon vertex. With such a vertex structure, the ribbon edges define a ternary six legged tree, and as trees dual to hexagons the three triangles may label the three square faces

$$(180)$$

of the A_4 associahedron in dimension 3. For any n we thus obtain index diagrams for certain codimension $n - 2$ faces of A_{2n-2}, which are always of dimension $n - 1$. There are $n!/2$ such faces, which can be seen inductively. Fixing one initial chord, there are $(n - 1)!/2$ ways to cut the remaining

$(2n-2)$-gon by the remaining chords. There are then n rotations of each such diagram.

Given a maximal chord diagram, there are associated linear orders with $n-1$ vertices. These are the internal orders of the dual decorated tree. Each vertex is labeled with a pair (u,v) of variables from the decorated diagram, representing a rooted globule with sides u and v. For the triangles, there are two vertices in the unique order,

$$
\begin{matrix}
(x,b) \bullet \\
 \big| \\
(b,a) \bullet
\end{matrix}
\quad
\begin{matrix}
(x,a) \bullet \\
 \big| \\
(a,b) \bullet
\end{matrix}
\quad
\begin{matrix}
(x,b) \bullet \\
 \big| \\
(x,a) \bullet
\end{matrix}
\tag{181}
$$

with globule labels determined as above, by contraction. Observe that each vertex on a linear order is a node on the dual tree. The orders are simply paths through the dual tree, with the root node at the top. Recall that these are themselves rooted trees, appearing in the Hopf algebra of rooted trees.

There remains only the sign problem in the symbol construction. This uses the orientation that was required for the differential on trees. The symbol obtains a factor of $(-1)^k$, where k is the number of backwards arrows, as follows. Orient every chord on the polygon with an arrow head at the white vertex. An arrow is backwards if its tail starts at a vertex to the right of its head, with the string of edges read clockwise from the root vertex and ending with the root edge. For example, only the first triangle has a backwards chord. Finally, the symbol for $G(a,b;x)$ is

$$
\mathcal{S}(G(a,b;x)) = -(1-\frac{x}{b})\otimes(1-\frac{b}{a})+(1-\frac{x}{a})\otimes(1-\frac{a}{b})+(1-\frac{x}{b})\otimes(1-\frac{x}{a}), \tag{182}
$$

reading the function assignments, as in (175), from the linear orders. This expression comes from a new differential, applied to an unchorded triangle. This contraction differential defines a differential graded algebra of polygons with a $\wedge$ product, but the symbol actually belongs to an associated $\otimes$ coalgebra. This is known as the *bar construction* [134][91]. For general polygons, the symbol is then obtained via a sum over all maximal sets P,

$$
\mathcal{S}(G) = \sum_P (-1)^k \sum_{\text{orders}} f(u_1,v_1) \otimes \cdots \otimes f(u_{n-1},v_{n-1}) \tag{183}
$$

using the above algorithm.

Example 6.4 The 12 octagons for $G(a,b,c;x)$ are given by chord rotations of the three diagrams

74
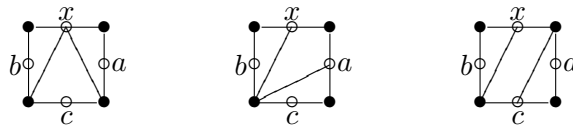
There are three diagrams with V shaped linear orders, which have symbol terms of the form

$$-f(b,x) \otimes f(a,b) \otimes f(c,b) - f(b,x) \otimes f(c,b) \otimes f(a,b)$$

$$-f(c,x) \otimes f(a,x) \otimes f(b,c) - f(c,x) \otimes f(b,c) \otimes f(a,x)$$

$$f(b,x) \otimes f(a,x) \otimes f(c,b) + f(b,x) \otimes f(c,b) \otimes f(a,x)$$

and the other 9 diagrams contribute terms like $f(a,x) \otimes f(b,a) \otimes f(c,b)$.

Polygon differentials are closely related to comultiplications for Hopf algebras of rooted trees. In the symbol calculus, the polygon label set $(a_1, \cdots, a_{n-1}; x)$ defines a polygon *cocycle*. That is, we consider cohomology only for the $\otimes$ structure and not for the original $\wedge$, whereas in general the coalgebra differential mixes $\otimes$ and $\wedge$. With both algebra and coalgebra structures, the polygons form a commutative Hopf algebra. It is commutative because the disjoint union of trees is taken to be commutative, but this could be modified to noncommutative forests.

Only a few basic function types occur in the symbol. In terms of these symbol pieces, the permutation group S_3 is given by [133]

$$x = \begin{pmatrix} 1 & 0 & 0 \\ 0 & 1 & 0 \\ 0 & 0 & 1 \end{pmatrix} \qquad \frac{1}{x} = \begin{pmatrix} 0 & 0 & 1 \\ 0 & 1 & 0 \\ 1 & 0 & 0 \end{pmatrix}$$

$$\frac{1}{1-x} = \begin{pmatrix} 0 & 1 & 0 \\ 0 & 0 & 1 \\ 1 & 0 & 0 \end{pmatrix} \qquad \frac{x}{x-1} = \begin{pmatrix} 0 & 1 & 0 \\ 1 & 0 & 0 \\ 0 & 0 & 1 \end{pmatrix} \qquad (184)$$

$$1 - \frac{1}{x} = \begin{pmatrix} 0 & 0 & 1 \\ 1 & 0 & 0 \\ 0 & 1 & 0 \end{pmatrix} \qquad 1 - x = \begin{pmatrix} 1 & 0 & 0 \\ 0 & 0 & 1 \\ 0 & 1 & 0 \end{pmatrix}$$

where function substitution is the group operation. For example, substituting $1/x$ into the variable in $1/(1-x)$ gives $x/(x-1)$. This means that $(231)(321) = (213)$. Observe that the sum of all six functions gives the ordinal 3, as did the sum of matrix hexagon edges. The coidentity $1/x$ is the inverse of x as an up down matrix reflection, and similarly for the other functions. Recall that such a matrix symmetry is captured by the permutation signature classes, with signature string reversal and sign flipping. In terms of logarithms, this symmetry is the additive inverse between $\log x$ and $-\log x$. As permutations, the Z and W twistor vertices of (150) give the variables $1/(1-x)$ and $1 - 1/x$.

Remark 6.5 This substitution S_3 is the form of the S_3 action on the argument z of the j-invariant for elliptic curves. That is, each function in z is also a ratio in terms of roots of a cubic polynomial. For example, for (312) we can take $z/(z-1) = (e_2 - e_3)/(e_2 - e_1)$. The roots clearly describe the

permutation. The flat ribbon graph for the j-invariant is a gluing of two trivalent ribbon vertices. This is a top down view of the basic pair of pants surface diagram, namely $\mathbb{CP}^1$ without $\{0, 1, \infty\}$.

The function assignment is motivated by homological cycles that are expressed as decorated trees, with the decorations taking values in the q-th roots of unity for $\mathbb{F}_{q+1}$ a field [91][135]. Thus the polylog arguments in $\mathbb{C}$ begin with the roots of unity.

6.5 Categorical Distributivity and Logarithms

This section is merely a categorical interlude. The importance of logarithm functions comes down to their higher arithmetic nature. Whereas addition for the integers mod k is characterised by the $+k$ operation, the complex logarithm has the property that $2\pi i$ can be added to any phase. The cyclicity of phases is a quantum arithmetic, according to the theory of mutually unbiased bases. So how do complex spaces become noncommutative?

Classically, twistor geometry uses sheaf cohomology on complex projective spaces [49][50]. Ostensibly, a quantum analog to the sheaf condition employs a functor on a *quantum* lattice. With constructive motives, spatial elements and algebraic ones should be unified. This means working with endofunctors $E : \mathbf{M} \to \mathbf{M}$ on one universal category $\mathbf{M}$, so that universal homology and cohomology provides a pair of endofunctors, E and $E^\vee$, such that $E \circ E^\vee$ and $E^\vee \circ E$ characterise integral invariants. Relations of the form $E \circ E^\vee \to E^\vee \circ E$ on functors are the categorical subject of *distributive laws* [136][137], where $\oplus\otimes \to \otimes\oplus$ is the canonical example. Quantum distributivity requires noncommutative categories, as in the braided distributivity of appendix C.

Braided distributivity suggests a weaker form of symbology, for noncommutative analogues of the logarithm. Let us consider what the logarithm represents abstractly.

Recall that a counting number $n \in \mathbb{N}$ stands for an n element set in the category **Set**, whose objects are sets and whose arrows are functions between sets. In **Set**, basic arithmetic is expressed in terms of functions. For instance, the product nm of two counting numbers n and m becomes the Cartesian product $\mathbf{n} \times \mathbf{m}$ of finite sets. This is drawn as a pullback square

$$
\begin{array}{ccc}
\mathbf{n} \times \mathbf{m} & \xrightarrow{\pi_L} & \mathbf{n} \\
{\scriptstyle \pi_R}\big\downarrow & & \big\downarrow \\
\mathbf{m} & \longrightarrow & \mathbf{1}
\end{array}
\tag{185}
$$

where π_L and π_R are projections onto left and right factors. Since the composition of projections is always a projection, there is a subcategory $\mathbf{Pr}$ of **Set** containing all the finite sets and all the projection arrows. The object

$\mathbb{N}$ is a limit of the finite $\mathbf{n}$. Addition $\mathbf{n} + \mathbf{m}$ is the disjoint union of the sets, and this is also represented by a square, with the empty set $\mathbf{0}$ replacing $\mathbf{1}$, and the reversed arrows are the obvious inclusions. We extend $\mathbf{Pr}$ to include these inclusions. Now there is a limiting successor function $(+1) : \mathbb{N} \to \mathbb{N}$, allowing an axiomatisation of arithmetic [7].

What about functions on infinite sets? Let us consider a convenient infinite set F, such as the complex number field, which has an addition and multiplication. F^n denotes the n-fold product, as for the domain of functions in n variables. For many purposes, the uncountable cardinality of F is troublesome, so we would like to begin with finite structures that we already understand. So for this fixed F, there should be an analogue of $\mathbf{Pr}$, still within the larger category. Take the collection of all F^n as objects. What is a suitable subset of the functions from F^n into F^m, replacing the basic squares in $\mathbf{Pr}$?

The arithmetic structure of $\mathbf{Set}$ suggests working with a collection of suitably arithmetic functions. This is the context of special functions, such as the polylogarithms. Natural analogues of addition and multiplication on the ordinals $\mathbb{N}$ are the exponential and logarithm functions. That is, the square for $\mathbf{n} \times \mathbf{m}$ may be mapped to a function product $\exp \mathbf{n} \cdot \exp \mathbf{m}$, while $\mathbf{n} + \mathbf{m}$ becomes $\log \mathbf{n} + \log \mathbf{m}$. The composition $\exp(\log z)$ behaves similarly to an identity arrow for the object F.

The symbol $\mathcal{S}$ acts on arithmetic functions and obeys a functorial rule. Since its arguments are actual complex numbers, it will help to view $\mathbb{C}$ itself as a category. In a sense we already do this, with $\mathbb{N}$ having the structure of $\mathbf{Pr}$. But if $\mathbb{N}$ and $\mathbb{C}$ are one dimensional structures then $\mathbf{Set}$, which contains them as sets, must become at least a two dimensional structure. It already is, because the Cartesian product of sets gives $\mathbf{Set}$ a monoidal structure, so that a 2-functor from $\mathbf{Set} \otimes \mathbf{Set}$ to $\mathbf{Set}$ gives the Cartesian product, and all sets in $\mathbf{Set}$ are secretly 1-arrows. Thus $\mathbb{C}$, as a continuum, is picking up this extension to an axiomatic arrow.

7   The Ribbon Particle Spectrum

In the Standard Model, the manifestly local Lagrangian contains a Higgs field, responsible for rest mass creation [138]. In 2012, the ATLAS [139] and CMS [140] experiments at the LHC discovered the Higgs boson. In the $\gamma\gamma$ decay channel it was observed at a higher than expected cross section, but most channels agree with Standard Model expectations. The observed Higgs mass $m_H = 126$ GeV was predicted some years ago by Dharwadker and Khachatryan [141] using the simple formula

$$m_H = \frac{1}{2}(m_{W^+} + m_{W^-} + m_Z) = m_W + \frac{m_Z}{2}, \qquad (186)$$

which is discussed below. The standard couplings run with scale, meaning that the fundamental particle masses effectively change. However, this does not prohibit algebraic relations between the masses, particularly in the low energy limit. We expect the emergent theory to pick out special scales in a different way to the Standard Model, wherein mass is generated only with empirical parameters. M theory expects both IR and UV inputs to the mass spectrum, and it is not clear at what scale the simplest symmetries should manifest themselves. In this chapter we study mass spectra using simple kinematic assumptions.

Twistor localisation is a factorisation process in a non local theory. The same happens here, only with braids instead of networks. With braids, localisation is the process of turning geometry into numbers, namely measurement outcomes. True arithmetic appears to require ribbon diagrams, extending the planar techniques that are associated to conformal structure.

Fundamental to the diagram techniques is the concept of S duality, or more generally, S, T and U dualities. It is duality that introduces complex cardinalities [142]. A $U(1)$ charge appears directly in the diagrams below, in the twists of ribbon strands. Such diagrams are used to frame knots in three dimensional spaces. In James Clerk Maxwell's original paper on electromagnetism [143], such twist loops were supposed to define vortices in the aether. This remains a useful insight into gauge construction.

The ribbon spectrum [102] represents the most fundamental set of localised IR states. It arises when the trivalent tree vertices are extended to braids and ribbons, and carries the quantum numbers for both the electroweak and the strong interaction. Kinematically, this is sufficient to discuss rest mass quantum numbers [120]. In the next chapter, braids and ribbons are studied in more detail.

7.1   The Mirror Transformation

The magnetic charges will be specified in a doubling of the Standard Model braid set. This hinges on a reversal of braid crossings in a B_3 particle diagram. Using the Burau representation of B_n, there are transformations that

act on both the matrices and the braid diagrams themselves. By definition, the *mirror transformation*

1. flips across a central horizontal axis

2. flips across a central vertical axis

3. changes all braid crossings, using the $t \mapsto 1/t$ map.

For the 2×2 matrices of B_3, this interchanges the diagonal elements, one for the other, and the off diagonal ones. Note that the diagram transformation only preserves the crossing site of a generator τ_i for τ_n in B_{2n}. In particular, the basic B_2 generator is conserved. In B_3, a knot in the set $\{\tau_1\tau_2^{-1}, \tau_2\tau_1^{-1}, \tau_2^{-1}\tau_1, \tau_1^{-1}\tau_2\}$ is fully fixed by the mirror map, with each crossing being sent to the inverse of the other. Similarly, a pair τ_i^{-1}, τ_{n-i} in B_n creates a $w = 0$ fixed point of the mirror map. Recall the Burau matrix

$$\tau_2 = \begin{pmatrix} 1 & -t & 0 \\ 0 & -t & 0 \\ 0 & -1 & -1 \end{pmatrix}, \tag{187}$$

in B_4, which is similar to the central τ_n generator for all B_{2n}. The top two rows look like τ_2 in B_3 and the bottom rows like τ_1. The mirror transformation sends τ_2 in B_4 to τ_2^{-1} by shifting the B_3 τ_2 down to its mirror τ_1^{-1} and similarly shifting the B_3 τ_1 up. Thus both the matrix and the diagram maintain the same crossing site τ_2, but the τ_1 and τ_3 generators are interchanged by the mirror.

Our braided ribbons will always be *double knots* in B_{2n}, meaning that there is an underlying knot in B_n. Since ribbon twists are separated from the braiding in B_n, the reversal of crossings under a mirror map can preserve the braid in B_n while flipping the direction of the ribbon twist. Full ribbon twists define a unit of electromagnetic charge [102]. The sign convention

$$+ \quad \text{⧓} \quad \text{⧓} \quad - \tag{188}$$

follows the B_2 convention, and the magnitude of charge q on each strand is set at $1/n$, where n is the total number of ribbon strands in a diagram. At a basic interaction vertex, at most $\Delta q = \pm 1$ is exchanged between particles. It is therefore sometimes possible to represent a half twist with the root of unity ω_6, so that $+1 \mapsto \omega_3$ and $-1 \mapsto \overline{\omega_3}$.

Note that whereas B_2 is generated by a half twist, charge generates $\mathbb{Z} \simeq B_2$ with a full twist. It would be better to label a half twist with the integer 1, and let a full set of three twists stand for $q = 6$. However, this disagrees with the physical convention, so we just remember the anomalous factor of 6.

Ribbons appear because we need the structure of a *tortile tensor* category [144]. These are braided $\otimes$ categories for which the braiding is compatible with the existence of dual objects. The definition is in appendix A. As in (A.2), writhe and ribbon twists are interchangeable for tortile category double knots. For this reason, we restrict attention to $w = 0$ knots in B_n, and consider all possible charge assignments. The particle spectrum consists of the fundamental set of such diagrams.

7.2   The Massless Electroweak and Strong Spectrum

In the massless particle scheme of [102], the permutations (213) and (312) underlie left and right handed fermion braids respectively. The full Standard Model particle spectrum is given by braided ribbons for B_3. It uses the writhe zero B_3 unknots, discussed further in chapter 8, along with charge information in the ribbon twists. A twisted ribbon, representing electromagnetic charge, takes one of four sign values: 0, $-$, $+$ or $-+$. Only the Z boson is permitted mixed $-+$ loops, to distinguish it from the photon. Its three $\pm$ strands may be considered a $W^{\pm}$ composition, as a bosonic analogy to fermion annihilation. Mixed charges for fermion braids are considered redundant, because ribbon twists are there to define the link writhe, and fermions trace to a knot. So using B_3 braids, the massless spectrum of the Standard Model is given by

$$e_L^- = [\tau_2\tau_1^{-1}, (---)] \quad e_R^+ = [\tau_1\tau_2^{-1}, (+++)] \quad (189)$$
$$e_L^+ = [\tau_2^{-1}\tau_1, (+++)] \quad e_R^- = [\tau_1^{-1}\tau_2, (---)]$$
$$\overline{\nu}_L = [\tau_2^{-1}\tau_1, (000)] \quad \nu_R = [\tau_1^{-1}\tau_2, (000)]$$
$$\overline{u}_L = [\tau_2\tau_1^{-1}, (++0)] \quad \overline{d}_R = [\tau_1\tau_2^{-1}, (00-)] \quad \mathbf{R}$$
$$\overline{u}_L = [\tau_2\tau_1^{-1}, (+0+)] \quad \overline{d}_R = [\tau_1\tau_2^{-1}, (0-0)] \quad \mathbf{G}$$
$$\overline{u}_L = [\tau_2\tau_1^{-1}, (0++)] \quad \overline{d}_R = [\tau_1\tau_2^{-1}, (-00)] \quad \mathbf{B}$$
$$u_L = [\tau_2^{-1}\tau_1, (--0)] \quad d_R = [\tau_1^{-1}\tau_2, (00+)] \quad \mathbf{R}$$
$$u_L = [\tau_2^{-1}\tau_1, (-0-)] \quad d_R = [\tau_1^{-1}\tau_2, (0+0)] \quad \mathbf{G}$$
$$u_L = [\tau_2^{-1}\tau_1, (0--)] \quad d_R = [\tau_1^{-1}\tau_2, (+00)] \quad \mathbf{B}$$
$$W^- = [I_2, (---)] \quad W^+ = [I_2, (+++)] \quad \gamma = [I_2, (000)]$$
$$Z_1 = [I_2, ((-+)00)] \quad Z_2 = [I_2, (00(-+))] \quad Z_3 = [I_2, (0(-+)0)]$$

The special Z boson comes with a color decomposition, according to the placement of its $(-+)$ mixed charges. Originally, in [102], a single Z boson with charge assignment $((-+)(-+)(-+))$ was used. Using the $\{1, \pm\omega_3\}$ charge representation, so that $(\pm\pm) = (\mp)$, we see that mixed charge assignments do not change the $W^{\pm}$ diagrams. That is, for the color free bosons, all possible charge assignments have now been given.

Only one choice of crossing pair is used for each observed particle, but the mirror particle set appears with duality. The mirror sends $e_L{}^-$ to a *mirror copy* of the positron $e_L{}^+$, and similarly for the other charged fermions. Thus matter antimatter annihilation will be viewed as a four object process with two $p\bar{p}$ annihilating pairs, one real and one mirror copy. The full ribbon spectrum is now parity conserving.

Only fermions with neutral strands, namely the neutrinos and quarks, exhibit non trivial mixing phenomena. Below we look at a braid picture for particle mixing. On a quark, for example, the two parallel strands will be swapped under the mirror transformation, and these strands may carry distinct charges. Thus the mirror transformation is participating in the strong interaction.

The chirality of the braids gives particle chirality. Antiparticles must use the inverse braid in B_3 so that braid composition represents annihilation to the identity photon braid. Using the underlying permutations and a $\{1, \omega_3, \overline{\omega_3}\}$ charge representation, fermions and bosons are related by the 3×3 Fourier transform [145], since 3×3 circulants are always transformed to diagonal matrices. This is a form of supersymmetry. Using a twisted F_3 transform, the left handed fermions are sent to the $W^\pm, \gamma$ bosons and the right handed ones to a Z boson color triplet. The required twist on F_3 is just the $(1, \omega_3, \overline{\omega_3})$ diagonal.

The important discrete symmetries of the Standard Model are

- **C**: charge conjugation on ribbon twists, sends a braid b to b^{-1}

- **P**: parity, sends $\tau_1{}^{-1}\tau_2$ to $\tau_2\tau_1{}^{-1}$

- **T**: time reversal, does the mirror crossing flip and conjugates charge.

With these choices, it is clear that the **CPT** transformation is the identity on particle states. The Standard Model **P** and **CP** violations have long motivated the idea of *mirror matter*, which restores the discrete symmetries for the full particle spectrum [146][147]. For us, however, the mirror matter is another aspect to the mass generation of ordinary baryonic matter. Since we do not expect the mirror states to be localised independently of the standard states, there is no expectation for new WIMP type dark matter particles. Rather, dark matter appears in the guise of black hole states. Since braid composition is annihilation, the ribbon states must be *mass states*. The electroweak states require the braid algebra.

As discussed in [102], the ribbon spectrum obeys the rules of the electroweak interaction. The full set of quantum numbers for the particles and the antiparticles should sum to zero, since these sets differ only in sign. This sign must be associated to the crossing changes in both B_3 and B_2. We are also interested in the specific braid parameter $t = i$, since $\pm i$ is the only complex phase fixed by $z \mapsto -1/z$.

Let us now derive the electroweak quantum numbers for one generation, algebraically [148]. The three valued rest mass quantum number is viewed via a Stern-Gerlach type experiment analogous to the measurement of spin [131]. This is what a mass spectrometer does when it separates a fixed velocity beam of mixed mass particles into three streams, separated by the ambient magnetic field. The three generations are labeled by the three directions of space, conveniently defined by the three Pauli operations X, Y and Z.

Stability of any quantum number requires at least two sequential measurements, so we need $l = 6$ words to account for operations on three objects. Ostensibly this is a high dimensional array, but a reduction to the one generation case leaves a 6×6 matrix of length 2 words. This should be split into B_3 and B_2 components, and is done fully in the next section.

Let us start with B_3, or rather the underlying S_3. Recall the group algebra for the three element group $C_3 \subset S_3$, from (C.1). A matrix representation for C_3 is given by the 3×3 1-circulant permutations: (123), (231) and (312). The relevant element of the group algebra is then

$$G_1 = \begin{pmatrix} a/2 & b & c \\ c & a/2 & b \\ b & c & a/2 \end{pmatrix} \qquad (190)$$

for $a, b, c \in \mathbb{C}$, such that $c = \pm b$ for a left right pair. We always work with the assumption that a triplet of equivalent operations may be cycled without altering the physical properties of the system [149].

The S_2 permutations in S_3 stand for an operation that fixes one object. To maintain invariance between the three directions, all three 2-circulant coefficients must be equal. This is then another 1-circulant. They can then contribute to the electroweak quantum numbers using

$$G_2 = \frac{u}{3} \begin{pmatrix} 1 & 1 & 1 \\ 1 & 1 & 1 \\ 1 & 1 & 1 \end{pmatrix}, \qquad (191)$$

for a parameter $u \in \mathbb{C}$. Now the copy of S_2 underlying B_2 has objects σ_X and I_2. These are used to create the 6×6 element of the Hopf algebra $\mathbb{C}S_6$,

$$G \equiv G_1 \otimes I_2 + G_2 \otimes \sigma_X, \qquad (192)$$

where two copies of G_1 form the diagonal blocks. As in [148], we impose the measurement projector condition $G^2 = G$ to obtain equations for a, b, c, u. The solutions give exactly the weak hypercharge $Y = a$ and weak isospin $T_3 = u$ for the leptons and quarks, such that the $U(1)$ charge quantum number is given by the Gell-Mann Nishijima formula $q = T_3 + \frac{Y}{2}$.

	Y	T_3		Y	T_3
$e_L{}^-$	-1	$-1/2$	$e_L{}^+$	$+1$	$+1/2$
$e_R{}^-$	-2	0	$e_R{}^+$	$+2$	0
ν_L	-1	$+1/2$	$\bar{\nu}_L$	$+1$	$-1/2$
ν_R	0	0	$\bar{\nu}_R$	0	0
u_L	$+1/3$	$+1/2$	$\bar{u}_L$	$-1/3$	$-1/2$
u_R	$+4/3$	0	$\bar{u}_R$	$-4/3$	0
d_L	$+1/3$	$-1/2$	$\bar{d}_L$	$-1/3$	$+1/2$
d_R	$-2/3$	0	$\bar{d}_R$	$+2/3$	0

This indicates that G_1 is responsible for the unbroken symmetry $U(1)_Y$ and G_2 for $SU(2)_T$. We can also use the canonical coordinates of a qutrit simplex to specify Y and T_3, as in the original Gell-Mann and Ne'eman model [150][151]. The three qutrit resonance decuplet has coordinates (x, y, z) such that $x + y + z = 3$ from the homogeneity of the monomials. Choosing $Y = 1 - z$ and $2T_3 = y - x$ gives the correct Y and T_3 values at the integral points. Then the charge quantum number is $q = 2 - x - z = y - 1$. Using these coordinates for the quark (d, u, s) triplet, the quark vectors are

$$u = (2/3, 5/3, 2/3) \qquad d = (5/3, 2/3, 2/3) \qquad s = (2/3, 2/3, 5/3). \quad (193)$$

The one qutrit quark triangle with coordinates $(0, 1, 0)$, $(1, 0, 0)$ and $(0, 0, 1)$ on the plane $x + y + z = 1$ also gives the three quark numbers. They are $2T_3 = y - x$ and $Y = 1/3 - z$, so that $q = 2/3 - x - z = y - 1/3$.

One generation of the Standard Model spectrum has also been considered in terms of ideals for the algebra $\mathbb{R} \otimes \mathbb{C} \otimes \mathbb{H} \otimes \mathbb{O}$, in [152]. This is geometrised using the octonion Fano plane over $\mathbb{F}_2$. Using the unit convention of appendix C, and the split octonion generators u_i and $\bar{u}_i$ [153], Furey's lepton and quark states are given by

$$\text{up: } iu_1 = \frac{1}{2}(-e_4 + ie_1) \quad \text{down: } i\bar{u}_1 = \frac{1}{2}(e_4 + ie_1) \quad \mathbf{R} \qquad (194)$$

$$\text{up: } iu_2 = \frac{1}{2}(-e_5 + ie_2) \quad \text{down: } i\bar{u}_2 = \frac{1}{2}(e_5 + ie_2) \quad \mathbf{G}$$

$$\text{up: } iu_3 = \frac{1}{2}(-e_6 + ie_3) \quad \text{down: } i\bar{u}_3 = \frac{1}{2}(e_6 + ie_3) \quad \mathbf{B}$$

$$\nu: u_0 = \frac{1}{2}(1 + ie_7) \qquad\qquad e^-: \bar{u}_0 = \frac{1}{2}(1 - ie_7)$$

Thus a bioctonion generator for modular arithmetic is a sum

$$\begin{pmatrix} 1 & 0 \\ e_i & 1 \end{pmatrix} = u_0 + \bar{u}_0 + u_i \qquad (195)$$
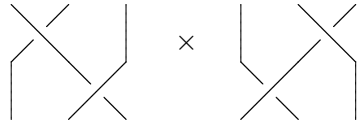
from a weak interaction vertex. Here the up quark is colored by the selection of a direction in the three dimensional space of off diagonal entries. The

generations are then obtained via the three possible embeddings of 2×2 operators in a 3×3 algebra.

The selected units $u \in \{1, ie_i\}$ all satisfy $u^2 = 1$, while the others satisfy $u^2 = -1$. The quaternion subalgebras fit the twistor complexification scheme for $SL_2(\mathbb{C})$ Minkowski space. If we think of the quaternion e_i as Pauli matrices, the 2×2 bioctonion matrix becomes a 4×4 matrix acting on $\mathbb{C}^4$.

7.3 Mirror Circulants

With the mirror transformation, an $e_L{}^- e_R{}^+$ annihilation

$$(196)$$

creates an annihilation process for a mirror $e_L{}^+$ and $e_R{}^-$. All four $w = 0$ unknots in B_3 appear in this set. Including also the crossing switched diagrams, such as the mirror of $e_L{}^-$, there are *eight* braid diagrams associated to charged lepton annihilation. Since annihilation is fundamental to the existence of rest mass, we interpret the two copies of $e_L{}^-$ as two components for rest mass generation. The mirror objects are viewed as dual states, nominally localisable at high energy.

The 2×2 Burau representations for the $e_L{}^-$ mirror pair gives a formal diagram sum with

$$\begin{pmatrix} 1 - 1/t & -t \\ 1 & -t \end{pmatrix} + \begin{pmatrix} -t & 1 \\ -t & 1 - 1/t \end{pmatrix} = \begin{pmatrix} 1 - t - 1/t & 1 - t \\ 1 - t & 1 - t - 1/t \end{pmatrix}.$$
$$(197)$$

Mirror pairs always give circulants in the group algebra $\mathbb{C}S_2$. The scalar $\delta^2 - 1 = 1 - t - 1/t$ defines an interesting choice of braid parameter $\delta = i(t^{-1/2} - t^{1/2})$. With the substitution $t \mapsto -t$, this becomes $\delta = t^{1/2} + t^{-1/2}$. At a root of unity t, this parameter corresponds to unitary representations of B_3 [95].

Note that the circulant was constructed with two diagrams of the *same* crossing configuration. Logically, $\mathbb{C}S_2$ must balance positive and negative crossings. Adding the two circulants together we obtain

$$-\begin{pmatrix} 2(t^{1/2} - t^{-1/2})^2 + 2 & (t^{1/2} - t^{-1/2})^2 \\ (t^{1/2} - t^{-1/2})^2 & 2(t^{1/2} - t^{-1/2})^2 + 2 \end{pmatrix}.$$
$$(198)$$

Circulants are also constructed for the larger representation below. As an $R_2(r)$ matrix, the circulant (197) corresponds to a parameter $r = i(1 - t - 1/t)/(1 - t)$, so that

$$t = \frac{1}{2} \pm \frac{1}{2}\sqrt{1 - 4/(1 - ir)}.$$
$$(199)$$

In particular, at $r = 0$ we have $t = \omega_3$. The other particle circulants have the same diagonal entry, and the off diagonal entries are permuted by $t \leftrightarrow 1/t$ and ± 1. That is, the charge free B_3 mirror pairs have distinct σ_X components

$$\begin{pmatrix} 0 & 1-t \\ 1-t & 0 \end{pmatrix} \qquad \begin{pmatrix} 0 & 1-1/t \\ 1-1/t & 0 \end{pmatrix} \qquad (200)$$

$$\begin{pmatrix} 0 & t-1 \\ t-1 & 0 \end{pmatrix} \qquad \begin{pmatrix} 0 & 1/t-1 \\ 1/t-1 & 0 \end{pmatrix}.$$

At a modular group value $t \in \{\omega_6, \omega_3\}$, the I_2 component can be either 0 or 2, and the off diagonals reduce to multiplicative generators of the cyclic group C_6, which can be embedded in S_6. As permutations, C_6 rightfully requires a 6×6 representation. Actually, the (234561) matrix can be decomposed into the form $H_1 \otimes I_2 + \otimes H_2 \sigma_X$, with

$$H_1 = \begin{pmatrix} 0 & 1 & 0 \\ 0 & 0 & 1 \\ 0 & 0 & 0 \end{pmatrix} \qquad H_2 = \begin{pmatrix} 0 & 0 & 0 \\ 0 & 0 & 0 \\ 1 & 0 & 0 \end{pmatrix}. \qquad (201)$$

These are not circulant, but insisting on a 2-circulant for H_2 and a 1-circulant for H_1 uniquely defines a dual permutation (651324) in S_6, such that the group algebra sum $(234561)+(651324)$ is the matrix $H \equiv (231) \otimes I_2 + (321) \otimes \sigma_X$. This matrix has the nice property that H^2 is the binary negation of H, meaning that all zeroes and ones are interchanged. Then $H^3 = H^2 + 2H$, which reduces to $H^3 = H^2$ under $\mathbb{F}_2$ arithmetic.

The ribbon twists require a representation of $B_2 \simeq \mathbb{Z}$. Let the Burau representation generate $m \in \mathbb{Z}$ with $(-Q)^m$, where Q is one half ribbon twist. Then a full twist is Q^{2m}, and the strand charge is $m/3$. We now need to identify strands in the matrices, but this occurs naturally in the full $n \times n$ representation for B_n, where generators are given by 2×2 crossing blocks. For charge, the twist generator becomes

$$\begin{pmatrix} 1-Q & Q \\ 1 & 0 \end{pmatrix}^{2m} \qquad (202)$$

where $m \in \{0, \pm 1\}$. Three charges form three blocks of a 6×6 matrix for the double knot. The two copies of B_3 must also use the 3×3 representation. The canonical choice is to select rows and columns to match the double knot strands, so that the braid b is embedded as $b \otimes I_2$. Alternatively, permuting with (142536), we can place two copies of b along a diagonal, as $I_2 \otimes b$. This is easier to work with. For example, the $e_L{}^+$ mirror B_3 braid is

$$\tau_2 \tau_1{}^{-1} = \begin{pmatrix} 1 & 0 & 0 \\ 0 & 1-t & t \\ 0 & 1 & 0 \end{pmatrix} \begin{pmatrix} 0 & 1 & 0 \\ 1/t & 1-1/t & 0 \\ 0 & 0 & 1 \end{pmatrix} \qquad (203)$$

and the full 6×6 particle operator should be

$$\begin{pmatrix} 1+Q^2-Q & 0 & 0 & Q-Q^2 & 0 & 0 \\ 0 & 1+Q^2-Q & 0 & 0 & Q-Q^2 & 0 \\ 0 & 0 & 1+Q^2-Q & 0 & 0 & Q-Q^2 \\ 1-Q & 0 & 0 & Q & 0 & 0 \\ 0 & 1-Q & 0 & 0 & Q & 0 \\ 0 & 0 & 1-Q & 0 & 0 & Q \end{pmatrix} \times$$

$$\begin{pmatrix} 0 & 1 & 0 & 0 & 0 & 0 \\ 1/t-1 & 2-t-1/t & t & 0 & 0 & 0 \\ 1/t & 1-1/t & 0 & 0 & 0 & 0 \\ 0 & 0 & 0 & 0 & 1 & 0 \\ 0 & 0 & 0 & 1/t-1 & 2-t-1/t & t \\ 0 & 0 & 0 & 1/t & 1-1/t & 0 \end{pmatrix} \quad (204)$$

so that charge acts on the ribbons at the base of a braid. The charge operators are

$$(+): \begin{pmatrix} 1+Q^2-Q & Q-Q^2 \\ 1-Q & Q \end{pmatrix} \quad (-): \begin{pmatrix} 1/Q & 1-1/Q \\ 1/Q+1/Q^2 & 1+1/Q^2-1/Q \end{pmatrix} \quad (205)$$

Note that when $Q = 1$, we get the 6×6 identity, and when $t = 1$ the permutation (231). This forces the convention of reading a braid word $\tau_i \tau_j$ from right to left, when composing the diagram from top to bottom. This 6×6 picture then recovers the $\mathbb{C}S_6$ objects that were used to derive the Standard Model quantum numbers.

For $\tau_1 \tau_2{}^{-1}$, and with the positive charge matrix evaluated at $Q = 0$, the 6×6 particle matrix reduces to a 6×3 matrix of two identical 3×3 blocks, which are both

$$\tau_1 \tau_2{}^{-1} = \begin{pmatrix} 1-t & 0 & t \\ 1 & 0 & 0 \\ 0 & 1/t & 1-1/t \end{pmatrix}.$$

At $Q = 1$ the same two blocks, up to sign, sit on the 6×6 diagonal. Note that we can also use $Q = \infty$ as a valid charge operation, letting Q take values in $\mathbb{CP}^1$. So the positive particle matrix takes the form $(+) \otimes b$ for the particle braid b. We can also define 4×4 matrices $(\pm) \otimes b$ using the 2×2 Burau representation.

A 6×6 particle determinant has no dependence on the parameter t. For example, we obtain $-8Q^9 + 12Q^8 - 6Q^7 + Q^6$, which evaluates to -1 at $Q = 1$ and 27 at $Q = -1$.

Consider the 2×2 circulants constructed from the larger representation. The mirror transformation works also on these matrices, exchanging τ_i for $\tau_{n-i}{}^{-1}$. The 2×2 generators τ and τ^{-1} give circulants

$$\begin{pmatrix} 1-t & 1+t \\ 1+t & 1-t \end{pmatrix} \quad \begin{pmatrix} 1-1/t & 1+1/t \\ 1+1/t & 1-1/t \end{pmatrix}. \quad (206)$$

The first matrix corresponds to an $R_2(r)$ matrix for the root of unity

$$t = \frac{-ir - 1}{ir - 1}.$$ (207)

That is, $t = \cos 2x + i \sin 2x$ when $r = \tan x$. Let $\phi_r = \tan^{-1}(1/r)$. Then the special braid parameter $\delta_t \equiv t^{1/2} + t^{-1/2}$ equals $-2 \sin \overline{\phi}_r$ and $\delta_{-t} = -2 \cos \overline{\phi}_r$. Summing the positive and negative contributions of (206), we obtain the circulant

$$\begin{pmatrix} \delta_{-t}^2 & \delta_t^2 \\ \delta_t^2 & \delta_{-t}^2 \end{pmatrix} = \begin{pmatrix} (1-t)(1-1/t) & (1+t)(1+1/t) \\ (1+t)(1+1/t) & (1-t)(1-1/t) \end{pmatrix}.$$ (208)

The products $(1 \pm t)(1 \pm 1/t)$ are *perfect polynomials*, because just like the number four, their product equals their sum. As a matrix product, multiplying matching entries is the *Schur product*, as noted in appendix C. One can substitute any polynomial into t, and δ^2 remains perfect. At the trigonometric values this matrix is a probability matrix, when multiplied by a factor of $1/4$. The Schur square root is the unitary circulant

$$\frac{-i}{2} \begin{pmatrix} \cos \overline{\phi}_r & i \sin \overline{\phi}_r \\ i \sin \overline{\phi}_r & \cos \overline{\phi}_r \end{pmatrix} = -i \sin \overline{\phi}_r R_2(-r).$$ (209)

These circulants are used in the next section to study 3×3 mixing matrices. Observe that (207) is the fractional linear transformation $-F_2$ on ir, where F_2 is the Hadamard gate [35]. It sends $r \in \{0, 1, \infty\}$ on the line $\mathbb{R}^+$ to $\{0, \pi/2, \pi\}$ on the unit circle.

So an $R_2(r)$ circulant is constructed from braids overlying the S_2 permutations, which are recovered at $t = 1$. The range $r \in \mathbb{F}$ covers all the normalised elements of the group algebra. For the 2×2 B_3 representation, at a root of unity t, the real parts of $(t^{1/2} - t^{-1/2})$ cancel, leaving a totally real square matrix. This reduces to $I_2 = (12)$ when $t = 1$. In other words, the group algebra for S_2 is viewed as a derivation of the braid algebra using both B_2 and B_3.

The 2×2 Burau representation of B_3 contained the complexified modular group generators. These may be extended to bioctonion operators using the u_i variables of appendix C [153], resulting in the new generators

$$\tau_1(j) = \begin{pmatrix} -t & 0 \\ -ie_j & 1 \end{pmatrix} \qquad \tau_1^{-1}(j) = \begin{pmatrix} -1/t & 0 \\ -ie_j/t & 1 \end{pmatrix}$$ (210)

$$\tau_2(j) = \begin{pmatrix} 1 & -ie_j t \\ 0 & -t \end{pmatrix} \qquad \tau_2^{-1}(j) = \begin{pmatrix} 1 & -ie_j \\ 0 & -1/t \end{pmatrix}$$

for the color index $j = 1, 2, 3$. Note that the signs of the braid entries take care of inverses for modular addition. The lower triangular matrices are the $u + e^- + \nu$ objects of beta decay, and the upper triangular ones use mirror

quark objects rather than down quarks. Down quarks would introduce an additional minus sign, creating a distinct set.

The braid circulants are extended to bioctonion operators in the obvious way. Observe that the classical off diagonal generator 1 for addition now looks like $-e_j/t$. The complex number t gives the B_3 braiding, and as a color object for up quarks, e_j must pick the neutral ribbon strand. The full Burau representation does not give modular operators, but is similarly extended to the bioctonions, and in this case it is clear how e_j can correspond to a strand.

Now the additive states of the weak interaction are given by bioctonion operators, while the annihilating mass states use braids. This must be a clue to the mixing phenomena for neutrinos and quarks. Eventually, in order to reduce the octonion algebra to complex numbers for the construction of unitary matrices, we need to think about projections from higher dimensional octonion spaces, although it is the categorical structure of these spaces that really matters.

7.4 Neutrino and Quark Mixing

The fundamental particles of the Standard Model are all massive, with the exception of the photon. When all other quantum numbers are fixed, there are three rest mass numbers for each fermion. The charged leptons, in increasing order of mass, are electrons ($e^\pm$), muons ($\mu^\pm$) and tau ($\tau^\pm$) particles. Neutrinos exhibit a mixing phenomenon. That is, if the three electroweak neutrinos are ν_e, ν_μ and ν_τ, there exists a second triplet of states ν_1, ν_2 and ν_3 such that the first triplet is transformed into the second by a non trivial 3×3 unitary transformation. The second set is interpreted directly as a set of mass states [154][155].

From an electroweak vertex, the propagating mass states supposedly transition from one to the other with a probability that depends on the distance L from the source and the energy E. For three states, the probability $P_{i \to j}$ is expressed as the square of the amplitude

$$A_{i \to j} = \sum_{k=1}^{3} V_{ik}{}^* V_{jk} \exp(-im_i{}^2 L/2E). \tag{211}$$

In the two neutrino case, this gives a probability

$$P_{i \to j} = \sin^2 2\theta_{ij} \, \sin^2 \frac{L(m_i{}^2 - m_j{}^2)}{4E} \tag{212}$$

in terms of a mixing angle θ_{ij}. The unitary 3×3 MNS neutrino matrix gives the transition amplitudes for all three states [156]. In contrast, the unitary

CKM matrix for quarks [157] contains amplitudes

$$\begin{pmatrix} V_{ud} & V_{us} & V_{ub} \\ V_{cd} & V_{cs} & V_{cb} \\ V_{td} & V_{ts} & V_{tb} \end{pmatrix} \tag{213}$$

that transition between the up and down quark triplets. It is usually factored as $V_u V_d{}^\dagger$. The Jarlskog invariant [158] measures **CP** violation in terms of the entries of the full CKM matrix, in a phase convention independent way. It is easily derived from any parameterisation of the full unitary matrix. Here we will only consider a cyclic ansatz for color and generation number, but this is closely related to the best parameterisation for the matrix.

Each 3×3 mixing matrix must be unitary and also respect unitarity, whereby the sum of norm squares for each row and column equals 1, conserving probabilities [159]. That is, $\sum_i V_{ij} V_{ik}{}^* = \delta_{jk}$ and $\sum_j V_{ij} V_{kj}{}^* = \delta_{ik}$.

In M theory, we consider the cyclic ansatz of *triality*. This gives the cyclicity of particle generations, leaving the probability set invariant under permutations of rows and columns. Given the existence of a single generation ribbon set, this suggests three unbroken $SU(2) \times U(1)$ factors, wherein the mixing of only two generations obeys the exact symmetry. Each factor should belong to the group algebra $\mathbb{C}S_3$, coming from the underlying braids.

The determinant condition on an $SU(2)$ matrix is the same as the unitarity condition. The only way to select an $SU(2) \times U(1)$ matrix that is a circulant sum is as the sum of a real diagonal and an imaginary 2-circulant, namely an extended $R_2(r)$ matrix. The required 3×3 R_2 factors are

$$R_{12}(r) = \begin{pmatrix} r & i & 0 \\ i & r & 0 \\ 0 & 0 & 1 \end{pmatrix} \quad R_{23}(r) = \begin{pmatrix} 1 & 0 & 0 \\ 0 & r & i \\ 0 & i & r \end{pmatrix} \quad R_{31}(r) = \begin{pmatrix} r & 0 & i \\ 0 & 1 & 0 \\ i & 0 & r \end{pmatrix} \tag{214}$$

giving a three parameter mixing matrix of the form

$$V = N R_{12}(a) R_{23}(b) R_{31}(c), \tag{215}$$

where a, b and c are real, and

$$N^{-2} = (a^2 + 1)(b^2 + 1)(c^2 + 1) \tag{216}$$

is the required normalisation factor. As a circulant sum, V then takes the form

$$V = N \begin{pmatrix} abc & -a-c & -b \\ -b & abc & -a-c \\ -a-c & -b & abc \end{pmatrix} \tag{217}$$

$$+ iN \begin{pmatrix} bc & ac-1 & ab \\ ac-1 & ab & bc \\ ab & bc & ac-1 \end{pmatrix}.$$

This is the general form for a cyclic decomposition in terms of generation pairs, because one is always free to scale the imaginary entries of R_{ij} to unit norm. Such matrices are always magic, in the sense that rows and columns have a constant sum.

Neutrino mixing is close to, but not equal to, the tribimaximal probability matrix [160][161]

$$\begin{pmatrix} 1/3 & 1/3 & 1/3 \\ 1/6 & 1/6 & 2/3 \\ 1/2 & 1/2 & 0 \end{pmatrix} \qquad (218)$$

This matrix has many complex representations, including $F_3 F_2$. It takes circulant mixing parameters $(a, b, c) = (1, \sqrt{2}, 0)$. When one parameter is zero there is necessarily a zero probability. Observationally, for both neutrinos and quarks, all the parameters a, b and c are observed to be non zero.

Each mixing parameter has a corresponding braid parameter $t = \pm(r - i)(r + i)$, which is a root of unity. This phase converts a mixing factor to an SL_2 matrix. The overall correcting phase for all three factors is

$$\phi_V \equiv \sqrt{\frac{(a+i)(b+i)(c+i)}{(a-i)(b-i)(c-i)}}. \qquad (219)$$

For the CKM quark mixing matrix, the conjugate numerator and denominator are near to $\pm\pi/24$, so that $\phi_V = \pi/12 + x$ for a small $x \sim 0.0035$, which happens to equal the parameter c for the quarks. This provides a potential further constraint on the parameters given below.

Neutrino experiments are not yet sufficiently accurate to pinpoint the parameters precisely. However, strong evidence for a non zero θ_{13} in neutrino mixing has come to light in recent years [162][163][164]. The accurate Daya Bay result [164] corresponds to an angle of around $9°$. Current estimates for the other two angles are $34.0° \pm 1.1$ (θ_{12}) and $45° \pm 7$ (θ_{23}) [165]. Current constraints, including the Δm^2 values, are:

$$\Delta(m_{12})^2 = 7.59 \pm 0.2 \times 10^{-5} \ \ \text{eV}^2$$
$$\Delta(m_{31})^2 = 2.43 \pm 0.13 \times 10^{-3} \ \ \text{eV}^2$$
$$\sin^2 2\theta_{13} = 0.092 \pm 0.017$$
$$\sin^2 2\theta_{23} > 0.92$$

Observe that $\theta_{13} + \theta_{12} \simeq \theta_{23}$. If the large mixing phase is $47 = 90 - \theta_{13} - \theta_{12}$, then the three phases satisfy a cyclic set of additive relations

$$9 + 34 = 47 \qquad (220)$$
$$47 + 9 = 34$$
$$34 + 47 = 9$$

under the $90°$ tangent rule. Thus the three phases give a 1-circulant, where the third column vector is considered a sum of the first two. A more cyclic representation in terms of the total angle

$$90 = 9.0 + 34.0 + 47.0 \tag{221}$$

sums all three vectors to obtain the democratic probability matrix. With these angles, all in agreement with the data, the neutrino mixing probabilities from V are given by

$$|V_\nu|^2 = \begin{pmatrix} 0.01 & 0.48 & 0.51 \\ 0.60 & 0.17 & 0.23 \\ 0.39 & 0.35 & 0.26 \end{pmatrix}. \tag{222}$$

Consider now the CKM mixing matrix. Recent experimental estimates [157] of the unsquared CKM amplitudes, for a complex CKM matrix V_{CKM}, are given by

$$\begin{pmatrix} 0.97427 \pm 0.00015 & 0.22534 \pm 0.00065 & 0.00351 \pm 0.00015 \\ 0.22520 \pm 0.00065 & 0.97344 \pm 0.00016 & 0.0412 \pm 0.0011 \\ 0.00867 \pm 0.00030 & 0.0404 \pm 0.0011 & 0.999146 \pm 0.000046 \end{pmatrix} \tag{223}$$

which is closely approximated by the three parameter product

$$V_{\text{CKM}} = N R_{12}(a) R_{23}(b) R_{31}(c) \tag{224}$$

for $a = -0.231$, $b = 24.0$ and $c = 0.00347$. These parameters correspond to the Euler angles of the standard parameterisation, but are now responsible for crucial phases in this kinematic CKM matrix. Observe that the CKM entry 0.999133 is recognised as $24/\sqrt{24^2 + 1}$. Such basic fractions are the reason for selecting r as a parameter, rather than the usual cosines and sines. The number 24^2 is a Postnikov volume for the S_4 permutohedron source coordinate $(1, 2, 3, 4)$. The small parameter c is close to $1/288$, where 288 is the volume for the target S_4 vertex $(4, 3, 2, 1)$. The remaining Cabibbo parameter a might be determined by (219) under the constraint $\pi/12 + c$. Note that the split octonion quarks fit on a cube, but the cube does have natural coordinates within the $\mathbb{Z}^4$ lattice. Recall that the cube vertex $(1, 1, 1, 1)$ has volume 24. Moreover, as a three dimensional cube, it collects the signature classes from S_4. Since such canonical volumes are intimately related to probabilities [84], either as V or $1/V$, it is not unlikely that they contribute in some way to fundamental probability arrays.

Since two factor products are effectively unordered, we interpret the three factor ordering as a noncommutative aspect of triality. As noted below, *all* unitary matrices in $U(3)$ have a neat parameterisation in terms of cyclic mixing matrices. The cyclicity of oscillations

$$\nu_e \to \nu_\mu \to \nu_\tau \to \nu_e$$

is now associated directly to three $t \mapsto 1/t$ braid maps. In other words, mirror particle pairing is driving the oscillations.

Although dynamical contributions are important, in some instances this cyclic approximation may roughly determine observables. For example, a simple B_s physics CKM parameter

$$2\beta_s \equiv 2\arg(V_{ts}\overline{V}_{tb}\overline{V}_{cs}V_{cb}) \tag{225}$$

is easily computed. Using the cyclic CKM phases, we obtain a $2\beta_s$ value of -0.0388, in agreement with Standard Model fits [166]. Note that the value -0.0388 comes mainly from the V_{ts} term. In terms of the parameters, the angle β_s is closely approximated by the product abc. Similarly, replacing strange quarks by down quarks, we obtain the value $\sin 2\beta = 0.649$, which is only a little lower than recent measurements indicate [167], and a non standard result. Such anomalies will be accurately measured by the LHCb experiment [168].

In [169], Gibbs proved that any 3×3 unitary matrix U could be written in the form

$$U = \begin{pmatrix} \psi_1 & 0 & 0 \\ 0 & \psi_2 & 0 \\ 0 & 0 & \psi_3 \end{pmatrix} V \begin{pmatrix} \phi_1 & 0 & 0 \\ 0 & \phi_2 & 0 \\ 0 & 0 & \phi_3 \end{pmatrix} \tag{226}$$

for a magic matrix V, and phase diagonals. This was extended to unitary matrices in any dimension by S. Lisi [170]. It follows that the circulant parameterisation, which is magic, characterises some essential behaviour of unitary mixing.

7.5 Koide Rest Mass Triplets

The leptons and quarks have the observed rest masses [171]

	m (MeV/c^2)
e^-	0.510998910(13)
μ^-	105.6583668(38)
τ^-	1776.84(17)
d	4.1 - 5.7
u	1.7 - 3.1
s	100 ± 30
c	1290 ± 110
b	4190 ± 180
t	172900 ± 1500

and the neutrino states satisfy the current bounds [165]

$$\Delta m_{12}{}^2 = 7.59 \pm 0.20 \times 10^{-5} \text{ eV}^2$$

$$\Delta m_{31}{}^2 = 2.43 \pm 0.13 \times 10^{-3} \text{ eV}^2$$

As a triplet of real numbers, a diagonal rest mass matrix is Fourier transformed to a Hermitian circulant. This is a basic rest mass operator. Alternatively, a Hermitian circulant matrix gives directly a triplet of rest mass eigenvalues. The off diagonal entries, responsible for mass splitting, are characterised by a single complex phase. There is one rational phase component which turns out to be universal, and a second phase component that only appears for the neutral stranded neutrinos, and possibly the quarks. Conjugation of this secondary phase is interpreted as a mirror process, under the $t \mapsto 1/t$ mirror map.

The twistor vertices (150) correspond to the permutations (231) and (312), which give the ϕ and $\overline{\phi}$ phase components of M. This conjugation showed up in the homogeneous transformations $Z \mapsto \phi Z$, $W \mapsto \phi^{-1} W$ [107][106]. The operators M are defined in terms of twistors in chapter 10.

First, recall the inverse pair of 3×3 circulant mutually unbiased bases

$$R_3 = \frac{1}{\sqrt{3}} \begin{pmatrix} 1 & \omega_3 & 1 \\ 1 & 1 & \omega_3 \\ \omega_3 & 1 & 1 \end{pmatrix} \quad R_3{}^{-1} = \frac{1}{\sqrt{3}} \begin{pmatrix} 1 & 1 & \overline{\omega_3} \\ \overline{\omega_3} & 1 & 1 \\ 1 & \overline{\omega_3} & 1 \end{pmatrix}. \quad (227)$$

Note that $R_3{}^2$, which is the natural increment from R_3 in the cyclic group, is the inverse only up to a factor of i. Thus R_3 is really a 12th root of I_3. However, bases are equivalent up to multiplication by a complex scalar. Along with I_3 and F_3, these are the 3×3 analogues of the Pauli unbiased bases, appropriate for describing real measurements with three outcomes. We need a Hermitian matrix, so one must sum R_3 and $R_3{}^{-1}$ with the same coefficient, to obtain the simplest mass matrix

$$H = \begin{pmatrix} 2 & \omega_6 & \overline{\omega_6} \\ \overline{\omega_6} & 2 & \omega_6 \\ \omega_6 & \overline{\omega_6} & 2 \end{pmatrix}. \quad (228)$$

Any multiple of I_3 may be added, since I_3 is another basis. The Schur square root of H

$$H_S = \begin{pmatrix} \sqrt{2} & \omega_{12} & \overline{\omega_{12}} \\ \overline{\omega_{12}} & \sqrt{2} & \omega_{12} \\ \omega_{12} & \overline{\omega_{12}} & \sqrt{2} \end{pmatrix} \quad (229)$$

contains the basic arithmetic phase $\pi/12$, as in (47). Using conjugate phase multiples of R_3 and $R_3{}^{-1}$, we have a general Hermitian circulant. Note that the special matrix H is fixed under the operation $H \mapsto H^2$. Testing a general diagonal parameter x and phase $\phi \neq 1$, simple algebra shows that only the sixth roots have fixed points, at $x \in \{2, -1\}$ for ω_6 and $x \in \{-2, 1\}$ for ω_3. However, if we let ϕ vary on iteration, then $x = x(\phi)$ can be fixed by maps $H \mapsto H^n$, in which case ϕ will eventually return to itself. At the Schur value $x = \sqrt{2}$, $\phi \simeq 4\pi/23$ rad fixes $H \mapsto H^3$. This cubic rule may be viewed as a ternary analogue of quantum mechanical projection $P^2 = P$. Appropriately,

the rational 4/23 appears in chapter 10 as an entropic probability for three unary fermion states.

The well known Koide formula [172][173] for the three charged lepton rest masses correctly predicted the τ mass, and has since been applied to neutrino triplets and hadrons [174]. This formula arises from a triplet of eigenvalues for a circulant $\sqrt{M}$ at some scale μ,

$$\sqrt{M} = \sqrt{\mu}(I_3 + z(231) + \overline{z}(312)) = \sqrt{\mu}\begin{pmatrix} x & \phi & \overline{\phi} \\ \overline{\phi} & x & \phi \\ \phi & \overline{\phi} & x \end{pmatrix}, \qquad (230)$$

where z is complex, $x^{-1} = |z|$ and $\phi = \arg(z)$. The eigenvalues are then

$$\sqrt{m_i} = \sqrt{\mu}(1 + 2|z|\cos(\arg(z) + \frac{2\pi i}{3})), \qquad (231)$$

for $i = 1, 2, 3$. The square root best displays the following empirical data, but now we can assume that each mirror component contributes equally to the mass operator M. Both charged leptons and neutrinos have mass triplets fitted with $x \simeq \sqrt{2}$, as in H_S. As discussed in [174][175], the charged lepton phase is 2/9, while the neutrino states are assigned a phase $2/9 + \pi/12$. The charged quark triplets are at first roughly fitted using phases 2/27 for the up triplet, and 4/27 for the down triplet. The quark $|z|$ value is related to the lepton value by basic trigonometry [176][177], with the lepton triangle inscribed inside the up quark one. This is

$$f(\sqrt{2}) \equiv |z| = \frac{1}{\sqrt{2}}\frac{\sin(\omega_{12}{}^5 - 4/27)}{\sin \omega_{12}}.$$

A natural charged lepton scale is given by $\mu_l = 313.8$ MeV, which equals the dynamical quark mass $m_p/3$. More recently it was observed [178] that the alternative (b, c, s) quark triplet fits the lepton value of $x = \sqrt{2}$ with a phase of 6/9. There is also a tripling of scales in $3\mu_l$, paired to the tripling of the 2/9 phase.

Quarks do not require a large secondary phase component, but might be corrected by a phase π/N. Now all fundamental Koide scales are empirically related to m_p, using basic braid parameters. Including mirror neutrinos, the table below contains the theoretical mass values for the Koide parameters. The leptons require a small phase adjustment to fit the accurate measurements. We set a somewhat arbitrary basic mass scale $\mu_0 = m_p/5$ MeV, for the proton mass m_p. In the table, all triplets then fit within current observational constraints, and the Koide eigenvalues therefore provide precise predictions for the rest masses.

	x	ϕ (rad)	μ (MeV)	m
e^-	$\sqrt{2}$	$2/9$	$5\mu_0/3$	0.51095
μ^-				105.65
τ^-				1776.82
u	$f(\sqrt{2}) = 1.76$	$2/27$	$120\mu_0$	2.0
c				1249
t				171546
d	$\sqrt{3}$	$4/25$	$3\mu_0$	5.0
s				83.3
b				4148
b	$\sqrt{2}$	$2/3$	$5\mu_0 = m_p$	4190
c				1356
s				92
ν_1	$\sqrt{2}$	$2/9 + \pi/12$	$5 \times 10^{-11}\mu_0$	0.00038
ν_2				0.0087
ν_3				0.0497
$\nu_1{}^m$	$\sqrt{2}$	$2/9 - \pi/12$	$5 \times 10^{-11}\mu_0$	0.0006
$\nu_2{}^m$				0.00117
$\nu_3{}^m$				0.0581

Recall that the universal $2/9$ is a basic path probability for the central point of the qutrit tetractys, and may be viewed as the volume 6 for the canonical coordinate $(1, 1, 1)$. Similarly, $2/27$ marks the coordinate $(2, 1, 0)$ and $2/3$ the coordinate $(0, 1, 2)$. We can take $120 = 5!$ as a volume for $(1, 1, 1, 1, 1)$, although it is not yet clear how these scales arise. The product $\sqrt{3}f(\sqrt{2})$ of up and down parameters equals 3.049, which is the side length of the Koide up quark triangle in the (r, ϕ) plane [176]. The lepton triangle has side length $\sqrt{6}$, which is similarly a product of the $\sqrt{2}$ and $\sqrt{3}$.

Note that we can always choose off diagonal entries of norm 1 in $\sqrt{M}$ by absorbing a scale into the parameter μ, which is where our arbitrary choice of units is hidden. Since a Hermitian matrix is a 1-circulant, it can only have a 2-circulant component equal to a multiple of the democratic matrix

$$D = \begin{pmatrix} 1 & 1 & 1 \\ 1 & 1 & 1 \\ 1 & 1 & 1 \end{pmatrix},$$
(232)

which is both a 1-circulant and 2-circulant. Taking a Hermitian matrix in the form

$$\frac{\pm i}{\sqrt{3}} \begin{pmatrix} 0 & v & -v \\ -v & 0 & v \\ v & -v & 0 \end{pmatrix} + \frac{1}{\sqrt{3}}D$$

it follows from normalisation that $v = \sqrt{2}$. The Hermitian matrices are in general the sum of three equal phased mixing factors, giving them an

interpretation as a *one time* operation. The reduction to one time variable is a homogeneous mixture of three, presumably responsible for setting the mass scale.

Consider again the mirror ansatz, where rest mass creation comes from braid pair localisation. For a boson there is only one mass state, because there are no braid crossings to generate a mirror. Since the 2/9 phase is observed to be universal amongst Standard Model particles, we use the secondary phase component to discuss the possibility of distinct mirror Koide states, which may be associated to observable phenomena.

A total phase conjugation does not alter the rest mass triplet, so only two mismatched phase components can generate distinct mirror states. For reasons that will be discussed in chapter 11, the Koide scale μ is thought to be fixed by the mirror triplet, just as ordinary matter sets the same scale for the mirror triplet. There is no CPT violation, because the mirror pair is its own annihilation pair. So in principle we permit distinct mass states for the second so called sterile neutrino triplet.

Now the neutrino $\sqrt{M}$ has a $2/9 - \pi/12$ mirror phase, where only the $\pi/12$ piece has been conjugated. With this phase, one may easily verify that the central mirror mass state corresponds precisely [179][180] to the current CMB temperature of 2.73 K, at 0.00117 eV. In a quantum universe, the CMB is not merely a cosmic relic of essentially arbitrary temperature, but a *local* observation of neutrino mass creation. The heavier particles are created at hotter horizons. We determine that the CMB was hotter in our imagined cosmic past precisely because there is an inverse duality between the mirror temperatures and their partner masses, which start out at zero at the conformal horizon.

The Koide coincidences lead to a significant reduction in the number of parameters required in the Standard Model. Mass is energy, and energy conservation is associated classically to local time symmetry [181]. In chapter 11, the nonlocal asymmetry of *cosmological* time is associated to the rest mass splittings and the generation of dynamics. In chapter 10 we also look at how entropy is described using these matrices and their quantum information content. In the eigenvalue space $\mathbb{R}^3$, the charged lepton Koide vector is rotated by $\pi/4$ from the $(1,1,1)$ vector, as originally noted in [182]. The $(1,1,1)$ vector sits at the centre of the word monoid tetractys, denoting mixed paths of type XYZ, which altogether represent the S_3 permutations that underlie mass circulants.

7.6 Symmetry Creation and the Higgs Boson

The electroweak theory of the Standard Model begins with the unbroken Lie symmetry $SU(2) \times U(1)$. In the gauge theory [183] this symmetry is *spontaneously broken* down to the $U(1)$ of electromagnetic charge. In the ribbon picture, *space* consists of only three (or six) abstract points, marked by a

horizontal cut on a braid diagram. So the redundant gauge is, in some way, specified with only three $U(1)$ phases, as in the mixing parameterisation.

The Higgs mechanism of the Standard Model [138] introduces a potential, contributing extra terms to the local Lagrangian to give rest masses to local states. In the emergent theory, we require spacetime to arise from quantum information, and so the symmetries that act upon spacetime must also be emergent. We know that $SU(2)$, for instance, is the set of unit quaternions, which may be considered independently of the representation theory of Lie groups. To a mathematician, quantum arithmetic replaces representation theory in the so called Langlands correspondence.

An exact $SU(2) \times U(1)$ symmetry appears in the MNS and CKM mixing matrices, with the circulant parameters. These $\mathbb{C}S_3$ objects may be constructed from braid mirror pairs. A braid on its own displays no natural classical symmetry. In the braid picture, what does the Higgs boson look like?

Dharwadker et al [141] correctly predicted the Higgs boson mass $m_H = 126$ GeV in 2009, using the relation

$$ m_H = \frac{1}{2}(m_{W^+} + m_{W^-} + m_Z) = \frac{m_Z}{2}(1 + 2\cos\theta_W), \qquad (233) $$

where θ_W is the Weinberg angle, which for us is close to $28°$. This is a Koide eigenvalue with parameter $x = 1$ and a scale set by m_Z. The Higgs is presumed to create a condensate of pairs with mass $2m_H$. Under the mirror ansatz, it is natural to split the pair so that each mirror sector claims one m_H. Consider the decomposition of a Koide matrix

$$ M = \mu_{WWZ} \begin{pmatrix} x & 1 & 1 \\ 1 & x & 1 \\ 1 & 1 & x \end{pmatrix} + \mu_{\gamma f \bar{f}} \begin{pmatrix} 0 & iy & -iy \\ -iy & 0 & iy \\ iy & -iy & 0 \end{pmatrix} \qquad (234) $$

into real and imaginary parts, giving a (W^+, W^-, Z) degenerate triplet and a $(\gamma, f, \bar{f})$ creation annihilation triplet. Since photons are the only massless states, this is an essentially unique way to view a Koide matrix in terms of real and imaginary parts. Here we take $x = \sec\theta_W \simeq 1.13$.

The Dharwadker geometry [185] is hypothesised to come from a particular *Steiner system* [186] known as the Witt design. This special set, called $S(5, 8, 24)$, is a collection of 759 length 8 subsets, known as octads, of a 24 letter alphabet, such that every 5 element subset of $S(5, 8, 24)$ is contained in exactly one octad. It may be constructed using the 24 dimensional parity cube, which is associated to a state space for 24 qubits, where 0 and 1 give the characteristic function for subsets of 24.

First, put all the length 24 binary strings in lexicographic order. Then, from the top, delete any string that does not differ in at least 8 places from any previous one. The resulting 4096 strings form the extended binary

Golay code [187]. The strings with exactly 8 plus signs are the $759 = 3 \times 253$ octads.

There are 24 quarks and leptons, not including antiparticles but including generation number [185]. A two sheeted Riemann surface representing the causal wave function is given a coloring by fermion discs, with quark color joining three quark discs together at a trivalent vertex, but all other particles are separated on the sheet. The surface is divided into 8 quadrants, for u, d, e^-, ν and their antiparticles. There is a total of 48 local regions for all quarks and leptons. The 24 double points are a state space for the higher dimensional parity cube. Alternatively, we could study the geometry of more complicated polytopes in lower dimension, such as the 24 vertex permutohedron.

The ambient space on the surface is supposed to be the fourth color of the four color mapping theorem, which states that any proper map in two dimensions requires no more than four colours. That is, the particle surface should model any two dimensional space, as a matter of principle. The fourth color is where the bosons live, under the supersymmetry that maps small fermion discs to large open boson spaces, as in open closed duality for a ribbon graph. The Higgs boson sits at the central zero point, on both the matter and antimatter sheets. Only the W and Z states have access to this point.

The four color theorem was proved only using a computer search. Mathematicians have hypothesised [188] that the maximum of 4 corresponds to the quantum algebra limit given by the braid parameter δ^2 at t a root of unity. This parameter can be expressed in the form $4\cos^2\theta$, which clearly has a maximal value of 4. For the braid circulants this factor of 4 showed up in the unnormalised 2×2 probability matrix, which has 4 braid components. These braid pieces are used in the ribbon scheme to distinguish two mirror states and two antiparticle states. Note also that the parity cube is associated to the Leech lattice in dimension 24, given by the standard construction. The projection of the 24 source axes on the cube give the fundamental roots ω_{24} in the complex plane.

It will be interesting to study anomalous observations using the emergent scheme. For instance, parity sign symmetries in M theory have been used [190] to explain the Wjj dijet anomaly [189]. Although an explanation in terms of multiple Z generations has been ruled out using local methods, the color Z triplet in the ribbon spectrum permits multiple states without altering the one generation characteristic [145].

Localisation should also clarify the meaning of bound state. The arithmetic structure of state spaces extends the qubit quantum mechanics that is usually applied to atomic or chemical bond structure. The simplest atom, the deuteron, has a formation energy that happens to equal the current constraint on $m_n - m_{\overline{n}}$, the difference between neutron and antineutron masses. Thus, as with the neutrinos, the neutrons could display a distinct

mirror behaviour [191], distinguishing free and bound states. Without the extra complication of charge, neutral particles are the perfect laboratory for studying gravity.

8 Knots, Ribbon Graphs and Motives

The general aim is to find a category **Mot** that describes a special class of spaces. Motives should provide a universal type of homology and cohomology, so that a category **Space** of spaces has an arrow **Mot** → **Space** that sends the universal cohomology to the usual one.

Unfortunately, universality is usually discussed in a 1-categorical sense. To a physicist, however, motives are about the emergence of classical geometry from quantum information. The numerical results of an experiment are invariants for the geometry of the experiment, and so we need to consider noncommutative and nonassociative geometries.
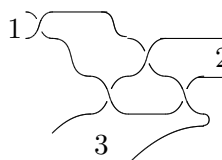
Usually, the functors go from a spatial category to an algebraic one, but since our geometric objects are always equipped with algebraic data, it makes more sense to work with endofunctors **Mot** → **Mot**. To start with, we seek the right diagram categories. Algebras for knots are a big clue about the structure of **Mot**, using the inspiration of three dimensional categories. In the following few sections we look at the Temperley-Lieb category **TL** of planar diagrams, and its connection to twistor diagrams.

A Temperley-Lieb generator on two points is a diagram in (153). However, the arc diagram represents (21) in the Temperley-Lieb algebra, while it gives the identity (12) in planar twistor diagrams [116][117]. And (21) for twistors is the identity for the Temperley-Lieb algebra. This basic confusion between (12) and (21) appears to be responsible for the ubiquitous 2×2 mixing circulants. Diagrammatically, such a sum is the duality of an open string vertex

$$(235)$$

The planar twistor diagrams for $n > 2$ are built with $4(n-2)$ ribbon vertices, including the boundary legs. These are the W and Z variables of causal structure. An extension to true braided ribbon diagrams will require a cyclic structure for braids. A particle braid in B_3 is usually drawn acyclically with three top inputs and three bottom outputs. But the standard trace joins these points in pairs. This could be used to create open ribbon legs.

For example, $\tau_1{}^{-1}\tau_2$ on the points $\{1, 2, 3\}$ is paired with two extra crossings to create a zero writhe ribbon vertex out of the figure eight knot.

$$(236)$$

This is not a twistor vertex, because the edge paths are no longer cyclic, due to the half twist on leg 1. A three crossing twistor vertex can only create a trefoil knot in B_2. As a traced braid on B_3, this would lead to a separated loop at one leg. Since knotting is related to the essential entanglement of causal states, the figure eight knot is a minimal three way linking diagram. The reversal of ribbon orientation at leg 1 gives the vertex a categorical direction, breaking the cyclicity again. The six new possibilities may be abbreviated to the edge vertices

$$\tag{237}$$

That is, including the standard cyclic twistor vertices, there is a set of eight vertices labeling the corners of a parity cube.

The figure eight knot is hyperbolic, in contrast to the trefoil knot, which is a torus knot [192]. Its complementary space in dimension three may be constructed from two ideal hyperbolic tetrahedra. This knot gives the smallest of all such hyperbolic volumes, at a normalised value of 2.0299. The holographic complement of the figure eight knot also has the property that its ribbon template diagram [31] contains *all* knots, as a branched surface. This is the so called universal template of Ghrist, which uses four letters for the knot monomials, just like RNA or DNA.

The figure eight knot is a writhe zero knot. Consider again the writhe zero links in the standard planar representation. For $a \in \mathbb{Z}$, consider the $w = 0$ braid words $t_{i,a}{}^\pm \equiv \tau_i{}^a \tau_{i\pm1}{}^{-a}$ in B_n. This includes the fundamental particle braids at $a = \pm1$. In B_n, there are $4(n-2)$ braids of the form $t_{i,\pm1}{}^\pm$. Observe that all $w = 0$ links in B_n are given as words in the $t_{i,a}{}^\pm$, since a general braid word $\tau_{i_1}{}^{a_1} \tau_{i_2}{}^{a_2} \cdots \tau_{i_k}{}^{a_k}$ satisfies $\sum a_i = 0$. For instance, $\tau_1{}^2 \tau_3{}^{-1} \tau_2{}^{-1}$ is expanded to $\tau_1{}^2 \tau_3{}^{-2} \tau_3{}^1 \tau_2{}^{-1}$. Another example is $\tau_1 \tau_4{}^{-1}$ in B_5.

$$\tag{238}$$

Recall that double knots in B_{2n} can have the writhe augmented by any $n \in \mathbb{Z}$ via the addition of a ribbon twist within B_{2n}. Therefore any link in B_n has a $w = 0$ ribbon representation in B_{2n} with particle generators $t_{i,a}{}^\pm$.

Let $q = t^{1/2} = \exp(2\pi i/r)$ be a root of unity braid parameter, so that $\delta^2 = q + q^{-1} + 2$ is the q-number $(\llcorner 2 \lrcorner_q)^2$. Then $\delta^2 = 4\cos^2 \pi/r$. The set $\{0, 1, \cdots, r-2\}$ may be considered a set of spin labels for a ribbon functor that describes quantum computation [?]. This functor sends a k qubit state space to a disc marked with $3k$ points. As a configuration space, the disc

has an action of the braid group B_{3k}. For each qubit there are three points, representing the three punctured Riemann sphere $\mathbb{CP}^1$. As a moduli space, $\mathbb{CP}^1$ is in fact a point, since it carries an essentially unique complex structure. Below it will be drawn as a ribbon graph.

This $\mathbb{CP}^1$ point is now a trivalent vertex, just like the vertices that appear in twistor scattering. As categorical diagrams, these basic vertices are pieced together to form *spin networks* [196]. In particular, a two qubit system for the modular functor corresponds to B_6 braids on the disc, which include the particle states.

8.1   Temperley-Lieb and Hecke Algebras

The Catalan numbers C_d, which enumerate the vertices of the associahedra, also give the dimension of the Temperley-Lieb algebra TL_{d+1} [193]. The diagram representation of TL_{d+1} has d generators e_i, $i = 1, \cdots, d$, such that
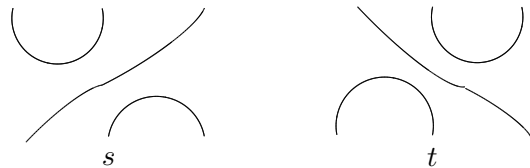
$$e_i{}^2 = \delta e_i \quad e_i e_{i\pm 1} e_i = e_i \tag{239}$$
$$e_i e_j = e_j e_i \quad |i - j| \geq 2$$

for $\delta \in \mathbb{C}$. An element of TL_{d+1} is a string diagram from $d + 1$ points to $d + 1$ points in the plane, such that non crossing arcs and loops are permitted. Note the similarity of the relations to those for the braid groups. Composition in TL_{d+1} is given by the vertical gluing of diagrams, as for braids. The generators of TL_3 are

$$\tag{240}$$

When a loop is created in a diagram, it acts as the scalar δ. This can be seen in the relation $e_i{}^2 = \delta e_i$. The identity 1 is, by definition, the same as a braid identity. The other two loop free diagrams in TL_3 are

$$\tag{241}$$

The pair $e_1 e_2$ and $e_2 e_1$ define a basis for TL_3, since for instance $e_1 e_2 \cdot e_2 e_1 = \delta e_1$. This is enumerated by $C_2 = 2$.

Compare this to the $d + 1$ leaved trees that define the vertices of A_d. We use the permutations in S_d to determine a diagram word. For example,

(231) is mapped to $e_2 e_3 e_1$. Now observe how (132) and (312) reduce to the same Temperley-Lieb diagram on the A_3 pentagon.

$$
\text{(242)}
$$

The TL_d pictures correspond directly to trees. Place a node on each downward arc in the picture, as it is built from generators. These are the tree nodes. Then one only needs to draw lines connecting nodes to other nodes on arcs below it, and include the arc segments going to the top.

Altogether there are 14 loop free pictures in TL_4. This equals C_4, the vertex number for the next associahedron, A_4, just as there were $C_3 = 5$ diagrams in TL_3. In other words, there is a second way to match trees to arc pictures, so that A_3 comes from TL_3, rather than TL_4.

The algebra TL_d is generalised to arc pictures from d to k points, for distinct d and k. Let $TL_{d,k}$ denote the vector space with basis given by all possible arc diagrams, equipped with formal addition of diagrams. We can restrict the coefficients to, say, the rational functions in Laurent polynomials in δ, with coefficients in $\mathbb{Z}$.

It is easy to check that the algebra TL_d gives a representation of the *positive* braids in the braid group B_d under the correspondence

$$
\tau_i \mapsto \delta e_i - 1 \tag{243}
$$

as follows. Plug $\tau_i = f(t)e_i - 1$ into the braid group relation $\tau_i \tau_{i+1} \tau_i = \tau_{i+1} \tau_i \tau_{i+1}$. Comparing the two sides forces $f(t)^2 = \delta f(t)$, so that $f(t) = \delta$ unless $f(t) = 0$. The negative generators τ_i^{-1} appear to require an inverse $(e_i{}^2 - 1)^{-1}$, but this is not obviously in TL_d. Inverses are discussed further below. Observe that τ_i mixes the two S_2 diagrams, as if it defines an open string vertex.

As usual, a nice choice of parameter is $\delta = (t^{1/2} + t^{-1/2})$, so that $\delta^2 = 2 + t + 1/t$, wherein we see the Alexander determinant for the writhe zero unknots in B_3. When $t = \omega_n$ there is a unitary representation of B_d, and then $\delta^2 = 4\cos^2 \pi/n$ [95]. These special values may be used to study the numerical range of the Jones polynomial $V_L(t)$.

Now the identity diagram in TL_2 and the generator e_1 look like the arc pictures in the Kauffmann bracket (133). This is important, because the Kauffmann bracket motivates a categorification of polynomial invariants like $V_L(t)$. What does it mean to categorify polynomials? Recall that a categorification of a number was a set, or vector space. The polynomial invariant should be derived from the diagram spaces, just as numbers give cardinalities of sets. This idea is the basis of *Khovanov homology* for links [194][197].

But we already have a space of planar diagrams associated to knots, namely TL_d. Actually, it is better to think in terms of a category **TL**, which has ordinal objects $d \in \mathbb{N}$ and arrow sets given by TL_d, along with algebras $TL_{d,k}$ giving arrows $d \to k$, which are arc pictures from d to k. Then we can also work with the union $\coprod_d B_d$ of all braid groups.

Let us look for diagram inverses within a single TL_d. Consider an arrow $2 \to 2$ which uses $TL_{2,4}$ and $TL_{4,2}$ to cancel the half loops of e_2 in TL_4.

$$(244)$$

It provides an inverse for e_2, but only via conjugation, and one obtains I_2 rather than I_4. One always obtains an identity I_n, where n is the number of through strands in a diagram. This n grades the Temperley-Lieb algebras into subalgebras $TL_{d,k,n}$ for $n \geq 0$. In order to obtain an identity arrow $4 \to 4$, we might conjugate once again with elements of $TL_{4,2}$ and $TL_{2,4}$. This diagram

$$(245)$$

is now weakly equivalent to the identity I_4, remembering the scalar multiple δ^2. But this does not provide true inverses.

Once we have a category, we can invent products between distinct algebras. A category **TL** is permitted to contain TL_d algebras for distinct values of δ. In this setting, we can look for braid inverses τ_i^{-1} in another copy of the Temperley-Lieb algebra.

Consider B_3, where there are two generators e_1 and e_2 giving the positive generators τ_1 and τ_2. The inverse τ_1^{-1} came from a mirror generator τ_2^*, along with $t \mapsto 1/t$ in the matrix. This suggests working with two mirror copies of TL_3, so that the mirror copy provides the correct site for the inverse braid crossing. Let the mirror category **TL*** be the union of all $TL_{d,k}{}^*$, so that e_i^* exists as a generator object in it. Then we choose the correct maps

$$\tau_i^{-1} \mapsto \delta(1/t)e_{n-i}{}^* - 1 \tag{246}$$

into **TL***, which is equipped with the mirror parameter $\delta(1/t)$. The condition $\tau_i\tau_i^{-1} = I$ now states that

$$I = (\delta(t)e_i - 1)(\delta(1/t)e_{n-i}{}^* - 1). \tag{247}$$

A product between a **TL** and **TL*** object has been used. With this product, the full braid group B_n is formally represented. At the unitary values, where $\delta(t) = \delta(1/t)$, the braid product gives a simple rule

$$\delta e_i e_{n-i}{}^* = e_i + e_{n-i}{}^* \tag{248}$$

for the mixed algebra product. Recall that $B_2 = \mathbb{Z}$ is the fundamental group for the unit circle, with $\exp(2k\pi i)$ sitting over 1, for $k \in \mathbb{Z}$. The negatives arise from winding in the anticlockwise direction around the circle, tracing a charge ribbon twist. This suggests labeling our second copy of **TL** with generators e_{-k}, so that

$$e_k + e_{-k} = \delta e_k e_{-k} \tag{249}$$

holds between addition and product in the double algebra. If the product annihilates, we are left with a decomposition of the scalar $\delta = e_k + e_{-k}$.

The Temperley-Lieb category contains Jones-Wenzl projectors p_i [198], satisfying $p^2 = p$. Assuming the usual braid parameters t and δ, the recursion rule is

$$p_d = p_{d-1} - f_d p_{d-1} e_{d-1} p_{d-1} \tag{250}$$

with $p_1 = 1$. The function f_2 is δ^{-1}, in $p_2 = 1 - \delta^{-1} e_1$. For p_3, basic algebra verifies that $f_3 = \delta^{-1}(1 - \delta^{-2})^{-1}$. At each step, projection follows from the projection $f_d p_d e_d p_d$.

The idempotents are often represented by box symbols, to disguise their exact diagrammatic nature. These boxes augment spin networks by creating vertices $d \to d$ that obey the recursion. The δ parameter is required for the TL_d relations at each step, for the generators e_d and e_{d-1}. The recursion hinges on the TL_d relations for all generators.

However, we could consider distinct TL_N, where the underlying t parameter varies with N. Each TL_N contains a distinct set of Jones Wenzl idempotents. One choice is t a $2N$th root of unity, matching matrix characters for B_N representations. Then as $N \mapsto \infty$, the braid phase t approaches 1 and δ^2 reaches the limit of 4. The coefficient f_N becomes small as $p_{\infty+1} \simeq p_\infty$. Comparing braid generators to projectors, the many relations start with $\tau_1 p_2 = -p_2$.

In general, the mirror transformation shifts the Burau matrix τ_i to $\tau_{n-i}{}^{-1}$, just as it transforms the corresponding braid diagram. Using the **TL** and **TL*** product, for any B_n,

$$(\delta(t)e_{n-j}{}^* - 1)(\delta(1/t)e_j - 1) \tag{251}$$

must pick out n identity strands. To each term we apply a Kauffman bracket (133), using the $t \mapsto 1/t$ inversion on the mirror term. By design, the resulting braid rule occurs at one generator site. Substituting the two brackets into the product, we have

$$f(t)I_2 \;\; = \;\; g(t) \; \diagup\!\!\!\!\!\diagdown \;\; + \;\; h(t) \; \diagdown\!\!\!\!\!\diagup \tag{252}$$

with

$$f(t) = 2 + \delta(t)^{-1}t^{1/2} + \delta(1/t)^{-1}t^{-1/2} \tag{253}$$
$$g(t) = t^{-1/4} + \delta(t)^{-1}t^{1/4} \quad h(t) = t^{1/4} + \delta(1/t)^{-1}t^{-1/4}$$

At the special unitary values $\delta = t^{1/2} + t^{-1/2}$, f becomes $\delta + 2$. There is a solution for $f = 1$ at the modular value $t = \overline{\omega_3}$. This is a local Jones type skein rule. Temperley-Lieb type relations are also related to Hecke algebras [199].

8.2 B_n and Khovanov Homology

In Khovanov homology [194][197] one has two choices for replacing a crossing, namely the two Kauffman uncrossings, I_2 and e_1 in TL_2. Under the above TL to tree algorithm, e_1 is the unique two leaved tree, which is the 1-ordinal 1. The identity gives an empty tree, because there is nowhere to draw a node. Then an arrow $I_2 \to e_1$ represents the fundamental inclusion of the empty set in a one point set. It is often written $0 \to 1$, so that multiple uncrossing choices are denoted by sequences like 001, or $--+$.

Given a link L with l crossings, Khovanov homology first writes down all possible diagrams with uncrossings in place of each crossing. That is, it takes the set of Kauffman bracket terms for all crossings in L. For example, when L is the trefoil knot $\tau_1{}^3$ in B_2, there are 8 *smoothings* given by the parity cube vertices [197]

$$\tag{254}$$

Each smoothing is assigned a polynomial in $t^{1/2}$. From the Temperley-Lieb algebra, there is a factor of $\delta = t^{1/2} + t^{-1/2}$ for each loop in the traced diagram. This is multiplied by $(-1)^k t^{k/2}$, where k is the number of 1 digits. This gives terms

$$(t^{1/2}+t^{-1/2})^2, \quad -t^{3/2}(t^{1/2}+t^{-1/2})^3, \quad 3t(t^{1/2}+t^{-1/2})^2, \quad -3t^{1/2}(t^{1/2}+t^{-1/2}), \tag{255}$$

where there is a copy of the term for each object. Then all terms are summed together to obtain

$$-t^3 + t^2 + t + t^{-1}. \tag{256}$$

The $w = 0$ unknot determinant is subtracted, giving $-t^3 + t^2 - 1$. There is also an overall factor of t for the writhe $w = 3$, recalling that the writhe factor turns the Kauffman bracket into the Jones polynomial. Finally, we obtain the standard form of the Jones polynomial for the trefoil knot,

$$V_{\tau^3} = t + t^3 - t^4. \tag{257}$$

The Khovanov diagram space is a *categorification* of the Jones polynomial, because we derived the polynomial from it in much the same way that ordinals come from counting sets. It can distinguish knots that are not distinguished by V_L.

The true Khovanov invariant $[L]$ is a sequence of graded modules, each coming from the diagram set at a given k. The shift map $0 \to 1$ is the fundamental flip operation on Kauffman pictures, and it defines the arrows of the parity cube. Note that this is *the reverse process* to the ordinal arrow between trees. And now the $0 \leftrightarrow 1$ pair is associated to the S_2 mixing, between twistor diagrams and Temperley-Lieb ones. So the diagrams give an invariant more powerful than the Jones polynomial, they appear in twistor theory, and they also correspond to rooted trees.

The Khovanov axioms use an abstract loop space V, which has the quantum dimension δ. It allows the gluing of two loops via a reverse flip, $m : V \otimes V \to V$, and the separation of a loop $\Delta : V \to V \otimes V$. On trees, these are the standard bialgebra vertices.

The $\{A_d\}$ and S_d operads define oriented polytopes in every dimension $d \in \mathbb{N}$. The Temperley-Lieb algebra has given us at least two ways to picture S_d and A_d. A permutation either (i) acts on the nodes of a tree with $d+1$ leaves, associated to TL_{d+1}, or (ii) comes from the d strands of B_d in TL_d. Case (i) uses point objects and case (ii) uses one dimensional edges or strings. Geometrically, the exchange of points and edges should define a Poincare duality for the one dimensional space. Categorically, there is a *shift operation* d^{-1} from TL_{d+1} to TL_d.

Remark 8.1 The tree differential of (5.3) also reduces the number of leaves by 1. It creates unions of rooted trees, and these underlying forest objects naively belong to multiple copies of the associahedron. However, in chapter 5 we saw that *noncommutative* forests are also counted by the Catalan numbers C_d, and the corresponding parking functions label simplex decompositions of the associahedra and other polytopes.

Consider again the positive knots, where the writhe w equals the number of crossings. This fixes the dimension of a Khovanov parity cube. This cube is a reduction of S_d for $d = w + 1$, the rooted trees with $w + 2$ leaves, and their diagrams in TL_{w+2}.

Take the codimension 1 faces on A_{2m} for $2m = w+1$. These are specified by the two node trees with node valency $m+2$, or by $k = 0$ sign strings from S_{2m+2}. To the positive writhe w knot in B_2 there is associated a *chorded braid* diagram [101]. This is a Feynman diagram with w loops, created as follows. For the trefoil knot, insert two horizontal chords on the braid,

connecting the first strand with the second.

$$a_1 \smile a_2 \qquad b_1 \qquad \qquad (258)$$

Ensure that at least one crossing lies between a pair of chords. The traced knot defines a planar loop with the two chords attached, forming a three loop diagram. Start at a_1 and trace a path along the braid to determine the positions of the vertices. There are two possible chordings on the trefoil. For harder knots, crossed chords are necessary [101]. For B_2 torus knots of odd writhe, there are $m = (w+1)/2$ chords. This corresponds to the leaf count of $m+1$ at *one node* on the A_{2m} face, that is the 1-ordinal m. These leaves count the loops in the Feynman diagram, or rather the number of cuts required to reduce it to a tree.

This knotty Feynman diagram is associated to the numerical zeta value $\zeta(w)$. This is also obtained from A_d using motivic methods, as discussed below. Such braid chord diagrams can be thickened into cyclic ribbon graphs.

8.3 Ribbons and Moduli Spaces

We have seen that two level rooted planar trees correspond to globule diagrams for a 2-category. The pointlike nature of arrow sources and targets is associated to the pointlike nature of particles in the Feynman formalism. But trees can be thickened to ribbons, drawn with a total of $2n$ lines. The Riemann sphere $\mathbb{CP}^1$ with three punctures is drawn as the interior of the flat ribbon diagram

$$ \qquad (259) $$

where the outside line is a loop about ∞, and the other loops traditionally mark the points 0 and 1. Although the continuum appears to be packed into the ribbon picture, we view ribbons as abstract geometric objects, prior to the existence of $\mathbb{C}$ itself.

There is a very fundamental reason for introducing ribbon graphs. Recall that for the associahedra A_d, the tree nodes correspond to the bracketing of letters in a word, such as $(a \otimes (b \otimes c))$. Consider the basic associator $(12) \to (21)$ of section (5.4). Ideally, the associator should be a *loop* rather

than an edge, because it describes a homotopy. Using the ribbon diagram

$$\tag{260}$$

the cyclic plat trace gives a picture of a Riemann sphere $\mathbb{CP}^1$ with 5 punctures, imagining the inside of the ribbon as the surface. What does this have to do with the associahedra?

Consider the complex equivalence classes of 5-punctured Riemann spheres, allowing for the degenerate cases where punctures collide. This defines a compactified *moduli space* $\mathcal{M}_{0,5}$ [200]. Now the real number points of the moduli space $\mathcal{M}_{0,5}$, which is a combinatorial gadget associated to points on the circle $\mathbb{RP}^1$, define a two dimensional space that is tiled [201] by 12 copies of the A_3 pentagon. In general, there are $(d+1)!/2$ copies of the A_d polytope in the moduli space tiling.

But the A_3 pentagon is the basic axiom for associativity in monoidal categories! In other words, the shape of the punctured sphere is encoding information about the structure of *all* punctured spheres. With a tree diagram, the cyclic trace yielded only a tetrahedron.

Similarly, the cyclic trace of the unique two leaved diagram $(1) \rightarrow (1)$ gives a picture of a 3-punctured sphere, and $\mathcal{M}_{0,3}$ is a point. A point is the A_1 associahedron. The empty polytope A_0 corresponds to a basic ribbon strip, traced into a loop. As a complex space, this is the disc. It will be useful to think of the edge of the disc as the unit circle in the complex plane. So in thickening trees to ribbons, we obtain actual pictures of the complex spaces. Physicists know these as string diagrams, but note that the legs on the string diagram come from the holes in the picture, and *not* from the thickened edges.

The simplification of real spinors in twistor scattering leads to a concrete tiling of punctured $\mathbb{RP}^1$ moduli by the associahedra A_d. The real points of the moduli spaces $\mathcal{M}_{0,n}$, indexed by $n \in \mathbb{N}$, form an operad in the sense that a composition

$$\mathcal{M}_{0,k+1} \times \mathcal{M}_{0,n_1+1} \times \cdots \times \mathcal{M}_{0,n_k+1} \rightarrow \mathcal{M}_{0,n} \tag{261}$$

may be defined using the structure of the A_d tree operad. The complex moduli spaces are similarly related to loop free string diagrams, but these require a higher dimensional operad structure. The real moduli compactification looks at configurations of points on $\mathbb{RP}^1$ [201]. It smooths the moduli by adding points that represent the limiting case of collisions between points,

which work to reduce the number of points in the configuration. These collisions are drawn as bubble offshoots of the original $\mathbb{RP}^1$, introducing strings of loops or, rather, glued polygons. And glued polygons may be viewed as chorded polygons.

The polytope picture for moduli spaces is used to describe relative cohomology invariants that happen to correspond to the n point Veneziano amplitudes [130][131]. These quantities are expressed in terms of the multiple zeta values, which have vanishing symbols. The chords of the n-gon are labeled (ij) and each chord indexes a variable u_{ij}, which is a function

$$\mathcal{M}_{0,n} \to \mathbb{CP}^1 \backslash \{0, 1, \infty\}$$

derived from simplex coordinates t_i. These are cross ratios

$$u_{ij} \equiv [ii + 1 \mid j + 1j] = \frac{(z_i - z_{j+1})(z_{i+1} - z_j)}{(z_i - z_j)(z_{i+1} - z_{j+1})} \tag{262}$$

such that the first three points z_1, z_2 and z_3 are sent to 1, ∞ and 0 respectively, and the remainder are relabeled as t_i. So for n points there are $n-3$ simplex coordinates, where a simplex is chosen with $0 < t_1 < \cdots < t_m < 1$.

Example 8.2 For $n = 5$, there is an edge simplex with coordinates t_1 and t_2. The five chords give

$$u_{13} = 1 - t_1 \quad u_{24} = \frac{t_1}{t_2} \quad u_{35} = \frac{t_2 - t_1}{t_2(1 - t_1)} \quad u_{41} = \frac{1 - t_2}{1 - t_1} \quad u_{52} = t_2$$

defining an affine space of dimension $n(n-3)/2 = 5$.

Each u_{ij} determines a differential form $\omega_{ij} = \mathrm{d} \log u_{ij}$. The face of the associahedron A_{n-2} is given by an equation $u_{ij} = 0$. This polytope correspondence creates pullbacks of differential forms on the lower dimensional associahedra, so that integrals are decomposed into an iterated expression. These multiple zeta value invariants form a rational algebra over a basis set of primitive integrals [128].

As usual, let $s_i = (p_1 + \cdots + p_i)^2$ give the sum of external momenta p_j. We introduce new coordinates x_i defined by $t_i = x_i x_{i+1} x_{i+2} \cdots x_{n-3}$ [130], and also hyperplanes $\alpha_{ij} \equiv x_i - x_j$. The Veneziano integrals then take the form

$$B_n = \int_0^1 \prod_{i=1}^{n-3} \mathrm{d}x_i \ x_i^{-\alpha(s_{i+1})-1} \prod_{1 < i < j < n} (1 - x_{i-1}x_i \cdots x_{j-2})^{-p_i p_j} \tag{263}$$

where the $\alpha(s_i)$ and the $p_i p_j$ are integers.

Example 8.3 Consider seven point amplitudes. This requires 14 affine coordinates u_{ij} representing the chords of a heptagon.

$$u_{13} = 1 - t_1 \quad u_{14} = \frac{1 - t_2}{1 - t_1} \quad u_{15} = \frac{1 - t_3}{1 - t_2} \quad u_{16} = \frac{1 - t_4}{1 - t_3}$$

$$u_{24} = \frac{t_1}{t_2} \quad u_{25} = \frac{t_2}{t_3} \quad u_{26} = \frac{t_3}{t_4} \quad u_{27} = t_4$$

$$u_{35} = \frac{t_3(t_1 - t_2)}{t_2(t_1 - t_3)} \quad u_{36} = \frac{t_4(t_1 - t_3)}{t_3(t_1 - t_4)} \quad u_{37} = \frac{(t_1 - t_4)}{t_4(t_1 - 1)}$$

$$u_{46} = \frac{(t_1 - t_4)(t_2 - t_3)}{(t_1 - t_3)(t_2 - t_4)} \quad u_{47} = \frac{(t_1 - 1)(t_2 - t_4)}{(t_1 - t_4)(t_2 - 1)}$$

$$u_{57} = \frac{(t_2 - 1)(t_3 - t_4)}{(t_2 - t_4)(t_3 - 1)}$$

The full motivic integral is

$$B_7 = \int_0^1 \prod_{i=1}^4 \mathrm{d}x_i \; x_i^{-\alpha(s_{i+1})-1}(1 - x_i)^{\beta_i} \prod_{1 < i < j < n} (1 - x_{i-1}x_i \cdots x_{j-2})^{-p_i p_j}$$

Here, β_i gives an integer ghost term. The ghost elimination from such integrals was crucial to the derivation of the dimension $d = 26$ for bosonic string theory. As in appendix C, in M theory the dimension 26 becomes the dimension of the traceless Hermitian elements of the exceptional 3×3 Jordan algebra over the octonions.

If the $\mathbb{RP}^1$ punctures stand for ribbon legs, a basic four leg vertex has a one dimensional moduli space tiled by three associator edges A_2, forming a triangle $\{0, 1, \infty\}$. These A_2 are given by the S_2 trees, now described by Temperley-Lieb diagrams with the edge extrapolating between I_2 and e_1. The bubble graph

(264)

for four points on $\mathbb{RP}^1$ has three places to put the second circle, representing the collision of two points. This is the same as putting two legs together in a BCFW factorisation, reducing the four valent particle graph to two trivalent factors.

9 Motivic Constructions

The word monoid, with its noncommutative monomials, replaces ordinary simplices in algebraic topology. It is equipped with numerical data. The divided simplices also contain natural representations of categorical polytopes. For example, we saw that the pentagon appears in one corner of the three qutrit tetractys.

On classical d dimensional simplices there is a boundary operation ∂_d, giving the face cells of the simplex. What replaces it for the graded word monoid?

We want the classical simplices at $l = 1$ to obey the usual rule $\partial^2 = 0$ for boundaries. At $l = 2$ the analogue is a $\partial^3 = 0$ rule, as follows. First, a solid simplex goes to all boundary elements under ∂, as usual. The second application of ∂ kills the classical elements, namely the undivided lines, edges and so on. However, it leaves the midpoints on all edges. Only the third application of ∂ kills these mixed paths.

For $l = 3$, we can similarly define a boundary operation such that $\partial^4 = 0$. When the classical faces are killed off, the edge pieces between the two middle points on each edge remain. Another ∂ kills the edges, and leaves the points for the last step. In this way, $\partial^{l+1} = 0$ for all word monoid simplices. Object labels are maintained throughout boundary operations.

Instead of coefficients in $\mathbb{Z}$, which do the canceling for $\partial^2 = 0$, now we require cancelation via a sum

$$a_1 + a_2 + \cdots + a_{l+1} = 0 \tag{265}$$

which is obeyed by the roots of unity $\omega_{l+1}{}^k$. The midpoints on the $l = 2$ simplices should then take on coefficients over $\{1, \omega_3, \overline{\omega_3}\}$, such as the Eisenstein integers. For $l = 3$, objects require the Gaussian integers $\mathbb{Z}[i]$. Combined with the $l = 2$ operations, this introduces ω_{24}.

In order for an $l = 2$ object to cancel out in a boundary, it must occur in *three* higher dimensional cells, rather than two. The midpoints on a triangle themselves define an inscribed triangle inside the $l = 2$ simplex. These three points must together pick out the zero sum for $\{1, \omega_3, \overline{\omega_3}\}$. For two qutrits, these are the points XY, YZ and ZX. The Pauli operators are a noncommutative analogue to $\{1, \omega_3, \overline{\omega_3}\}$.

As usual, simplices for homology define the d-chains in a space M, only now there is a double (d, l) index. The simplex labels are commutative, but the tensor cubes carry all noncommutative monomials. As algebraic data, this is a non abelian coefficient structure for cohomology. Recall that singular cohomology is defined by dualising singular homology [45]. Given coefficients $\mathbb{Z}$, the collection of arrows from the d-chains into the object $\mathbb{Z}$ give the object of d-cochains. Similarly for other abelian coefficient sets, when $l > 1$.

9.1   Comments on Quantum Homotopy

Given divided simplices for $l > 1$, a generic chain complex has a double (d, l) grading. The usual planar notion of homotopy $f : C_\bullet \to D_\bullet$ between two complexes is extended to higher dimension. A cubic segment of such a homotopy

$$(266)$$

introduces length three paths to replace the $\partial_{d+1} f_d$ and $f_{d+1} \partial_d$ paths on the squares [45]. The higher l face carries boundary operations δ such that $\delta^{l+1} = 0$, so that an object in the source $C_{d,l}$ is equally likely to be killed off whatever path it takes to the target.

The classical cone is a homotopy between a d-simplex and a single point. The single point represents the minimal space, because classical homotopy requires a base point to define the trivial loop. In quantum homotopy, this can be relaxed to n base points, since groupoids are just as nice as groups to a category theorist. Moreover, typical groupoids have objects indexed by $n \in \mathbb{N}$, such as the groupoid of braid groups B_n. Now a quantum cone extends the classical cone with its noncommutative internal simplex, sitting over the n points. For example, internal to the two qutrit cone over a triangle is a triangular simplex

$$(267)$$

113

This was an index simplex for the hexagon S_3. The $\pm$ signs of $l = 1$ homotopy are replaced by the cubed roots of unity, or their noncommutative analogue, the Pauli operators. At $l = 2$ there is always a simplex prism inside the cone.

When the other genus zero categorical polytopes are triangulated, classical cones can be created given a base point. For example, the 24 triangles on A_4 are extended to a fifteenth vertex. Each of the boundary triangles then represents a vertex on a dual S_4 permutohedron, and the signatures of the S_4 vertices give a parity cube. The homotopy class π_2 should look at maps using all this structure.

Classical twistor constructions rely on relative homotopy and homology. For single basepoints, the group $\pi_k(M, A)$ is defined for a subspace $A \to M$ [45]. One takes the space ΩA of paths into A, which is a bundle over A, and evaluates $\pi_{k-1}(\Omega A)$ in terms of $\pi_{k-1}(M)$ and $\pi_{k-1}(A)$. Divided simplices automatically provide quantum subsets. Homotopy classes are distinguished by relative contractibility, which is now dictated at *every point* by tree edges and tree differentials.

In the triangulated categories of classical motives, homology and cohomology is constructed from derived functors, using natural chains of objects

$$\cdots \to TTA \to TA \to A$$

associated to an object A. When the arrows are weak equivalences, T is thought of as a projector. Our algebraic projectors instead arose from pairings $X, \overline{X}$ of letters from the word monoid, resulting generally in $l = 2k$ tensor cubes. They all have a noncommutative structure. If a matrix $T \otimes T \to T$ generates such a long sequence, the associated homology maps $H_k \to H_{k-1}$ are a reduction in the quantum grading $2l \mapsto l$, but the simplex dimension is preserved. However, the secondary polytopes associated to the simplices are of distinct dimension, and act as homological cells.

9.2 The Crans-Gray Tensor Product

Recall that distributivity is naturally a three dimensional structure on categorical tensor operations, just as arithmetic knots guide us towards a three dimensional picture for $\mathbb{Z}$. In [14], Crans noted that a natural tensor product for higher dimensional categories was not dimension preserving. In particular, the horizontal composition of two 2-arrows gives a 3-arrow, just as branched 2-surfaces contain three dimensional knots. A generic category of dimension ≥ 2 has such dimension raising compositions, so that beyond dimension 3, space is created from the algebra of surfaces.

To begin with, the Gray tensor product breaks interchange. Put two objects U in $\mathbf{C}_1$ and V in $\mathbf{C}_2$ into a formal pair (U, V). Let g_i be a 1-arrow in $\mathbf{C}_1$ and f_j a 1-arrow in $\mathbf{C}_2$. Then the formal pairs $(g_i, 1_{V_i})$ and $(1_{U_j}, f_j)$ satisfy $(g_1, 1_V)(g_2, 1_V) = (g_1 g_2, 1_V)$ and $(1_U, f_1)(1_U, f_2) = (1_U, f_1 f_2)$. Now

for each pair f and g there is only an isomorphism $\sigma_{fg} : (1_U, f)(g, 1_V) \Rightarrow (g, 1_V)(1_U, f)$. That is, the diagram

$$
\begin{array}{ccccc}
U & \longrightarrow & V & \longrightarrow & W \\
{\scriptstyle 1}\downarrow & \Downarrow\alpha & {\scriptstyle 1}\downarrow & \Downarrow 1 & \downarrow{\scriptstyle 1} \\
U & \longrightarrow & V & \longrightarrow & W \\
{\scriptstyle 1}\downarrow & \Downarrow 1 & {\scriptstyle 1}\downarrow & \Downarrow\beta & \downarrow{\scriptstyle 1} \\
U & \longrightarrow & V & \longrightarrow & W
\end{array}
\tag{268}
$$

may be different, via an isomorphism, from the diagram

$$
\begin{array}{ccccc}
U & \longrightarrow & V & \longrightarrow & W \\
{\scriptstyle 1}\downarrow & \Downarrow 1 & {\scriptstyle 1}\downarrow & \Downarrow\beta & \downarrow{\scriptstyle 1} \\
U & \longrightarrow & V & \longrightarrow & W \\
{\scriptstyle 1}\downarrow & \Downarrow\alpha & {\scriptstyle 1}\downarrow & \Downarrow 1 & \downarrow{\scriptstyle 1} \\
U & \longrightarrow & V & \longrightarrow & W
\end{array}
\tag{269}
$$

Note that these are the usual pictures for interchange, which is now broken. When the crucial four 2-arrows sit on the faces of a tetrahedron, σ_{fg} is the resulting internal 3-arrow. When the Mac Lane pentagon is broken on the six faces of a parity cube, one can fill the cube with a cyclically invariant 3-arrow.

In general, the composition of a p-arrow and a q-arrow results in a $(p + q - 1)$-arrow. Thus categorical structure permits ribbon spectra to generate information in arbitrarily high dimension. The full continuum of the underlying surfaces cannot be constructed until dimension ω, so there is a correspondence between dimensions 2 and ω, a known feature of quantum gravity.

10 Entanglement and Entropy

The *black hole qubit* correspondence [24][25] is a detailed relationship between black hole entropy formulas in M theory and measures of entanglement for multiple qudits. In particular, the extremal BPS solutions have eight charges, a magnetic set (p^0, p^1, p^2, p^3) and an electric (q_0, q_1, q_2, q_3). These correspond to the eight coefficients of an unnormalised three qubit state ψ_{ijk}, so that the black hole entropy is given by

$$S = \frac{\pi}{2} \sqrt{-\Delta(\psi_{ijk})} \qquad (270)$$

where $\Delta(\psi)$ is Cayley's hyperdeterminant [84]. The hyperdeterminant is a natural generalisation of a matrix determinant for a $2 \times 2 \times 2$ qubit tensor cube, which is just the parity cube for a 0, 1 alphabet. In the next section, we see how this invariant is connected to twistor geometry [202].

An acceptable measure of quantum entanglement must show the correct invariance under the equivalence relations of the physical system. These are taken to be the local operations with classical communication (LOCC), or stochastic local operations (SLOCC). Here locality means that transformations act on each qudit separately [203]. For an n qubit system we usually consider a SLOCC group $GL_2(\mathbb{C})^{\otimes n}$, where GL_2 acts locally on each qubit. For a general mixed qudit Hilbert space on n objects, the SLOCC group will be $GL_{k_1}(\mathbb{C}) \otimes \cdots \otimes GL_{k_n}(\mathbb{C})$. When the classical groups are the primary consideration, determinant zero matrices are mostly ignored. But it is now precisely these matrices that shift the entanglement class, and we instead consider the entanglement classification using the underlying categorical combinatorics.

The axiomatic nature of category theory is a good argument for certain choices of entanglement measure, which are by no means yet settled. In some current schemes, an entanglement class can contain both separable states and maximally entangled ones! Here we consider only maximally entangled states, meaning n-partite n qudit systems. For example, for three qubits there are two tripartite classes, one bipartite and one totally separable class. Separability literally means that the state is expressible in terms of $j < n$ components. For four or more qubits, an entanglement measure may require a free parameter, every value of which defines a distinct class. Insisting on restricted coefficient sets at least limits the cardinality of such entanglement schemes.

The interesting invariants may be constructed using *secondary polytopes* [84], introduced below. These polytopes are indexed by finite geometries. For example, one index is the two qutrit word monoid simplex, namely a triangle with edges divided into two. Combinatorially, this is a hexagon, and is used to construct the three dimensional associahedron A_4 via the usual chordings. The natural invariants associated to secondary polytopes

are constructed using matrix minors, as for Grassmannians.

10.1 Entanglement with Trees and Strings

Recall that the $2n$ particle scattering amplitudes include a helicity configuration with n negative and n positive helicities, for $n \geq 2$. Given $2n$ legs on a diagram, there are clearly $h = \begin{pmatrix} 2n \\ n \end{pmatrix}$ ways to assign $\pm$ signs to the legs. Observe that this is $n+1$ times the Catalan number C_n.

It is also the number of minors in the $n \times 2n$ matrix of Grassmannian coordinates, where an $n \times n$ block has been fixed at I_n. These minors are a basis for $\mathbb{C}^h$. When $n = 2$, the Minkowski space Grassmannian gives a basis for $\bigwedge^2(\mathbb{C}^4)$ and the six minors v_{ij} satisfy the Plücker relation

$$V = v_{12}v_{34} - v_{13}v_{24} + v_{23}v_{14} = 0. \tag{271}$$

In [202], the minors for $n = 2$ and $n = 3$ are used to study entanglement for n fermions with two single particle states, $-$ and $+$. When $n = 2$, there is only one true bipartite entanglement class, given by $V \neq 0$. A measure of this entanglement is given by

$$\eta \equiv 8|V| \in [0,1]. \tag{272}$$

When $V = 0$, the two particle system is separable. This means that V can be written in the twistor form $v_{ij} = Z_i W_j - W_i Z_j$ for two 4-vectors Z and W. Now the lowest dimension associahedron related to the Minkowski trees was the geometric point A_1, where two legs are joined in a double root

$$\begin{array}{c} - \quad + \\ \diagdown\!\!\diagup \\ \| \\ +\, - \end{array} \tag{273}$$

to give the 1-ordinal 1. This now represents the unique entanglement class for $n = 2$. A full four leg tree gives $h = 3C_2$, where $C_2 = 2$ counts the objects on the associator edge A_2.

When $n = 3$, there are now $20 = 4C_3$ minors in the 3×6 Grassmanian matrix [202]. We call them V_{ijk}, where as before the index ijk labels the selected columns. The *triple root* trees

$$\begin{array}{c} - \ - \ + \\ \diagdown\!\!\diagdown\!\!\diagup \\ \| \| \\ +\, +\, - \end{array} \tag{274}$$

give the associator edge, with its MHV and $\overline{\text{MHV}}$ source and target. Now $C_2 = 2$ will count the number of tripartite entanglement classes. The first

entanglement measure is $|T_{123}| \in [0,1]$, defined as follows. Let V_{ijk} also denote the numerical coefficient of $v_i \wedge v_j \wedge v_k$ in the full state. Since the ijk index tracks the choice of $\pm$ signs, let the source $s = V_{123}$ and target $t = V_{456}$. The remaining 18 3-forms fit into two helicity conjugate 3×3 matrices,

$$A = \begin{pmatrix} V_{156} & V_{164} & V_{145} \\ V_{256} & V_{264} & V_{245} \\ V_{356} & V_{364} & V_{345} \end{pmatrix} \quad B = \begin{pmatrix} V_{423} & V_{431} & V_{412} \\ V_{523} & V_{531} & V_{512} \\ V_{623} & V_{631} & V_{612} \end{pmatrix}. \quad (275)$$

The measure is defined by

$$T_{123} = 4[(\mathrm{Tr}(AB) - st)^2 - 4\sqrt{\det(AB)}^{-1}\mathrm{Tr}(A^\dagger B^\dagger) + 4s \det A + 4t \det B]. \quad (276)$$

This is chosen to be twice the quartic form $q(x)$ for the *Freudenthal triple system* $\mathbb{C} \oplus \mathbb{C} \oplus J \oplus J$ for the 3×3 matrix Jordan algebra J, where

$$x = \begin{pmatrix} s & A \\ B & t \end{pmatrix} \quad (277)$$

and A and B are in J. The definition is in appendix C. Let us look at the special case of diagonal A and B. This gives eight dimensional vectors

$$V = V_{123} + V_{156} + V_{264} + V_{345} + V_{423} + V_{531} + V_{612} + V_{456}, \quad (278)$$

which specialise further to a three qubit state when indices in $\{1, 2, 3\}$ are replaced by 0, and $\{4, 5, 6\}$ by 1. In this case, the entanglement measure is given by Cayley's hyperdeterminant Δ for a $2 \times 2 \times 2$ three qubit tensor cube, to be discussed further in the next two sections [84]. That is, $T_{123} = 4\Delta(V)$, where

$$\Delta(V) = V_{123}{}^2 V_{456}{}^2 + V_{612}{}^2 V_{345}{}^2 + V_{531}{}^2 V_{264}{}^2 + V_{423}{}^2 V_{156}{}^2 \quad (279)$$
$$-2V_{123}V_{456}(V_{612}V_{345} + V_{531}V_{264} + V_{423}V_{156})$$
$$-2(V_{612}V_{345}V_{531}V_{264} + V_{531}V_{264}V_{423}V_{156} + V_{423}V_{156}V_{612}V_{345})$$
$$+4(V_{123}V_{345}V_{156}V_{264} + V_{456}V_{423}V_{531}V_{612}).$$

Unlike for qubits, the three fermions are distinguishable by their indices, using the six letter alphabet. Consider now an example where $T_{123} = 0$, but the entanglement is still tripartite [202]. Let Φ be the normalised state with $V_{123} = 1/\sqrt{3}$, $V_{456} = 0$, $B \equiv 0$ and

$$A = \frac{1}{\sqrt{3}} \begin{pmatrix} 1 & 0 & 0 \\ 0 & 0 & 0 \\ 0 & 0 & 1 \end{pmatrix}. \quad (280)$$

How do we distinguish this state, known as a $|W\rangle$ state, from a $T_{123} \neq 0$ one? With the Jordan algebra J, one can define a dual state $\tilde{V}$. This turns out to be

$$\tilde{V}_{ijk} = 3\epsilon^{abcdef} V_{ibc} V_{ajk} V_{def}, \qquad (281)$$

which may be taken as a definition for the triality inspired dual. In the example, $\tilde{\Phi}$ is non zero, and this counts as a second entanglement measure. The duality is defined separately for s, t, A and B using triality for J. For $\tilde{\Phi}$, $\tilde{s}$, $\tilde{t}$ and $\tilde{A}$ are all zero, but $\tilde{B}$ is not. Let $C(A)^T$ by the transpose cofactor matrix of A. Then

$$\tilde{B} = 3s C(A)^T = \frac{3}{3\sqrt{3}} \begin{pmatrix} 0 & 0 & 0 \\ 0 & 1 & 0 \\ 0 & 0 & 0 \end{pmatrix}, \qquad (282)$$

from $\tilde{V}_{531} = V_{156} V_{123} V_{345}$. The $1/3$ coefficient comes from the single nonzero C_{ij} determinant. It is also a result that

$$T_{123} = -c\epsilon^{abcdef} V_{abc} \tilde{V}_{def}, \qquad (283)$$

for a normalisation constant c. This shows the origin of the quartic terms in $\Delta(V)$. So $T_{123}(\Phi)$ is zero precisely because of the complementarity of A and its cofactor matrix, but it is constructed from two non zero components, and the existence of a dual signifies an entanglement class distinct from the $T_{123} \neq 0$ class.

We could also specialise T_{123} to a three unary state system, using $1, 4 \mapsto X$, $2, 5 \mapsto Y$ and $3, 6 \mapsto Z$. This is a qutrit. Now each leaf on the signed tree is paired to its conjugate root leg. The hyperdeterminant Δ then becomes an expression in the 1-circulant three qutrit words, for XYZ the identity,

$$\Delta = (1 - 4V_{XYZ}{}^2)(V_{ZXY}{}^2 + V_{YZX}{}^2) \qquad (284)$$
$$-2V_{ZXY}{}^2 V_{YZX}{}^2 + 8V_{XYZ}{}^2 V_{ZXY} V_{YZX}.$$

If the 1-circulants form a 3×3 Hermitian Koide matrix with diagonal $V_{XYZ} = xI_3$ and off diagonal complex phases ϕ and $\overline{\phi}$, then we have a normalised state such that $T_{123} = (4/3)(\tan^2 \phi)(4x^2 - 1)$.

Remark 10.1 Since any SLOCC transformation of a three term W state returns another W state, mixing matrices with three non zero parameters may be viewed as triplets of W states. When the $(1/3, 1/3, 1/3)$ vector is in the Φ basis, the degenerate tribimaximal mixing matrix consists of two W states and one separable one.

For the three qubit state Υ with coefficients a_{ijk}, consider a projective

coordinate fix of $a_{000} = 1$. Cayley's hyperdeterminant is then reduced to

$$\Delta(\Upsilon) = a_{111}^2 + a_{100}^2 a_{011}^2 + a_{010}^2 a_{101}^2 + a_{001}^2 a_{110}^2 \qquad (285)$$
$$+ 4(a_{011} a_{110} a_{101} + a_{111} a_{100} a_{010} a_{001})$$
$$- 2(a_{100} a_{011} a_{111} + a_{010} a_{101} a_{111} + a_{001} a_{110} a_{111}$$
$$+ a_{100} a_{010} a_{101} a_{011} + a_{010} a_{001} a_{110} a_{101} + a_{100} a_{001} a_{110} a_{011}).$$

In [204] it was noted that the entanglement condition $\Delta(\Upsilon) = 0$ is equivalent to an ordinary determinant $D = a_{111}$ for the 3×3 matrix

$$M(\Upsilon) = \begin{pmatrix} a_{100} & \sqrt{a_{100} a_{010} - a_{110}^2} & \sqrt{a_{100} a_{001} - a_{011}^2} \\ \sqrt{a_{100} a_{010} - a_{110}^2} & a_{010} & \sqrt{a_{010} a_{001} - a_{011}^2} \\ \sqrt{a_{100} a_{001} - a_{101}^2} & \sqrt{a_{010} a_{001} - a_{011}^2} & a_{001} \end{pmatrix}.$$
$$(286)$$

The entries are written so that the set of a_{ijk} are the six 2×2 minors. When $\Delta(\Psi) \neq 0$ the determinant D differs from a_{111}, which then characterises the entanglement. Note that this matrix is really a two qutrit rather than three qubit matrix, as are the Jordan algebra elements above. It matches the commutative path array when the parity 110 terms are zero, as for the $|W\rangle$ state. The qutrit state is then $(\sqrt{a_{100}}, \sqrt{a_{010}}, \sqrt{a_{001}})$, and none of the matrix entries are zero. The $|W\rangle$ state, with $D = 0$, characterises null twistors, as shown in [26]. This now follows directly from the 2×2 minors of the qutrit matrix, which are essentially the Minkowski elements in $SL_2(\mathbb{C})$. This gives each of the three qubit subspaces of the qutrit space an interpretation in twistor variables, as expected. In contrast, the GHZ state is given by $M(\Upsilon) \equiv 0$, with $a_{111} \neq 0$. This requires the twistor variables Z and W to specify distinct null directions.

The two tripartite classes given above ($T_{123} \neq 0$ and $\tilde{V} \neq 0$) are known respectively as the GHZ and $|W\rangle$ states for three qubits [205]. A biseparable state is given by the example $1/\sqrt{2}(V_{123} + V_{156})$ and a GHZ state by

$$\Psi = \frac{1}{\sqrt{3}}(\sqrt{2} V_{135} + V_{246}). \qquad (287)$$

Note that the four classes for three qubits do not distinguish the three *labeled* biseparable sets, such as $(AB)(C)$. Does the Catalan number C_{n-1} count the number of n-partite classes for n fermions?

In terms of categorical structure, it was shown in [206] that the two tripartite classes for three qubits, W and GHZ, correspond to two kinds of commutative Frobenius algebras on $\mathbb{C}^2$ in the symmetric monoidal category of qudit Hilbert spaces. Take trivalent nodes for the multiplication m and comultiplication Δ, and truncated strings

$$\qquad (288)$$

for the unit $\eta : I \to A$ and counit $\epsilon : A \to I$ respectively. The compatibility condition looks like

$$\text{(289)}$$

as an algebra diagram, stating that the order of nodes does not matter. For diagrams with no loops one can then introduce the shorthand

$$S_{mn} \quad = \quad \text{(290)}$$

for a vertex from m to n strings. In particular, S_{02} and S_{20} give the arc diagrams of duality, so that we may consider a straightening law

$$= \quad \text{(291)}$$

involving an arrow $A \to A \otimes A \otimes A \to A$. This is part of the structure of a *compact* category [137], for which writhe pieces are unimportant. The category of finite dimensional Hilbert spaces is an example of a compact category, with duals A^*. This straightening law underlies the protocol for quantum teleportation [207]. Now the GHZ and W states are given respectively by [206] the laws

$$= \qquad \circ \quad = \quad \text{(292)}$$

noting the scalar loop, as in the Temperley-Lieb algebra. The so called induced tripartite state is given by the diagram S_{03}

$$\text{(293)}$$

which we see is just an A_2 associahedron tree. The diagram calculus of GHZ and W states for the symmetric monoidal category captures multipartite entanglement for *any* number of qubits. However, the higher dimensional polytopes are expressing coherence laws for higher dimensional categories, so symmetric monoidal categories cannot be the whole story.

10.2 Secondary Polytopes and Hyperdeterminants

The associahedra and permutohedra are examples of secondary polytopes [84]. In this section we see how secondary polytopes can generate determinant type invariants.

To begin with, for any finite set S of n points in an embedding space $\mathbb{R}^k$, let $C(S)$ be the convex hull of the set, possibly with points in its interior. We consider triangulations with vertices in S, including the hull edges. For example, four points in the plane with one central point define two possible diagrams.

 (294)

Observe that a square configuration of four points would not have allowed a central subdivision. For the square configuration, the triangulations would be the chorded source and target of A_2. Thus the *geometry* of the points dictates the diagram set. We only allow certain nice triangulations, as indicated in the examples below.

Given a triangulation T for any S, let $\xi_T : S \to \mathbb{R}$ be the characteristic function defined by the sum

$$\xi_T(p) = \sum_{\{\sigma : p \in \sigma\}} \mathrm{Vol}(\sigma) \qquad (295)$$

over simplices σ in T. The volumes will be neatly normalised so that the underlying field is not crucial to the combinatorial arguments. Let $\mathbb{R}^S$ be the vector space of all ξ_T for all T. The dimension of $\mathbb{R}^S$ is just n.

The *secondary polytope* $\Sigma(S)$ is the convex hull in $\mathbb{R}^S$ of all vectors ξ_T for all triangulations T. For the four point configuration above, the normalised volume vectors are $(3, 3, 3, 0)$ and $(2, 2, 2, 3)$, giving the secondary interval between these points. The dimension of $\Sigma(S)$ is $n - k - 1$, since every cone over T in $\mathbb{R}^S$ shares a $k + 1$ dimensional subspace with every other, determining the codimension for $\Sigma(S)$.

Example 10.2 The A_4 polytope in $\mathbb{R}^3$ is determined by the 14 triangulations of the planar two qutrit simplex, which is a squashed hexagon.
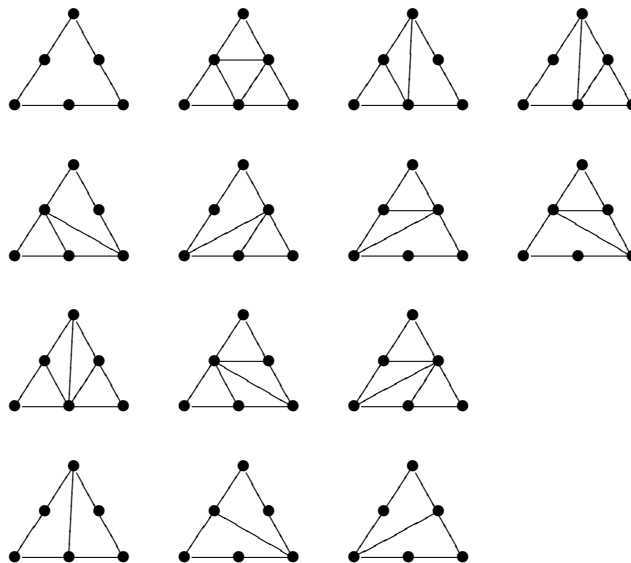
The area of a minimal piece inside any triangulated simplex is normalised to 1. Note that this process is dual to assigning integral volumes to vertices, as in the Postnikov procedure. Zero area triangles are permitted along a simplex edge. For example, on the tetractys three qutrit simplex, the possible areas are $0, 1, 2, 3, 4, 6$ and 9. Note that these values were Postnikov volumes for a hexagon piece of the tetractys. These volumes take values $V \in \{2^{i_2} 3^{i_3} \cdots l^{i_l}\}$ for $i_k \leq d-1$. For A_4, the volumes are $0, 1, 2$ or 4, and these occur in a square chunk of the hexagon simplex.

Example 10.3 The qubit intervals in the word monoid of length $n-1$ are squashed cubes. Consider the three qubit parity cube, at $n = 4$. As an interval it has four triangulations, matching the interval partitions $(1, 1, 1)$, $(1, 2)$, $(2, 1)$ and (3). Recall from chapter 5 that these partitions label the vertices of the parity square. The four vectors of the secondary polytope are $(3, 3, 3, 3)$, $(1, 2, 2, 1)$, $(1, 3, 2, 2)$ and $(2, 2, 3, 1)$. For the $2 \times 2 \times 2$ cube in $\mathbb{R}^3$, we expect a four dimensional secondary polytope on the eight vertices.

Example 10.4 The permutohedra S_d are secondary polytopes for the triangular prism $\Delta^1 \times \Delta^{m-1}$ in $\mathbb{R}^m$ on a simplex Δ^{m-1} [84], where Δ^1 is the interval. The prism clearly has $2m$ points, so the secondary polytope is of dimension $m-1$, for $d = m$. For example, the hexagon S_3 of dimension 2 comes from the six point prism $\Delta^1 \times \Delta^2$. The ξ_T vectors form $2 \times m$ matrices, using the prism decomposition. For the permutation $(d(d-1)\cdots 1)$ in S_d, one may take a triangulation such that the ξ_T vectors are $(d-k+1, k)$, and the other ξ_T are permutations of these vectors.

Divided simplices are canonically coordinatised. Let S sit in the integral lattice $\mathbb{Z}^k$, so that $p \in S$ is a commutative monomial $X_p = X_1^{i_1} \cdots X_k^{i_k}$ with k variables. That is, integer vectors are replaced by index vectors. For example, when $k = 2$ let S be the monomials $X^i Y^j$ for $i \in \{1, 2, \cdots, m_i\}$ and $j \in \{1, 2, \cdots, m_j\}$. For any $m_i \times m_j$ matrix M defining a form $\sum M_{ij} X^i Y^j$, the S-*discriminant* is either 1, when $m_i \neq m_j$, or equal to the determinant $\det M$ when M is square. We think of the variables X, Y as coefficients for polynomials, such as $f(x) = X_0 + X_1 x + X_2 x^2$, and the form M as an invariant for sets of functions. For the trilinear $X^i Y^j Z^h$ there is a *hyperdeterminant* for any form

$$\sum_{i}^{m_i} \sum_{j}^{m_j} \sum_{h}^{m_h} M_{ijh} X^i Y^j Z^h \tag{296}$$

In [72], this polynomial type generates generalised Catalan numbers, where $\sum M_{i00} X^i = C(X)$ is the usual Catalan number generating function. For the braid parameter $t(X)$ in (199), with $X^{-1} = 1 - ir$, we have $C(X) = t(X) \cdot X^{-1}$. The ternary function [72] is then

$$\frac{t(X)t(Y)t(Z) \cdot X^{-1}Y^{-1}Z^{-1}}{1 - t(X) - t(Y) - t(Z)}. \tag{297}$$

At the pseudoidentity $r = 0$ we have $X = 1$ and $C(1) = \omega_6$, the whole infinite sum of Catalan numbers. In this case the ternary generating function evaluates to -1.

The Cayley hyperdeterminant $\Delta(V)$ for qubits is a $2 \times 2 \times 2$ example. Recall that $\Delta(V)$ is quartic by the triality of (281). The arguments come from an A_4 particle configuration. Triality on A_4 itself is made manifest by the simplex triangulations. Look at the $21 = 3 \times 7$ edges, indicated by triangulations that may omit a boundary triangle. Two of these edge sets come with a left right reflection asymmetry, leaving only 5 diagram types.

 (298)
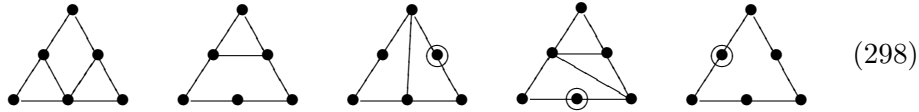
Any simplex is coordinatised on $\mathbb{Z}^d$ by the monomial indices [84]. For example, the monomial $X^3 Y^2 Z$ for 6 qutrits is given the coordinate vector $(3, 2, 1)$ of entry sum $n = 6$ in $\mathbb{R}^3$. The homogeneity of a word monoid simplex monomial means that all points lie in the hyperplane

$$x_1 + x_2 + \cdots + x_n = d. \tag{299}$$

This fixes a volume normalisation factor for the simplex. Integral coordinates may be abbreviated so that $(3, 2, 1)$ becomes 321. The two qutrit labels from the word monoid give the A_4 index triangle its coordinates: $(2, 0, 0)$, $(0, 2, 0)$, $(0, 0, 2)$, $(1, 1, 0)$, $(1, 0, 1)$ and $(0, 1, 1)$.

Recall that planar paths in steps X and Y ending at a point (m, n), and so of total length $m + n$, correspond to the (m, n) shuffles in S_{m+n}. The paths XY and YX therefore stand for the $(1, 1)$ shuffles in S_2, which is all of S_2, namely $\{I_2, \sigma_X\}$. The noncommutative paths always form a tensor cube. Commutativity naturally reduces an $l = 2$ matrix to a symmetric matrix, such as

$$\begin{pmatrix} 200 & 110 & 101 \\ 110 & 020 & 011 \\ 101 & 011 & 002 \end{pmatrix}, \tag{300}$$

which uses the shorthand for triangle coordinates. Observe that all permutations of a vector occur in such an array.

Finally, the *shuffle polytope* $N_{m,n}$ [84] has amongst its vertices all the (m, n) shuffles in the permutohedron S_{m+n}. Thus $N_{1,1}$ is the edge S_2. The polytope $N_{3,3}$ determines an invariant for two cubic polynomials

$$f(z) = X_0 + X_1 z + X_2 z^2 + X_3 z^3 \quad g(z) = Y_0 + Y_1 z + Y_2 z^2 + Y_3 z^3 \tag{301}$$

whose coefficients X_i and Y_j define integral coordinates in $\mathbb{R}^8$. The vertices of $N_{3,3}$ specify terms in R, but it is difficult to compute. By definition, $N_{3,3}$ is the convex hull of all integral vectors in $\mathbb{R}^8$ such that $c_{i_0 i_1 \cdots j_3}$ is non zero.

The index simplex for a secondary polytope is dual to tropical curves. Tropical polynomials like (2.2) may be used to draw cyclic tree diagrams, more suited to the symmetry of $N = 4$ planar Yang-Mills theory.

10.3 Entropy and Black Holes

Given an ensemble of N classical states with probabilities p_i such that $\sum_i p_i = 1$, the entropy

$$S = -\sum_i p_i \log p_i \tag{302}$$

may be considered a measure of distance from equipartition, where the equipartition for N states gives $S = \log N$. For $N = 2$, the associated free energy is considered in [44] in connection with the tropical logarithm and arithmetic. In information theory many alternative measures exist, but the intuition of arithmetic is crucial to the motivic point of view [208].

We consider how such measures arise combinatorially. First let S be a generating set in the integer lattice $\mathbb{Z}^k$. The secondary polytope for S is known as the *Chow polytope* for the toric variety defined by S. In this case there is a *principal S-determinant* for S, such that a triangulation T is associated to a coefficient

$$c_T = \pm \prod_{\sigma \in T} \text{Vol}(\sigma)^{\text{Vol}(\sigma)}. \tag{303}$$

As noted in [84], the expression $\prod_i V^V$ is the same as

$$\exp(\sum V_i \log V_i) \tag{304}$$

where $\sum V_i \log V_i$ is in the form of a negative entropy, where V_i is a probability.

Consider the two qutrit index simplex. When a minimal triangle is normalised to area 1, the 14 c_T take the values 1, 4 or 16. The renormalised probabilities over all 14 vertices of A_4 are then 1/92, 1/23 and 4/23. The latter probability showed up in chapter 7, as a phase for the ternary operator H.

Recall that certain simplex volumes take values $V_c \in \{2^{c_2} 3^{c_3} \cdots d^{c_d}\}$ for $c_k \leq n-1$, as in chapter 5 [72]. The secondary polytopes thus exhibit a wide variety of volume numbers. In (5.3), the Catalan number $C_4 = 14$ labeled integral volume hypersimplices for coordinates in $\mathbb{Z}^4$. This particular set contains 11 distinct volumes. Prime volumes of the form $1^{c_1} 2^{c_2} 3^{c_3} \cdots p_k{}^{c_k}$ are examples of V_c volumes for c vectors with non zero entries only at prime sites, satisfying the condition $c_1 + \cdots + c_i \geq i$ for all $i \leq k$. This reduces the example of C_4 to 9 distinct prime factorisations, up to $1^1 2^1 3^2$.

Now the c vectors for C_4 are canonical coordinates for four 4-dits. The tetrahedral four 4-dit simplex then contains an integral A_4 polytope, just

as one corner of the tetractys contains the pentagon A_3. These pentagon coordinates were

$$(1,1,1) \qquad (2,0,1) \qquad (1,2,0) \qquad (2,1,0) \qquad (3,0,0)$$

and they have volumes in $\{1,2,3,4,6\}$, wherein we recognise the universal $6/27$.

A volume thus represents both scale and probability. The probability measures the likelihood of ending up in a particular region, where this likelihood increases with volume. On the other hand, the only probability 1 event is a maximal density experiment, namely black hole creation within a small volume. In the first instance, some fixed classical region defines the total probability 1. In the second, the smallest possible region defines the probability 1. The black hole state has a definite local mass, while the uncertainty of position sharpens a measure of momentum. Partitions are then an important aspect of duality for M theory.

For a general 1-ordinal $n \in \mathbb{N}$ with prime decomposition $n = p_1{}^{c_1} \cdots p_k{}^{c_k}$, let $E_n = \log n$ represent an energy eigenvalue for a state $|n\rangle$ including c_i objects of type p_i. These are additive eigenvalues, since $E_n = c_1 \log p_1 + \cdots + c_k \log p_k$ where $\log p_i$ is the energy of a prime state. Then the partition function is

$$Z(s) = \sum_n e^{-sE_n} = \sum e^{-s \log n} = \sum \frac{1}{n^s} = \zeta(s) \qquad (305)$$

the Riemann zeta function, for $s = 1/kT$. This system is known as the Riemann gas. Now the coordinate V_c volumes can be written in terms of the prime decomposition

$$V_c = 1^{c_1} 2^{c_2 + c_4 + c_6 + \cdots} 3^{c_3 + c_6 + c_9 + \cdots} 5^{c_5 + c_{10} + \cdots}. \qquad (306)$$

In this case, the Riemann energy eigenvalue is

$$E_c = \log 2 \left(\sum_j c_{2j} \right) + \log 3 \left(\sum_j c_{3j} \right) + \cdots + \log p_k \left(\sum_j c_{pj} \right). \qquad (307)$$

For example, when $c = (2,1,1,0)$ for the integral $V_c = 6$, we have $E_c = \log 6$. However, $c = (3,0,0,1)$ has $E_c = \log 2$, whereas $V_c = 4$. So it is only the prime c vectors that give $E_c = \log V_c$ directly, and E_c is otherwise divided out by divisors. In a sense, the Riemann gas only sees the primes.

With canonical coordinates, the prime volumes pick out certain vertices on the simplices and polytopes. For example, allowing prime powers, five vertices are selected on the parity cube (101). Recall from chapter 5 that there were 70 forest orders at $n = 4$. It so happens that the length squared

$$1^2 + 2^2 + 3^2 + \cdots + 24^2 = 70^2$$

126

of the 24 dimensional integral source vector of S_{24} is the square of 70, which as a volume defines a 70 dimensional vector $(2484, 0, \cdots, 0, 1)$. But 70 is also the volume of the prime vector $(25, 1, 0, 0, 1, 0, 1)$ in dimension 7, using the prime decomposition of 70. As usual, the first coordinate is selected to maintain the coordinate sum for S_d. In this way quantum geometry can reduce the dimension of classical arithmetic, by adding noncommutative information to the underlying spaces.

In the STU model of M theory, the macroscopic black hole entropy for extremal states is the square root of Cayley's hyperdeterminant. This is extended beyond three qubits to the tripartite entanglement of seven qubits, where $S = \pi\sqrt{|T|}$ for a suitable invariant T [24][25]. In the three qubit case, the charge cube corresponds to the quantum state via

$$(p^0, p^1, p^2, p^3, q_0, q_1, q_2, q_3) \quad \leftrightarrow \quad (a_{000}, a_{001}, a_{010}, a_{011}, -a_{111}, a_{110}, a_{101}, a_{100}), \tag{308}$$

so that pairs (p^i, q_i) sit on opposite corners of the parity cube. The minus sign ensures a real entropy, as can be seen when a_{111} defines a 3×3 determinant. The real amplitudes reduce the local symmetry to $SL_2(\mathbb{R})$, and integral values give the total U duality group $SL_2(\mathbb{Z})^{\otimes 3}$. We see that electric magnetic duality flips signs in signature classes for S_4. Altogether, the three dualities correspond to the three binary operations on the ribbon spectrum: crossing flips, left right symmetry, and charge conjugation.

In the thermodynamic interpretation of black hole geometries [209][210] it is indeed the horizon area A that corresponds to an entropy $S \sim A/4G$. Taking $G = 1$, we see directly the factor of 4 that arises naturally in both entanglement geometry and braid algebras. Using the four letter ribbon template [31] for braids, we can also model the attractor surfaces [211] that are supposed to control the pathological behaviour of microscopic states in the continuum theory. The full four qubit structure for STU states is also related to the j-invariant for elliptic curves.

11 Information in the Emergent Cosmology

The relativistic Big Bang cosmology of the twentieth century cannot be correct. This is not to say that it lacks useful working descriptions or partially correct observations, but as a fundamental subject cosmology demands conceptual clarity. Accurate predictions cannot come from false foundations. It is no longer scientifically reasonable to phrase our description of the cosmos in terms of general relativity, with a dash of quantum physics.

This old approach produces numerous anomalies. First, only 4.5 percent of the observed mass in our universe is baryonic matter, the remainder constituting the problem of dark energy and dark matter. Dark matter was not predicted by theorists, but observed first in the anomalous rotation of galaxies by Zwicky [212] in the 1930s. It has since become clear that basically all galaxies show a flat rotation curve at high radius [213], in line with the hypothesis that extra mass lies in the galactic halo.

None of the localisable WIMP type dark matter candidates can agree with astrophysical observation, since the dark matter characteristics of a galaxy depend on properties that cannot be attributed to states with an essentially independent cosmic evolution [214]. The data does however agree with the hypotheses of conformal gravity [215] and modified Newtonian dynamics, as mentioned below.

The so called dark energy component of the universal energy budget was hypothesised after the observation of apparent dimming for distant supernovae, which act as standard candles for distance measurement [216][217]. It is often attributed to a cosmological constant term in Einstein's equations, although this can hardly be considered a physical explanation of anything [218]. Moreover, this constant was only considered by Einstein as a means of ruling out an expanding universe, before observations confirmed that the universe *was* expanding. The natural alternative is a quantum cosmology, perhaps with a variable speed of light as one looks back in time, or a dependence of supernovae characteristics on evolving particle properties.

The Friedman equations for an isotropic and homogeneous classical spacetime predict a constant density for the equation of state $p = -\rho$, generally accepted in the dark energy paradigm and in agreement with observation. In terms of the Hubble expansion parameter $H = \dot{a}/a$, the flat universe critical density is

$$\rho_c = \frac{3H^2}{8\pi G} \tag{309}$$

where G is Newton's constant. The cosmological density parameters are then defined by

$$\Omega \equiv \frac{\rho}{\rho_c} = \frac{8\pi G}{3H^2}\rho \tag{310}$$

so that $\Omega = 1$ expresses flatness. The classical spacetime evolves from the Big Bang epoch, where nucleosynthesis occurs at a temperature of around

100 keV. It becomes transparent at the recombination epoch, when hydrogen is formed, at about 0.3 eV. Everything depends on the temperature of the environment, and evolves slowly by one cosmic clock.

One cornerstone of classical cosmology is the evolution of structure formation [219]. Historically, this is analysed with a strictly classical image of colliding galaxies and star formation. Large scale structure is associated to the supposedly initial perturbations, seen in the cosmic microwave background radiation. In this framework, it takes billions of years from the Big Bang for complex spiral galaxies to form, and yet they are observed at high redshift [220].

Such anomalies were in fact predicted by the alternative idea of primordial black holes [221][222]. In this situation, the conditions at the Big Bang epoch are based on thermodynamic principles, and our cosmological boundary is associated to *actual* black hole horizons. We assume that the boundary is conformal, with particle states becoming massless as the speed of light approaches infinity [223][224]. In the quantum picture, this Big Bang is an *observer dependent* phenomenon, with the local constancy of the speed of light depending on our notion of present time.

Another observational issue is the lithium problem, namely the conflict between the theoretical value of lithium abundance and that observed, which is much less. Hydrogen and helium fractions are a success of Big Bang nucleosynthesis, but beyond this it fails. Moreover, recent studies of stellar mass black hole accretion discs indicate that the full cosmic lithium fraction can be created locally in hot regions near the black hole [225][226].

Direct detection dark matter experiments have now ruled out most WIMP scenarios [227][228]. There remains the oscillation results of DAMA [229], which observed a variation in event rates with a phase that is correlated with Earth's relative galactic motion, rather than solar system motion. Heaven forbid that we should imagine a classical aether as an explanation, with the Earth sweeping through a fixed sea of classical dark matter particles. However, alternative mechanisms defining our galactic motion are possible.

An increasingly popular view holds that neutrino condensates are responsible for gravitational states in the cosmic environment. McElrath [233] has recovered the vierbein of general relativity using condensate arguments. Recently, Alexander obtained an interesting evolving equation of state from a neutrino condensate ansatz [234]. This all suggests that neutrinos are closely related to the cosmic microwave background radiation, as discussed previously in [179][180]. The Koide relation offers further quantitative evidence for this idea, recovering the precise CMB temperature from the mirror neutrino states.

In an M theory based on quantum measurement, cosmology must be observer dependent [232]. Even the holographic principle [230], which places quantum information at horizons, usually requires the input of a classical boundary. Notably, Padmanabhan [231] has studied atoms of spacetime

using the thermodynamics of general relativity, and its associated entanglement entropy.

A basic foundation for the emergent view must lie in the physical dualities of M theory, linking small and large scales. Whether representing distances or couplings, the only natural unit is that for energy. In a quantum world the only *certain* experiment is that of black hole creation, when the conditions of an experiment push local density limits. A small distance is defined by such a large energy probe, in the experimenter's laboratory. This contrasts with the largest possible distances, which are cosmological ones. The laboratory does not exist without the second consideration.

The easiest way to encode both conditions into the abstract experimental constraints is to start with two distinct notions of *time*, since time is closely connected to the concept of energy. This is accommodated in the new cosmology, which views the dark sector of the universe entirely in terms of black hole quantum states. Using classical methods, Penrose [224], Carr and Hawking [221] and others have studied the black hole picture. However, the necessary observer dependence cannot happen within general relativity, because although spacetime is dynamical, its content cannot be discussed without favouring the observer that knows the universal geometry. That is, there is no interaction between distinct observers. More simply, it contains no Planck's constant $\hbar$.

Consider the Big Bang epoch. We now imagine [224] that all matter is massless at the observer's boundary, meaning that the speed of light is essentially infinite [235]. Initially, it does not concern us what form the matter takes here, because we *cannot observe it*. We just say that as our cosmological time progresses, the mass M of the observable universe should be seen to increase.

What matters is that the boundary we observe in the distant past is like the horizons we observe when we look at black holes. Classically we identify these boundaries, to create Penrose's cyclic universe [224]. Quantum gravitationally, we identify them only in our mind, because they have no concrete reality outside observation, and the boundaries are dissolved by quantum geometry. Cosmological conditions become local ones, because there is no observation without locality.

Usually, the local clocks of the laboratory are identified with the clocks that govern the distant past. Thus we begin with the concept of dual clocks.

11.1 Mirror Clocks and the Dark Sector

An observer selects two clocks. The *cosmological* clock estimates the elapsed time since the Big Bang, with either an estimate of universal mass M or measurement of the CMB temperature T. The *laboratory* clock uses the local dynamics of a few massive objects to define an orbital tick. Each clock covers the full range of energy scales. Our cosmological clock measures time from

our Big Bang, through to the present and into local future horizons. The laboratory clock keeps time for both low and high energy local experiments.

With respect to the dualities of M theory, these two clocks must be related, but they are not identified. One is mainly used to observe particles and the other the environment, or horizons. Crucially, we do not assume that other observers, whether in distant galaxies or nearby, share our estimate of cosmological epoch.

Implicitly, dual clocks occur already in black hole thermodynamics. In black hole complementarity [236][237], quantum information resides in both the particle states and in the local environment. The mirror particles of baryonic matter are now assumed to contribute to the infrared internal black hole states, while the external states that are accessible to us are a complex mix of local and nonlocal information.

Thus our cosmological boundary, beyond the dark ages, is defined by future horizons, describing an abundance of primordial black holes. These black holes seed a dispersive structure evolution. The entropic arrow of the observer's cosmic time drives the irreversible dynamics of quantum gravity. As Riofrio [238] notes, one may invoke Kepler's law for the universal mass M,

$$GM = tc^3, \tag{311}$$

where t marks this passage of cosmic time as *measured* by an observer's estimate of the CMB temperature. Newton's constant G and c may be set to 1, and M then increases exactly with the arrow of cosmic time, from the massless boundary. We attribute the missing factor of π in Kepler's law to the difference between the cosmic radial time and the time defined by an orbital clock. This factor of π now differentiates the rational and non rational Koide phase factors, with the universal 2/9 arising in the laboratory.

Where do dual clocks occur in the rest mass quantum numbers? Recall that neutrinos, which define the CMB temperature, have Koide phases

$$\delta_\nu = \frac{2}{9} \pm \frac{\pi}{12}. \tag{312}$$

In chapter 7, the $\pm\pi/12$ conjugation recovered both the neutrino mass triplet and the CMB temperature, at 0.00117 eV [179][180]. There are two other mirror mass states in the triplet, one at a future time and one in the past. The past one occurs at around $z = 7$, which is the observed reionization epoch.

The mirror neutrino braids have flipped crossings under the $t \mapsto 1/t$ Burau map. Since t is a root of unity for unitary braids, this is indeed a phase conjugation. Note that the two clocks should still exist as we approach conformal boundaries, where the Koide scales must vanish. Since local observation is directly associated to cosmological conditions, we most easily observe the cosmological conditions for light states, namely the neutrinos. Indeed, it appears that only the neutrinos carry the $\pi/12$ Koide phase.

Now the mirror mass triplets also define triplets of photon energies. When all massive states and all photons are created via Hawking radiation, in principle out of the entropic vacuum that replaces classical horizons, the observer's past universal mass M may be interpreted as a black hole mass. Then the Hawking temperature T, as a measure of cosmic time, appears in a modified form of (311),

$$\frac{1}{t} = \frac{8\pi kT}{\hbar} = \frac{c^3}{GM},\qquad(313)$$

with k Boltzmann's constant. At the CMB temperature, the Koide factor of 3 appears once more in $8\pi T \simeq 0.03$ eV, which is close to the tripled neutrino mass scale $3\mu_\nu$. This is an additional coincidence between neutrinos and the CMB. Recall that the charged lepton scale is also set by an internal phenomenon, namely the dynamical quark scale, with $3\mu_l$ equal to the proton mass.

The exact value of $\Omega_d = 3/\pi$ for the total dark sector density was obtained by Riofrio [238] using an horizon pair production argument. We split Ω_d into $\Omega_{dm} = 3/4\pi$ for dark matter and $\Omega_\Lambda = 9/4\pi$ for dark energy. The factor of three in $\Omega_{dm}/\Omega_\Lambda$ is now attributed to the quark color quantum number, as it appears in the Koide triplets. Since quarks are already internal, in the domain of confinement, and dynamical quarks account for most of the baryonic rest mass, each dynamical quark contributes roughly $1/3 - 1/\pi$ to the total baryonic fraction $\Omega_b = 1 - 3/\pi$.

Yet another occurrence of the factor of 3 is in the universal shear viscosity to entropy ratio of the quark gluon plasma [239], which has an observed [240] minimum value of $1/4\pi$ and a maximum of $3/4\pi$. These quantities were notably associated to the Rindler causal horizon in [241]. The color kinematic duality of $N = 8$ supergravity [120][121] is a strong theoretical argument for this link between color number and kinematic states.

Consider that the rational phases of a Koide operator come from the laboratory clock. The time p ranges from 0 to 1 radians, and may be interpreted as a probability. The basic probabilities should be associated to the Koide scale parameters r, since scale is itself a time measure. Recall that r in $\sqrt{M}$ ranges from 0 for fermion creation and annihilation to ∞ for an identity matrix, representing boson rest mass. Let p then define a triplet (p, q, q) with $p + 2q = 1$, in a probability circulant

$$C = \begin{pmatrix} p & q & q \\ q & p & q \\ q & q & p \end{pmatrix}\qquad(314)$$

which is also a mixed boson Koide matrix. At $p = 0$, $r = 0$ stands for the condition of the creating horizon. Letting p/q arise as a 2×2 r parameter in a Schur square root, a few simple rationals are given, with the corresponding braid phase t.

p	q	r	t
1/2	1/4	1	$\pi/2$
1/4	3/8	$1/\sqrt{3}$	$\pi/3$
1/3	1/3	$1/\sqrt{2}$	1.23
2/3	1/6	$\sqrt{2}$	1.91
4/27	24/56	$1/\sqrt{6}$	0.78
2/27	26/56	$1/\sqrt{13}$	0.54
1/17	8/17	1/4	$0.49 = 28°$
1	0	∞	π

Recall that r and $1/r$ determine complementary phases, so that $0.49 = \pi - 2\tan^{-1} 4$. The angle $28° \sim \theta_W$ follows from $r = 1/4$ regardless of the probability interpretation. The IR Standard Model parameter zoo still requires further unraveling, but the Koide triplets already strongly constrain data.

11.2 Modified Newtonian Dynamics

In [242] Milgrom noted that in the weak acceleration limit pertaining to outer galactic motions, one could modify Newtonian gravity according to the rough law

$$\frac{GM}{r^2} = \frac{a^2}{a_0} \tag{315}$$

where a_0 is a characteristic acceleration. For a circular orbit this gives

$$a = \frac{\sqrt{GMa_0}}{r} \tag{316}$$

which indicates a constant speed $v = \sqrt[4]{GMa_0}$ at the galactic rim, in line with the observation of rotation curves. MOND is a candidate theory to explain the dark sector without any additional matter states. The observed value of a_0 is around 1.2×10^{-10} ms^{-2}. Relativistic variants of MOND exist.

One variant of MOND adds an additional $1/r$ term to the usual $1/r^2$ behaviour of Newtonian gravity. For large r, the non standard $1/r$ term dominates. In classical mechanics [243] a 19th century theorem of Bertram states that closed Keplerian orbits can only exist for the laws $1/r^2$ and r. The observational reality of closed orbits in galactic rotations then demands a transformation from the function r to $1/r$. This is exactly the behaviour of T duality in M theory.

11.3 Further Observational Comments

The furthest human experiment to date is the Voyager II journey beyond the solar system [244]. In [245], the anomalous acceleration towards the sun that is observed in the Pioneer spacecraft is attributed to the speed of light

variation over this distance. This variation agrees with the cosmological rate of variation determined by Riofrio. The Riofrio study [238] also provides a quantitative explanation for the apparent dimming of type Ia supernovae [216][217].

The rotation curves of spiral galaxies are clearly dictated by the luminosity of the galaxy [246]. In particular, the observed Tully-Fisher relation [247] shows that the smaller the galaxy, the greater the dark matter fraction. The total density fraction for the dark sector, Ω_d, can only be an average for the galaxy distribution. We interpret this fact as follows, on the basis that mirror states are complementary to baryonic ones. Lower mass galaxies are interpreted as *younger* objects, according to the definition of the cosmic clock, in the same way that the light neutrinos are associated to the most local cosmic conditions. This is true irrespective of the stellar ages observed within them, because we are chiefly concerned with the black hole content of the galaxy.

Theoretically, one expects a correspondence between the emergent de Sitter geometry and a conformal field theory at the boundary. In the twistor picture, this has become a breaking of conformal structure by higher categorical geometry.

A Category Theory

Categories are the foundation of relational mathematics. A *set* is a zero dimensional category, because everything in a set is an element, pictured as a pointlike object. A one dimensional category $\mathbf{C}$, or 1-category for short, has both zero dimensional *objects* and *arrows* between objects. If the head of an arrow meets the tail of another, they compose to form another arrow in $\mathbf{C}$. That is, an arrow f has *source* and *target* objects. Instead of equations relating elements of sets, categories relate arrows using commutative diagrams. For example, the square

$$
\begin{array}{ccc}
A & \overset{h}{\longrightarrow} & B \\
{\scriptstyle f}\downarrow & & \downarrow{\scriptstyle k} \\
C & \underset{g}{\longrightarrow} & D
\end{array}
\tag{317}
$$

says that $gf = kh$, if it commutes, and A, B, C and D are source and target objects. Diagrams of any shape are possible. A 1-category $\mathbf{C}$ is associative on arrows, so that $h(fg) = (hf)g$, and it always contains at least identity arrows $1_A : A \to A$ for every object A, that represent the object at the arrow level. Thus a set only has identity arrows.

Since categories replace sets, we need maps between categories. A *functor* $F : \mathbf{C} \to \mathbf{D}$ sends objects A to objects $F(A)$ and arrows f, g to arrows such that $F(gf) = F(g) \circ F(f)$. This is the covariant rule. A contravariant functor satisfies $F(gf) = F(f) \circ F(g)$. We can also say that a contravariant functor is a covariant functor $\mathbf{C}^{\mathrm{op}} \to \mathbf{D}$ from the *opposite category* $\mathbf{C}^{\mathrm{op}}$, which is the same as $\mathbf{C}$ with all arrows formally reversed.

Example A.1 $\mathbf{Vect}_{\mathbb{F}}$ is the category of vector spaces over the field $\mathbb{F}$. Every vector space V is an object in the category. The arrows are the linear maps between vector spaces.

Example A.2 $\mathbf{Set}$ is the category of all sets, with functions as arrows. The empty set is an *initial* object, since it is included in any other set in only one way. A one element set is terminal. All one element sets A and B are equivalent, because the unique maps ! in the squares

$$
\begin{array}{ccc}
A & \overset{!}{\longrightarrow} & B \\
{\scriptstyle 1_A}\downarrow & & \downarrow{\scriptstyle 1_B} \\
A & \underset{!}{\longleftarrow} & B
\end{array}
\qquad\qquad
\begin{array}{ccc}
B & \overset{!}{\longrightarrow} & A \\
{\scriptstyle 1_B}\downarrow & & \downarrow{\scriptstyle 1_A} \\
B & \underset{!}{\longleftarrow} & A
\end{array}
$$

ensure that they commute. The two element set $\Omega = \{0, 1\}$ in $\mathbf{Set}$ gives it the structure of a *topos* [7]. In particular, Ω allows characteristic functions $A \to \Omega$, which send some elements of A to 1 and others to 0, thereby defining a subset of A using an arrow.

Note that two objects A and B are *equivalent* when there exist two arrows $f : A \to B$ and $g : B \to A$ such that both $fg = 1_B$ and $gf = 1_A$ hold. Arrows can be equal, but distinct objects can only be equivalent.

Why categories? Many familiar structures are already categories. For instance, a group is a 1-category with only one object. Arrow composition is the group operation and every arrow has an inverse, such that they compose to the identity. Note that the axioms of a category have automatically given the group its identity, and a group homomorphism is nothing but a functor between two groups. A *groupoid* is a category in which every 1-arrow is invertible. This extends groups to categories with multiple objects.

So the category **Grp** of all groups is really a *category of categories*, containing all one object categories with inverses, and all functors between them. Now comes the interesting part. Categories of categories have another level of structure, namely 2-arrows between the 1-arrows. Let F and G be functors with the same source and target categories. These 2-arrows are *natural transformations* $\eta : F \Rightarrow G$, given by a collection of arrows η_A in the target category, such that for every f in the source category the squares

$$
\begin{array}{ccc}
F(A) & \xrightarrow{\ F(f)\ } & F(B) \\
\eta_A \big\downarrow & & \big\downarrow \eta_B \\
G(A) & \xrightarrow[\ G(f)\ ]{} & G(B)
\end{array}
\qquad (318)
$$

all commute. The 2-arrows are two dimensional pieces of a diagram, because they fill an area between two 1-arrows. Such 2-arrows may compose both horizontally and vertically, as in this globule


$$(319)$$

piece of a 2-category. Natural transformations were originally introduced for cohomology, since cohomology is a functor from a category of spaces to the algebraic category that gives the invariants. Now a 2-category is a collection of objects, 1-arrows, 2-arrows and identities, such that every equation on 1-arrows can be weakened by 2-arrows between the paths.

There is no reason to stop at dimension 2. Categories are naturally defined for any ordinal dimension n. Things get much more interesting in dimension 3, with the appearance of *tricategories* [75][76]. Up to dimension 2, all categories are essentially *strict*. This means that every bicategory is equivalent, at the level of 2-arrows, to an ordinary 2-category [77]. Bicategories will be discussed below.

A.1 Limits and Universality

As with sets, categories can have natural closure conditions, such as the existence of certain limiting objects [137][47]. A *limit* in a 1-category is defined over any diagram D in the category. It is an object L, with an arrow from L to each object in D, such that given any other object Q in the category, and arrows from Q down to D, there is always a unique arrow $Q \to L$ so that the whole diagram commutes.

Thus the *pullback* limit of a pair of arrows, f and x, if it exists, is a unique square in a set of diagrams

$$
\begin{array}{ccc}
Q & & \\
& \searrow^{h} & \\
k \searrow & L \longrightarrow A & \\
& \downarrow^{f} & \\
& Z \xrightarrow{x} B &
\end{array}
$$
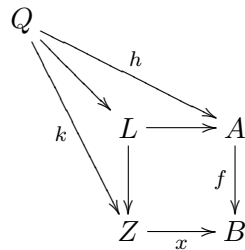
given by the following condition. For any pair of arrows h and k, there is a unique arrow $Q \to A$ such that the diagram commutes. Note that an arrow $L \to B$ also exists by composition.

Example A.3 Pullbacks characterise the behaviour of the differential form functor in the de Rham cohomology of manifolds. Given $f : \mathbb{R}^m \to \mathbb{R}^n$, there is a pullback f^* from 0-forms on $\mathbb{R}^n$ to forms on $\mathbb{R}^m$, defined by $f^*(w) = wf$ [45]. The pullback f^* extends to all differential forms.

Similarly, a *colimit* is an object C, along with arrows from D to C, so that for any other object Q and arrows from D to Q, there is a unique $C \to Q$ making the diagram commute.

Example A.4 The direct limit of a sequence $\{X_i\}$.

$$
\cdots X_i \longrightarrow X_{i+1} \longrightarrow X_{i+2} \longrightarrow X_{i+3} \longrightarrow \cdots \longrightarrow X_n \quad\nearrow C
$$
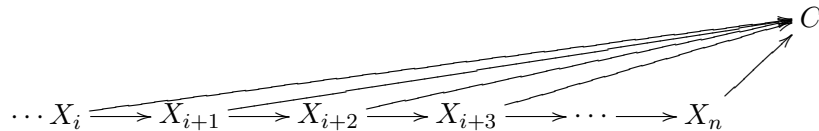
Limits are instances of *universality*, the idea that a single object essentially contains the structure of a larger piece of the category. In particular, *motives* are a universal cohomology theory, in some category of cohomology functors. However, the 1-categorical limit concept is too limiting, not least because a category of functors is already a 2-category! We need higher dimensional limit concepts. On that note, observe that there is a unique limit

only in the sense that all limits must be equivalent. Let us look then at equivalences between categories.

Let $1_{\mathbf{C}}$ and $1_{\mathbf{D}}$ be the identity functors on two categories $\mathbf{C}$ and $\mathbf{D}$. There is an *adjunction* $F \dashv G$, for functors $F : \mathbf{C} \to \mathbf{D}$ and $G : \mathbf{D} \to \mathbf{C}$, if there exist natural transformations $\eta : 1_{\mathbf{C}} \Rightarrow GF \Rightarrow$ and $\epsilon : FG \Rightarrow 1_{\mathbf{D}}$. It helps to draw out the arrows. In simple cases, F and G may compose to the identity itself.

Example A.5 F and G are both the same functor $\vee : \mathbf{Vect} \to \mathbf{Vect}$, namely the duality functor on a category of vector spaces. There is a natural equivalence $(V^{\vee})^{\vee} \simeq V$ between the double dual of a vector space and itself.

Example A.6 Let K be a finite extension of the number field $\mathbb{F}$ defined by the splitting property, namely that the extension splits certain polynomials into linear factors. For example, $\mathbb{C}$ splits quadratics over the reals. Let S be some subset of K. The field $\mathbb{F}(S)$ closes S under the field operations. This gives a lattice of extensions between $\mathbb{F}$ and K. To any such nice extension K/L we consider the group of automorphisms of K which fix the elements of L. This is the *Galois group* $\mathrm{Gal}(K/L)$. For example, $\mathrm{Gal}(\mathbb{C}/\mathbb{R})$ is the two element group, containing the trivial automorphism and complex conjugation. The subgroups of $\mathrm{Gal}(K/\mathbb{F})$ are in one to one correspondence with the extensions between $\mathbb{F}$ and K. This is an adjunction between the lattice of extensions and the subgroups.

A *monad* is an endofunctor $T : \mathbf{C} \to \mathbf{C}$ with natural transformations $\mu : T^2 \Rightarrow T$ and $\eta : 1_{\mathbf{C}} \Rightarrow T$ such that $\mu(T\eta) = \mu(\eta T)$ and

$$
\begin{array}{ccc}
T^3 & \xrightarrow{\ T\mu\ } & T^2 \\
{\scriptstyle \mu T}\downarrow & & \downarrow{\scriptstyle \mu} \\
T^2 & \xrightarrow{\ \ \mu\ \ } & T
\end{array}
\tag{320}
$$

Note how this axiom resembles associativity for a binary product. Every adjunction defines a monad with $T = GF$. Monads define T-algebras, which are pairs (X, h) for X an object in $\mathbf{C}$ and $h : TX \to X$ the algebra structure, so that $Th \cdot h = \mu_X h$ [77].

A *multicategory* allows arrows with multiple sources.

$$\tag{321}$$
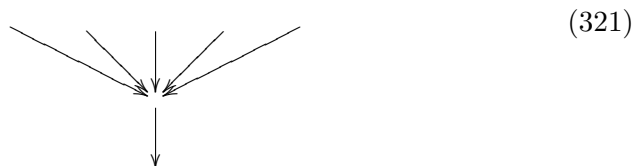
On such tree diagrams the arrow orientations are often omitted, and it is understood that processes occur downwards on the tree. An *operad* is a

multicategory on one object [248]. That is, for every $n \in \mathbb{N}$ there is an object $X(n)$, including an identity 1 in $X(1)$, so that the collection has a composition

$$X(n) \times X(k_1) \times X(k_2) \times \cdots \times X(k_n) \to X(k_1 + k_2 + \cdots + k_n) \qquad (322)$$

given by an associative $x \cdot (x_1, x_2, \cdots, x_n)$ such that $x \cdot (1, 1, \cdots, 1) = x$. This last identity rule extends n leaves on a tree by a secondary leaf. Similarly, the generic composition uses the tree $X(n)$ as a base for grafting the other components. Special sequences of polytopes of real dimension n form operads, and these are an important theme of the book. Operads are often defined with a permutation group action, but the weaker definition is more suited to noncommutative geometries.

A.2 Monoidal, Braided and Tortile Categories

In category theory, *coherence* of a structure means providing a finite set of axioms that are sufficient to force commuting diagrams wherever necessary. The primary example is Mac Lane's proof of coherence for monoidal categories [77], which are examples of bicategories.

A *bicategory* $\mathbf{B}$ is the general form for two dimensional axioms, as in categories of 1-categories, functors and natural transformations. Thus it contains 0-arrows, 1-arrows and 2-arrows, along with weak identities 1_A for all 0-arrows A, and a left identity λ_f and right identity ρ_f for all 1-arrows f. The 1-arrows and 2-arrows from A to B form a 1-category $\mathbf{B}(A, B)$. The identities satisfy

$$(323)$$

It turns out that any bicategory is weakly equivalent to a 2-category, where all the λ_f and ρ_f are strictly identities. For objects A, B and C, there is a functor

$$\otimes : \mathbf{B}(B, C) \times \mathbf{B}(A, B) \to \mathbf{B}(A, C) \qquad (324)$$

and associator 2-arrows $\psi_{fgh} : f \otimes (g \otimes h) \to (f \otimes g) \otimes h$ such that

$$\psi_{fg1}(f \otimes \rho_g) = \rho_{f \otimes g} \qquad \psi_{1fg}\lambda_{f \otimes g} = \lambda_f \otimes g \qquad \psi_{f1g}(f \otimes \lambda_g) = \rho_f \otimes g. \quad (325)$$

The *interchange law* for 2-arrows ψ, ϕ, ψ' and ϕ' states that $(\psi \otimes \phi)(\psi' \otimes \phi') = \psi\psi' \otimes \phi\phi'$, interchanging the two inner arrows. That is, the composition of

four 2-arrows

$$
\begin{array}{ccc}
A \longrightarrow B \longrightarrow C \\
\downarrow \qquad \Downarrow\phi' \quad \downarrow \quad \Downarrow\psi' \quad \downarrow \\
A \longrightarrow B \longrightarrow C \\
\downarrow \qquad \Downarrow\phi \quad \downarrow \quad \Downarrow\psi \quad \downarrow \\
A \longrightarrow B \longrightarrow C
\end{array}
\tag{326}
$$

should give a 2-arrow in **B**. Here, the 2-arrows are globules, defined from one source object to one target object. This may be generalised to the concept of double category, based on square building blocks.

A bicategory with one object is a monoidal category. Since there are only two non trivial levels of arrow, it may be described using objects and 1-arrows with extra structure, understanding that the objects are really the 1-arrows and the 1-arrows are really 2-arrows. The identity on the one object is usually denoted I, and acts as a unit for $\otimes$. The objects can be composed using the monoidal product $\otimes$. The bicategory interchange law becomes the Mac Lane pentagon axiom [77]

$$
\begin{array}{ccc}
& {}_{\psi}\,((A \otimes (B \otimes C)) \otimes D) \xrightarrow{\ \psi\ } (A \otimes ((B \otimes C) \otimes D))\,{}_{\psi} & \\
(((A \otimes B) \otimes C) \otimes D) & & (A \otimes (B \otimes (C \otimes D))) \\
& {}_{\psi}\quad ((A \otimes B) \otimes (C \otimes D)) \quad {}_{\psi} &
\end{array}
\tag{327}
$$

Rather than keep track of the same set of objects all the time, this law is abbreviated to bracket sets. A bracketed object is replaced by a binary rooted tree with four leaves. For instance,

$$
\tag{328}
$$

stands for the object $((A \otimes B) \otimes (C \otimes D))$.

Example A.7 The category **Set** with Cartesian product $\times$ is a monoidal category. So is **Vect**$_{\mathbb{F}}$ with tensor product $\otimes$.

In these standard examples, the tensor product is symmetric. But it turns out that the condition of commutativity on $\otimes$ is a four dimensional structure. The three dimensional structure that underlies commutativity is that of a *braided monoidal* category. Like monoidal categories, these have only two non trivial levels of arrow, but now there is one 0-arrow and one 1-arrow. The 0-arrow gives the $\otimes$, as above. The 1-arrow adds the structure of a *braiding*, which is a collection of arrows $\gamma_{AB} : A \otimes B \to B \otimes A$ such that

the hexagon

$$A \otimes (B \otimes C) \xrightarrow{\gamma_{A(BC)}} (B \otimes C) \otimes A \tag{329}$$

$$\psi \nearrow \qquad \psi \searrow$$

$$(A \otimes B) \otimes C \qquad\qquad\qquad B \otimes (C \otimes A)$$

$$\gamma_{AB} \otimes 1_C \searrow \qquad \nearrow 1_B \otimes \gamma_{AC}$$

$$(B \otimes A) \otimes C \xrightarrow{\psi} B \otimes (A \otimes C)$$

and another hexagon with inverse associators ψ^{-1}, commute [64]. Braids are actually just that: knotted string diagrams. String diagrams are dual to the usual arrow diagrams, because a string stands for an object A, while a braid object on a set of strings is an arrow. Thus a braid arrow γ_{AB} is a braid crossing

$$\begin{array}{cc} A & B \end{array} \tag{330}$$

and γ_{BA} is the opposite crossing, taking B over A. A *tortile* braided monoidal category $\mathbf{C}$ has a dual object A^* for every object A in $\mathbf{C}$, and twist maps $\theta_A : A \to A$ that twist the object ribbons. As explained in [144], ribbons are necessary to make a braiding compatible with the existence of duals. Duals come from adjunctions. We can assume that A^* is a *right dual*, since in tortile categories this automatically makes it a left dual also. From the adjunction $A \dashv A^*$ there is a unit and counit

$$\eta_A : I \to A^* \otimes A \qquad \epsilon_A : A \otimes A^* \to I \tag{331}$$

where I is the monoidal identity. These are drawn as arcs

$$\eta \qquad \epsilon \tag{332}$$

so that I is an empty diagram. The arrow $(1_A \otimes \eta_A)(\epsilon_A \otimes 1_A)$ should be the identity 1_A, as should $(\eta_A \otimes 1_{A^*})(1_{A^*} \otimes \epsilon_A)$. For every A, the twist θ_A satisfies the compatibility condition

$$A \otimes B \xrightarrow{\gamma_{AB}} B \otimes A \tag{333}$$

$$\theta_{A \otimes B} \downarrow \qquad\qquad \downarrow \theta_B \otimes \theta_A$$

$$A \otimes B \xleftarrow{\gamma_{BA}} B \otimes A$$

In string diagrams, this just says that the braiding of ribbons does not interfere with the ribbon twists. Tortile categories introduce both ribbons and arc segments. Only full twists will be permitted on ribbons, so that

141

ribbon diagrams are doubled braid diagrams, with a unique underlying braid [144]. Finally, the definition of *tortile tensor* category includes the condition $\theta_{A^*} = (\theta_A)^*$. That is, if a ribbon A is twisted, the twisting on the dual object A^* must define the dual of the twisted A. This is because A and A^* are connected by a ribbon arc, and the twists can propagate along a ribbon

$$\tag{334}$$

to the other side. A single braid crossing within a ribbon diagram, thought of as a double knot, adds ± 1 to the writhe of the braid. Recall that a braid's *writhe w* is the sum $j - k$, where j is the number of over crossings and k the number of under crossings. This quantity is important in the definition of knot and link invariants. For a double knot, the *twist number* is given by

$$\theta_K = \frac{1}{2}(j - k) \tag{335}$$

This is always an integer, noting that two ribbons create four braid crossings when they cross. Let ξ_K denote $j - k$ when each ribbon crossing only contributes ± 1. That is, $\xi_K = w/4$. Then the *linking number* of the two underlying knots is given by

$$l_K = \xi_K + \theta_K \tag{336}$$

Now we can extend any single knot to a double knot by replacing each strand segment with a parallel double strand segment, ie. a ribbon, and adding full twists on the new ribbons.

The total number of twists $n = n_+ - n_-$ and ξ_K together give an equivalence between double knots, because $\xi_K + n$ is conserved under ambient isotopy in $\mathbb{R}^3$. We can see this by observing that a writhe component on the underlying knot is turned into a full twist.

$$\tag{337}$$

A *ribbon functor* is a functor between ribbon categories that preserves the essential structures. In particular, modular functors are used to model quantum computation [**?**].

In general, the categorical dimension is not restricted. Even the $\otimes$ structure will be broken by physical considerations in dimension 3. It is too laborious to write out the rules for categories with more than two or three levels of arrow, so one must focus on basic geometric elements, namely trees, braids and ribbons. We will soon see that trees contain structure into arbitrary high categorical dimension.

A.3 Tricategories and Higher Dimensions

In 1995, Gordon, Power and Street found a coherence theorem for tricategories [75]. It shows that not every tricategory is triequivalent to a strict 3-category, with simple identity arrows. Although the definition is essentially unique, its precise form is still a mystery. One axiom is given by the A_4 polytope, which generalises the Mac Lane pentagon to dimension 3. Instead of strict natural transformations, the category provides 2-arrows to fill in the squares. A convenient concept is the *pseudonatural transformation*, where the square filling arrows are assumed to be invertible. For example, given objects A, B, C and D and bicategories of arrows $T(A, B)$ between them, there is a pseudonatural transformation

$$
\begin{array}{ccc}
T(A,B) \times T(D,A) \times T(C,D) & \xrightarrow{\otimes \times 1} & T(D,B) \times T(C,D) \\
{\scriptstyle 1 \times \otimes} \downarrow & \Downarrow & \downarrow {\scriptstyle \otimes} \\
T(A,B) \times T(C,A) & \xrightarrow{\otimes} & T(C,B)
\end{array}
\tag{338}
$$

on the $\otimes$ composition functor. And since a tricategory has three dimensional arrows, diagrams of composed pseudonatural transformations are subject to *modification* 3-arrows. For example, the cube

$$\tag{339}$$

is filled with a modification. A weak identity axiom is given by the (left) triangular prism 3-arrow

$$\tag{340}$$

with faces filled by 2-arrows. Although tricategories are not all strict, they are all triequivalent to a special tricategory **Gray** of 2-categories with a Gray tensor product [249]. This is mentioned in chapter 9.

B   Braid Groups

To Maxwell, electromagnetism was a theory of circular vortices in the aether [143]. Later in the 19th century, Lord Kelvin proposed knotted vortices as atoms for space. Knots had already been studied by great mathematicians, such as Gauss, who first defined a linking number invariant.

The first true knot invariant is due to Alexander, in the 19th century. Little progress was made on finding invariants that were good at distinguishing knots, until 1983, when Jones [96] defined the Jones polynomial. This was followed shortly thereafter by a two variable analogue [250]. The basic link invariants are defined in chapter 5.

A braid group B_n on n string pieces has $n-1$ generators τ_i, for $i = 1, 2, \cdots, n-1$. Each generator represents an over under crossing, and the inverse τ_i^{-1} is the under over crossing. A braid $b \in B_n$ is a word in the generators. Since B_1 has only one string, which cannot knot itself, B_1 is the trivial group 1. With only one over $(+1)$ or under (-1) crossing, B_2 is isomorphic to $\mathbb{Z}$. For B_3, we have

$$\tag{341}$$

The group multiplication is given by adjoining a braid to the bottom of another braid, so that $\tau_1 \tau_2 \neq \tau_2 \tau_1$. For all n, the group relations are

$$\tau_i \tau_{i+1} \tau_i = \tau_{i+1} \tau_i \tau_{i+1} \quad \text{for } i = 1, 2, \cdots, n-2 \tag{342}$$
$$\tau_i \tau_j = \tau_j \tau_i \quad \text{for } |i - j| \geq 2$$

A braid $b \in B_n$ has an underlying permutation in S_n, given by the connection of endpoints at the top of the diagram to points at the bottom. Thus S_n is given by the braids in B_n, where the crossing information is forgotten.

A braid diagram is a projection onto the plane of a link diagram in three dimensions. A *link* is formed by tracing the braid, by joining each top point to the same point at the bottom of the diagram, as in the B_3 example

$$\tag{343}$$
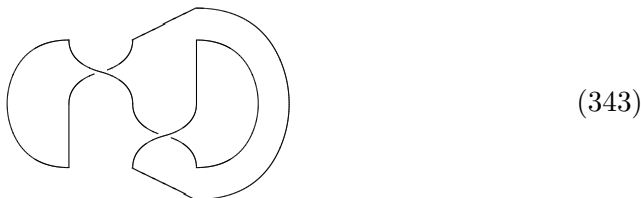
which is unknotted. Observe that the trace can form links with various numbers of loops. A *knot* is a one loop link. Markov [251] showed that a traced braid is equivalent to a link, in the sense that two distinct braid representations of the same link in three dimensions are simply related to

144

each other. A link is deformed into an equivalent link by *ambient isotopy* in dimension 3. If we are not allowed to flip knot pieces around in the third dimension, braids are only equivalent up to *planar isotopy*. The Reidemeister moves [252]

$$\tag{344}$$

$$R1 \qquad\qquad R2$$

$$R3$$

define the equivalence relation between different braid diagrams for the same link.
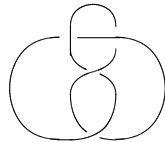
Example B.1 The Hopf link
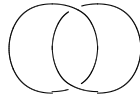
Example B.2 The trefoil knot

is *chiral*, being distinct from its mirror image.

Example B.3 The unique four crossing knot is the achiral figure eight knot.

This is the first true B_3 knot, since the trefoil is represented by $\tau_1{}^3$ in B_2. It has the braid word $\tau_1\tau_2{}^{-1}\tau_1\tau_2{}^{-1}$.

The unknot, trefoil and figure eight knots are all *prime* with respect to connected sum [253]. This operation $K_1 \sharp K_2$ cuts a small piece from two knots, and joins the knots at these points.

$$\text{(345)}$$

That is, it flips two vertical arcs to two horizontal arcs. This is a fundamental binary operation on planar string diagrams. The collection of all knots along with connected sum form a monoid, with unit the unknot. There is no canonical listing of prime knots by prime ordinals in the monoid $\mathbb{N}$, although this question is studied.

Let j be the number of positive crossings in $b \in B_n$ and k the number of negative crossings. The *writhe w* of a link is the integer $w = j - k$. For the trefoil above, $w = +3$, whereas the mirror trefoil with reversed crossings has $w = -3$.

Braid strands may be replaced by ribbon segments, allowing ribbon twists. The diagram still has an underlying link picture [144], obtained by shrinking all ribbons to strands. As we saw in appendix A, in a ribbon category a writhe component on the underlying link is turned into a full ribbon twist

$$\text{(346)}$$
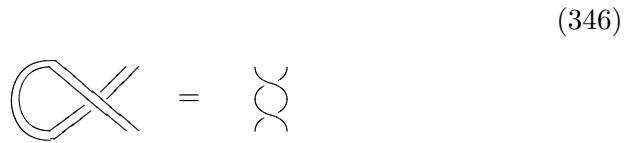
Observe that a braid crossing, as represented on the plane, consists of three string pieces: one over string and two under strings. The crossing can be used to represent a product $a \circ b = c$ of the under string segments. Algebras of such link arcs are known as *racks* or *quandles* [254]. The Reidemeister moves define their rules.

There is a category **Br** of all B_n braid groups, with objects $n \in \mathbb{N}$ and arrow sets B_n for $n \to n$. This is a collection of groups forming a *groupoid*, which is a category in which all arrows are invertible.

C   Basic Algebra

An *algebra* is usually a vector space over a field equipped with a binary product $m(a, b)$ on vectors. The field provides additive and multiplicative inverses. In constructive number theory, we are more interested in diagram algebras. A vector is then a formal sum of basis diagrams, and the coefficients belong to a restricted set, not necessarily forming a field. Products are defined using a composition of diagrams.

Many known algebras can be thought of as diagram algebras. In particular, given a diagram representation for permutations in the permutation group S_d on d objects, the group algebra of formal combinations of $\sigma \in S_d$ is a diagram algebra. Such algebras are often also *bialgebras* or *Hopf algebras*, which are defined below.

In order to be useful, diagrams should have an interpretation in category theory. A one dimensional category consists of directed edges, or 1-arrows, but we often start with undirected edge diagrams that encode parts of the categorical structure. With rooted trees, for instance, there is an obvious choice of direction, downwards on the branches.

A *monoid* is a set with a binary composition $a \circ b$ or, equivalently, a 1-category with only one 0-arrow giving the source and target of 1-arrows. Arrow composition is literally the gluing of arrows

$$\rightarrow \rightarrow \rightarrow \quad \cdots \tag{347}$$

in a diagram segment of the category, so that the composed path itself defines an arrow in the category. To begin with, binary operations are associative. This says that the two paths in

$$
\begin{array}{ccc}
a, b, c & \xrightarrow{\ m \times 1_c\ } & a \circ b, c \\
{\scriptstyle 1_a \times m} \big\downarrow & & \big\downarrow \\
a, b \circ c & \longrightarrow & a \circ b \circ c
\end{array}
\tag{348}
$$

commute, where m is the binary composition map $\mathcal{C} \times \mathcal{C} \to \mathcal{C}$ on the category $\mathcal{C}$. Weakened associativity comes from higher dimensional arrows, starting with a 2-arrow filling this square. We should always think of $\psi_{abc} : ((a \circ b) \circ c) \Rightarrow (a \circ (b \circ c))$ as being at least two dimensional. Usually, bracketed objects such as $((a \circ b) \circ c)$ are represented by tree diagrams, and ψ_{abc} is a transformation of trees. As the number of product structures grows, so does the categorical dimension.

C.1 Bialgebras and Hopf Algebras

Multiplication takes two objects a and b and returns $m(a, b)$, as in the tree

$$\begin{array}{c} a \qquad b \\ \diagdown \diagup \\ | \\ m(a,b) \end{array} \qquad (349)$$

Dually, comultiplication sends one object to two,

$$\begin{array}{c} a \\ | \\ \diagup \diagdown \\ \Delta(a) = x \otimes y \end{array} \qquad (350)$$

An ordinary *algebra* object A in a category $\mathbf{C}$ comes with a map $m : A \otimes A \to A$, such that associativity

$$
\begin{array}{ccc}
A \otimes A \otimes A & \xrightarrow{m \otimes 1_A} & A \otimes A \\
\scriptstyle{1_A \otimes m} \downarrow & & \downarrow \scriptstyle{m} \\
A \otimes A & \xrightarrow{\quad m \quad} & A
\end{array}
\qquad (351)
$$

holds. Note that $\mathbf{C}$ carries the whole algebra in the object A. Often there is also an object I in $\mathbf{C}$, such that there exists a unit arrow $\eta : I \to A$ with the property that $\eta \cdot m : I \otimes A \to A$ is essentially 1_A, and similarly for $m \cdot \eta$. Comultiplication obeys coassociativity

$$
\begin{array}{ccc}
A \otimes A \otimes A & \xleftarrow{\Delta \otimes 1_A} & A \otimes A \\
\scriptstyle{1_A \times \Delta} \uparrow & & \uparrow \scriptstyle{\Delta} \\
A \otimes A & \xleftarrow{\quad \Delta \quad} & A
\end{array}
\qquad (352)
$$

and often comes with a counit $\epsilon : A \to I$. In a category of vector spaces, the object I is the base field. A *bialgebra* object A has both a multiplication m and comultiplication Δ, such that

$$
\begin{array}{ccc}
A \otimes A & \xrightarrow{\quad m \quad} & A \\
\scriptstyle{\Delta \times \Delta} \downarrow & & \downarrow \scriptstyle{\Delta} \\
A \otimes A \otimes A \otimes A & \xrightarrow{\quad m \times m \quad} & A \otimes A
\end{array}
\qquad (353)
$$

Example C.1 A *Frobenius algebra* is a bialgebra object A with (m, Δ) and natural transformations $\eta : I \to A$ and $\epsilon : A \to I$, such that (m, η) forms a commutative monoid and (Δ, ϵ) forms a cocommutative monoid, and

$$(1 \otimes m)(\Delta \otimes 1) = \Delta m$$

A *Hopf algebra* H is a bialgebra, along with an arrow $S : H \to H$ called the *antipode* [255]. The antipode satisfies

$$
\begin{array}{ccc}
H \otimes H & \xrightarrow{\;\;S \otimes 1_H\;\;} & H \otimes H \\
{\scriptstyle \Delta}\nearrow & & \searrow{\scriptstyle m} \\
H & & H \\
{\scriptstyle \epsilon}\searrow & & \nearrow{\scriptstyle \eta} \\
& I &
\end{array}
\tag{354}
$$

Example C.2 Functions on a group G with values in a given field. The multiplication is defined by $(f_1 \cdot f_2)(g) = f_1(g)f_2(g)$. Given g and h in G, $\Delta(f)(g,h) \equiv f(gh)$, using the group product. The unit sends a scalar λ to the constant function $g \mapsto \lambda$. The counit sends f to $f(1)$, for the identity $1 \in G$. The antipode exists because G has inverses. It is defined by $S(f)(g) = f(g^{-1})$. Let us check the antipode rule. The path $\eta\epsilon$ sends f to $f(1) \cdot 1$, where 1 is the constant function. The other way, Δf acts on (g,h) and $S \times 1_A$ then works on (g^{-1}, h^{-1}), giving $f(1)$ for all $g, h \in G$, and so defining the function $f(1) \cdot 1$.

Example C.3 Given a field $\mathbb{F}$, the *group algebra* $\mathbb{F}C_3$ over the three element group $C_3 = \{(0), (1), (2)\}$ is the set of all formal linear combinations $v = a_0(0) + a_1(1) + a_2(2)$. Here C_3 is represented using mod 3 arithmetic. The field operations extend to products and scalar multiples for elements v and w. Thus $m(v,w)$ is the product vw, and the unit sends $\lambda \in \mathbb{F}$ to $\lambda(0)$, noting that (0) is the identity for C_3. The counit sends v to (0), and $\Delta(g) \equiv g \otimes g$ for $g \in C_3$. For general v, linearity fixes $\Delta(v)$. The antipode is similarly defined using $S(g) = g^{-1}$, so that $S(v) = a_0(0) + a_2(1) + a_1(2)$. Any finite group defines such a Hopf algebra.

Example C.4 [256] The renormalisation algebra is closely related to the Hopf algebra of rooted trees. A basis object is a rooted tree. Then H is a vector space over all such trees, using coefficients in $\mathbb{Q}$. The product is generated by the disjoint union of two trees, producing a *forest*. The empty tree e gives the unit, sending $\lambda \in \mathbb{Q}$ to λ, and the counit maps every non empty tree to 0, and e to 1. The comultiplication uses tree cuts, that split a tree into two pieces by removing one edge. An admissible cut set for a tree T is such that any path from a leaf down strikes at most one cut. For example,

where lone tree nodes are included. The single left and right cuts give the factor of 2. In general, Δ satisfies $\Delta(e) = e \otimes e$ and

$$\Delta(T) = T \otimes e + (I \otimes R_+)\Delta(R_-(T))$$

where R_+ is the operation of grafting two trees by attaching them to two extra base edges, and R_- is the inverse operation that removes the two root edges. The antipode for the same example is

$$S\,\overset{\bullet}{\diagdown}\!\!\overset{\bullet}{\diagup} = \overset{\bullet}{\diagdown}\!\!\overset{\bullet}{\diagup} + \; 2\,\bullet\,\overset{\bullet}{\underset{\bullet}{|}} - \; \bullet\,\bullet\bullet$$

The minus signs pick up the even number of cuts. Each cut, including the empty cut, can be represented by a box around the smaller piece so that the diagrams correspond to nested boxes. This generalises nested boxes around single path trees, which are the same as sequences of bracketings. In renormalisation, subdivergences are subgraphs of Feynman graphs, defined by the partition boxes.

C.2 Shuffles and Lattice Paths

The Hopf algebras $\mathbb{C}S_d$ over the permutation groups are of particular interest, although $\mathbb{Q}$ coefficients are more appropriate for most purposes [82].

A permutation σ in S_d, which acts on the sequence $(123\cdots d)$, is a *shuffle* if

1. $\sigma^{-1}(1) < \sigma^{-1}(2) < \cdots < \sigma^{-1}(m)$

2. $\sigma^{-1}(m+1) < \sigma^{-1}(m+2) < \cdots < \sigma^{-1}(m+n)$

for $m+n = d$. That is, the sequence σ^{-1} breaks up into two strictly ordered pieces, one of length m and one of length n. Altogether, there are

$$\binom{m+n}{m}$$

(m,n) shuffles. Note that when $m = n$, this is similar to the Catalan number C_n. For fixed m and n, the sum over all shuffles of type (m,n) in S_d is an element h_{mn} in the Hopf algebra $\mathbb{Z}S_d$. For example, for $m = 2$ and $n = 1$, $h_{21} = (123) + (132) + (312)$.

Let s_{mn} be a permutation in S_d that lets $(s_1 \cdots s_m) \in S_m$ act on the first m objects and $(s_{m+1} \cdots s_d) \in S_n$ act on the rest. Then the group algebra product $h_{mn}s_{mn}$ is thought of as a product of the partial permutations in S_m and S_n. For example, $h_{21} \cdot (213) = (213) + (231) + (321)$. This is a graded product for the infinite direct sum $\oplus \mathbb{Z}S_d$ over all d.

The (m,n) shuffles are in one to one correspondence with paths on a planar lattice [84]. The point $(0,0)$ is the source and (m,n) the target, defining a block of mn lattice squares. The variables $\sigma^{-1}(k)$ within the shuffle are used to label horizontal steps if $k \leq m$, and vertical steps for $k > m$. Shuffles are often written as words in two letter types, as in $X_1 Y_1 X_2 Y_2$ for $m = n = 2$.

## C.3 Octonions, Jordan Algebras and Spinors

This section makes a few remarks that rely on some knowledge of representation theory. The nonassociative octonions $\mathbb{O}$ [257] are real linear combinations

$$a_0 + a_1 e_1 + a_2 e_2 + a_3 e_3 + a_4 e_4 + a_5 e_5 + a_6 e_6 + a_7 e_7 \tag{355}$$

of 1 and the seven other units e_i. The products $e_i e_j$ satisfy [153]

$$e_i e_j = -\delta_{ij} + \epsilon_{ijk} e_k$$

where the antisymmetric ϵ_{ijk} has norm 1 on the seven lines of a Fano plane
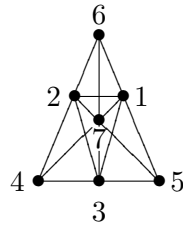
and ϵ_{ijk} is chosen to be positively oriented on the cycles

$$615 \quad 534 \quad 426 \quad 673 \quad 471 \quad 572 \quad 213.$$

The projective Fano plane is the seven lines in the cube $\mathbb{F}_2{}^3$. The line orientation is recovered from an oriented cube with faces of type

$$\tag{356}$$

and the central e_7 placed at the source and target. It uses the labeling

$$\tag{357}$$

By definition, the conjugate of $a \in \mathbb{O}$ is $a_0 - \sum_1^7 a_i e_i$. The *norm* of $a \in \mathbb{O}$ is $N(a) \equiv a\bar{a}$, satisfying $N(ab) = N(a)N(b)$.

The bioctonions $\mathbb{CO}$ are the complexification of $\mathbb{O}$ defined by complex coefficients [258], such that the complex unit i commutes with all e_i. It has an octonion conjugate and a complex conjugate $\overline{a_0} + \sum \overline{a_i} e_i$. The bioctonions

contain the *split octonion* algebra [153]. This may be defined using the 2×2 rational matrices

$$A \equiv \begin{pmatrix} x & a \\ b & y \end{pmatrix} \qquad \overline{A} \equiv \begin{pmatrix} y & -a \\ -b & x \end{pmatrix} \qquad (358)$$

with x, y in $\mathbb{Q}$ and a, b in a three dimensional space V^3. The matrix product is

$$\begin{pmatrix} x_1 & a_1 \\ b_1 & y_1 \end{pmatrix} \begin{pmatrix} x_2 & a_2 \\ b_2 & y_2 \end{pmatrix} = \begin{pmatrix} x_1 x_2 + a_1 \cdot b_2 & x_1 a_2 + y_2 a_1 - b_1 \times b_2 \\ x_2 b_1 + y_1 b_2 + a_1 \times a_2 & y_1 y_2 + b_1 \cdot a_2 \end{pmatrix}.$$
$$(359)$$

The 8 basis elements of the split algebra are then given by

$$u_0 = \begin{pmatrix} 0 & 0 \\ 0 & 1 \end{pmatrix} \qquad \overline{u}_0 = \begin{pmatrix} 1 & 0 \\ 0 & 0 \end{pmatrix} \qquad (360)$$

$$u_i = \begin{pmatrix} 0 & 0 \\ e_i & 0 \end{pmatrix} \qquad \overline{u}_i = \begin{pmatrix} 0 & -e_i \\ 0 & 0 \end{pmatrix}$$

for e_i the three octonion units e_1, e_2 and e_3. Then $A\overline{A} = \overline{A}A$ equals $(xy - a \cdot b)I_2$. There are two copies of the split octonions in $\mathbb{CO}$, with the second one given by iu_j.

A (formally real) Jordan algebra $\mathcal{J}_n$ [257] has a nonassociative product $a \circ b$ such that

$$a \circ (b \circ a^2) = (a \circ b) \circ a^2. \qquad (361)$$

We are interested in the 3×3 matrix Jordan algebras over $\mathbb{R}$, $\mathbb{C}$, $\mathbb{H}$, $\mathbb{O}$ and $\mathbb{CO}$. These are the 3×3 Hermitian matrices with commutative Jordan product $a \circ b \equiv (ab + ba)/2$.

The 2×2 Hermitian matrices over $\mathbb{O}$ also form a Jordan algebra, and it has projections

$$\begin{pmatrix} X\overline{X} & X\overline{Y} \\ Y\overline{X} & Y\overline{Y} \end{pmatrix} \qquad (362)$$

for (X, Y) in $\mathbb{O}^2$ of norm 1. By definition, the projective line $\mathbb{OP}^1$ is the set of all 2×2 projections P such that the trace of P equals 1. This agrees with the projective lines $\mathbb{FP}^1$ over the other fields. The 3×3 algebra over $\mathbb{O}$ can only give a Moufang plane $\mathbb{OP}^2$ [259], and there is no $\mathbb{OP}^3$. The line $\mathbb{OP}^1$ is basically the sphere $S^8 \simeq \mathbb{O} \cup \infty$, just as $\mathbb{CP}^1$ is the sphere S^2. The 2×2 algebra over $\mathbb{O}$ is an instance of a *spin factor* [257] because the elements

$$\begin{pmatrix} x + y & a \\ \overline{a} & x - y \end{pmatrix} \qquad (363)$$

with x and y real may be considered as elements (a, y, x) in $\mathbb{O} \oplus \mathbb{R} \oplus \mathbb{R}$, and similarly for a rational basis. The matrices in $SL_2(\mathbb{O})$ give the spin group Spin$(9,1)$, which is the double cover of the Lorentz group in dimension 9.

The group $SL_2(\mathbb{O})$ acts on $\mathbb{O}^2$ as a left handed spinor representation, just as for the twistor $SL_2(\mathbb{C})$.

For octonions, the 2×2 spacetime has dimension 10, and for the bioctonions [258] it should have real dimension 20. This happens to equal the number of minors D_{ij} for a 3×6 Grassmannian matrix in $\text{Gr}(3,6)$. Such minors are fundamental to scattering combinatorics, and $\text{Gr}(3,6)$ represents the six particle case with a $- - - + ++$ helicity configuration. In chapter 10, the $-+$ pairs represent a fermion, so that $\text{Gr}(3,6)$ is a three fermion state space. The 2×2 algebra over $\mathbb{O}$ appears in the 3×3 algebra under the isomorphism [257]

$$\mathcal{J}_3(\mathbb{O}) \simeq \mathcal{J}_2(\mathbb{O}) \oplus \mathbb{O}^2 \oplus \mathbb{R} \simeq \mathbb{R}^3 \oplus V_8 \oplus S_8{}^+ \oplus S_8{}^-.$$

Here V_8, $S_8{}^+$ and $S_8{}^-$ are the three components of triality for the octonion number field. $S_8{}^+$ and $S_8{}^-$ are right and left handed spinor representations. Triality is the trilinear map

$$t : V_8 \times S_8{}^+ \times S_8{}^- \to \mathbb{R} \tag{364}$$

associated to the multiplication structure of a division algebra. Trialities with norms are always specified in terms of spinors, since they give representations of $\text{Spin}(n)$. All three components are just $\mathbb{R}^8$ as vector spaces. An automorphism of the triality is a triplet (f_1, f_2, f_3) of norm preserving maps such that

$$t(f_1(v_1), f_2(v_2), f_3(v_3)) = t(v_1, v_2, v_3)$$

for all v_i. It turns out that the automorphisms of $\mathbb{O}$ form the Lie group G_2, and this is contained in the triality automorphism group $\text{Spin}(8)$. Remarkably, any $g \in \text{Spin}(8)$ defines a unique triplet (g, g_+, g_-) in $\text{Spin}(8)^3$ such that

$$t(g(v_1), g_+(v_2), g_-(v_3)) = t(v_1, v_2, v_3).$$

The outer automorphisms of $\text{Spin}(8)$ form the permutation group S_3, which allows any permutation of the spaces V_8, $S_8{}^+$ and $S_8{}^-$.

For the full bioctonion algebra $\mathcal{J}_3(\mathbb{C}\mathbb{O})$ we define a trilinear form by [260]

$$T(a, b, c) \equiv (a, b \circ c) = \frac{1}{2}(a, bc) + \frac{1}{2}(a, cb) \tag{365}$$

where (x, y) is the inner product $\text{tr}(x \circ y)$, and the last step uses ordinary matrix product. The complex 3×3 matrices form a subalgebra of $\mathcal{J}_3(\mathbb{C}\mathbb{O})$. There is also a commutative *Freudenthal product*

$$a \times b \equiv a \circ b - \frac{1}{2}\text{tr}(a)b - \frac{1}{2}\text{tr}(b)a + \frac{1}{2}\text{tr}(a)\text{tr}(b)I_3 - \frac{1}{2}(a, b)I_3 \tag{366}$$

and associated cubic form

$$(a, b, c) \equiv (a, b \times c) = (a \times b, c). \qquad (367)$$

Then the determinant of $a \in \mathcal{J}$ is given by $\det(a) = (a, a, a)/3$. It is known as the cubic norm of a.

Let D_{ij} denote the minor determinant at position ij in any $n \times n$ complex matrix D. The cofactor matrix C_{ij} has entries $(-1)^{i+j} D_{ij}$ for $i, j = 1, 2, \cdots, n$. The adjugate is the transpose $D^* \equiv C_{ij}{}^T$. There is then a bilinear form on matrices in $\mathcal{J}_3(\mathbb{C})$ given by [202]

$$\beta(A^*, B) = 3(A, A, B). \qquad (368)$$

The *Freudenthal triple system* for $\mathcal{J}(\mathbb{F})$ is the larger algebra

$$\mathbb{F} \oplus \mathbb{F} \oplus \mathcal{J} \oplus \mathcal{J}$$

with elements 2×2 matrices A as in (358), such that $x, y \in \mathbb{F}$ and a and b are $\mathcal{J}$. For $\mathcal{J}$ the 3×3 complex matrices, the Freudenthal triple is a 20 complex dimensional space. The *quartic form* of the system is

$$q(A) \equiv 2(\beta(a, b) - xy)^2 - 8\beta(a^*, b^*) + 8x \det(a) + 8y \det(b). \qquad (369)$$

Under a suitable equivalence relation on the Freudenthal triple system for complex matrices [202], any matrix in the algebra may be transformed into elements with $b = 0$, $y = 0$ and $x = 1$, and a diagonal a in the set

$$\begin{pmatrix} 0 & 0 & 0 \\ 0 & 0 & 0 \\ 0 & 0 & 0 \end{pmatrix} \quad \begin{pmatrix} 1 & 0 & 0 \\ 0 & 0 & 0 \\ 0 & 0 & 0 \end{pmatrix} \quad \begin{pmatrix} 1 & 0 & 0 \\ 0 & 1 & 0 \\ 0 & 0 & 0 \end{pmatrix} \quad \begin{pmatrix} 1 & 0 & 0 \\ 0 & 1 & 0 \\ 0 & 0 & k \end{pmatrix}$$

for $k \in \mathbb{C}$. In this case, the quartic form often reduces to $8\det(a)$, which takes values in $\{0, 8k\}$.

There is an $SU(3)$ color subgroup of G_2 that makes the split octonions u_0 and $\overline{u}_0$ singlets and the u_i and $\overline{u}_i$ a triplet and antitriplet [153]. Octonion structure can thus be used to specify the quarks. The automorphisms of $\mathcal{J}_3(\mathbb{O})$ are the Lie group F_4, which is generated by a pair of traceless Hermitian matrices over $\mathbb{O}$. This is a $52 = 2 \times 26$ dimensional group. It has an $SU(3) \times SU(3)$ flavor color subgroup, associated to the decomposition

$$26 \mapsto (8, 1) \oplus (3, 3) \oplus (\overline{3}, \overline{3}). \qquad (370)$$

This is in turn related to the 27 dimensional representation of the group E_6, which has decomposition [153]

$$(\overline{3}, 3, 1) \oplus (3, 1, 3) \oplus (1, \overline{3}, \overline{3}) \qquad (371)$$

under $SU(3) \times SU(3) \times SU(3)$. The last factor is the color symmetry. The $(\overline{3}, 3)$ part is the lepton factor. All leptons and quarks fit into a complex octonion 3×3 matrix, written as a combination of the $\{u_0, u_i, \overline{u}_0, \overline{u}_i\}$. Particle states are discussed in chapter 7.

C.4 Tensor Algebra and Distributivity

For two $n \times n$ matrices J and K, the *Schur product* S is given entry by entry as $S_{ij} \equiv J_{ij} \cdot K_{ij}$. This is a kind of word concatenation, as in the example

$$\begin{pmatrix} X\overline{X} & X\overline{Y} \\ Y\overline{X} & Y\overline{Y} \end{pmatrix} = \begin{pmatrix} X & X \\ Y & Y \end{pmatrix} \circ_S \begin{pmatrix} \overline{X} & \overline{Y} \\ \overline{X} & \overline{Y} \end{pmatrix} \qquad (372)$$

for a dual pair of vectors, resulting in a Jordan algebra projection. For a general square matrix, if the entries are projections $(P_{ij})^2 = P_{ij}$, then the Schur product clearly defines a matrix projection. The Schur product is a submatrix of the tensor product.

We imagine that everything is a category, rather than a set. Recall that the tensor product $A \otimes B$ of two 2×2 matrices A and B, with commutative entries, is defined as the 4×4 matrix

$$\begin{pmatrix} A_{11}B_{11} & A_{11}B_{12} & A_{12}B_{11} & A_{12}B_{12} \\ A_{11}B_{21} & A_{11}B_{22} & A_{12}B_{21} & A_{12}B_{22} \\ A_{21}B_{11} & A_{21}B_{12} & A_{22}B_{11} & A_{22}B_{12} \\ A_{21}B_{21} & A_{21}B_{22} & A_{22}B_{21} & A_{22}B_{22} \end{pmatrix}. \qquad (373)$$

This generalises to any pair of matrices. Given a tensor product on objects in a category V with addition and multiplication, the *symmetric algebra* on V is the space of all objects $v_1 \otimes v_2 + v_2 \otimes v_1$. The *exterior algebra* $\bigwedge^k V$ is the space spanning all k-fold *wedge products* $v_1 \wedge \cdots \wedge v_k$ for $1 \cdots \leq k-1 \leq k$, where $v_1 \wedge v_2$ is defined as $v_1 \otimes v_2 - v_2 \otimes v_1$. Then $v_1 \wedge v_2 = -v_2 \wedge v_1$.

Consider a category with the three composition types $.$, $\otimes$ and $\oplus$. Let $.$ give horizontal composition and $\otimes$ vertical. As with matrices, the category also contains objects I_n for $n \in \mathbb{N}$ that act as identities for the $.$ product. Then the object $(A \otimes I_m)(I_n \otimes B)$
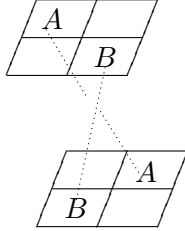
A	I_n
I_m	B

usually specifies a unique object $A \otimes B$ by the bicategory interchange law. Similarly for $B \otimes A$. What about $\oplus$ in the third dimension? Using matrix dimensions as a guide, observe that $(A \oplus B) \otimes (B \oplus A)$ should distribute to

$$(A \otimes B) \oplus (B \otimes A) \oplus (A \otimes A) \oplus (B \otimes B),$$

whereas $(A \otimes B) \oplus (B \otimes A)$ would be $(A \oplus B) \otimes (B \oplus A)$ if basic interchange held.

That is, basic distributivity is breaking interchange in the third dimension

by creating the AA and BB terms. Distributivity is fundamentally a three dimensional structure. In a higher category, a *distributive law* is a natural transformation $\lambda : \otimes\oplus \to \oplus\otimes$ between two operation endofunctors, such that $\lambda \cdot (\otimes)_R = (\otimes)_L$ and

$$
\begin{array}{ccc}
& \oplus\otimes\oplus \longrightarrow \otimes\oplus\oplus & \\
\oplus\oplus\otimes & & \otimes\oplus \\
& \oplus\otimes &
\end{array}
\tag{374}
$$

commutes, along with similar laws for a source $\oplus\otimes\otimes$. Observe that λ resembles a braiding. Already with $\otimes$ and $\oplus$ we have a string of adjunctions for distributivity [136]. That is, if **Mon** is a category of monoids with $\otimes$ and **Ab** is a category of additive groups with $\oplus$, then there is a category **Ring** that inherits the two operations through the four adjunctions in the square

$$
\begin{array}{ccc}
& \mathbf{Ring}_{\otimes\oplus} & \\
\mathbf{Mon}_{\otimes} & & \mathbf{Ab}_{\oplus} \\
& \mathbf{Set} &
\end{array}
\tag{375}
$$

and a distributive law gives an arrow inside the square, which is nominally a 3-arrow filling a tetrahedron. As a string diagram, the usual distributive axiom is naturally symmetric, allowing strings to slide past one another through a vertex. A braiding gives a choice between the usual law and a broken distributivity, with the axiom taking the form

$$
\neq
\tag{376}
$$

Note that only a pair of opposite crossings on the left will block the string slide. Each crossing is a braiding $\lambda_{\otimes\oplus}$ on the two functor objects. Since our physical spaces emerge from braided structures, broken distributivity for arithmetic is a fundamental feature of quantum algebra.

Remark C.5 The Jacobi rule (161) for Lie algebras is often expressed as a triplet of trees. The (s, t, u) Mandelstam variables act on three particles (234), once the leg 1 is fixed. They permute these three legs according to the 1-circulants in S_3. Thus a braided version of the Jacobi rule replaces the S_3 permutations by a braid triplet in B_3. With suitably chosen crossings, these form an annihilation triplet (γ, e_L, e_R), as in the bottom pieces of the broken distributivity diagrams. This three term braided Jacobi rule is then a form of broken distributivity. There is a left and right handed version, each using two fermion braids and the resulting photon.

References

[1] M. Marcolli, arXiv:0907.0321

[2] A. Connes and M. Marcolli, *Noncommutative Geometry, Quantum Fields and Motives* (AMS Colloquium Publ., 2007)

[3] A. Grothendieck, http://en.wikipedia.org/wiki/Alexander_Grothendieck

[4] R. Street, J. Pure Appl. Alg. **49**, 283335(1987)

[5] E. H. Spanier, *Algebraic Topology* (McGrawHill, 1966)

[6] S. Eilenberg and N. Steenrod, *Foundations of Algebraic Topology* (Princeton, 1952)

[7] I. Moerdijk and S. Mac Lane, *Sheaves in geometry and logic: a first introduction to topos theory* (Springer, 2000)

[8] M. J. Duff, Int. J. Mod. Phys. A **11**, 56235642(1996)

[9] E. Witten, Not. Amer. Math. Soc., 11241129(1998)

[10] S. Wagon, *The Banach Tarski Paradox* (Cambridge, 1993)

[11] G. Peano, Math. Annalen, **36**, 157160(1890)

[12] Philosophy Encyclopedia, http://plato.stanford.edu/entries/fregelogic

[13] J. W. Cannon and W. P. Thurston, Geom. Top. **11**, 13151355(2007)

[14] S. E. Crans, Theory Appl. Cat. **5**, 1269(1999),
http://home.tiscali.nl/secrans/papers/tpgc.html

[15] E. Witten, Commun. Math. Phys. **121**, 351399(1989)

[16] A. Hughston and M. Hurd, Proc. Roy. Soc. London **A378**, 141154(1981)

[17] Z. Bern, J. J. Carrasco, L. Dixon, H. Johansson and R. Roiban, arXiv:1103.1848v2

[18] R. Kallosh and T. Kugo, arXiv:0811.3414v2

[19] F. Cachazo, L. Mason and D. Skinner, arXiv:1207.4712v1

[20] T. Adamo and L. Mason, arXiv:1207.3602v1

[21] B. Greene, *The fabric of the cosmos: space, time and the texture of reality* (Random House, 2004)

[22] G. A. J. Sparling, Proc. Roy. Soc. A **463**, 2083(2007)

[23] I. Bars, arXiv:hepth/0502065v3

[24] L. Borsten, M. J. Duff and P. Levay, arXiv:1206.3166v1

[25] L. Borsten, D. Dahanayake, M. J. Duff, H. Ebrahim and W. Rubens, Phys. Rev. A **80**, 032326 (2009)

[26] P. Levay, arXiv:quantph/0403060v1

[27] A. Hodges, arXiv:1204.1930v1

[28] J. Fuchs, *Affine Lie Algebras and Quantum Groups* (Cambridge, 1992)

[29] J. Fuchs, I. Runkel and C. Schweigert, Contemp. Math. **431**, 203224 (2007), arXiv:math/0511590

[30] I. Runkel, J. Fuchs and C. Schweigert, arXiv:math/0602079

[31] R. W. Ghrist, Topology **36**, 423448 (1997)

[32] J. Birman and R. F. Williams, Topology **22**, 120 (1983)

[33] E. Witten, arXiv:0706.3359v1

[34] G. V. Belyi, Math. USSR Izvestiya **14**, 247 (1980)

[35] M. A. Nielsen, and I. L. Chuang, *Quantum Computation and Quantum Information* (Cambridge, 2000)

[36] http://cornellmath.wordpress.com/2007/07/30/sumdivergentseriesii/,

[37] T. Apostol, *Introduction to analytic number theory* (SpringerVerlag, 1976)

[38] D. E. Knuth, *Surreal numbers* (AddisonWesley, 1974)

[39] G. H. Hardy and E. M. Wright, *An introduction to the theory of numbers* (Oxford, 1979)

[40] J. Franel and E. Landau, Gotting. Nachr., 108206 (1924)

[41] K. Ford, Ann. Math. **150**, 283311 (1999)

[42] A. Gathmann, arXiv:math/0601322v1

[43] M. Joswig, *Essentials of tropical combinatorics* (Springer, 2012)

[44] A. Connes, and C. Consani, arXiv:0911.3537v1

[45] R. Bott, and L. W. Tu, *Differential Forms in Algebraic Topology* (SpringerVerlag, 1982)

[46] F. Hirzebruch, *Topological Methods in Algebraic Geometry* (Springer, 1978)

[47] C. McLarty, *Elementary categories, elementary toposes* (Oxford, 1992)

[48] C. Piron, *Foundations of Quantum Physics* (W.A. Benjamin, 1976)

[49] R. Penrose and W. Rindler, *Spinors and spacetime: spinor and twistor methods in spacetime geometry* (Cambridge, 1988)

[50] R. S. Ward, and R. O. Wells, *Twistor Geometry and Field Theory* (SpringerVerlag, 1990)

[51] J. Schwinger, Proc. Nat. Acad. Sci. U.S.A. **46**, 570 (1960)

[52] W. K. Wootters and B. D. Fields, Annal. Phys. **191**, 363381 (1989)

[53] J. Lawrence, Phys. Rev. A **84**, 022338 (2011)

[54] M. Combescure, arXiv:0710.5642

[55] M. Combescure, J. Math. Phys. **50**, 032104 (2009)

[56] M. Kapranov, www.math.unihamburg.de/home/schreiber/Kapranov_Streetfest.pdf

[57] P. Johnstone, *Stone spaces* (Cambridge, 1982)

[58] A. Joyal and R. Street, Adv. Math. **88**, 55113 (1991)

[59] B. Coecke, arXiv:quantph/0510032v1

[60] B. Coecke, S. Perdix and E. O. Paquette, arXiv:0808.1029v1

[61] B. Coecke and D. Pavlovic, arXiv:quantph/0608035

[62] R. Jozsa, arXiv:quantph/0508124v2

[63] M. Batanin, Adv. Math. **136**, 39103 (1998)

[64] A. Joyal and R. Street, Adv. Math. **102**, 2078 (1993)

[65] M. Batanin, Adv. Math. **211**, 684725 (2007)

[66] M. Batanin, www.maths.mq.edu.au/ street/BatanAustMSMq.pdf

[67] M. Batanin, arXiv:math.CT/0301221

[68] L. Loomis, *An introduction to abstract harmonic analysis* (D. van Nostrand, 1953)

[69] N. Koblitz, *Padic numbers, padic analysis and zeta functions* (D. van Nostrand, 1996)

[70] J. Neukirch, *Algebraic number theory* (SpringerVerlag, 1999)

[71] D. V. Chistyakov, Theor. Math. Phys. **109**, 14951507(1996)

[72] A. Postnikov, arXiv:math/0507163v1

[73] D. Tamari, Bull. Soc. Math. France **82**, 5396(1954)

[74] J. D. Stasheff, Trans. Amer. Math. Soc. **108**, 275292(1963)

[75] R. Gordon, A. J. Power and R. Street, Mem. Amer. Math. Soc. **117**, 558(1995)

[76] N. Gurski, http://users.math.yale.edu/ mg622/tricats.pdf

[77] S. Mac Lane, *Categories for the working mathematician* (SpringerVerlag, 1998)

[78] D. BarNatan, in *Proceedings of the Georgia international topology conference* (International Press, 1997), www.math.toronto.edu/drorbn/papers/nat/nat.pdf

[79] J. Loday, http://wwwirma.ustrasbg.fr/ loday/PAPERS/Dichotomy.pdf

[80] L. Solomon, J. Alg. **41**, 255268(1976)

[81] M. D. Atkinson, Bull. London Math. Soc. **24**, 545551(1992)

[82] J. L. Loday and M. Ronco, Adv. Math. **139**, 293309(1998)

[83] Online database of integer sequences, http://oeis.org

[84] I. M. Gelfand, M. M. Kapranov, and A. V. Zelevinsky, *Discriminants, Resultants and Multidimensional Determinants* (Birkhauser, 1994)

[85] S. L. Devadoss, arXiv:math/0102166v1

[86] W. Zhao, J. Pure Appl. Alg. **186**, 311327(2004)

[87] L. Foissy, arXiv:1007.1547v3

[88] R. P. Stanley, *Enumerative Combinatorics* (Cambridge, 1999)

[89] J. Pitman and R. Stanley, Disc. Comput. Geom. **27**, 603634(2002)

[90] J. L. Loday, arXiv:math/0510380v1

[91] H. Gangl, A. B. Goncharov and A. Levin, arXiv:math/0508066v1

[92] J. Birman, Can. J. Math. **28**, 264290(1976)

[93] C. Kassel and V. Turaev,
emphBraid groups (Springer, 2008)

[94] V. Turaev, Sem. Bourbaki **878**, 389409(1999)

[95] V. F. R. Jones, Ann. Math. **126**, 335388(1987)

[96] V. F. R. Jones, Bull. Amer. Math. Soc. **12**, 103111(1985)

[97] Knot Atlas, http://katlas.math.toronto.edu/wiki/Main_Page

[98] L. Kauffman, Topology **26**, 395407(1987)

[99] D. Kreimer, Adv. Theor. Math. Phys. **2**, 303(1998), arXiv:qalg/9707029

[100] S. Bloch, H. Esnault and D. Kreimer, arXiv:math/0510011v1

[101] D. J. Broadhurst and D. Kreimer, Phys. Lett. B **393**, 403412(1997)

[102] S. O. BilsonThompson, arXiv:hepph/0503213v2

[103] R. Penrose, Rep. Math. Phys. **12**, 6576(1977)

[104] J. C. Baez and J. Huerta, arXiv:1003.3436v2

[105] S. Mandelstam, Phys. Rev. **112**, 1344(1958)

[106] N. ArkaniHamed, F. Cachazo, C. Cheung and J. Kaplan, arXiv:0907.5418

[107] N. ArkaniHamed, J. L. Bourjaily, F. Cachazo, S. CaronHuot, and J. Trnka,
arXiv:1008.2958

[108] N. ArkaniHamed, J. L. Bourjaily, F. Cachazo, and J. Trnka,
arXiv:1012.6032v1

[109] L. Mason and D. Skinner, JHEP **12**, 018(2010), arXiv:1009.2225

[110] R. Penrose, Twistor workshop, Oxford, 2009

[111] F. Cachazo, P. Svrcek and E. Witten, JHEP **0409**, 6(2004)
arXiv:hepth/0403047v2

[112] S. J. Parke and T. R. Taylor, Phys. Rev. Lett. **56**, 24592460(1986)

[113] Z. Bern, G. Chalmers, L. Dixon and D. A. Kosower, Phys. Rev. Lett. **72**,
2134(1994) arXiv:hepth/9312333

[114] R. Britto, F. Cachazo and B. Feng, Nucl. Phys. B **715**, 499522(2005)
arXiv:hepth/0412308

[115] R. Britto, F. Cachazo, B. Feng and E. Witten, Phys. Rev. Lett. **94**,
181602(2005) arXiv:hepth/0501052

[116] A. Hodges, http://www.twistordiagrams.org.uk

[117] N. ArkaniHamed, http://strings2012.mpp.mpg.de/

[118] A. Postnikov, http://math.mit.edu/ apost/courses/18.318

[119] D. Speyer and L. K. Williams, arXiv:math/0312297v1

[120] Z. Bern, J. J. M. Carrasco and H. Johansson, Phys. Rev. Lett. **105**, 061602(2010) arXiv:1004.0476

[121] Z. Bern and T. Dennen, arXiv:1103.0312v1

[122] N. ArkaniHamed, http://pirsa.org/11080047

[123] E. Witten, Commun. Math. Phys. **252**, 189(2004) arXiv:hepth/0312171

[124] M. Spradlin and A. Volovich, Phys. Rev. D **80**, 085022(2009) arXiv:0909.0229v1

[125] M. Spradlin and A. Volovich, arXiv:1105.2024v2

[126] A. B. Goncharov, M. Spradlin, C. Vergu and A. Volovich, Phys. Rev. Lett. **105**, 151605(2010) arXiv:1006.5703v2

[127] A. Goncharov, Adv. Math. **114**, 197318(1995)

[128] M. Hoffman, http://www.usna.edu/Users/math/meh/mult.html

[129] J. M. Borwein and W. Zudilin, http://carma.newcastle.edu.au/MZVs

[130] F. C. S. Brown, C. R. Acad. Sci. Paris Ser. I **342**, 949954(2006) arXiv:math/0606419v1

[131] M. D. Sheppeard, Ph.D. thesis, Canterbury (2007), http://hdl.handle.net/10092/1436

[132] L. Lewin, *Polylogarithms and Associated Functions* (North Holland, 1981)

[133] C. Duhr, H. Gangl and J. R. Rhodes, arXiv:1110.0458v1

[134] S. Crans, J. Pure Appl. Alg. **101**, 3557(1995)

[135] A. B. Goncharov, arXiv:math/0202154v2

[136] J. Beck, Lect. Notes Math. **80**, 119140(1969) doi:10.1007/BFb0083084

[137] M. Barr and C. Wells, *Toposes, triples and theories* (SpringerVerlag, 1985)

[138] P. Higgs, Phys. Rev. **145**, 11561163(1966)

[139] ATLAS Collaboration, https://twiki.cern.ch/twiki/bin/view/AtlasPublic/HiggsPublicResults

[140] CMS Collaboration, https://twiki.cern.ch/twiki/bin/view/CMSPublic/PhysicsResultsHIG

[141] A. Dharwadker and V. Khachatryan, arXiv:0912.5189v1

[142] T. Dimofte and S. Gukov, arXiv:1106.4550v1

[143] J. C. Maxwell, Phil. Trans. Roy. Soc. London **155**, 459512 (1865)

[144] M. C. Shum, J. Pure Appl. Alg. **93**, 57110 (1994)

162

[145] M. D. Sheppeard, http://vixra.org/abs/1004.0083

[146] L. B. Okun, arXiv:hepph/0606202v2

[147] H. M. Hodges, Phys. Rev. D **47**, 456459 (1993)

[148] C. A. Brannen, http://brannenworks.com/E8/HopfWeakQNs.pdf

[149] M. D. Sheppeard, http://keamonad.blogspot.com

[150] M. GellMann and Y. Ne'eman, *The Eightfold Way* (Benjamin, 1964)

[151] C. Itzykson and J. B. Zuber, *Quantum Field Theory* (McGrawHill, 1985)

[152] C. Furey, arXiv:1002.1497v3

[153] S. Catto, arXiv:hepth/0302079v1

[154] B. Pontecorvo, Sov. Phys. JETP **26**, 984(1968)

[155] S. Eidelman et al, Phys. Lett. B **592**, 1(2004)

[156] Z. Maki, M. Nakagawa and S. Sakata, Prog. Theor. Phys. **28**, 870 (1962)

[157] M. Kobayashi and T. Maskawa, Prog. Theor. Phys. **49**, 652657 (1973)

[158] C. Jarlskog, Phys. Rev. Lett. **55**, 1039(1985)

[159] Particle Data Group,
http://pdg.lbl.gov/2012/reviews/rpp2012revvudvus.pdf

[160] P. F. Harrison and D. H. Perkins, Phys. Lett. B **530**, 167 (2002),
arXiv:hepph/0202074

[161] P. F. Harrison and W. G. Scott, Phys. Lett. B **547**, 219 (2002),
arXiv:hepph/0210197

[162] T2K Collaboration, http://t2kexperiment.org/forphysicists/

[163] MINOS Collaboration,
http://wwwnumi.fnal.gov/PublicInfo/forscientists.html

[164] Daya Bay Collaboration, arXiv:1203.1669v2

[165] Particle Data Group,
http://pdg.lbl.gov/2012/reviews/rpp2012revneutrinomixing.pdf

[166] Particle Data Group,
http://pdg.lbl.gov/2012/reviews/rpp2012revckmmatrix.pdf

[167] D0 Collaboration, arXiv:1005.2757v1

[168] M. D. Sheppeard, http://vixra.org/abs/1008.0015

[169] P. Gibbs, http://vixra.org/abs/0907.0002

[170] S. Lisi, http://math.stackexchange.com/q/29819

[171] J. Beringer et al, Phys. Rev. D **86**, 010001 (2012)

[172] Y. Koide, Lett. Nuovo Cimento **34**, 201 (1982)

[173] Y. Koide, Phys Lett. B **120**, 161165 (1983)

[174] C. A. Brannen (2008), http://www.brannenworks.com/koidehadrons.pdf

[175] PhysicsForums, http://www.physicsforums.com/showthread.php?t=551549

[176] D. Look, http://home.comcast.net/ davelook/site/

[177] M. D. Sheppeard, http://pseudomonad.blogspot.co.nz/2010/07

[178] A. Rivero, arXiv:1111.7232

[179] G. Dungworth, http://www.galaxyzooforum.org/index.php?topic=277933.0

[180] M. D. Sheppeard and G. Dungworth, http://vixra.org/abs/1102.0010

[181] E. Noether, http://de.wikisource.org/wiki/Invariante_Variationsprobleme

[182] R. Foot, Int. J. Mod. Phys. D **13**, 21612192(2004), arxiv:quantph/0402130

[183] W. Greiner and B. Muller, *Gauge Theory of Weak Interactions* (Springer, 2000)

[184] LHC Higgs Cross Sections, arXiv:1201.3084v1

[185] A. Dharwadker, http://www.dharwadker.org/standard_model

[186] http://mathworld.wolfram.com/SteinerSystem.html

[187] http://en.wikipedia.org/wiki/Binary_Golay_code

[188] V. F. R. Jones, personal communication, Adelaide, 1995

[189] CDF Collaboration, http://wwwcdf.fnal.gov/physics/ewk/2011/wjj/

[190] D. K. Ghosh, M. Maity and S. Roy, Phys. Rev. D **84**, 035022(2011)

[191] Z. Berezhiani and R. N. Mohapatra, Phys. Rev. D **52**, 6607-6611(1995)

[192] S. Friedl and N. Jackson, arXiv:1102.3742v1

[193] N. Temperley and E. Lieb, Proc. Roy. Soc. A **322**, 251(1971)

[194] M. Khovanov, Duke Math. J. **101**, 359426(2000), arXiv:math/9908171v2

[195] M. H. Freedman, M. Larsen and Z. Wang, Commun. Math. Phys. **9**, 605622(2000)

[196] R. Penrose, in *Combinatorial Mathematics and its Applications* (Academic Press, 1971)

[197] D. Bar Natan, arXiv:math.GT/0410495

[198] H. Wenzl, C. R. Math. Rep. Acad. Sci. Canada **9**, 59(1987)

[199] http://en.wikipedia.org/wiki/IwahoriHecke_algebra

[200] M. Mulase, http://www.math.ucdavis.edu/ mulase/texfiles/2001moduli.pdf

[201] S. Devadoss, Contemp. Math. **239**, 91114(1999)

[202] P. Levay and P. Vrana, Phys. Rev. A **78**, 022329(2008), arXiv:0806.4076v1

[203] V. Coffman, J. Kundu and W. K. Wootters, Phys. Rev. A **61**, 052306(2000), arXiv:quantph/9907047v2

[204] O. Holtz and B. Sturmfels, J. Alg. **316**, 634648(2007),

[205] F. Verstraete, J. Dehaene and B. De Moor, Phys. Rev. A **68**, 012103(2003)

[206] B. Coecke and A. Kissinger, arXiv:1002.2540

[207] S. Abramsky and B. Coecke, Proceedings of the 19th IEEE conference on Logic in Computer Science (LiCS'04) (2004), http://arxiv.org/abs/quantph/0402130

[208] I. Shunsuke, *Information theory for continuous systems* (World Scientific, 1993)

[209] J. D. Bekenstein, Phys. Rev. D **7**, 23332346(1973)

[210] S. W. Hawking, Comm. Math. Phys. **43**, 199220(1975)

[211] S. Ferrara and A. Marrani, arXiv:0708.1268v2

[212] F. Zwicky, Helv. Phys. Acta **6**, 110127(1933)

[213] V. C. Rubin and W. K. Ford, Astrophys. J. **159**, 379(1970)

[214] DM Portal, http://lpsc.in2p3.fr/mayet/dm.php

[215] P. D. Mannheim and D. Kazanas, Astrophys. J. **342**, 635638(1989)

[216] S. Perlmutter et al, Astrophys. J. **517**, 565586(1999)

[217] A. G. Riess et al, Astronom. J. **116**, 10091038(1998)

[218] K. S. Thorne, R. H. Price and D. M. McDonald, *Black Holes, the membrane paradigm* (Yale, 1986)

[219] D. Sijacki, V. Springel and M. G. Haehnelt, arXiv:0905.1689v2

[220] D. R. Law et al, arXiv:1207.4196v1

[221] B. J. Carr and S. W. Hawking, Month. Not. Roy. Astro. Soc. **168**, 399(1974)

[222] S. W. Hawking, Commun. Math. Phys. **43**, 199(1975)

[223] J. Magueijo, Rep. Prog. Phys. **66**, 2025(2003), arXiv:astroph/0305457

[224] R. Penrose, http://accelconf.web.cern.ch/accelconf/e06/PAPERS/THESPA01.PDF

[225] F. Iocco and M. Pato, Phys. Rev. Lett. **109**, 021102(2012), arXiv:1206.0736v2

[226] F. Iocco, arXiv:1206.2396v2

[227] XENON Collaboration, http://xenon.astro.columbia.edu/

[228] CDMS Collaboration, http://cdms.physics.ucsb.edu/

[229] DAMA Collaboration, http://people.roma2.infn.it/ dama/web/home.html

[230] G. 'tHooft, arXiv:grqc/9310026v2

[231] T. Padmanabhan, Phys. Rev. D **82**, 124025(2010), arXiv:1007.5066v2

[232] T. Banks and W. Fischler, arXiv:hepth/0102077v1

[233] B. McElrath, arXiv:0812.2696v1

[234] S. Alexander, http://pirsa.org/12050017

[235] L. Riofrio, http://riofriospacetime.blogspot.com/

[236] G. 'tHooft, Nucl. Phys. B **256**, 727745(1985)

[237] L. Susskind, L. Thorlacius and J. Uglum, Phys. Rev. D **48**, 37433761(1993), arXiv:hepth/9306069v2

[238] L. Riofrio, http://riofriospacetime.blogspot.com/2006/09/recentgmtc3paper.html

[239] J. P. Blaizot, E. Iancu and A. Rebhan, arXiv:hepph/0303185v2

[240] D. A. Teaney, arXiv:0905.2433v1

[241] G. Chirco, C. Eling and S. Liberati, arXiv:1005.0475v2

[242] M. Milgrom, Astrophys. J. **270**, 365370(1983)

[243] H. Goldstein, *Classical Mechanics* (AddisonWesley, 1970)

[244] Jet Propulsion Laboratory, http://voyager.jpl.nasa.gov

[245] Y. H. Sanejouand, arXiv:0908.0249v4

[246] V. C. Rubin, N. Thonnard and W. K. Ford, Astrophys. J. **238**, 471(1980)

[247] R. B. Tully and J. R. Fisher, Astron. Astrophys. **54**, 661673(1977)

[248] T. Leinster, *Higher operads, higher categories*, arXiv:math/0305049

[249] J. W. Gray, *Formal category theory: adjointness for 2categories* (Springer, 1974)

[250] P. Freyd, D. Yetter, J. Hoste, W. B. R. Lickorish, K. Millett and A. Ocneanu, Bull. Amer. Math. Soc. **12**, 239246(1985)

[251] W. B. R. Lickorish, *An introduction to knot theory* (Springer, 1997)

[252] K. Reidemeister, Abh. Math. Sem. Univ. Hamburg **1**, 2432(1926)

[253] D. Rolfsen, *Knots and links* (Publish or Perish, 1976)

[254] R. Fenn and C. Rourke, J. Knot Th. Ramif. **1**, 343406(1992)

[255] E. Abe, *Hopf algebras* (Cambridge, 1980)

[256] D. Kreimer, *Knots and Feynman Diagrams* (Cambridge, 2000)

[257] J. Baez, http://math.ucr.edu/home/baez/octonions

[258] M. Rios, arXiv:1005.3514

[259] R. Moufang, Math. Ann. **110**, 416430(1935)

[260] K. McCrimmon, in *A Taste of Jordan Algebras* (Springer, 2003)